Title

Synthesis, Characterization, and Reactivity of Pentamethylcyclopentadienyl Complexes of Divalent Cobalt and Nickel

Author

Smith, M.E.

Publication Date

1993-10-01

LBL-34753
UC-401

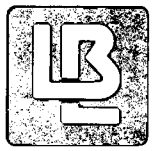

Lawrence Berkeley Laboratory
UNIVERSITY OF CALIFORNIA

CHEMICAL SCIENCES DIVISION

Synthesis, Characterization, and Reactivity of Pentamethylcyclopentadienyl Complexes of Divalent Cobalt and Nickel

M.E. Smith
(Ph.D. Thesis)

October 1993

Prepared for the U.S. Department of Energy under Contract Number DE-AC03-76SF00098

DISCLAIMER

LBL-34753

Synthesis, Characterization, and Reactivity of Pentamethylcyclopentadienyl Complexes of Divalent Cobalt and Nickel

Michael Edward Smith

Lawrence Berkeley Laboratory
University of California
Berkeley, California 94720

October 1993

This work was supported by the Director, Office of Energy Research, Office of Basic Energy Sciences, Chemical Sciences Division of the U.S. Department of Energy under contract number DE-AC03-76SF00098.

Abstract

Synthesis, Characterization, and Reactivity of Pentamethylcyclopentadienyl Complexes of Divalent Cobalt and Nickel

by

Michael Edward Smith

Doctor of Philosophy in Chemistry

University of California at Berkeley

Professor Richard A. Andersen, Chair

The divalent transition metal complexes $[(C_5Me_5)M(X)]_n$ (M = Co, X = Cl, n = 2; M = Co or Ni, X = acetylacetonate, n = 1) react with MeLi to produce the carbyne-bridged trinuclear cluster complexes, $(C_5Me_5)_3M_3(\mu_3\text{-}CH)(\mu\text{-}H)$ (M = Co or Ni), with evolution of methane. The complexes have three-fold symmetry in the solid-state and exhibit physical properties and chemical reactivity that are dominated by their electronic configurations of 46 electrons (M = Co) and 49 electrons (M = Ni) (48 electrons exactly fill the bonding molecular orbitals for trinuclear clusters with this geometry). The carbyne-hydride cluster complexes react with oxidizing agents, producing either the cobalt(III) cluster species, $(C_5Me_5)_3Co_3(\mu_3\text{-}CH)_2$, or decomposition to nickel(II) salts and oxidized organic products. $(C_5Me_5)_3Ni_3(\mu_3\text{-}CH)(\mu\text{-}H)$ is unreactive towards dihydrogen, but $(C_5Me_5)_3Co_3(\mu_3\text{-}CH)(\mu\text{-}H)$ reacts with one equivalent of dihydrogen to produce $(C_5Me_5)_3Co_3(\mu_3\text{-}CH)(\mu_2\text{-}H)_3$. This 48-electron complex is not chemically reactive, but 2D EXSY NMR experiments indicate that the carbyne and hydride protons exchange in an intramolecular fashion *ca.* once per second.

Monomeric $(C_5Me_5)Ni(acac)$ exhibits a temperature dependent singlet-triplet spin equilibrium. Both acetylacetonate species show an "ene-allyl" distortion of the C_5Me_5 ring in the solid state, which is produced by selective population of a metal-ring antibonding orbital and is more pronounced for the nickel species. Addition of PMe_3 to the nickel complex produces the 20-electron complex, $(C_5Me_5)Ni(acac)(PMe_3)$, which is paramagnetic, consistent with molecular orbital theory. $(C_5Me_5)Co(acac)$ does not coordinate additional phosphine.

The halide-bridged dimers, $[(C_5Me_5)M(X)]_2$ (M = Co, X = Cl, Br; M = Ni, X = Br), react with phosphines to produce the corresponding monomeric species, $(C_5Me_5)M(X)(PR_3)$. These complexes also exhibit "ene-allyl" distortions in the solid-state since they are isoelectronic with the acac complexes. The phosphine adducts are unreactive towards methyl anion sources, and the synthesis of $(C_5Me_5)M(Me)(PEt_3)$ was accomplished by reacting $(C_5Me_5)M(acac)$ with MeLi in the presence of PEt_3.

The mixed-ring metallocenes, $(C_5Me_5)M(C_5H_5)$ (M = Mn, Fe, Co, Ni), were studied to investigate the possibility of static Jahn-Teller distortions being present in metallocenes with E symmetry electronic ground states. In contrast to some earlier work with D_5 symmetrical metallocenes, no definitive evidence for static Jahn-Teller distortions was found in the crystallographic analysis of the mixed-ring metallocenes.

RA Anderson

Acknowledgments

After spending five plus years at Berzerkeley, there have been far more people who have contributed to my life and my research than I can mention here. However, there are a few people who stand above the rest. First and foremost is my advisor, Dick Andersen. You have always made me think hard about my chemistry, from both a practical and a theoretical point of view. I don't know if I've made you more famous, but the time I've spent in your research group has certainly made me a better, and hopefully wiser, chemist. Whenever somebody asks me what color a compound is, I'll always think of you. Maybe the Giants can make it in the playoffs with the new screwy three-division arrangement.

I'd also like to thank my undergraduate advisor, Greg Girolami. Without the year and a half I spent in your lab, Greg, I have no idea what I would have been doing the last five years. Although considering the earthquakes, firestorm, hostage situations, and riots, I don't know exactly how grateful I should be. You were a wonderful influence on me, and showed me how fun organometallic chemistry could be.

Phil Matsunaga deserves special mention. He took a know-it-all hot shot from Illinois and showed him how to make air-sensitive compounds. He also was a good friend the years we were here together, with many pathetically long nights in lab or on the diffractometer. If it weren't for the "gross-out" game, I would have jumped off the balcony years ago. Good luck with the future, and I'm sure I'll see you soon. (You have got to produce "Bullet in the Head"!)

As for the rest of the Andersen group, Marc Weydert and my evil twin, Wayne Lukens, helped me spend five years as an honorary hilloid (that means machine hits every two hours and giving Norm a hard time). Without these two

gentlemen, I would be even more ignorant than I am now about spectroscopy and many other things (like how foul-smelling French cigarettes are). Other group members of the past - Rob Rosen, Steve Stults, Sharon Beshouri, Brian Campion, and Mitch Smith - and present - Dave Schwartz, Chad Sofield, and Mark Petrie - have made graduate school much more enjoyable. I must also acknowledge my half-brother and -sister from the distant past, Rick Michelman and Melinda Burn, for near-constant entertainment and (for one of them) introducing me to my wife. Finally, Claus Lugmair worked with me for three semesters, and we had a tremendous amount of fun together. Good luck at San Diego and wherever life takes you. To the new generation - Jennifer, Kris, Pat, and Laura - have a great time.

The following is an abbreviated list of the many friends I've made here at Cal. The 5th floor gang: Mike Chan, Dave Sable (my first roomie), and Dave Eichhorn (Armstrong group); Bill Casteel, Byron Shen, George Lucier, and Prof. Rika Hagiwara (the Bartlett boys); Phil Bonasia and Victor Christou (Arnold group); and Gene Pruss (Stacy Group). I also consider Graham Ball an honorary member of the gang. I've also made good friends in other parts of the department, especially the Heathcock Group. Tony Watson and I spent innumerable lunches together, talking about everything, and I consider being best man at his wedding a highlight of my short life. My roommate, Dave Clark, and Doris Stoermer have been two good friends that have made the last three years much better, and you two had better visit us in the bayou. Finally, to the Latvians (Neo and otherwise, especially Phil Carter and Steve Keller), the basketball gang (esp. Don Arnold and Bob Harris), and the volleyball gang (esp. Tom Boussie, Todd McDermott, and Tim Lewis), thanks for putting up with a competitive, loud-mouthed white boy who isn't nearly as athletically inclined as he thinks he is.

If you're still reading this, you are either bored or I haven't mentioned you yet. I'd like to thank my close friends outside chemistry, starting with my best man, Tim Mickna ("Some call him Tim"). There is no way I can ever sum up our friendship, so I'll just say thanks from the bottom of my heart. Also, Joe Quinn, Paul DiSalvo, Trent Austin, and Jim Fleck have made both my college and graduate years (and in Jim's case, high school) great fun, and have helped me kill a substantial number of brain cells. To all of you, cheers.

Finally, and most importantly, I must thank my family. Mom, Dad and Jeff, you've made me everything I am today, and I love you very much (sorry about the gray hair). My newly discovered family, Allen, Barbara, Lisa, Jeff, Rachel, and Alex, I have also grown to love you in just the short time since we met. And Allison, you are everything to me, and I consider myself the luckiest man on the face of the Earth.

To

My Family

Table of Contents

Introduction

The study of the interactions of hydrocarbon fragments with metal centers is an extremely important field because of its direct relationship to many catalytic processes used in industry today. The variety of organometallic species that have been synthesized and studied since the discovery of Zeise's salt in 1827[1] is immense. However, complexes with bridging alkyl groups, especially methyl groups, form a small and extremely interesting class of compounds. Although there are examples of complexes with bridging methyl groups that involve many different geometries and a variety of metallic elements,[2] there are only four structurally characterized dimeric, methyl-bridged complexes involving first-row transition metals (Figure 1). The first two complexes in Figure 1, [(1,3-dimethylallyl)Ni(μ_2-Me)]$_2$[3] and [(C_5Me_5)Cr(Me)(μ_2-Me)]$_2$,[4] both exhibit a symmetrical coordination environment about each metal atom and a $\angle$M-C-M angle around °, which is within the range seen for most of the symmetrical bridging methyl species known, going back to the first structurally characterized bridging methyl complex, [$(Me)_2Al(\mu_2\text{-}Me)]_2$.[5] However, the two iron cations shown in Figure 1 have methyl groups that exhibit an asymmetric interaction with one of the two metal centers.[6] This type of interaction, where a hydrogen atom of an alkyl group is preferentially associated with a metal center, producing a weakening of the carbon-hydrogen bond, has been termed *agostic* by M. L. H. Green.[7] Agostic interactions have been proposed as models for C-H bond activation at metal centers, making the study of these and all bridging methyl groups very important for trying to understand the processes occurring in many catalytic systems.

Figure 1. First-Row Homobimetallic Bridging-Methyl Complexes.[3,4,6]

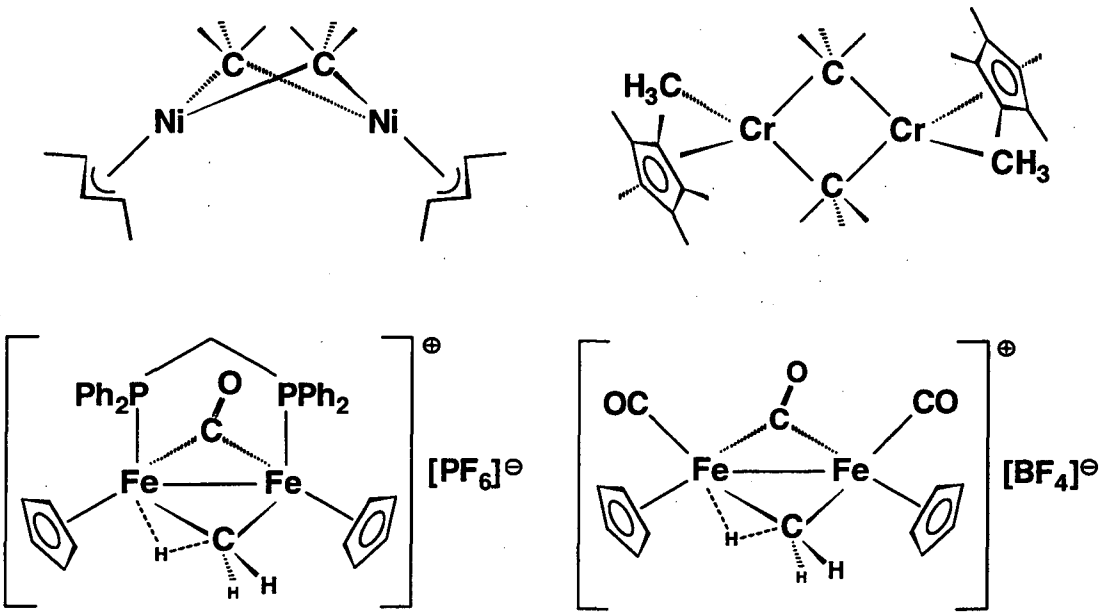

The dearth of bridging-methyl complexes involving first-row transition metals led to this work, which initially involved the attempts to synthesize complexes of the type $[(C_5Me_5)M(\mu\text{-}CH_3)]_n$ (M = Co, Ni, $n \geq 2$), where C_5Me_5 is shorthand for the pentamethylcyclopentadienyl anion. However, generation of the coordinatively unsaturated fragment, "$(C_5Me_5)M(CH_3)$," in the absence of coordinating ligands does not produce the desired methyl-bridged species, but instead results in the isolation of clusters of the general formula $(C_5Me_5)_3M_3(\mu_3\text{-}CH)(\mu\text{-}H)$ (M = Co, Ni). These clusters differ from most triangular, trinuclear metal clusters in that they have less (46 for Co) or more (49 for Ni) electrons than the most stable electronic configuration for this class of compounds, which has 48 electrons, exactly filling all of the bonding molecuar orbitals.[8] This difference in electronic configuration plays a large role in the

physical properties and chemical reactivity of these clusters, and allows insight into the nature of the bonding in the cluster compounds.

Initial studies of the cluster compounds were hampered by our inability to isolate the desired carbyne-hydride clusters from by-products with similar molecular geometries. This led to the investigation of $(C_5Me_5)M(acac)$ complexes as soluble, easily purified starting materials for synthesizing $(C_5Me_5)_3M_3(\mu_3\text{-}CH)(\mu\text{-}H)$ (M = Co, Ni). However, the unusual physical properties reported for $(C_5Me_5)Ni(acac)$[9] warranted an in-depth study of the acac complexes. Due to a large difference in the energies of the molecular orbitals derived from the d_{xz} and d_{yz} metal orbitals, these complexes exhibit a distorted ground-state geometry, termed an "ene-allyl" distortion by Mason.[10] The implications of this distortion and its effects on the physical properties and reactivity of the acac complexes is described.

Initial reports in the literature of $[(C_5Me_5)Co(\mu\text{-}Cl)]_2$, the original starting material used to generate "$(C_5Me_5)Co(CH_3)$," concluded that this complex exists as a mixture of two species in solution: the dimeric form indicated above and a solvated monomer, $(C_5Me_5)Co(Cl)(S)$, where S is the reaction solvent.[11] However, there are some unusual features of the reported characterizational data that indicated that a reexamination of this complex and the related bromide complexes for cobalt and nickel was warranted. Also, the isolable phosphine adducts, $(C_5Me_5)M(X)(PR_3)$ (M = Co, X = Cl, Br; M = Ni, X = Br), synthesized by addition of the phosphine to the appropriate dimeric halide species,[11,12] were investigated as electronic analogues of $(C_5Me_5)M(acac)$, where the three-electron, bidentate acac ligand has been substituted for by two unidentate ligands, the one-electron halide ligand and the two-electron phoshine ligand. Comparison of these two classes of species will lead to a better understanding of the nature of the bonding interactions in both class of complexes.

The last chapter is a departure from the rest of the work presented here. Even though a large number of metallocene complexes involving virtually every metal in the periodic table are known, there is still some debate involving the solid-state structures of the C_5-symmetrical metallocenes, $(C_5R_5)_2M$ (M = Mn, Fe, Co, Ni; R = H, Me).[13] Solution properties of these complexes indicate that the metallocenes with ^2E ground states exhibit a dynamic Jahn-Teller distortion that can only be detected by EPR at extremely low temperatures (< 10 K).[14] However, reports of X-ray crystallographic evidence for a static Jahn-Teller distortion at room temperature have clouded the issue. Presented in this work is a review of the pertinent data for these metallocenes and a summary of ours and previous work with $(C_5Me_5)M(C_5H_5)$ (M = Mn,[15] Fe,[16] Co, Ni), and the relationship of all of this data to the electronic ground states of these compounds.

References

1. Zeise, W. C., *Pogg. Ann.*, **1831**, *21*, 497.

2. Bursten, B. E.; Cayton, R. H., *Organometallics*, **1986**, *5*, 1051; and references therein.

3. Krüger, C.; Sekutowski, J. C.; Berke, H.; Hoffmann, R., *Z. Naturforsch.*, **1978**, *33B*, 1110.

4. Noh, S. K.; Sendlinger, S. C.; Janiak, C.; Theopold, K. H., *J. Am. Chem. Soc.*, **1989**, *111*, 9127.

5. Huffman, J. C.; Streib, W. E., *J. Chem. Soc., Chem. Commun.*, **1971**, 911.

6. (a) Dawkins, G. M.; Green, M.; Orpen, A. G.; Stone, F. G. A., *J. Chem. Soc., Chem. Commun.*, **1982**, 41.
(b) Casey, C. P.; Fagan, P. J.; Miles, W. H., *J. Am. Chem. Soc.*, **1982**, *104*, 1134.

7. Brookhart, M.; Green, M. L. H., *J. Organomet. Chem.*, **1983**, *250*, 395.

8. Pinhas, A. R.; Albright, T. A.; Hofman, P.; Hoffmann, R., *Helv. Chim. Acta*, **1980**, *63*, 29.

9. Bunel, E. E.; Valle, L.; Manriquez, J. M., *Organometallics*, **1985**, *4*, 1680.

10. Gerloch, M. R.; Mason, R., *J. Chem. Soc.*, **1965**, 296.

11. Kölle, U.; Fuss, B.; Belting, M.; Raabe, E., *Organometallics*, **1986**, *5*, 980.

12. Kölle, U.; Fuss, B.; Khouzami, F.; Gersdorf, J., *J. Organomet. Chem.*, **1985**, *290*, 77.

13. (a) Powell, P., "Principles of Organometallic Chemistry," 2nd Ed., Chapman and Hall: London, **1988**.
(b) Freyberg, D. P.; Robbins, J. L.; Raymond, K.N.; Smart, J. C., *J. Am. Chem. Soc.*, **1979**, *101*, 892.
(c) Raymond, K. N., unpublished results.

14. Ammeter, J. H.; Swalen, J. D., *J. Chem. Phys.*, **1972**, *57*, 678.

15. Matsunaga, P. T.; Andersen, R. A., unpublished results.

16. Zanin, I. E.; Antipin, M. Y.; Struchkov, Y. T.; Kudinov, A. R.; Ruebinskaya, M. I., *Metalloorganicheskaya Chimiya*, **1992**, *5*, 579.

Chapter 1

Synthesis, Characterization and Reactivity of Trinuclear Pentamethylcyclopentadienyl Cobalt and Nickel Clusters with Triply-Bridging Methylidyne Groups

Initial attempts to generate complexes of the type $[(C_5Me_5)M(\mu\text{-}CH_3)]_n$ (M = Co, Ni, $n \geq 2$) produced cluster compounds of the type $(C_5Me_5)_3M_3(\mu_3\text{-}CH)(\mu\text{-}H)$ (M = Co, Ni) instead. Cluster compounds containing triply-bridging methylidyne ligands have been known for some time. Markó first reported $Co_3(CO)_9(\mu_3\text{-}CH)$ in 1962,[1] and a host of other carbonyl clusters containing bridging carbyne ligands have been reported since then.[2] More closely related to the compounds studied here are the cobalt and rhodium clusters reported by Vollhardt[3] and Maitlis,[4] respectively, which have the general formula $(C_5R_5)M_3(\mu_3\text{-}CH)_2$ (M = Co, R = H; M = Rh, R = Me). Also important are the complexes of the type $(C_5R_5)_3Ni_3(\mu_3\text{-}CR')$ (R = H, R' = Me, Et, ^{i}Pr; R = Me, R' = Me) synthesized by Pasynkiewicz, *et al.*[5] However, these and the vast majority of cluster compounds containing a triangular, trinuclear metal core triply-bridged by one or more carbyne ligands are diamagnetic, with an overall electron count of 48 electrons, a condition that results when all of the bonding molecular orbitals are filled.

In contrast, the cluster compounds, $(C_5Me_5)_3M_3(\mu_3\text{-}CH)(\mu\text{-}H)$, have electron counts of 46 (M = Co) and 49 (M = Ni). These molecules with the electronic configurations that are two electrons short and one electron in excess, respectively, of the condition where all of the bonding molecular orbitals are occupied by a pair of electrons, have been observed for other cluster types. For example, the Fischer-Palm carbonyl clusters, $(C_5R_5)_3M_3(\mu_3\text{-}CO)_2$, are isoelectronic with the carbyne-hydride clusters described here.[6] The electronic

configuration affects the physical and structural properties of these clusters, as well as their reactivity. Investigation of these novel clusters will, it is hoped, provide new insight into the nature of the bonding in cluster complexes, and this in turn should provide a rationalization for their reaction chemistry, or lack thereof.

Synthesis

Initial studies of $(C_5Me_5)_3M_3(\mu_3\text{-}CH)(\mu\text{-}H)$ were spurred by the initial synthesis of the cobalt species from the reaction of $[(C_5Me_5)Co(\mu\text{-}Cl)]_2$ with two equivalents of MeLi (eq. 1). This reaction produces $(C_5Me_5)_3Co_3(\mu_3\text{-}CH)(\mu\text{-}H)$ as black prisms in ~60% yield. However, a small but significant amount of a second complex, $(C_5Me_5)_3Co_3(\mu_3\text{-}CH)_2$, was always present, based on infrared and ^1H NMR spectral data. The two species crystallize in the same space group (see X-ray discussion below), making separation effectively impossible. Hence, a different route that gave one compound in pure form was desired. The corresponding reactions of MeLi with $[(C_5Me_5)Co(\mu\text{-}Br)]_2$ and $[(C_5Me_5)Ni(\mu\text{-}Br)]_2$ were unsuccessful since unreacted starting material was the only product isolated in each case (eq. 2). Since $[(C_5Me_5)Ni(\mu\text{-}Cl)]_2$ could not be synthesized (see Chapter 3), other starting materials were pursued.

$$[(C_5Me_5)Co(\mu\text{-}Cl)]_2 + 2\ MeLi \xrightarrow[0\ ^\circ C]{Et_2O} (C_5Me_5)_3Co_3(\mu_3\text{-}CH)(\mu\text{-}H) + \ldots \quad (1)$$

$$[(C_5Me_5)M(\mu\text{-}Br)]_2 + 2\ MeLi \xrightarrow[0\ ^\circ C]{Et_2O} \text{no reaction} \quad (2)$$

$M = Co, Ni$

Maitlis described the synthesis of $(C_5Me_5)_3Rh_3(\mu_3\text{-}CH)_2$ from the reaction of $[(C_5Me_5)RhCl(\mu\text{-}Cl)]_2$ with $AlMe_3$.[4] Since $[(C_5Me_5)Co(\mu\text{-}Cl)]_2$ is easily oxidized to $[(C_5Me_5)CoCl(\mu\text{-}Cl)]_2$, a cobalt(II) starting material that is not easily oxidized to a cobalt(III) species seemed to be a desirable metal complex, since $(C_5Me_5)_3Co_3(\mu_3\text{-}CH)_2$ is observed as a by-product in the reaction shown in eq. 1. Also, a starting material that could be synthesized for both cobalt and nickel was desirable in order to systematize the synthetic reaction as much as possible. The acetylacetonate compounds, $(C_5Me_5)M(acac)$ (M = Co, Ni), fit these criteria. Reaction of $(C_5Me_5)M(acac)$ with MeLi in diethyl ether solution produces the corresponding clusters, $(C_5Me_5)_3M_3(\mu_3\text{-}CH)(\mu\text{-}H)$, in yields as good as or much better than those from the metal halides (eq. 3). More importantly, since both the nickel and cobalt starting materials are accessible and easily purified by sublimation, both clusters could be synthesized with high purity. Performing the synthesis with freshly prepared MeLi yielded the best results.

$$(C_5Me_5)M(acac) + MeLi \xrightarrow[0\ ^\circ C]{Et_2O} (C_5Me_5)_3M_3(\mu_3\text{-}CH)(\mu\text{-}H) \quad (3)$$

M = Co, 66% yield

M = Ni, 61% yield

Characterization

Identification of $(C_5Me_5)_3M_3(\mu_3\text{-}CH)(\mu\text{-}H)$ was complicated initially by the lack of information present in the initial characterizational data. The infrared spectrum contains features attributable to $M\text{-}C_5Me_5$ modes, but no hydride bands are obvious. The carbyne C-H stretch is expected to appear around 3000 cm^{-1},[7] which is obscured by the mineral oil mull, as well as the other C-H features. Neither compound melts up to 330 °C in a sealed capillary, and neither compound sublimes up to 200 °C under diffusion pump vacuum ($\approx 10^{-4}$ torr).

This lack of volatility also complicates the mass spectrum of $(C_5Me_5)_3Co_3(\mu_3\text{-}CH)(\mu\text{-}H)$ since it does not yield a molecular ion, but only a broad envelope of peaks (*ca.* 30 amu wide) centered around 600 amu. Fortunately, the nickel analogue is somewhat more cooperative, yielding a molecular ion in the electron-impact mass spectrum whose isotopic pattern indicates the presence of three nickel atoms (nickel has two major naturally abundant isotopes, ^{58}Ni (68%) and ^{60}Ni (26%)). High resolution electron-impact mass spectroscopy confirms that the observed ion has a formula of $C_{31}H_{47}Ni_3$.

Solid-state magnetic susceptibility measurements of $(C_5Me_5)_3Co_3(\mu_3\text{-}CH)(\mu\text{-}H)$ and $(C_5Me_5)_3Ni_3(\mu_3\text{-}CH)(\mu\text{-}H)$ are extremely informative. The variable temperature magnetic susceptibility of $(C_5Me_5)_3Co_3(\mu_3\text{-}CH)(\mu\text{-}H)$ is shown in Figure 1. The compound displays approximate Curie-Weiss behavior at low and high temperatures, with a linear regression analysis of the data yielding a low temperature moment (5-50 K) of 2.42 μ_B and a high temperature moment (160-300 K) of 2.72 μ_B. This data indicates that the cobalt cluster has two unpaired electrons **per cluster**. The magnetic susceptibility data of $(C_5Me_5)_3Ni_3(\mu_3\text{-}CH)(\mu\text{-}H)$ is shown in Figure 2. $(C_5Me_5)_3Ni_3(\mu_3\text{-}CH)(\mu\text{-}H)$ exhibits Curie-Weiss behavior, yielding a moment of 1.90 μ_B with a small Weiss constant (θ = -6 K). This value indicates that $(C_5Me_5)_3Ni_3(\mu_3\text{-}CH)(\mu\text{-}H)$ has one unpaired electron **per cluster**. The magnetic susceptibility data provided important clues about the true identity of the cluster compounds.

Figure 1. Plot of $1/\chi_M$ vs. T for $(C_5Me_5)_3Co_3(\mu_3\text{-}CH)(\mu\text{-}H)$

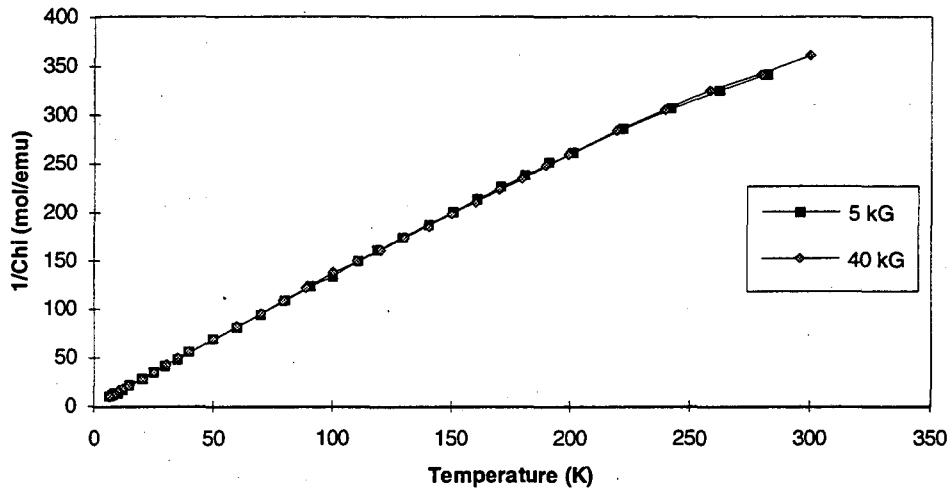

Figure 2. Plot of $1/\chi_M$ vs. T for $(C_5Me_5)_3Ni_3(\mu_3\text{-}CH)(\mu\text{-}H)$

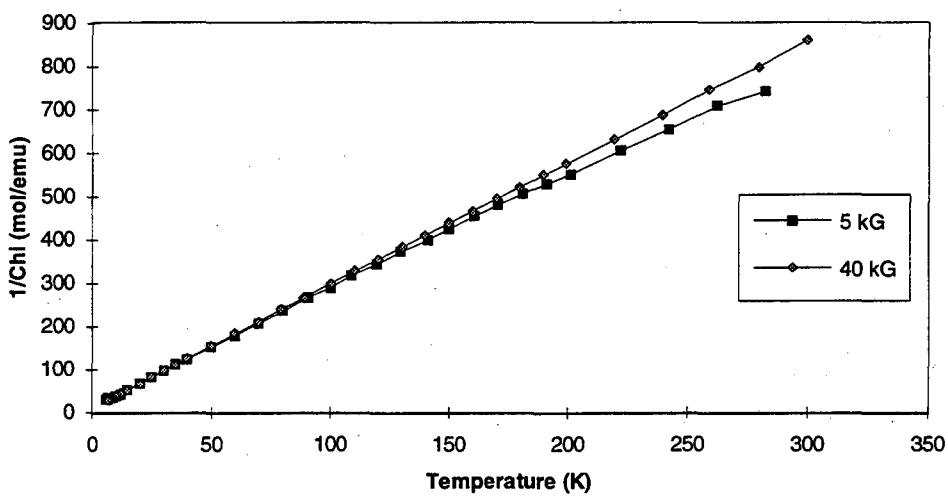

X-ray crystallographic analysis of the clusters was necessary to definitively determine the identity of the two species. The crystal structures of $(C_5Me_5)_3Co_3(\mu_3\text{-}CH)(\mu\text{-}H)$ and $(C_5Me_5)_3Ni_3(\mu_3\text{-}CH)(\mu\text{-}H)$ are shown in Figures 3 and 4, respectively. The structures are isomorphous, with both compounds crystallizing in $R\bar{3}$ (No. 148), and the molecules having crystallographically

imposed three-fold symmetry (hence, only one-third of the atoms are labeled). Figure 5 shows the nickel analogue looking down the three-fold axis. The bond distances and angles for both structures are listed in Tables 1 through 4. Unfortunately, both structures exhibit a minor disorder of the carbyne group to the opposite side of the triangular face of the metal core, and this disorder obscures whatever evidence there might be for the position of the hydride ligand. This is why the hydride ligands in these clusters are merely denoted by μ, since it is not possible to determine the exact geometry of the hydride ligand by X-ray crystallography. Nevertheless, since there is no evidence of a terminal hydride ligand in the infrared spectra (which would be expected to produce a reasonably intense absorption in the region of 1800-2250 cm^{-1}),[7] the assignment of a bridging geometry to the hydride ligand is reasonable. Even though the molecule has crystallographically imposed three-fold symmetry, a triply-bridging geometry cannot be definitively assigned to the hydride ligand. The hydride ligand could bridge two metal centers along one edge of the trimetallic core, and if the position of the hydride is disordered across the three potential bridging sites, the structure would still maintain rigorous three-fold symmetry. Since the packing in the crystalline lattice is dominated by the C_5Me_5 ligands, a disorder of the sterically insignificant hydride ligand would have no measurable effect on the final structure solution.

Figure 3. ORTEP Diagram of $(C_5Me_5)_3Co_3(\mu_3\text{-}CH)(\mu\text{-}H)$.

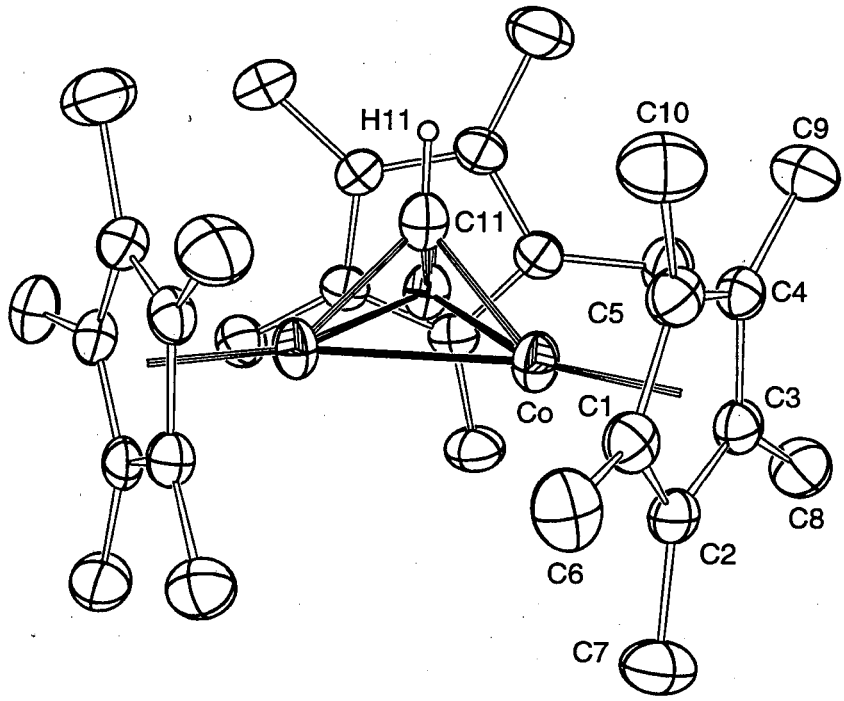

Figure 4. ORTEP Diagram of $(C_5Me_5)_3Ni_3(\mu_3\text{-}CH)(\mu\text{-}H)$.

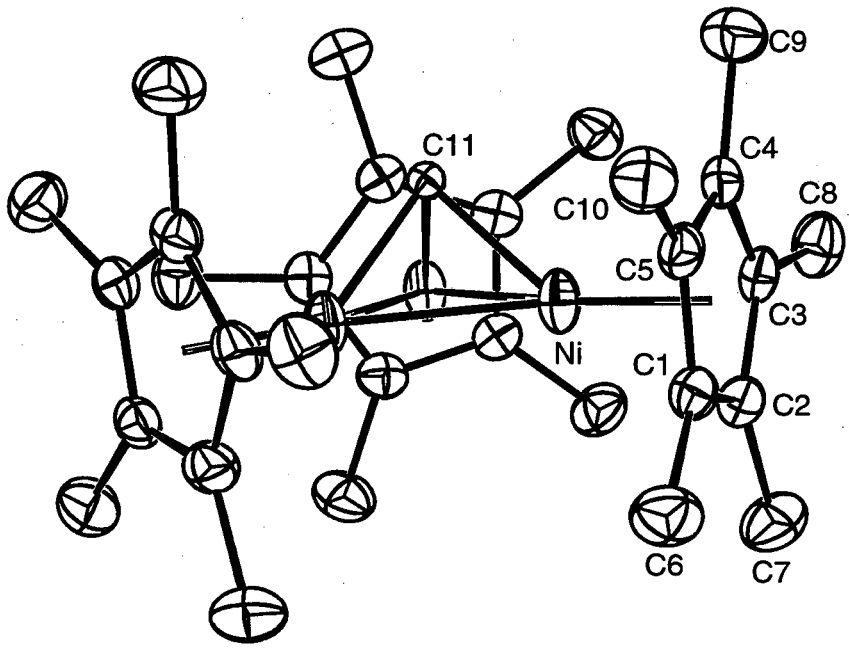

Figure 5. ORTEP View of $(C_5Me_5)_3Ni_3(\mu_3\text{-}CH)(\mu\text{-}H)$ Along the 3-Fold Axis.

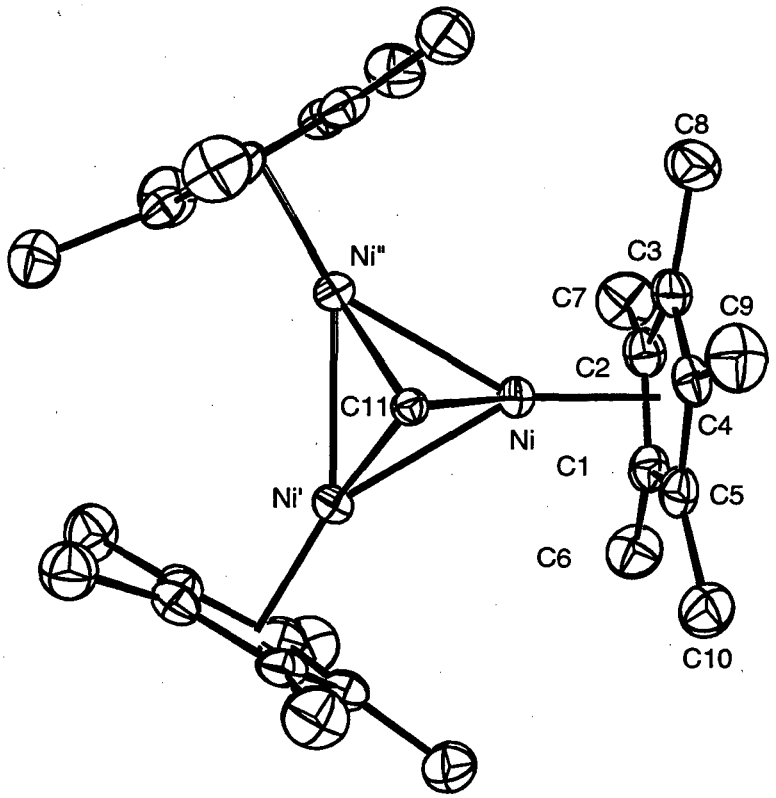

Table 1. Bond Distances for $(C_5Me_5)_3Co_3(\mu_3\text{-}CH)(\mu\text{-}H)$ (Å).

Co-Co	2.439 (1)	C1-C2	1.417 (7)
Co-C1	2.113 (5)	C1-C5	1.433 (7)
Co-C2	2.116 (5)	C2-C3	1.414 (7)
Co-C3	2.123 (5)	C3-C4	1.438 (7)
Co-C4	2.111 (5)	C4-C5	1.418 (7)
Co-C5	2.114 (5)		
Co-C11	1.856 (4)	Co-Cp	1.73

Cp is the ring centroid of atoms C1-C5.

Table 2. Bond Angles for $(C_5Me_5)_3Co_3(\mu_3\text{-}CH)(\mu\text{-}H)$ (°).

Co-Co-Co	60.00	C2-C1-C5	107.8 (4)
Co-C11-Co	82.10 (3)	C1-C2-C3	108.9 (4)
		C2-C3-C4	107.4 (4)
Cp-Co-Co	150	C3-C4-C5	108.1 (4)
Cp-Co-C11	138	C1-C5-C4	107.8 (4)

Table 3. Bond Distances for $(C_5Me_5)_3Ni_3(\mu_3\text{-}CH)(\mu\text{-}H)$ (Å).

Ni-Ni	2.415 (1)	C1-C2	1.415 (6)
Ni-C1	2.140 (4)	C1-C5	1.436 (6)
Ni-C2	2.135 (4)	C2-C3	1.431 (6)
Ni-C3	2.141 (4)	C3-C4	1.430 (6)
Ni-C4	2.119 (4)	C4-C5	1.411 (6)
Ni-C5	2.140 (4)		
Ni-C11	1.913 (7)	Ni-Cp	1.76

Cp is the ring centroid of atoms C1-C5.

Table 4. Bond Angles for $(C_5Me_5)_3Ni_3(\mu_3\text{-}CH)(\mu\text{-}H)$ (°).

Ni-Ni-Ni	60.00	C2-C1-C5	108.0 (4)
Ni-C11-Ni	78.26 (3)	C1-C2-C3	108.4 (4)
		C2-C3-C4	107.2 (4)
Cp-Ni-Ni	151	C3-C4-C5	108.8 (4)
Cp-Ni-C11	138	C1-C5-C4	107.7 (4)

The solution properties of the complexes are consistent with the proposed molecular constitution but do not definitively prove their nature. Neither complex exhibits a ^1H NMR spectrum at any temperature. Solution magnetic moment measurements indicate the presence of two unpaired electrons in $(C_5Me_5)_3Co_3(\mu_3\text{-}CH)(\mu\text{-}H)$ (2.28 μ_B) and one unpaired electron in $(C_5Me_5)_3Ni_3(\mu_3\text{-}CH)(\mu\text{-}H)$ (1.77 μ_B). This agrees with the results obtained from solid-state measurements, although the solution value for the cobalt cluster is low. The Evans' method will give low magnetic moments when the θ value of a complex cannot be accurately determined due to curvature in the plot of $1/\chi_M$ vs. T, as is the case for $(C_5Me_5)_3Co_3(\mu_3\text{-}CH)(\mu\text{-}H)$ (-38 K is the averaged θ value for the data from 160-300 K).

The EPR spectra of the cluster compounds yield results that are in accord with the magnetic susceptibility results. $(C_5Me_5)_3Co_3(\mu_3\text{-}CH)(\mu\text{-}H)$ does not

exhibit a solution EPR spectrum in methylcyclohexane at temperatures down to 1.8 K. However, doping $(C_5Me_5)_3Co_3(\mu_3\text{-}CH)(\mu\text{-}H)$ into the diamagnetic and isomorphous complex $(C_5Me_5)_3Co_3(\mu_3\text{-}CH)_2$ (2% solid solution, by weight) allows observation of a powder EPR spectrum at 1.7 K (Figure 6). The sample exhibits two very broad signals, one at g = 2.157 and a second at g = 4.268. The second signal is a half-field signal and is due to a "forbidden transition" in even-spin systems (the transition has $\Delta m_s = \pm 2$).[8] This half-field signal confirms that $(C_5Me_5)_3Co_3(\mu_3\text{-}CH)(\mu\text{-}H)$ has an even number of unpaired electrons, which is consistent with magnetic susceptibility measurements.

Figure 6. EPR Spectrum of $(C_5Me_5)_3Co_3(\mu_3\text{-}CH)(\mu\text{-}H)$, 2 wt. % Doped in $(C_5Me_5)_3Co_3(\mu_3\text{-}CH)_2$ (1.7 K).

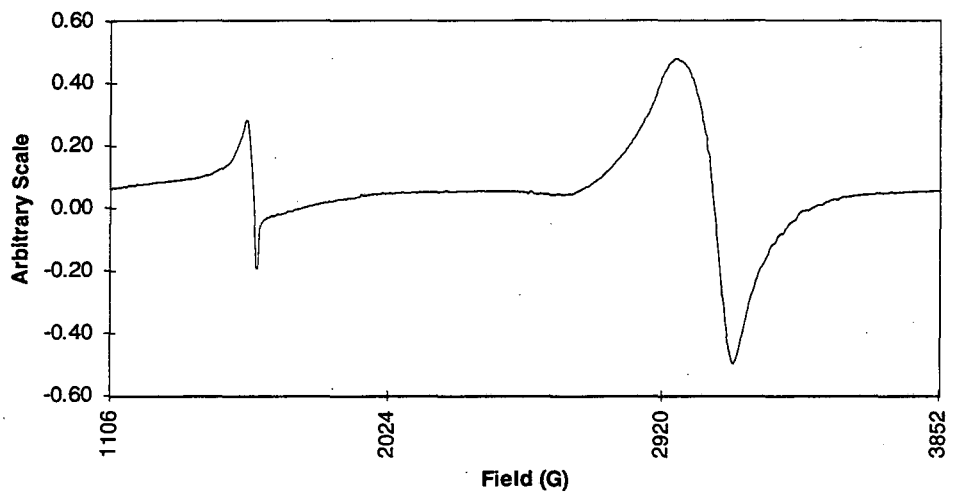

The room temperature solution EPR spectrum of $(C_5Me_5)_3Ni_3(\mu_3\text{-}CH)(\mu\text{-}H)$ exhibits a single resonance with $g_{iso} = 2.046$. This value, combined with the magnetic susceptibility data, indicates the presence of incomplete quenching of orbital angular momentum, since both values are higher than the expected spin-only values (1.90 μ_B vs. 1.73 μ_B, and 2.046 vs. 2.0023). The low

temperature EPR spectrum of $(C_5Me_5)_3Ni_3(\mu_3\text{-}CH)(\mu\text{-}H)$ is shown in Figure 7. This spectrum shows an axial splitting of the signal, with $g_\perp$ = 2.114 and $g_\parallel$ = 2.009, which indicates that the unpaired electron resides in an orbital with axial symmetry.

Figure 7. EPR Spectrum of $(C_5Me_5)_3Ni_3(\mu_3\text{-}CH)(\mu\text{-}H)$ in C_7H_{14} Glass (91 K).

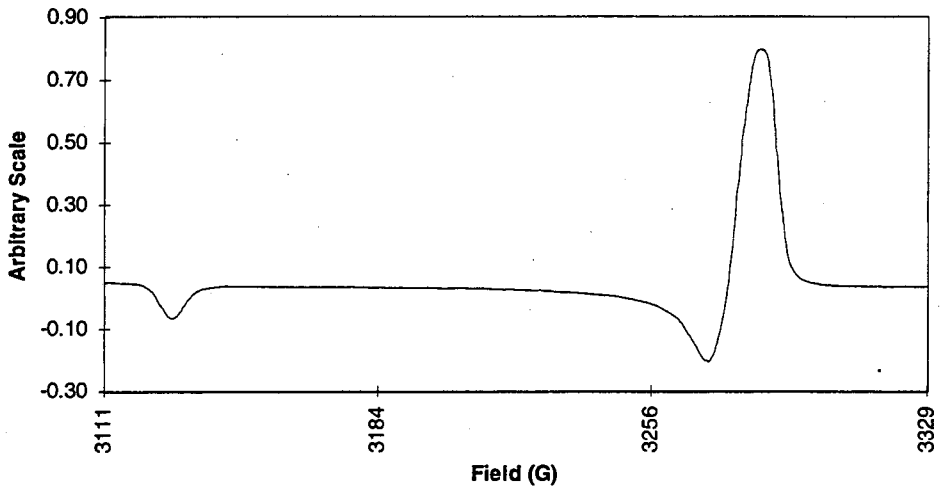

Orbital Considerations

All of the characterizational results for $(C_5Me_5)_3Co_3(\mu_3\text{-}CH)(\mu\text{-}H)$ and $(C_5Me_5)_3Ni_3(\mu_3\text{-}CH)(\mu\text{-}H)$ can be explained by utilizing the molecular orbital diagram in Figure 8, first presented by Pinhas and co-workers[9] and later modified by Dahl and co-workers,[6b] for $(C_5Me_5)_3M_3(\mu_3\text{-}L)_2$, where M = Co or Ni and L = CO, CS, S and other ligands capable of forming μ_3-bridging geometries. Although these ligands vary in electronic properties and thus perturb the absolute energy levels of the orbitals, the relative ordering of the 3e" and $2a_2'$ orbitals indicated in the diagram does not change.[6b] Since the $(C_5Me_5)_3M_3(\mu_3\text{-}CH)(\mu\text{-}H)$ clusters still have three-fold symmetry (as determined by X-ray crystallography), the 3e" levels remain orbitaly degenerate, since

reduction of the molecular symmetry from D_{3h} to C_{3v} by removal of the horizontal mirror plane of symmetry does not remove this degeneracy (the symmetry labels technically change to 7e and $4a_2$ in C_{3v} symmetry - however, the D_{3h} labels will be used in the discussion in order to reduce confusion). Hence, it is reasonable to apply the molecular orbital diagram in Figure 8 to $(C_5Me_5)_3Co_3(\mu_3\text{-}CH)(\mu\text{-}H)$ and $(C_5Me_5)_3Ni_3(\mu_3\text{-}CH)(\mu\text{-}H)$ for the purpose of interpreting the physical properties of these clusters with respect to their electronic configurations.

Figure 8. Symmetry Orbital Diagram for $(C_5Me_5)_3M_3(\mu_3\text{-}L)_2$ (48 electrons).[6b]

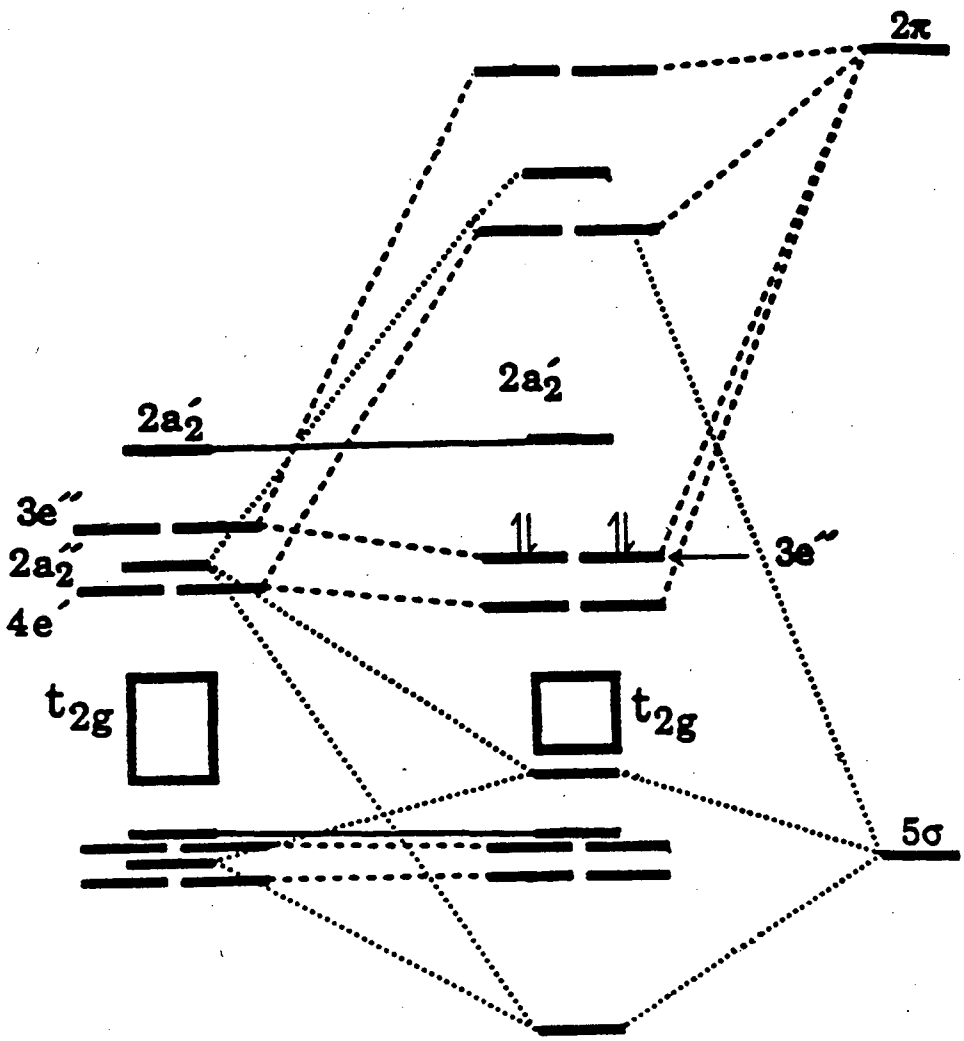

$(C_5Me_5)_3Co_3(\mu_3\text{-}CH)(\mu\text{-}H)$ has a total electron count of 46 electrons. Inspection of Figure 8 shows that this total predicts that the 3e" level will be half-occupied, and that this cluster compound will have two unpaired electrons. The magnetic susceptibility and EPR data for this complex agree with this deduction. Although none of the techniques utilized in this work produced direct evidence of a bridging hydride ligand in this compound, there must be a one-electron ligand present in the cluster to produce the results observed, since the hypothetical cluster "$(C_5Me_5)_3Co_3(\mu_3\text{-}CH)$" would have 45 electrons and hence an odd number of unpaired electrons. Also, the crystallographic data only indicates the presence of the μ_3-CH ligand, which means that the one-electron ligand must be a hydride, since that is the only ligand which would be expected to be unobservable in an X-ray crystallographic study. Unfortunately, the disorder problem precludes analysis by neutron diffraction, which is the standard method for definitive identification of hydride ligands that cannot be observed by X-ray methods. Comparison to the nickel analogue, $(C_5Me_5)_3Ni_3(\mu_3\text{-}CH)(\mu\text{-}H)$, which can be more definitively characterized by mass spectroscopy, also argues for the presence of the bridging hydride group in the cobalt cluster.

There is some confusion in the literature about the electronic ground state expected for 46-electron clusters of this type. Dahl has reported that $(C_5Me_5)_3Co_3(\mu_3\text{-}CO)_2$ is effectively diamagnetic in the solid state and exhibits a singlet-triplet spin equilibrium in solution.[6a] However, the room temperature X-ray crystal structure of this complex shows no evidence of distortion of the cluster from D_{3h} to a lower symmetry to remove the degeneracy of the 3e" molecular orbitals, which calculations by Pinhas and co-workers indicate would be necessary to pair the electrons in the 3e" orbitals.[9] $(C_5Me_5)_3Rh_3(\mu_3\text{-}CO)_2$, reported by Stone and co-workers,[10a] was shown to be diamagnetic in both solution and the solid-state. The low temperature X-ray crystal structure of this

rhodium cluster does exhibit a reduction of the overall symmetry of the cluster to C_{2v},[10b] which is in line with the predictions of Pinhas' model for a diamagnetic, 46-electron cluster.[9] In contrast to the C_5Me_5 clusters, $(C_5H_5)_3Co_3(\mu_3\text{-}CO)_2$ is paramagnetic in solution, with a solution magnetic moment of 3.0 ± 0.2 μ_B, indicating the presence of two unpaired electrons in the cluster.[11] The X-ray crystal structure of $(C_5H_5)_3Co_3(\mu_3\text{-}CO)_2$ has D_{3h} symmetry, as would be predicted from the magnetic moment of this compound. Finally, the tetrahydride cluster, $(C_5Me_5)_3Co_3(\mu_3\text{-}H)(\mu_2\text{-}H)_3$, reported recently by Theopold, *et al.*,[12] is paramagnetic in solution, with a broad, highly shifted ^1H NMR signal for the C_5Me_5 ligand (δ +63 in toluene-d_8 solution at 20 °C). The X-ray structure of this complex has three cobalt-cobalt distances that are identical within the error of the experiment, indicating that the complex has virtual, but not crystallographically imposed, three-fold symmetry. Thus, the paramagnetism observed in $(C_5Me_5)_3Co_3(\mu_3\text{-}CH)(\mu\text{-}H)$ is consistent with the results observed for most of the C_3-symmetrical 46-electron clusters in the literature, where the only anomaly is the diamagnetism of $(C_5Me_5)_3Co_3(\mu_3\text{-}CO)_2$ at low temperatures (< 170 K).

$(C_5Me_5)_3Ni_3(\mu_3\text{-}CH)(\mu\text{-}H)$ has a total electron count of 49 electrons, which predicts that the there is one unpaired electron in the $2a_2'$ level shown in Figure 8. This is also completely consistent with the characterizational data found for this compound, since the low-temperature EPR spectrum of $(C_5Me_5)_3Ni_3(\mu_3\text{-}CH)(\mu\text{-}H)$ predicts that the unpaired electron resides in a level with axial symmetry, and the $2a_2'$ orbital has axial symmetry. Also, the $2a_2'$ orbital would be expected to have a small orbital contribution to the magnetic moment,[13] which is reflected in the positive deviation from spin-only values observed for μ_{eff} and g_{iso} in this compound. Again, the solid-state structural data does not present direct evidence for the hydride ligand, but Pasynkiewicz, *et al.* have synthesized

the 48-electron cluster $(C_5Me_5)_3Ni_3(\mu_3\text{-}CMe)$,[5] and it is diamagnetic with a sharp ^1H NMR spectrum, just as predicted by Dahl's molecular orbital model (Figure 8). Hence, the existence of the bridging hydride ligand in $(C_5Me_5)_3Ni_3(\mu_3\text{-}CH)(\mu\text{-}H)$ is necessary to explain the physical properties observed for the complex.

The electronic structure of these clusters has a direct effect on the bond distances and angles observed in the solid-state structures of these complexes. The most important values for the X-ray structures of $(C_5Me_5)_3Co_3(\mu_3\text{-}CH)(\mu\text{-}H)$ and $(C_5Me_5)_3Ni_3(\mu_3\text{-}CH)(\mu\text{-}H)$ are listed in Table 5. Since the metal ions in both compounds have the same formal charge ("+7/3"), and the structures are isomorphous, direct comparison of bond lengths and angles can be interpreted with respect to electronic structures. Even though nickel is smaller than cobalt (by 0.03 Å for the divalent ions with coordination number 6)[14] inspection of Table 5 shows that the metal-carbyne carbon bond distance is *ca.* 0.06 Å longer in the nickel cluster than in the cobalt cluster, and this difference makes the M-C-M angle smaller in $(C_5Me_5)_3Ni_3(\mu_3\text{-}CH)(\mu\text{-}H)$. This can be rationalized by looking at the metal orbitals that contribute to the 3e" and $2a_2'$ molecular orbitals that are involved (Figure 9). These symmetry orbital conclusions were made by Dahl and Wilson,[15] and indicate that the $2a_2'$ level involves an in-plane, metal-metal antibonding interaction, while the 3e" orbitals are predominantly out-of-plane, metal-capping ligand and metal-ring antibonding orbitals. Thus, the larger metal-carbyne carbon and metal-ring carbon distances (which are 0.02 Å longer in the nickel analogue) in the nickel cluster are consistent with adding two electrons to the 3e" molecular orbitals. The observed differences in most of the bond distances and angles for the two cluster compounds are completely consistent with this analysis. An apparent contradiction is the contraction of the metal-metal bond distances when going from cobalt to nickel. This may be explained by noting that the shortening is smaller than the shortening expected based on the

differences in ionic radii (0.024 Å vs. 0.030 Å), indicating that the one electron in the metal-metal antibonding $2a_2'$ molecular orbital of the nickel cluster does have an effect on the metal-metal bond distances.

Figure 9. Metal Orbitals in the $2a_2'$ and 3e" Levels in $(C_5Me_5)_3M_3(\mu_3\text{-}L)_2$.[15]

HOMO and LUMO designations are for 48 electron species (see Figure 8).

Table 5. Important Bond Distances and Angles in $(C_5Me_5)_3M_3(\mu_3\text{-}CH)(\mu\text{-}H)$.

M	d(M-M)	d(M-ring C)[a]	d(M-C11)[b]	∠(M-C11-M)
Co	2.439	2.115	1.856	82.1°
Ni	2.415	2.135	1.913	78.3°

[a]Averaged value, in Å.
[b]C11 is the μ_3-carbyne carbon; distance in Å.

Mechanistic Studies

An important aspect of the study of the cluster compounds, $(C_5Me_5)_3M_3(\mu_3\text{-}CH)(\mu\text{-}H)$, is the determination of how the clusters are formed. The investigations were performed on the nickel system because characterization (by mass spectroscopy) is considerably easier for $(C_5Me_5)_3Ni_3(\mu_3\text{-}CH)(\mu\text{-}H)$ than for the cobalt analogue. Furthermore, the CD_3Li used for the labeling study contained a significant amount of LiBr, which

produced intractable reaction products in the cobalt system but did not interfere with isolation of the nickel cluster. Figure 10 postulates three net reactions that are required to produce $(C_5Me_5)_3M_3(\mu_3\text{-}CH)(\mu\text{-}H)$. First, metathesis of $(C_5Me_5)M(acac)$ with MeLi would be expected to produce the coordinatively unsaturated fragment, "$(C_5Me_5)M(Me)$." An attempt was made to trap this fragment with PEt_3; and $(C_5Me_5)M(Me)(PEt_3)$ was indeed isolated in high yield (Chapter 3). However, inspection of a ^1H NMR sample containing $(C_5Me_5)Ni(acac)$ and PEt_3 showed that the phosphine was coordinated to the nickel atom, since the C_5Me_5 and acac signals were shifted from their expected positions and there were no signals for uncoordinated PEt_3. Two other broad resonances were observed that increased in intensity and shifted when additional PEt_3 was added, indicating that the signals were due to coordinated phosphine, and that this phosphine was exchanging with the free phosphine in solution. Subsequent isolation and X-ray crystallographic analysis of $(C_5Me_5)Ni(acac)(PMe_3)$ (Chapter 2) proved that phosphines are not "innocent" with respect to their use as trapping agents, at least in this system. Thus, the presence of "$(C_5Me_5)M(Me)$" has yet to be definitively proven, although it is a reasonable assumption.

Figure 10. Proposed Mechanism for Formation of $(C_5Me_5)_3M_3(\mu_3\text{-}CH)(\mu\text{-}H)$.

$$(C_5Me_5)M(acac) + MeLi \longrightarrow "(C_5Me_5)M(Me)" + Li(acac)$$

$$3\ "(C_5Me_5)M(Me)" \longrightarrow (C_5Me_5)_3M_3(\mu_3\text{-}CH) + 2\ CH_4$$

$$(C_5Me_5)_3M_3(\mu_3\text{-}CH) \xrightarrow{[H]} (C_5Me_5)_3M_3(\mu_3\text{-}CH)(\mu\text{-}H)$$

possible [H]: solvent, trace H_2O, MeLi, CH_4, $(C_5Me_5)_3M_3(\mu_3\text{-}CH)$

The next step in Figure 10 assembles three "$(C_5Me_5)M(Me)$" fragments into the trimetallic core with concomitant evolution of methane. Since three body collisions are usually considered highly improbable from a mechanistic standpoint,[16] it is most likely that the "$(C_5Me_5)M(Me)$" fragments assemble in a stepwise fashion, producing a bimetallic intermediate before forming the $(C_5Me_5)_3M_3(\mu_3\text{-}CH)$ core. The evolution of methane was shown in the preparation of $(C_5Me_5)_3Ni_3(\mu_3\text{-}CH)(\mu\text{-}H)$ in a sealed NMR tube from $(C_5Me_5)Ni(acac)$ and MeLi in tetrahydrofuran-d_8 solution. Since the resulting nickel cluster has no ^1H NMR signal, the resulting solution exhibited a number of small, unidentified signals. Subsequent removal of gaseous products by repeated freeze-pump-thaw cycles resulted in the disappearance of only one signal, at δ 0.185 ppm. Pressurization of this degassed sample with 1 atmosphere of methane gas caused the signal at δ 0.185 ppm to reappear, definitively assigning this signal as being due to methane. Thus, methane is produced in the formation of $(C_5Me_5)_3M_3(\mu_3\text{-}CH)(\mu\text{-}H)$, tentatively confirming the second step of the proposed mechanism. This result is not quantitative since methane is not very soluble in tetrahydrofuran-d_8 and further experiments are

necessary to determine the absolute amount of methane generated in the reaction.

The final step shown in Figure 10 is the most perplexing and the most important. A simple metathesis reaction, followed by methane evolution, would produce clusters with the formula $(C_5Me_5)_3M_3(\mu_3\text{-}CH)$, where M is a divalent metal ion [M(II,II,II)]. However, the clusters scavenge a hydrogen atom from some source, resulting in a net oxidation of one electron and producing $(C_5Me_5)_3M_3(\mu_3\text{-}CH)(\mu\text{-}H)$ [formally M(III,II,II)]. This may not be unexpected for the cobalt analogue, since the molecular orbital model in Figure 8 indicates that $(C_5Me_5)_3Co_3(\mu_3\text{-}CH)$ would be three electrons short of the desired 48-electron configuration (indeed, there are no 45-electron clusters with the $M_3(\mu_3\text{-}L)_2$ geometry reported in the literature). However, $(C_5Me_5)_3Ni_3(\mu_3\text{-}CH)$ would be a 48-electron cluster, the ideal electron count for these systems. Still, both species scavenge a hydrogen atom, producing the $(C_5Me_5)_3M_3(\mu_3\text{-}CH)(\mu\text{-}H)$ cluster compounds.

The source and spectroscopic signature of the hydride ligand was determined by attempts to selectively deuterate $(C_5Me_5)_3Ni_3(\mu_3\text{-}CH)(\mu\text{-}H)$ by several methods, using mass spectroscopy as the analytical method. The product obtained from the ^1H NMR study of the reaction of $(C_5Me_5)Ni(acac)$ and MeLi in deuterated tetrahydrofuran showed no evidence of deuterium incorporation, so the solvent can be ruled out as a source of the hydride ligand. Likewise, attempts to exchange any of the hydrogen atoms by pressurizing a hexane solution of $(C_5Me_5)_3Ni_3(\mu_3\text{-}CH)(\mu\text{-}H)$ under 18 atmospheres of D_2 gas for periods of up to a week were unsuccessful, indicating that once the hydride has been scavenged by the cluster compound, it is not readily exchanged. The source of the hydride ligand was determined when the synthetic reaction was performed with D_3CLi. High resolution mass spectroscopy indicated that the

cluster formed in this reaction had a molecular weight that is exactly two mass units higher than that of the all protio compound (Figures 11 and 12). Comparison of the infrared spectra of this product to that of $(C_5Me_5)_3Ni_3(\mu_3\text{-}CH)(\mu\text{-}H)$ shows only two differences: the deuterated product has a sharp absorption at 2164 cm^{-1}, indicative of a μ_3-CD stretch,[17] and the replacement of a band at 981 cm^{-1} in the $(C_5Me_5)_3Ni_3(\mu_3\text{-}CH)(\mu\text{-}H)$ spectrum with a band at 682 cm^{-1} in its deuteride. The ratio of the wavenumber values of the two differing low energy bands is 981/682 = 1.438, in reasonable agreement with the idealized value of 1.414 expected for the ratio ν(X-H)/ν(X-D) if the vibrational mode were a pure harmonic oscillator.[18a] This stretch is in the region associated with triply bridging hydride ligands, and thus leads to the assignment of the deuterated product as $(C_5Me_5)_3Ni_3(\mu_3\text{-}CD)(\mu_3\text{-}D)$.[18b] Thus, the hydride ligand is derived from methyllithium. The moderate yields of the cluster compounds (typically 50 - 60%) indicate that the hydride ligand could be scavenged from the carbyne group of another ligand (eq. 4). The C-H bond of the carbyne group would be expected to be a more accessible source of the hydride ligand than either MeLi or methane, since the carbon is bound to three metal centers that act as electron withdrawing groups.

$$2\ (C_5Me_5)_3Co_3(\mu_3\text{-}CH) \longrightarrow (C_5Me_5)_3Co_3(\mu_3\text{-}CH)(\mu\text{-}H) + (C_5Me_5)_3Co_3(\mu_3\text{-}C) \quad (4a)$$

$$(C_5Me_5)_3Co_3(\mu_3\text{-}C) \longrightarrow \text{decomposition} \quad (4b)$$

Figure 11. Molecular Ion Envelope for $(C_5Me_5)_3Ni_3(\mu_3\text{-}CH)(\mu\text{-}H)$.

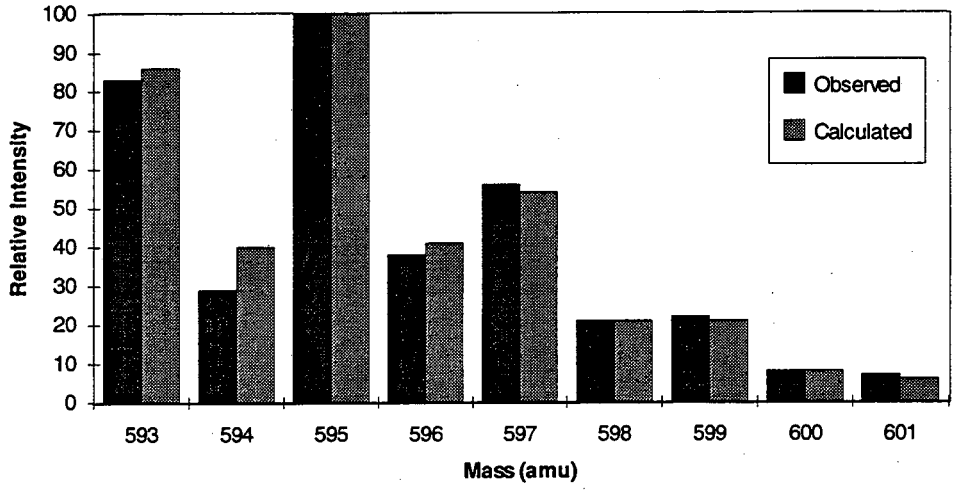

Figure 12. Molecular Ion Envelope for $(C_5Me_5)_3Ni_3(\mu_3\text{-}CD)(\mu\text{-}D)$.

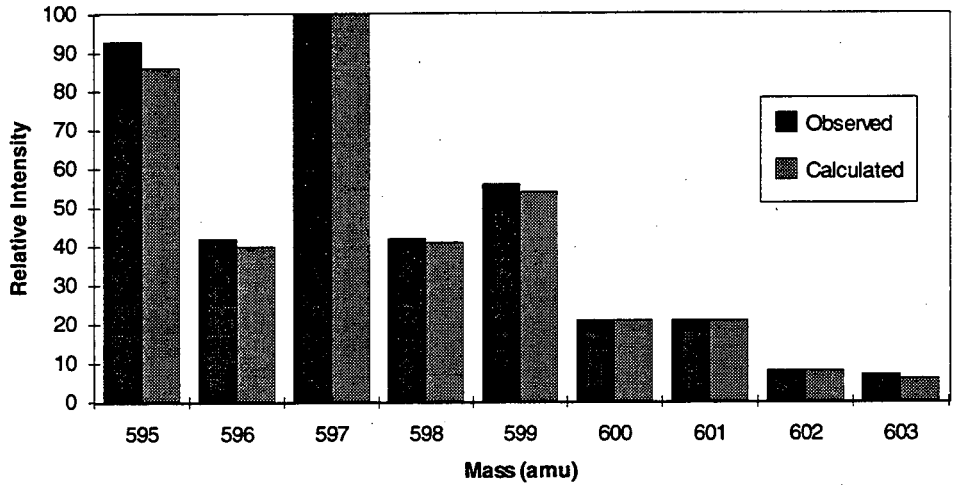

Oxidation Reactions

The discovery that $(C_5Me_5)_3Co_3(\mu_3\text{-}CH)(\mu\text{-}H)$ was contaminated with $(C_5Me_5)_3Co_3(\mu_3\text{-}CH)_2$ when synthesized from $[(C_5Me_5)Co(\mu\text{-}Cl)]_2$ led to the initial hypothesis that small amounts of $[(C_5Me_5)CoCl(\mu\text{-}Cl)]_2$ in the starting material were producing the contaminating bis-carbyne cluster. However, attempts to react $[(C_5Me_5)CoCl(\mu\text{-}Cl)]_2$ with MeLi in diethyl ether solutions produce no reaction (eq. 5), and reaction of $AlMe_3$ in CH_2Cl_2 with the cobalt(III) halide species (based on the precedent in rhodium(III) chemistry)[4] only reduces the starting material to $[(C_5Me_5)Co(\mu\text{-}Cl)]_2$ (eq. 6).

$$[(C_5Me_5)CoCl(\mu\text{-}Cl)]_2 + 4\ MeLi \xrightarrow[0\ °C]{Et_2O} \text{no reaction} \quad (5)$$

$$[(C_5Me_5)CoCl(\mu\text{-}Cl)]_2 + 4\ AlMe_3 \xrightarrow{CH_2Cl_2} [(C_5Me_5)Co(\mu\text{-}Cl)]_2 \quad (6)$$

However, oxidation of $(C_5Me_5)_3Co_3(\mu_3\text{-}CH)(\mu\text{-}H)$ with concentrated HCl produces $(C_5Me_5)_3Co_3(\mu_3\text{-}CH)_2$ in low yields (eq. 7), along with a substantial amount of $CoCl_2$ precipitate. Oxidation with one equivalent of CCl_4 produces better yields of the bis-carbyne (eq. 8), but no $CHCl_3$, which might be expected to form by hydride abstraction from the starting material, was observed in the ^1H NMR spectrum. The yields presented are based on the mass balance of cobalt. Performing the oxidation with DCl produces $(C_5Me_5)_3Co_3(\mu_3\text{-}CD)_2$, as judged by the sharp infrared band at 2158 cm^{-1}, which is very close to the C-D stretching frequency observed in $(C_5Me_5)_3Ni_3(\mu_3\text{-}CD)(\mu\text{-}D)$. Vollhardt has reported deuterium scrambling into the carbyne position of the cluster species

$(C_5H_5)_3Co_3(\mu_3\text{-}CH)(\mu_3\text{-}CR)$ (R = H, $SiMe_3$) upon treatment with F_3CCO_2D,[3] with a ν(C-D) of 2210 cm^{-1} observed for $(C_5H_5)_3Co_3(\mu_3\text{-}CD)(\mu_3\text{-}CSiMe_3)$.[17]

$$(C_5Me_5)_3Co_3(\mu_3\text{-}CH)(\mu\text{-}H) + HCl \xrightarrow{Et_2O} (C_5Me_5)_3Co_3(\mu_3\text{-}CH)_2 + CoCl_2 + \ldots \quad (7)$$
15% yield

$$(C_5Me_5)_3Co_3(\mu_3\text{-}CH)(\mu\text{-}H) + CCl_4 \xrightarrow{\text{toluene}} (C_5Me_5)_3Co_3(\mu_3\text{-}CH)_2 + \ldots \quad (8)$$
27% yield

$(C_5Me_5)_3Co_3(\mu_3\text{-}CH)_2$ crystallizes as red-violet prisms from pentane solution. The compound has 48 electrons and is diamagnetic, as predicted by molecular orbital theory for a cluster of this type (Figure 8). The ^1H NMR spectrum of $(C_5Me_5)_3Co_3(\mu_3\text{-}CH)_2$ consists of two singlets at δ 1.74 and 16.99, corresponding to the pentamethylcyclopentadienyl and carbyne protons, respectively. The significant downfield shift of the carbyne proton resonance is consistent with that seen for other μ_3-carbyne species, with values of δ 13.18 and 18.37 observed for this resonance in $(C_5Me_5)_3Rh_3(\mu_3\text{-}CH)_2$[4] and $(C_5H_5)_3Co_3(\mu_3\text{-}CH)_2$,[3] respectively. The corresponding signals in the series of diamagnetic, 48-electron cluster compounds, $M_3(CO)_9(\mu_3\text{-}CH)(\mu\text{-}H)_3$, appear at δ 11.4, 9.75, and 9.36 for M = Fe,[19] Ru,[20] and Os,[2b] respectively. No solution EPR signal is observed for $(C_5Me_5)_3Co_3(\mu_3\text{-}CH)_2$.

Inspection of Figure 8 indicates that the 48-electron bis-carbyne cluster would be expected to be inert, and indeed the complex is air- and water-stable. It is possible that any $[(C_5Me_5)CoCl(\mu\text{-}Cl)]_2$ present in solution when $(C_5Me_5)_3Co_3(\mu_3\text{-}CH)(\mu\text{-}H)$ is synthesized from $[(C_5Me_5)Co(\mu\text{-}Cl)]_2$ could act as an oxidant, thus producing the bis-carbyne complex. Since $(C_5Me_5)Co(acac)$

can be easily isolated without cobalt(III) impurities, this could explain why the use of the acac starting material yields pure $(C_5Me_5)_3Co_3(\mu_3\text{-}CH)(\mu\text{-}H)$, while the chloride starting material produces a mixture of the two clusters.

The X-ray crystal structure of $(C_5Me_5)_3Co_3(\mu_3\text{-}CH)_2$, shown in Figure 13, is extremely informative. The complex crystallizes in $R\bar{3}$ (No. 148) in a well-ordered fashion, so that all of the hydrogen atoms can be located and refined (the disorder observed in the $(C_5Me_5)_3M_3(\mu_3\text{-}CH)(\mu\text{-}H)$ structures cannot occur in this system since the bridging ligands are identical). The bond distances and angles (Tables 6 and 7, respectively) are consistent with the results seen for the two carbyne-hydride clusters and the orbital model (Figure 8) used to explain these results. $(C_5Me_5)_3Co_3(\mu_3\text{-}CH)_2$ has two more electrons than $(C_5Me_5)_3Co_3(\mu_3\text{-}CH)(\mu\text{-}H)$, and these electrons reside in the 3e" level, which is mostly metal-capping ligand antibonding in nature. Even though cobalt(III) is considerably smaller than cobalt(II) (by as much as 0.10 Å, based on ionic radii for a coordination number of 6),[14] the metal-carbyne carbon bond distance is longer (1.867 Å vs. 1.856 Å) and the cobalt-C(11)-cobalt angle is smaller (80.6° vs. 82.1°) in the bis-carbyne species. This is the same result that is observed when comparing $(C_5Me_5)_3Co_3(\mu_3\text{-}CH)(\mu\text{-}H)$ and $(C_5Me_5)_3Ni_3(\mu_3\text{-}CH)(\mu\text{-}H)$, and supports the molecular orbital model presented in Figures 8 and 9. The cobalt-cobalt distance is *ca.* 0.02 Å shorter in $(C_5Me_5)_3Co_3(\mu_3\text{-}CH)_2$ than in $(C_5Me_5)_3Co_3(\mu_3\text{-}CH)(\mu\text{-}H)$, a difference that is significantly smaller than would be expected based on the change in radii upon change in oxidation state. Inspection of Figure 9 reveals that the 3e" orbitals, while predominantly metal-ligand antibonding in nature, also have some metal-metal antibonding character,[15] which may be responsible for this observation.

Figure 13. ORTEP Diagram of $(C_5Me_5)_3Co_3(\mu_3\text{-}CH)_2$.

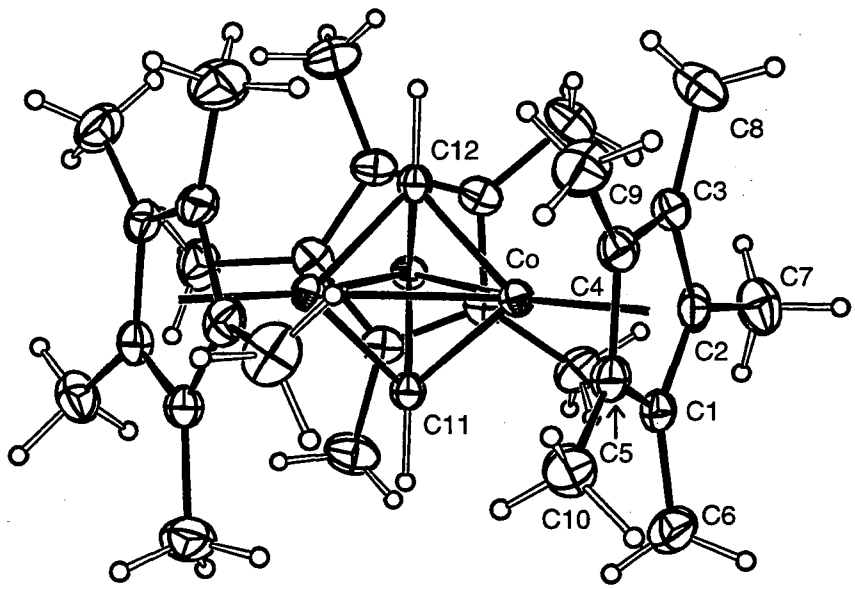

Table 6. Bond Distances for $(C_5Me_5)_3Co_3(\mu_3\text{-}CH)_2$ (Å).

Co-Co	2.413 (1)	C1-C2	1.432 (3)
Co-C1	2.113 (2)	C1-C5	1.420 (3)
Co-C2	2.108 (2)	C2-C3	1.425 (3)
Co-C3	2.103 (2)	C3-C4	1.418 (3)
Co-C4	2.097 (2)	C4-C5	1.437 (4)
Co-C5	2.110 (2)		
Co-Cp	1.72	C11-H11	1.10 (1)
Co-C11	1.866 (1)	C12-H12	1.12 (1)
Co-C12	1.867 (2)		

Cp is the ring centroid of atoms C1-C5.

Table 7. Bond Angles for $(C_5Me_5)_3Co_3(\mu_3\text{-}CH)_2$ (°).

Co-Co-Co	60.00 (1)	C2-C1-C5	107.6 (2)
Co-C11-Co	80.58 (8)	C1-C2-C3	108.4 (2)
Co-C12-Co	80.52 (2)	C2-C3-C4	107.8 (2)
C11-Co-C12	83.43 (5)	C3-C4-C5	108.2 (2)
		C1-C5-C4	108.0 (2)
Cp-Co-Co	150		
Cp-Co-C11	139		
Cp-Co-C12	138		

Since $(C_5Me_5)_3Co_3(\mu_3\text{-}CH)_2$ crystallizes in $R\bar{3}$, with cell parameters that are extremely similar to those of $(C_5Me_5)_3Co_3(\mu_3\text{-}CH)(\mu\text{-}H)$, it is not surprising to discover that these two cluster species co-crystallize to form a solid solution. This is why the synthetic route to $(C_5Me_5)_3Co_3(\mu_3\text{-}CH)(\mu\text{-}H)$ that utilized $[(C_5Me_5)Co(\mu\text{-}Cl)]_2$ was ultimately abandoned. The inability to separate the two compounds by fractional crystallization is also responsible for the initial difficulties in identifying $(C_5Me_5)_3Co_3(\mu_3\text{-}CH)(\mu\text{-}H)$. In fact, initial attempts to obtain the X-ray crystal structure of $(C_5Me_5)_3Co_3(\mu_3\text{-}CH)(\mu\text{-}H)$ resulted in a structural solution that appeared to indicate the presence of a second bridging ligand. The ligand was really a partially occupancy carbyne ligand resulting from the presence of a significant amount of $(C_5Me_5)_3Co_3(\mu_3\text{-}CH)_2$ in the crystalline lattice. However, once the two species could be prepared and characterized in pure form, the ability of the two species to form solid solutions was utilized to obtain the powder EPR spectrum of $(C_5Me_5)_3Co_3(\mu_3\text{-}CH)(\mu\text{-}H)$ by using $(C_5Me_5)_3Co_3(\mu_3\text{-}CH)_2$ as a diamagnetic host lattice.

The corresponding oxidation reactions of $(C_5Me_5)_3Ni_3(\mu_3\text{-}CH)(\mu\text{-}H)$ are substantially less informative. Reaction of the nickel cluster with dilute HCl produces an intractable orange oil (eq. 9). Similarly, oxidation of $(C_5Me_5)_3Ni_3(\mu_3\text{-}CH)(\mu\text{-}H)$ with CCl_4 produces $NiCl_2$ and several organic products (eq. 10), with the main product being the fulvene shown. This compound appears to be the product of a reaction between a pentamethylcyclopentadienyl anion and a halocarbon radical, but the system is very complicated and no attempt to identify the other organic products was made. As with the cobalt analogue, no $HCCl_3$ was observed when the reaction was performed in a sealed NMR tube.

$$(C_5Me_5)_3Ni_3(\mu_3\text{-}CH)(\mu\text{-}H) + HCl \xrightarrow{Et_2O} NiCl_2 + \text{intractable oil} \quad (9)$$

$$(C_5Me_5)_3Ni_3(\mu_3\text{-}CH)(\mu\text{-}H) + CCl_4 \xrightarrow{\text{toluene}} NiCl_2 + \text{ 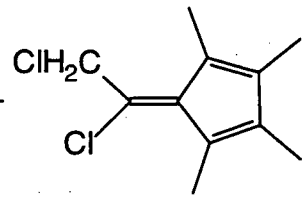 } + \ldots \quad (10)$$

The final attempts at controlled oxidation of the cluster compounds, $(C_5Me_5)_3M_3(\mu_3\text{-}CH)(\mu\text{-}H)$, with nitrous oxide were also unsuccessful. The cobalt compound was largely unreactive, with only a small amount of an insoluble residue isolated in the recovery of the starting material. The nickel analogue did not react with N_2O, as judged by infrared and mass spectroscopy. This is curious, since the nickel species exhibited considerably greater reactivity towards HCl and CCl_4, as judged by the extensive decomposition observed in these reactions. It is possible that the single unpaired electron in the $2a_2'$ orbital of $(C_5Me_5)_3Ni_3(\mu_3\text{-}CH)(\mu\text{-}H)$ makes it more susceptible to radical reactions than the cobalt analogue, but less reactive towards nitrous oxide. Also, it is important to note that cobalt is quite stable as a trivalent cation, as shown by the tremendous stability of $(C_5Me_5)_3Co_3(\mu_3\text{-}CH)_2$. On the other hand, this oxidation state is unstable for nickel, and hence the corresponding bis-carbyne product is not accessible for nickel. Precipitation of nickel(II) chloride and oxidation of the pentamethylcyclopentadienyl ligand is the only reaction path available for $(C_5Me_5)_3Ni_3(\mu_3\text{-}CH)(\mu\text{-}H)$ when presented with an oxidizing environment.

Reactions with Ethylene and Carbon Monoxide

$(C_5Me_5)_3Co_3(\mu_3\text{-}CH)(\mu\text{-}H)$ and $(C_5Me_5)_3Ni_3(\mu_3\text{-}CH)(\mu\text{-}H)$ exhibit virtually identical reaction chemistry with respect to ethylene and carbon monoxide.

Neither species shows any evidence of reaction with ethylene. Reaction of $(C_5Me_5)_3Co_3(\mu_3\text{-}CH)(\mu\text{-}H)$ with CO produces a mixture of two known carbonyl compounds, $(C_5Me_5)Co(CO)_2$[21] and $(C_5Me_5)_3Co_3(\mu_3\text{-}CO)_2$,[6a] as judged by infrared spectroscopy (eq. 11). Similarly, reaction of $(C_5Me_5)_3Ni_3(\mu_3\text{-}CH)(\mu\text{-}H)$ with CO produces the known compound, $[(C_5Me_5)Ni(\mu\text{-}CO)]_2$ (eq. 12).[22] No significance should be placed on the lack of $(C_5Me_5)_3Ni_3(\mu_3\text{-}CO)_2$ in the reaction product, since the nickel reaction was performed under substantially higher pressures of CO (18 atm vs. 3 atm). No evidence of the fate of either the carbyne or hydride ligand was observed in either reaction.

$$(C_5Me_5)_3Co_3(\mu_3\text{-}CH)(\mu\text{-}H) + CO \xrightarrow{\text{hexane}} \begin{matrix}(C_5Me_5)_3Co_3(\mu_3\text{-}CO)_2 \\ + \\ (C_5Me_5)Co(CO)_2\end{matrix} \qquad (11)$$

$$(C_5Me_5)_3Ni_3(\mu_3\text{-}CH)(\mu\text{-}H) + CO \xrightarrow{\text{hexane}} [(C_5Me_5)Ni(\mu\text{-}CO)]_2 \qquad (12)$$

Reactions with Dihydrogen

As mentioned earlier, $(C_5Me_5)_3Ni_3(\mu_3\text{-}CH)(\mu\text{-}H)$ shows no evidence of reaction with H_2 or D_2, as judged by infrared and mass spectroscopy. However, reaction of $(C_5Me_5)_3Co_3(\mu_3\text{-}CH)(\mu\text{-}H)$ with H_2 at high pressures ($\geq$ 12 atm) and prolonged reaction times generates the 48-electron, diamagnetic cluster compound $(C_5Me_5)_3Co_3(\mu_3\text{-}CH)(\mu_2\text{-}H)_3$ (eq. 13). The μ_2 assignment for the hydride ligands is based on the presence of a strong infrared stretch at 1675 cm^{-1}, which is in the region expected for doubly-bridging metal hydrides.[18b,23] This green, crystalline compound exhibits a molecular ion in the mass spectrum, using fast-atom bombardment techniques. A second signal, corresponding to $(M - H_2)^+$ is also seen using FAB techniques, and this signal is the only one

observed in the electron-impact mass spectrum. This is certainly due to loss of dihydrogen in the gas phase, since $(C_5Me_5)_3Co_3(\mu_3\text{-}CH)(\mu\text{-}H)$ does not yield a molecular ion in the mass spectrum. It should be noted that these are the only conditions under which the conversion of $(C_5Me_5)_3Co_3(\mu_3\text{-}CH)(\mu_2\text{-}H)_3$ back to $(C_5Me_5)_3Co_3(\mu_3\text{-}CH)(\mu\text{-}H)$ can be achieved. Reaction of $(C_5Me_5)_3Co_3(\mu_3\text{-}CH)(\mu_2\text{-}H)_3$ with CO produces the same two carbonyl species observed when the reaction is performed with the monohydride (shown in eq. 11), and heating to 200 °C under high vacuum only results in decomposition. The trihydride species does not react with ethylene.

$$(C_5Me_5)_3Co_3(\mu_3\text{-}CH)(\mu\text{-}H) + H_2 \xrightarrow{\text{hexane}} (C_5Me_5)_3Co_3(\mu_3\text{-}CH)(\mu_2\text{-}H)_3 \quad (13)$$

The difference in reactivity with dihydrogen for $(C_5Me_5)_3Co_3(\mu_3\text{-}CH)(\mu\text{-}H)$ and $(C_5Me_5)_3Ni_3(\mu_3\text{-}CH)(\mu\text{-}H)$ can again be traced to their electronic configuration. The 3e" level for $(C_5Me_5)_3Co_3(\mu_3\text{-}CH)(\mu\text{-}H)$ is only half-occupied, and since these orbitals are out-of-plane, metal-ligand orbitals (Figure 9), it is reasonable to expect that a molecule of dihydrogen approaching the hydride-capped face of the cluster would be able to interact and add its two electrons to the cluster, producing the stable, 48-electron species, $(C_5Me_5)_3Co_3(\mu_3\text{-}CH)(\mu_2\text{-}H)_3$. However, the occupied orbital in H_2 is not of the proper symmetry to interact with the 3e" molecular orbital of the cluster. For H_2 to interact with the core, the hydride ligand would have to move to either a μ_2 or terminal geometry, thus reducing the symmetry of the cluster and opening a coordination site at a metal atom. This would presumably require a significant amount of reorganization energy, and could be the reason that the otherwise electronically-favored formation of $(C_5Me_5)_3Co_3(\mu_3\text{-}CH)(\mu_2\text{-}H)_3$ is so slow. On the other hand,

the half-occupied $2a_2'$ orbital in $(C_5Me_5)_3Ni_3(\mu_3\text{-}CH)(\mu\text{-}H)$ is an in-plane, metal-metal orbital, which is expected to be relatively inaccessible to incoming ligands. It would be difficult for dihydrogen to associate with the nickel cluster, since the orbitals that extend outward from the metal core (3e") are filled. Thus, any exchange of the hydride ligand with free dihydrogen would most likely require the breaking of a nickel-nickel bond, with scrambling of the hydrides and subsequent reformation of the bond and elimination of dihydrogen. Since no deuterium scrambling is observed, this is obviously a high energy process.

$(C_5Me_5)_3Co_3(\mu_3\text{-}CH)(\mu_2\text{-}H)_3$ can be thought of as an analogue of $(C_5Me_5)_3Co_3(\mu_3\text{-}CH)_2$, with one, three-electron carbyne ligand replaced by three, one-electron hydride ligands. Then, the molecular orbital model shown in Figure 8 predicts that this complex will be diamagnetic. The ^1H NMR spectrum confirms this, exhibiting three singlets at δ 16.92, 1.77, and -32.06 with an intensity ratio of 1:45:3. These correspond to the carbyne, pentamethylcyclopentadienyl, and hydride ligands, respectively. The hydride signal is somewhat broader ($\nu_{1/2} \approx$ 10 Hz at room temperature) than the other two signals ($\nu_{1/2} < 5$ Hz). When the spectrum is measured at 90 °C, both the carbyne and hydride signals are substantially broadened ($\nu_{1/2} \approx 10 \times \nu_{1/2}$ at room temperature), indicating the possibility of proton exchange between the two sites. When D_2 is substituted for H_2 in the synthesis of the trihydride cluster, the room temperature spectrum of the partially deuterated cluster exhibits two resonances in the hydride region at δ -32.09 and -32.12. Inspection of the ^2H NMR spectrum of this sample reveals that deuterium is present in the carbyne and hydride positions, but not in the C_5Me_5 ligand. Unfortunately, the lower resolution of the ^2H NMR experiment makes it impossible to resolve the two expected signals in the hydride region, and instead a single broad absorption at δ -32 is observed. Based on trends in isotopic shifts, the signals at δ -32.09 and -32.12 are assigned to the hydride

signals of two isomers, $(C_5Me_5)_3Co_3(\mu_3\text{-}CH)(\mu_2\text{-}H)_2(\mu_2\text{-}D)$ and $(C_5Me_5)_3Co_3(\mu_3\text{-}CD)(\mu_2\text{-}H)(\mu_2\text{-}D)_2$, respectively.

More detailed NMR experiments were performed on $(C_5Me_5)_3Co_3(\mu_3\text{-}CH)(\mu_2\text{-}H)_3$ to determine the nature of the exchange process. Spin saturation experiments indicate that the carbyne proton exchanges into a hydride position approximately once per second at 30 °C. Figure 14 shows a 2-dimensional EXSY experiment that definitively assigns the exchange mechanism observed in the NMR experiments as intramolecular.

Figure 14. ^1H NMR 2D EXSY Spectrum of $(C_5Me_5)_3Co_3(\mu_3\text{-}CH)(\mu_2\text{-}H)_3$.

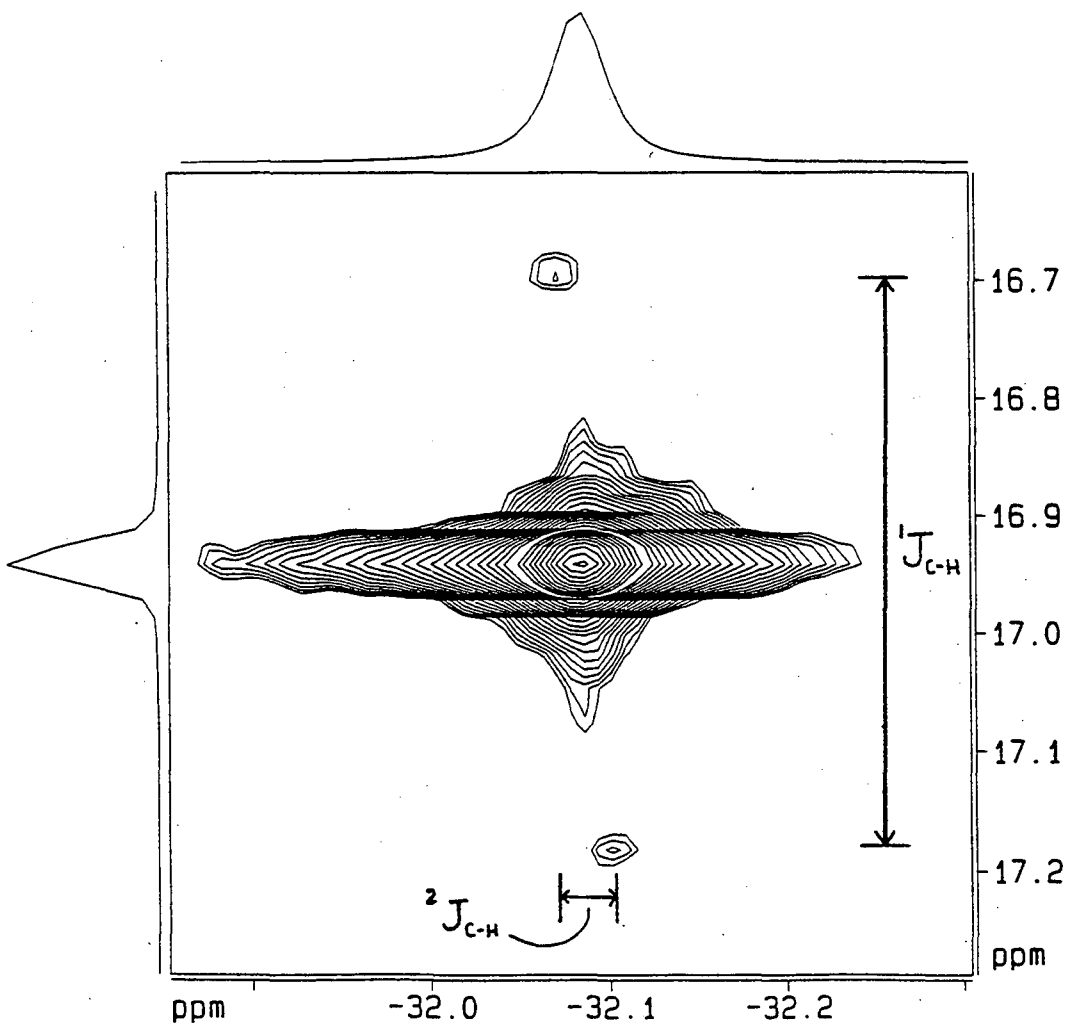

The EXSY experiment measures the spin saturation transfer information at all frequencies in the spectral window, then correlates them as a two-dimensional contour plot. The vertical dimension shows the region of the spectrum containing the carbyne proton resonance and the horizontal dimension shows the hydride region. The couplings indicated in Figure 14 are for the carbyne and hydride protons interacting with a ^{13}C atom in the carbyne ligand ($^{1}J_{C-H}$ = 147 Hz for the carbyne hydrogen and $^{2}J_{C-H}$ = 9 Hz for the hydride ligands). The large cross peak at the center of Figure 14 is due to the exchange process occurring in cluster molecules that have a ^{12}C atom in the carbyne site (natural abundance ≈ 99%). The small cross peaks to either side of the large peak are due to the 1% of the cluster molecules that have a ^{13}C atom in the carbyne site. Since the concentration of molecules with a ^{12}C atom in the carbyne site is *ca.* 99 times that of the clusters with a ^{13}C atom in the carbyne site, any intermolecular exchange process would exchange a ^{13}C-labeled carbyne proton with a ^{12}C hydride atom 99% of the time. However, the small cross peaks occur only between the ^{13}C satellite signals of the carbyne proton and hydride resonances, with no cross peaks for the ^{12}C signals, indicating that the carbyne proton of a ^{13}C-labeled molecule only exchanges with a hydride proton of another ^{13}C-labeled molecule. Since the ^{13}C-labeled molecules are present in a very small concentration, the exchange must occur within a given molecule, thus proving that the exchange mechanism is intramolecular.

This exchange process is not without precedent. The previously mentioned clusters, $M_3(CO)_9(\mu_3\text{-}CH)(\mu\text{-}H)_3$, where M = Ru and Os, exhibit an exchange process between the carbyne and hydride proton sites at elevated temperatures, with rates of 1.1 x 10^{-2} sec^{-1} and 3.6 x 10^{-3} sec^{-1} measured by spin saturation techniques at 80 °C.[24] The mechanism proposed by Shapley and co-workers for this site interconversion is shown in Figure 15.[24] This

intramolecular mechanism is also consistent with the observed results for $(C_5Me_5)_3Co_3(\mu_3\text{-}CH)(\mu_2\text{-}H)_3$, where the three solid circles would represent $(C_5Me_5)Co$ fragments instead of $(CO)_3M$ fragments. Perhaps even more interesting is the iron carbonyl analogue, $Fe_3(CO)_9(\mu_3\text{-}CH)(\mu\text{-}H)_3$, which apparently exists as a mixture of three tautomers in C_6D_6 solution at room temperature, assigned as $Fe_3(CO)_9(\mu_3\text{-}CH)(\mu\text{-}H)_3$ (84%), $Fe_3(CO)_9(\mu_3\text{-}HCH)(\mu\text{-}H)_2$ (12%), and $Fe_3(CO)_9(\mu_3\text{-}HCH_2)(\mu\text{-}H)$ (4%).[19] Although the existence of a triply-bridging methyl group should probably be viewed with some skepticism (4% abundance is certainly near the limit of detection in a ^1H NMR experiment), the series of three carbonyl cluster complexes certainly confirm the presence of a proton exchange mechanism occurring between μ_3-carbyne and hydride sites, and furthermore indicate that this process is more facile for the first-row transition metal complex than for the second- and third-row transition metal complexes in this system. All of this corroborates the phenomena observed for $(C_5Me_5)_3Co_3(\mu_3\text{-}CH)(\mu_2\text{-}H)_3$, where interconversion occurs fairly quickly at room temperature.

Figure 15. Proposed Exchange Mechanism for $(L_nM)_3(\mu_3\text{-}CH)(\mu\text{-}H)_3$.[24]

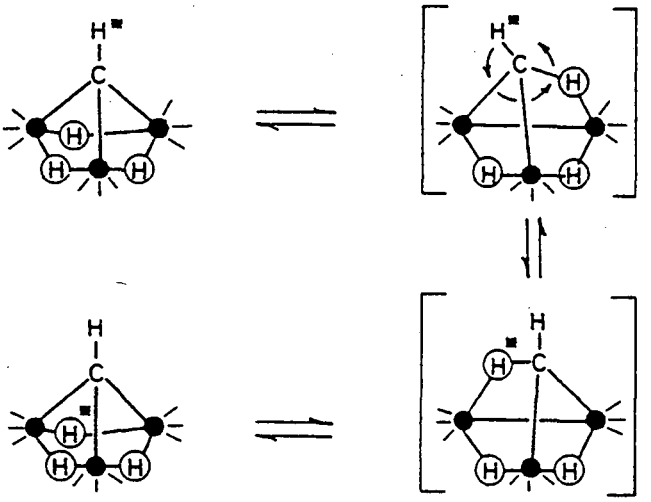

A final note regarding the exchange processes occurring for $(C_5Me_5)_3Co_3(\mu_3\text{-}CH)(\mu_2\text{-}H)_3$. This complex has 48 electrons, and thus would not be expected to exchange its hydride ligands with free dihydrogen, based on the explanation given for $(C_5Me_5)_3Ni_3(\mu_3\text{-}CH)(\mu\text{-}H)$. Indeed, when $(C_5Me_5)_3Co_3(\mu_3\text{-}CH)(\mu_2\text{-}H)_3$ is placed under 18 atmospheres of D_2 for one week, no evidence of deuterium incorporation is observed (this lack of exchange with D_2 was noted by Shapley for $M_3(CO)_9(\mu_3\text{-}CH)(\mu\text{-}H)_3$, [M = Ru, Os], as well).[24] However, preliminary EXSY experiments on the partially deuterated product generated by the reaction of $(C_5Me_5)_3Co_3(\mu_3\text{-}CH)(\mu\text{-}H)$ with D_2 indicate that at least one more species, $(C_5Me_5)_3Co_3(\mu_3\text{-}CH)(\mu_2\text{-}H)_2(\mu_2\text{-}D)$, is present in solution, although in smaller amounts than the isomers containing two deuterium atoms. The possibility of intermolecular exchange occurring during the initial synthesis of the trihydride cluster needs to be explored more thoroughly using deuterium labeling and more sophisticated NMR techniques.

References

1. Bor, G.; Markó, L.; Markó, B., *Chem. Ber.*, **1962**, *95*, 333.

2. (a) Shapley, J. R.; Cree-Uchiyama, M. E., St. George, G. M., *J. Am. Chem. Soc.*, **1983**, *105*, 140; and references therein.
(b) Calvert, R. B.; Shapley, J. R., *J. Am. Chem. Soc.*, **1977**, *99*, 5225; and references therein.

3. Fritch, J. R.; Vollhardt, K. P. C., *Angew. Chem., Int. Ed. Engl.*, **1980**, *19*, 559.

4. Vazquez de Miguel, A.; Isobe, K.; Bailey, P. M.; Meanwell, N. J.; Maitlis, P. M., *Organometallics*, **1982**, *1*, 1604.

5. Pasynkiewicz, S.; Poplawska, J.; Lehmkuhl, H.; Krüger, C, *Organometallics*, **1988**, *7*, 2038.

6. (a) Olson, W. L.; Stacy, A. M.; Dahl, L. F., *J. Am. Chem. Soc.*, **1986**, *108*, 7646; and references therein.
(b) North, T. E.; Thoden, J. B.; Spencer, B.; Bjarnason, A.; Dahl, L. F., *Organometallics*, **1992**, *11*, 4326; and references therein.

7. Kegley, S. E.; Pinhas, A. R., "Problems and Solutions in Organometallic Chemistry," University Science Books: Mill Valley, CA, **1986**.

8. Drago, R. S., "Physical Methods in Chemistry," W. B. Saunders: Philadelphia, **1977**.

9. Pinhas, A. R.; Albright, T. A.; Hofmann, P.; Hoffmann, R., *Helv. Chim. Acta*, **1980**, *63*, 29.

10. (a) Green, M.; Hankey, D. R.; Howard, J. A. K.; Louca, P.; Stone, F. G. A., *J. Chem. Soc., Chem. Commun.*, **1983**, 757.
(b) Bray, A. C.; Green, M.; Hankey, D. R.; Howard, J. A. K.; Johnson, O.; Stone, F. G. A., *J. Organomet. Chem.*, **1985**, *281*, C12.

11. Barnes, C. E.; Orvis, J. A.; Staley, D. L.; Rheingold, A. L.; Johnson, D. C., *J. Am. Chem. Soc.*, **1989**, *111*, 4992.

12. Kersten, J. L.; Rheingold, A. L.; Theopold, K. H.; Casey, C. P.; Widenhoefer, R. A.; Hop, C. E. C. A., *Angew. Chem., Int. Ed. Engl.*, **1992**, *31*, 1341.

13. Jolly, W. H., "The Synthesis and Characterization of Inorganic Compounds," Prentice-Hall: Englewood Cliffs, NJ, **1970**.

14. Douglas, B.; McDaniel, D. H.; Alexander, J. J., "Concepts and Models of Inorganic Chemistry," 2nd. Ed., John Wiley and Sons: New York, **1983**.

15. Olson, W. L.; Dahl, L. F., *J. Am. Chem. Soc.*, **1986**, *108*, 7657.

16. Lowry, T. H.; Richardson, K. S., "Mechanism and Theory in Organic Chemistry," 3rd Ed., Harper and Row: New York, **1987**.

17. Fritch, J. R., Ph.D. Thesis, University of California, Berkeley, **1980**.

18. (a) Andrews, J. A.; Jayasooriya, U. A.; Oxton, I. A.; Powell, D. B.; Sheppard, N.; Jackson, P. F.; Johnson, B. F. G.; Lewis, J., *Inorg. Chem.*, **1980**, *19*, 3033.
(b) Cooper, C. B., III; Shriver, D. F.; Onaka, S., *Adv. Chem. Ser.*, **1978**, *167*, 232.

19. Dutta, T. K.; Vites, J. C.; Jacobsen, G. B.; Fehlner, T. P., *Organometallics*, **1987**, *6*, 842.

20. Keister, J. B.; Horling, T. L., *Inorg. Chem.*, **1980**, *19*, 2304.

21. King, R. B.; Bisnette, M. B., *J. Organomet. Chem.*, **1967**, *8*, 287.

22. Mise, T.; Yamazaki, H., *J. Organomet. Chem.*, **1979**, *164*, 391.

23. Anson, C. E.; Jayasooriya, U. A.; Kettle, S. F. A.; Stanghellini, P. L.; Rossetti, R., *Inorg. Chem.*, **1991**, *30*, 2282.

24. VanderVelde, D. G.; Holmgren, J. S.; Shapley, J. R., *Inorg. Chem.*, **1987**, *26*, 3077.

Chapter 2

Chemical and Physical Properties of Pentamethylcyclopentadienyl Acetylacetonate Complexes of Cobalt(II) and Nickel(II)

A substantial portion of organometallic synthesis involves the selection of ligands that impart desirable qualities to the metal complexes being made. For metathesis reactions, the acetylacetonate anion (referred to as acac from here on) is just such a ligand. In this chapter the focus is on the simplest acac, $CH(MeCO)_2^-$, since substitution of the methyl groups by other groups leads to an enormous number of compounds, called β-keto-enolates.[1] Many of its organometallic complexes are soluble in non-polar or slightly polar solvents, yet its alkali and alkaline-earth salts are insoluble in the same solvents. Also, the acac group usually coordinates to a metal in a bidentate fashion by way of both oxygen atoms, yet is monovalent, so metathesis reactions with unidentate, monovalent anions can yield coordinatively unsaturated organometallic complexes. In short, acac compounds are ideal starting materials for preparation of metal alkyl complexes with low coordination number.

The acac complexes of the d-transition metals have a varied and often unusual chemistry. The physical properties of the binary compounds were intensively studied in the 1960's, presumably because they were used in the early metallocene syntheses.[2] The simple divalent salts of the first row metals are mostly oligomeric with a general formula of $[M(acac)_2]_n$, with n = 2 (M = Fe),[3] 3 (M = Mn, Ni, Zn),[4] or 4 (M = Fe, Co),[5] where one or both of the oxygens of the chelating acac ligand bridge to another metal center. For transition metal complexes containing acac and other ligands in the coordination sphere, the variety of coordination modes is large. The acac ligand is usually a bidentate chelate, but can also be unidentate, bound either through an oxygen, as in

$Pt(acac\text{-}O)_2(PEt_3)_2$,[6] or the central carbon (called a γ or C^3 linkage), as in $Me_3Pt(acac\text{-}C^3)(bpy)$[7a] and $Pd(acac)(acac\text{-}C^3)(PEt_3)$.[7b] Consideration of other more exotic coordination types, including bridging modes, brings the total number of reported coordination modes for the acac monoanion to eleven.[8] More closely related to this work is the structural characterization of complexes with the formula $(C_5Me_5)M(acac)$. For d^6 metal complexes, such as $[(C_5Me_5)Rh(acac)](BF_4)_2$, the complex is a dimer with the oxygen atoms chelating one rhodium and the C^3 carbon bridging to the other rhodium.[9] $(C_5Me_5)Ru(acac)$ was initially reported to be a 16 electron monomer with an unprecedented distorted geometry,[10] but reexamination of the crystallographic data showed it to be a C^3 bridged dimer,[11] just like the 18 electron Rh example. Investigation of the physical properties of the complexes $(C_5Me_5)M(acac)$ for M = Co (d^7) and Ni (d^8), which are potentially 17- and 18-electron monomers, would show insight into the nature of the bonding in these complexes.

Initial Studies

Manriquez first reported the synthesis of $(C_5Me_5)M(acac)$ for M = Co and Ni.[12] Both complexes are synthesized by metathesis of the corresponding anhydrous metal acac with one equivalent of $Li(C_5Me_5)$ in thf (eq. 1).

$$M(acac)_2 + (C_5Me_5)Li \xrightarrow{THF} (C_5Me_5)M(acac) + Li(acac) \quad (1)$$
$$M = Co, Ni$$

The reported analytical and mass spectroscopic data confirm the elemental compositions of the $(C_5Me_5)M(acac)$ compounds and indicate that both

complexes are monomers in the gas phase. However, no further information has been published about the chemical or physical properties of these materials.

Solid-State Physical Properties

A detailed study of the properties of the two acac complexes reveals some interesting and subtle differences. The infrared spectra of both $(C_5Me_5)Co(acac)$ and $(C_5Me_5)Ni(acac)$ exhibit acac C-O/C-C stretching frequencies that are *ca.* 50 cm^{-1} lower in energy than in the corresponding $M(acac)_2$ compounds (1530-1550 cm^{-1} vs. 1590-1600 cm^{-1}).[13] The variable-temperature magnetic susceptibility of $(C_5Me_5)Co(acac)$ obeys the Curie-Weiss law, with a small θ value and a magnetic moment somewhat higher (1.93 μ_B) than the spin-only value for one unpaired electron (1.73 μ_B) (Figure 1). However, the variable-temperature magnetic susceptibility of $(C_5Me_5)Ni(acac)$ shows an unusual result (Figure 2). Even with doubly-sublimed material, a paramagnetic signal grows in above 150 K, with the signal being essentially diamagnetic below this temperature.

Figure 1. Plot of $1/\chi_M$ vs. T for $(C_5Me_5)Co(acac)$.

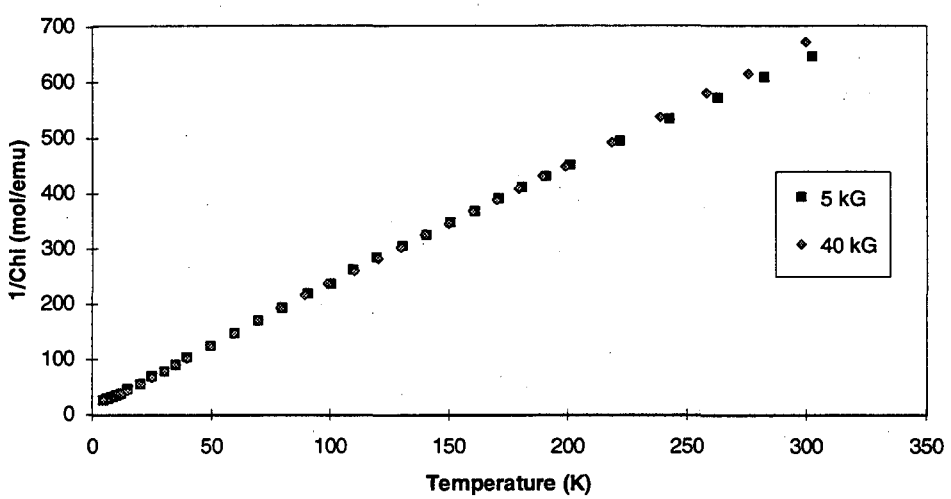

Figure 2. Plot of χ_M vs. T for $(C_5Me_5)Ni(acac)$.

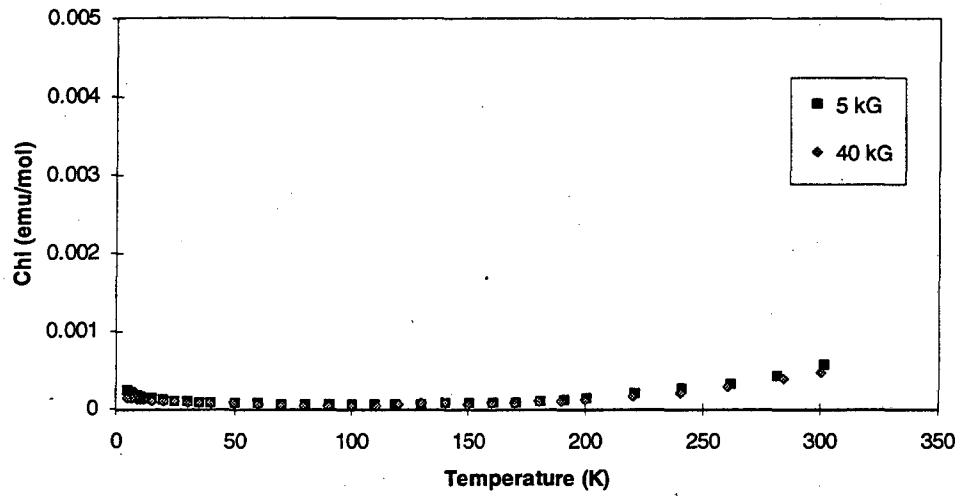

The X-ray crystal structures of $(C_5Me_5)Co(acac)$ and $(C_5Me_5)Ni(acac)$ are shown in Figures 4 and 5, respectively. The two compounds are isomorphous, crystallizing in the space group $P\bar{1}$ (No. 2) and having two crystallographically independent molecules in the asymmetric unit. Selected bond distances and angles for both structures are in Tables 1 through 4. The averaged values in the tables utilize the labels in the Scheme shown in Figure 3, which assumes that all of the monomers have an effective mirror plane of symmetry that contains the metal atom and bisects the C_5Me_5 and acac ligands.

Figure 3. Labeling Scheme for C_5Me_5 Ring in $(C_5Me_5)M(acac)$.

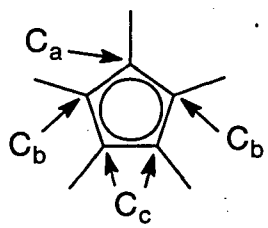

Figure 4. ORTEP Diagram of the Asymmetric Unit of $(C_5Me_5)Co(acac)$.

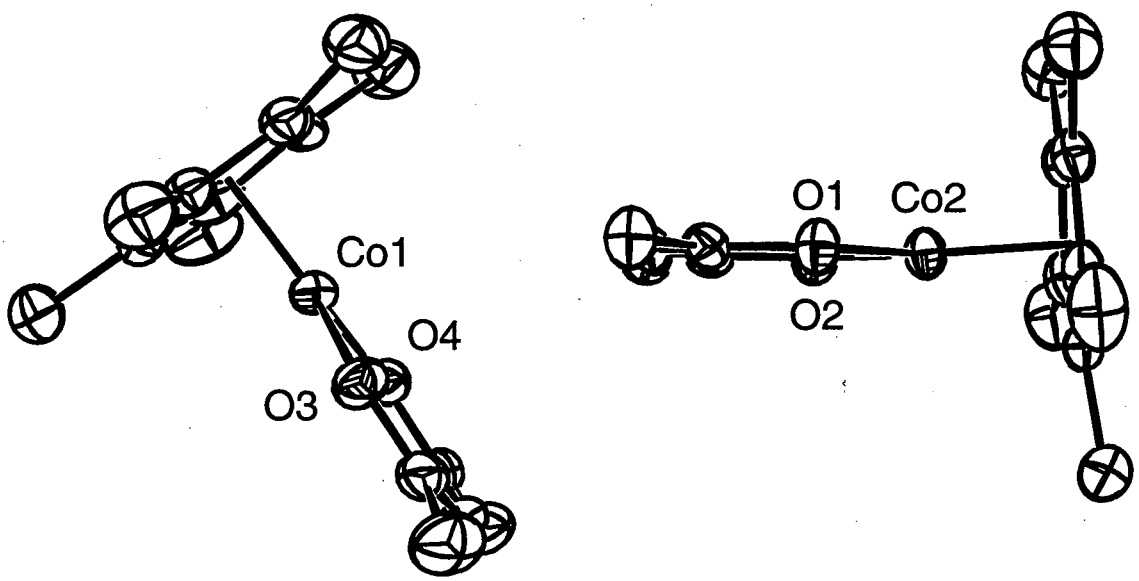

Figure 5. ORTEP Diagram of the Asymmetric Unit of $(C_5Me_5)Ni(acac)$.

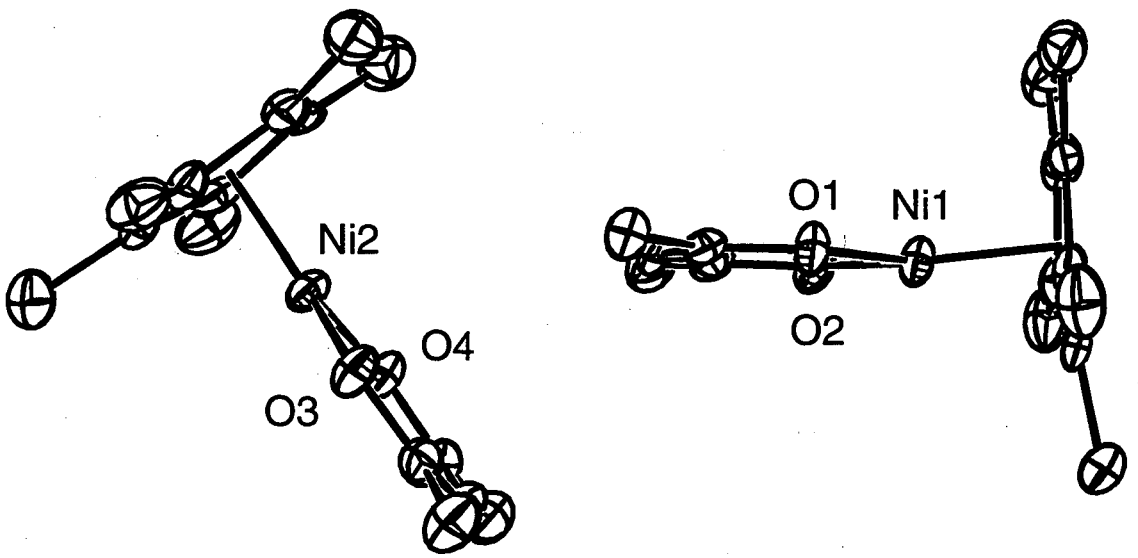

Table 1. Bond Distances for $(C_5Me_5)Co(acac)$ (Å).

Co1-O1	1.883 (3)	O1-C2	1.278 (5)
Co1-O2	1.887 (3)	O2-C4	1.283 (5)
Co2-O3	1.876 (3)	O3-C22	1.276 (6)
Co2-O4	1.872 (3)	O4-C24	1.284 (6)
Co-O (ave)	1.880 (2)	O-C (ave)	1.280 (3)
Co1-C6	2.066 (5)	C6-C7	1.423 (7)
Co1-C7	2.118 (4)	C7-C8	1.412 (7)
Co1-C8	2.054 (4)	C8-C9	1.444 (7)
Co1-C9	2.091 (4)	C9-C10	1.398 (6)
Co1-C10	2.085 (5)	C6-C10	1.425 (7)
Co2-C26	2.093 (5)	C26-C27	1.419 (7)
Co2-C27	2.088 (5)	C27-C28	1.431 (7)
Co2-C28	2.050 (5)	C28-C29	1.407 (7)
Co2-C29	2.092 (5)	C29-C30	1.431 (7)
Co2-C30	2.052 (5)	C26-C30	1.412 (7)
Co-C_a (ave)	2.105 (3)	C_a-C_b (ave)	1.418 (4)
Co-C_b (ave)	2.056 (2)	C_b-C_c (ave)	1.428 (4)
Co-C_c (ave)	2.089 (2)	C_c-C_c (ave)	1.409 (5)
Co1-Cp1	1.70	Co-Cp (ave)	1.69
Co2-Cp2	1.69		

Cp1 and Cp2 are the ring centroids of atoms C6-C10 and C26-C30, respectively.

Table 2. Bond Angles for $(C_5Me_5)Co(acac)$ (°).

O1-Co1-O2	95.3 (1)	C7-C6-C10	108.8 (4)
O3-Co1-O4	95.4 (1)	C6-C7-C8	106.6 (4)
		C7-C8-C9	108.8 (4)
O-Co-O (ave)	95.3 (1)	C8-C9-C10	107.2 (4)
		C6-C10-C9	108.3 (4)
Cp1-Co1-O1	133	C27-C26-C30	107.7 (4)
Cp1-Co1-O2	131	C26-C27-C28	107.2 (4)
Cp2-Co2-O3	132	C27-C28-C29	109.3 (4)
Cp2-Co2-O4	133	C28-C29-C30	106.4 (4)
		C26-C30-C29	109.2 (4)
Cp-Co-O (ave)	132		
		C_b-C_a-C_b (ave)	106.5 (3)
		C_a-C_b-C_c (ave)	109.0 (2)
		C_b-C_c-C_c (ave)	107.6 (2)

Table 3. Bond Distances for $(C_5Me_5)Ni(acac)$ (Å).

Ni1-O1	1.890 (4)	O1-C2	1.280 (5)
Ni1-O2	1.883 (3)	O2-C4	1.282 (6)
Ni2-O3	1.868 (4)	O3-C22	1.290 (5)
Ni2-O4	1.876 (4)	O4-C24	1.294 (5)
Ni-O (ave)	1.879 (2)	O-C (ave)	1.287 (3)
Ni1-C6	2.074 (5)	C6-C7	1.432 (8)
Ni1-C7	2.143 (4)	C7-C8	1.417 (9)
Ni1-C8	2.074 (5)	C8-C9	1.474 (6)
Ni1-C9	2.196 (5)	C9-C10	1.382 (9)
Ni1-C10	2.188 (5)	C6-C10	1.460 (8)
Ni2-C26	2.183 (5)	C26-C27	1.361 (9)
Ni2-C27	2.200 (5)	C27-C28	1.467 (7)
Ni2-C28	2.062 (5)	C28-C29	1.423 (10)
Ni2-C29	2.123 (4)	C29-C30	1.409 (8)
Ni2-C30	2.060 (5)	C26-C30	1.465 (8)
Ni-C_a (ave)	2.133 (3)	C_a-C_b (ave)	1.420 (4)
Ni-C_b (ave)	2.068 (3)	C_b-C_c (ave)	1.467 (4)
Ni-C_c (ave)	2.192 (3)	C_c-C_c (ave)	1.372 (6)
Ni1-Cp1	1.75	Ni-Cp (ave)	1.75
Ni2-Cp2	1.75		

Cp1 and Cp2 are the ring centroids of atoms C6-C10 and C26-C30, respectively.

Table 4. Bond Angles for $(C_5Me_5)Ni(acac)$ (°).

O1-Ni1-O2	98.0 (2)	C7-C6-C10	108.6 (5)
O3-Ni2-O4	98.7 (2)	C6-C7-C8	106.3 (4)
		C7-C8-C9	108.6 (5)
O-Ni-O (ave)	98.3 (1)	C8-C9-C10	107.6 (5)
		C6-C10-C9	108.0 (4)
Cp1-Ni1-O1	131	C27-C26-C30	108.2 (5)
Cp1-Ni1-O2	130	C26-C27-C28	107.5 (5)
Cp2-Ni2-O3	130	C27-C28-C29	108.7 (5)
Cp2-Ni2-O4	131	C28-C29-C30	105.8 (5)
		C26-C30-C29	108.9 (6)
Cp-Ni-O (ave)	131		
		C_b-C_a-C_b (ave)	106.1 (3)
		C_a-C_b-C_c (ave)	108.7 (3)
		C_b-C_c-C_c (ave)	107.8 (2)

Both molecules of both compounds exhibit a "T-shaped" geometry, where the least-squares planes defined by the C_5Me_5 ligand and the M(acac) fragment are all within 5.5° of perpendicular for a given molecule. However, the nickel complex shows a substantial distortion of the C_5Me_5 ring relative to the cobalt complex. The range of averaged carbon-carbon ring distances is 0.08 Å in (C_5Me_5)Ni(acac), while it is only 0.02 Å in (C_5Me_5)Co(acac). Also, the averaged metal-C_b and metal-C_c distances differ by more than 0.12 Å in (C_5Me_5)Ni(acac) but only by *ca.* 0.03 Å in (C_5Me_5)Co(acac). The significance of these distortions will be commented upon shortly.

Solution Behavior

In all respects, (C_5Me_5)Co(acac) exhibits the solution behavior expected for a monomeric, low-spin, 17-electron cobalt(II) complex. Its solution EPR yields an eight-line pattern (due to splitting by ^{59}Co with I = 7/2) with a g value of 2.099 (Figure 6). When the solution is frozen to a glass, the signal exhibits a rhombic distortion (Figure 7). (C_5Me_5)Co(acac) does not exhibit a ^{1}H NMR signal at room temperature, and yields a solution magnetic moment (from Evans' NMR method) of 1.86 μ_B at room temperature. All of these results indicate that the symmetry about the metal center is low (hence the rhombic distortion), and that the complex has one unpaired electron with incomplete quenching of the angular momentum.[14]

Figure 6. Room Temperature EPR Spectrum of $(C_5Me_5)Co(acac)$ in C_7H_{14}.

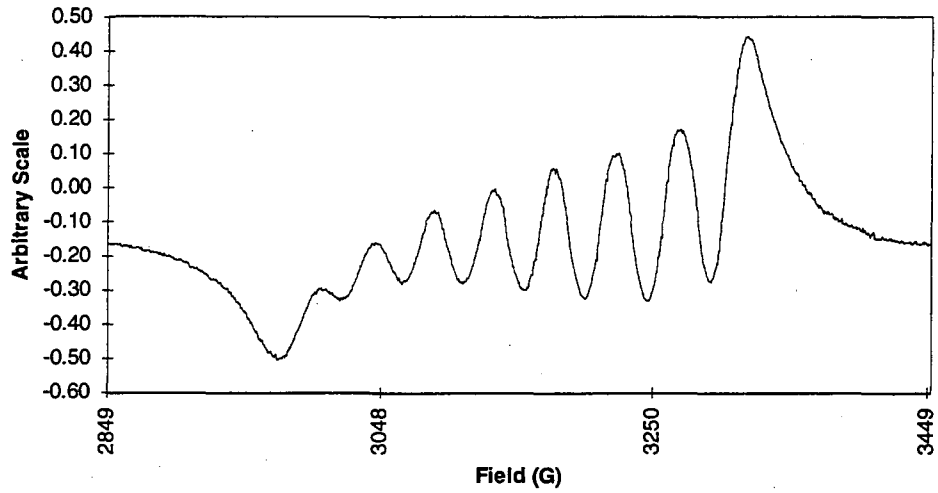

Figure 7. EPR Spectrum of $(C_5Me_5)Co(acac)$ in C_7H_{14} Glass (2 K).

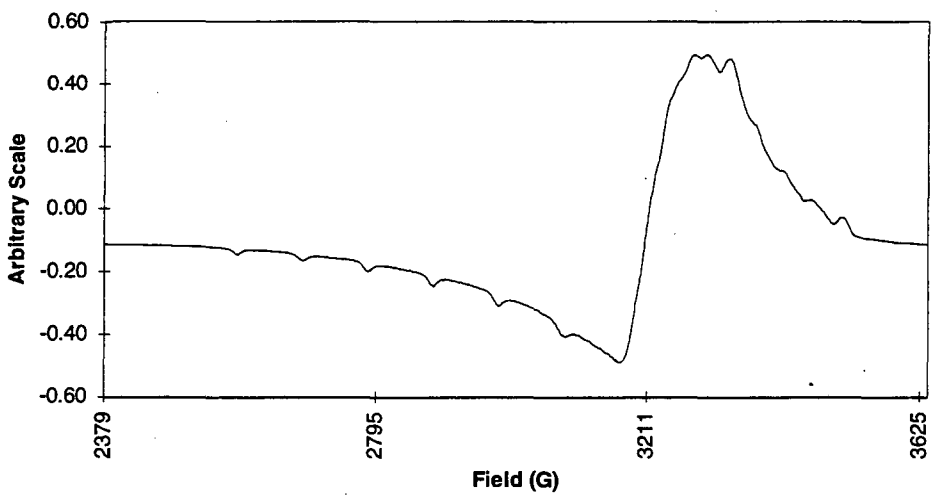

$(C_5Me_5)Ni(acac)$ does not exhibit an EPR signal in solution at room temperature or at liquid helium temperature. The ^1H NMR behavior of the nickel complex is more informative. Manriquez' ^1H NMR data indicates that the resonances for $(C_5Me_5)Ni(acac)$ are spread over a range of 75 ppm at room temperature.[12] At first glance, this is a very odd result for an 18-electron

nickel(II) complex. The variable temperature behavior of the ^1H NMR signals shows that the situation is quite complex (Figures 8 and 9). The plots of chemical shift vs. inverse temperature demonstrate non-linear behavior with the signals moving towards the diamagnetic region of the spectrum upon lowering of the temperature. Furthermore, the signals sharpen upon cooling ($\nu_{1/2} \approx 10$ Hz for $C_5\underline{Me}_5$ at -80 °C) and broaden upon warming ($\nu_{1/2} \approx 40$ Hz for $C_5\underline{Me}_5$ at 90 °C). Virtually identical traces were obtained in toluene-d_8 and tetrahydrofuran-d_8 solution, the difference being a small chemical shift difference for the C_5Me_5 resonance at low temperature. Therefore, the averaged chemical shifts are nearly identical in these two solvents and the methyl groups on the cyclopentadienyl ring are equivalent, as are the methyl groups on the acac ligand. The molecule in solution is either highly symmetric or it is non-rigid. The solution magnetic moment at room temperature (from Evans' NMR method) is 1.32 μ_B.

Figure 8. δ vs. 1/T for $(C_5Me_5)Ni(acac)$: C_5Me_5 Resonance.

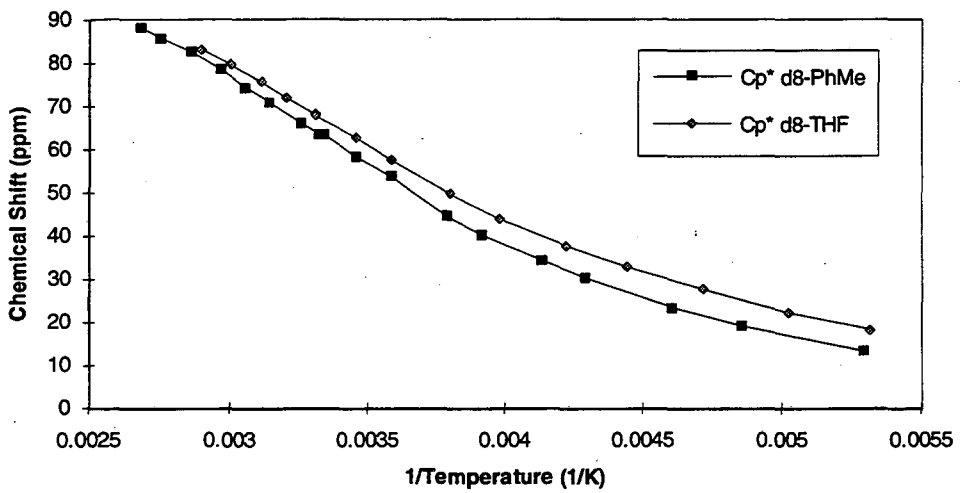

Figure 9. δ vs. 1/T for $(C_5Me_5)Ni(acac)$: acac Resonances.

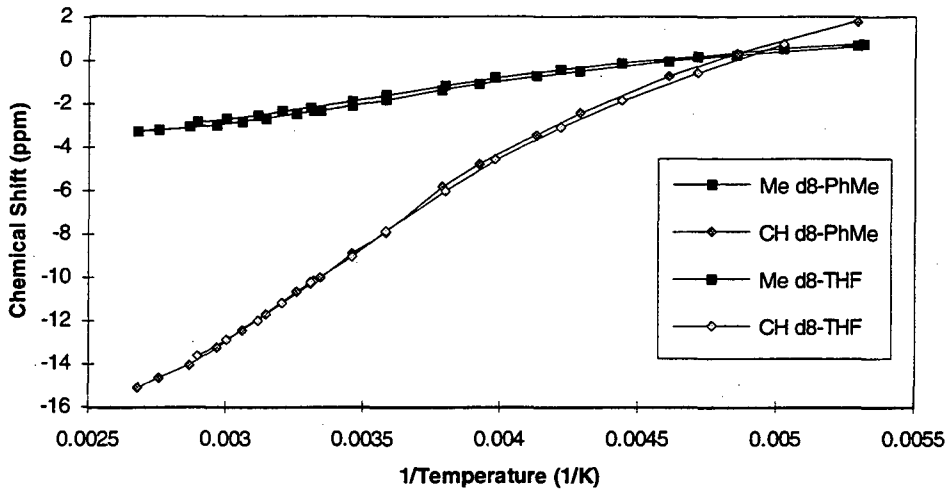

Ground-State Distortions

The variation in bond lengths observed in the crystal structure of $(C_5Me_5)Ni(acac)$ can be attributed to an "ene-allyl" distortion, first proposed by Mason and co-workers in 1964.[15] Dahl has obtained information on this phenomenon in the single crystal X-ray crystallography studies on $(C_5Me_5)Co(CO)_2$[16a] and $[(C_5H_5)Ni(C_3H_4)]_2$.[16b] Both complexes are d^8 metal centers and they have C_s symmetry (by considering one half of the $(C_5H_5)Ni(allyl)$ dimer). In both of the crystal structures analyzed by Dahl, the cyclopentadienyl rings show an "ene-allyl" distortion, where the carbon-carbon bond distances in the ring approximate an alkene fragment and an allyl fragment connected by two single bonds (Figure 10). Dahl attributes this distortion to the asymmetric interaction of the ML_2 fragment (C_{2v} symmetry) with the p_π HOMO of the C_5R_5 ring (which is a pair of degenerate e_1" symmetry orbitals in the local D_{5h} symmetry of the ring). Inspection of Figure 11 shows that antibonding combinations of the d_{xz} and d_{yz} metal orbitals with the two ligands produce two molecular orbitals of substantially different energy (labelled $1b_1$ and $1b_2$).

Subsequent combination with the e_1" orbitals of the C_5Me_5 ring splits the e_1" levels, producing a fully populated orbital (b_2*) and an empty orbital (b_1*) for a metal with a d^8 configuration (for clarity, these labels indicate the parentage, not the actual symmetry, of the hybrid orbitals). For the conjugated π system, the bond lengths should directly reflect the non-cylindrical charge density present on the ring in the b_2* orbital.[16a] Inspection of Figure 11 shows that the b_2* orbital has a single node running through the cyclopentadienyl ring parallel to the plane of the ML_2 fragment, which produces the localization of the π bonding that is responsible for the alternation of carbon-carbon bond lengths that is observed in the cyclopentadienyl rings of $(C_5Me_5)Co(CO)_2$ and $[(C_5H_5)Ni(C_3H_4)]_2$.

Figure 10. "Ene-allyl" Distortion in a C_5Me_5 Ring, with Labeling Scheme.

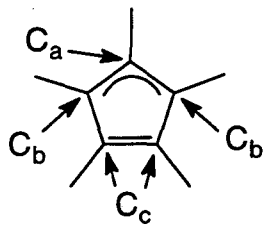

Figure 11. Symmetry Orbital Diagram for a C_s $CpML_2$ Molecule (d^8 system).[17]

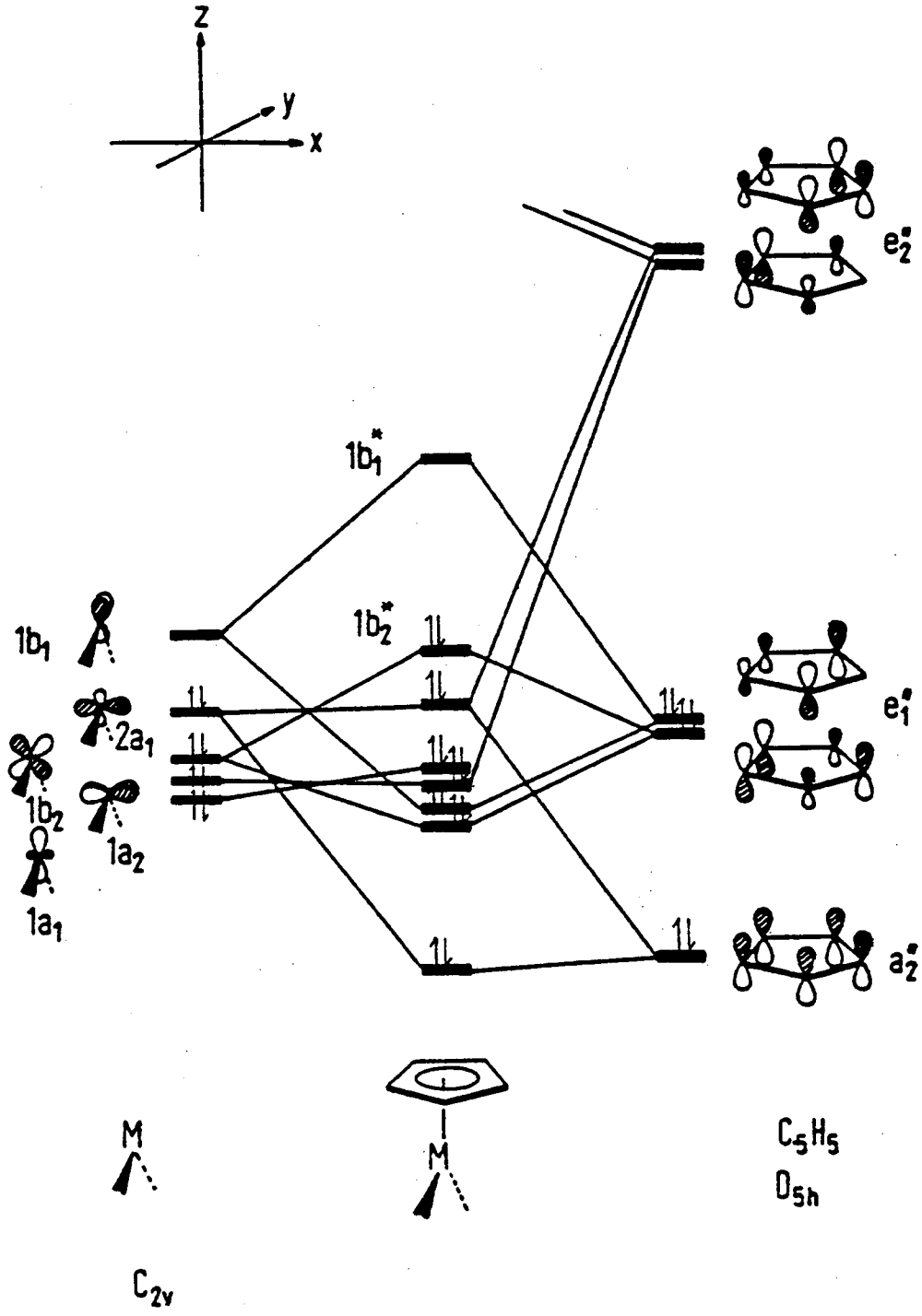

The X-ray crystallographic data for $(C_5Me_5)Co(acac)$ and $(C_5Me_5)Ni(acac)$ are in complete agreement with the "ene-allyl" model. The two compounds are isomorphous (Figures 4 and 5). This makes the structural comparisons very persuasive since the packing effects cancel. Furthermore, there are two independent molecules in the asymmetric unit, allowing for more data to be averaged and hence to produce a more accurate measurement of any distortion or distortions present. The averaged bond distances and angles listed in Tables 1 through 4 show that the alternation in carbon-carbon bond distances in the C_5Me_5 ring is completely analogous to that shown by Dahl, and that $(C_5Me_5)Ni(acac)$ has large distortions (relative to those seen in $(C_5Me_5)Co(CO)_2$), while the variations in the $(C_5Me_5)Co(acac)$ bond distances are the smallest of the four complexes shown in Figure 12.

Figure 12. Averaged Bond Lengths (Å) of "Ene-allyl" Systems.[16]

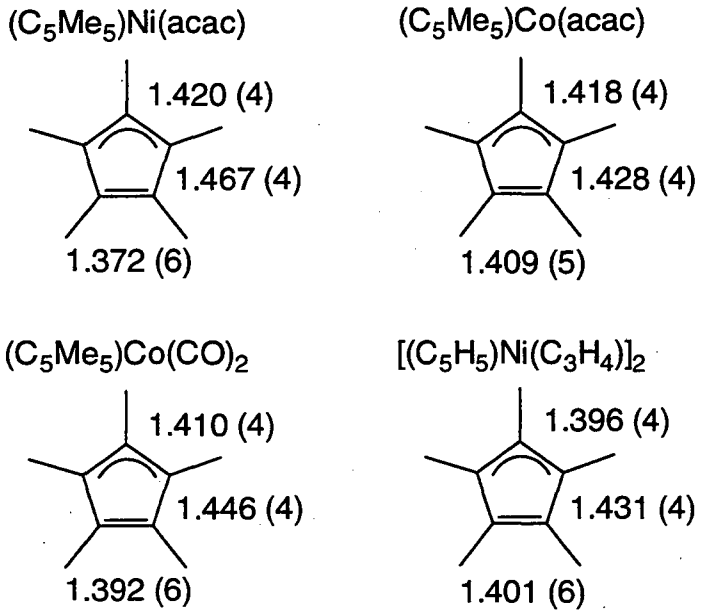

The other distortion observed in "ene-allyl" systems is the puckering of the C_5Me_5 ring from planarity, due to the reduced π bonding between the C_b and C_c carbons in the ring (Figure 13). One way to observe this distortion is to calculate the angle between the two planes containing the "ene" and "allyl" portions of the C_5Me_5 ligand, referred to here as the fold angle (ω in Figure 13). Also useful is a comparison of the differences in the metal-carbon bond distances to C_b and C_c. Table 5 summarizes this information for the four complexes in Figure 12, where $\Delta = |d(M\text{-}C_b) - d(M\text{-}C_c)|$. The table does not have a fold angle value for $(C_5Me_5)Co(CO)_2$ (which was not reported), but Dahl reports that the C_b carbon atoms of $(C_5Me_5)Co(CO)_2$ are displaced 0.017 Å out of the least-squres plane of the C_5Me_5 ligand, towards the cobalt atom, indicating that the fold angle is significant in this compound. Also, $(C_5Me_5)Ni(acac)$ has an ω value that is twice as large as that of $(C_5Me_5)Co(acac)$. Comparison of the Δ values for all of the complexes again indicates that the "ene-allyl" distortion is the largest for $(C_5Me_5)Ni(acac)$, while it is quite small for $(C_5Me_5)Co(acac)$. This distortion is visually striking when one molecule each of $(C_5Me_5)Co(acac)$ and $(C_5Me_5)Ni(acac)$ are viewed down their metal-ring centroid vectors (Figures 14 and 15). The Ni(acac) fragment in Figure 15 is obviously displaced away from the "alkene" portion of the ring when compared to the cobalt structure. Again, the data in Table 5 indicates that $(C_5Me_5)Ni(acac)$ exhibits the largest distortion, although the low value of Δ for $[(C_5H_5)Ni(C_3H_4)]_2$ is deceptive, since the unusually long Ni-C_a distance in this structure indicates that the Ni(allyl) fragment has slipped towards the "alkene" section of the cyclopentadienyl ring, possibly due to steric interactions with the biallyl ligand.[16b]

Figure 13. Ring Puckering due to Selective Population of the b_2^* Orbital.

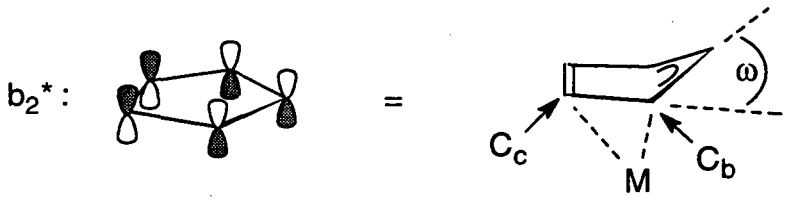

Table 5. Summary of Important Structural Values in "Ene-allyl" Systems.[16]

Compound	d(M-C_a)[a]	d(M-C_b)[a]	d(M-C_c)[a]	Δ	ω[b]
$(C_5Me_5)Ni(acac)$	2.133 (3)	2.068 (3)	2.192 (3)	0.124	9.3
$(C_5Me_5)Co(acac)$	2.105 (3)	2.056 (2)	2.089 (2)	0.033	4.2
$(C_5Me_5)Co(CO)_2$	2.102 (4)	2.067 (3)	2.103 (3)	0.036	--
$[(C_5H_5)Ni(C_3H_4)]_2$	2.167 (4)	2.090 (3)	2.095 (3)	0.005	3.4

[a]Averaged values in Å.

[b]Angle in degrees.

Figure 14. ORTEP Diagram of one molecule of $(C_5Me_5)Co(acac)$.

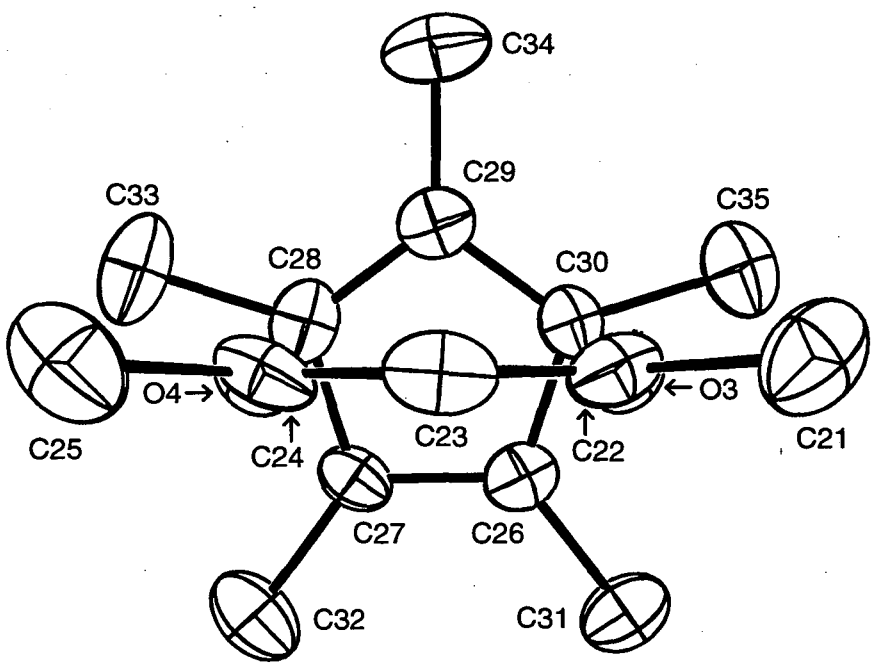

Figure 15. ORTEP Diagram of one molecule of $(C_5Me_5)Ni(acac)$.

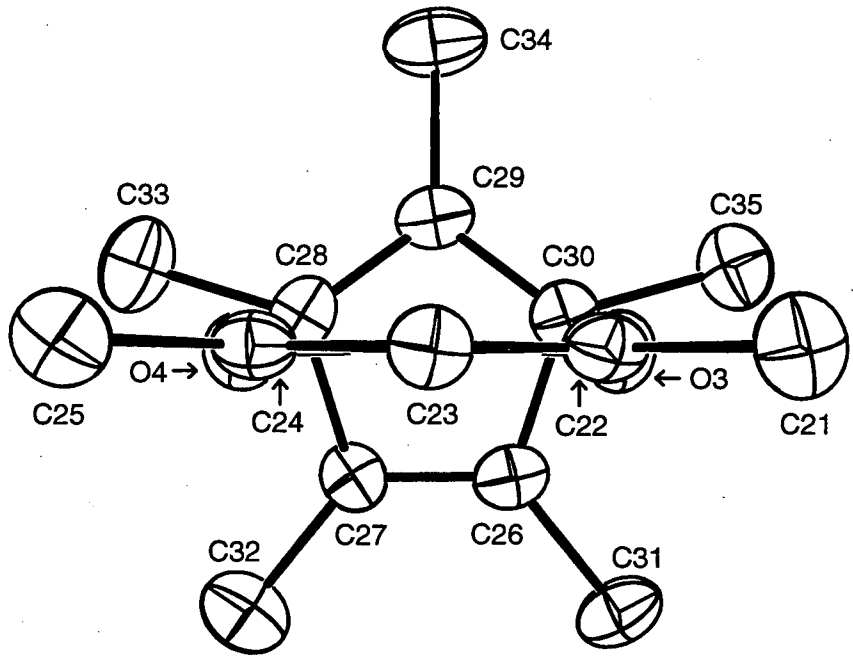

Spin-Equilibrium Phenomena

All of the spectroscopic results for $(C_5Me_5)Ni(acac)$ can be explained by postulating that $(C_5Me_5)Ni(acac)$ has a diamagnetic ground state and a paramagnetic excited state that is thermally accessible. The solution magnetic moment is obviously too low for one unpaired electron per molecule, but definitely shows that a paramagnetic species is present in solution. The variable temperature ^1H NMR spectra show non-linear behavior, indicative of a temperature-dependent equilibrium. The fact that the ^1H NMR signals sharpen and move towards the diamagnetic region upon cooling suggests that the diamagnetic state is lower in energy than the paramagnetic state since paramagnetic species usually have signals that broaden and shift away from the diamagnetic region upon cooling.[18] This is consistent with the solid state

magnetic result which shows a diamagnetic ground state with a low-lying paramagnetic state that becomes populated at *ca.* -120 °C.

The observed phenomena can be rationalized by considering the frontier molecular orbitals for monomeric $CpML_2$ (Figure 11) used to rationalize the "ene-allyl" distortion in the solid state. Since the b_1* combination has a large overlap with the acac orbitals in $(C_5Me_5)Ni(acac)$ and the b_2* m.o. has no overlap, b_2* is substantially lower in energy than b_1*. Placement of the electrons in the orbitals predicts that the last electron pair resides in the b_2* orbital, producing a diamagnetic ground state. However, if the energy gap between b_2* and b_1* is on the order of kT, thermal population of b_1* would occur.[19] This would mean that a high-spin, paramagnetic state is thermally accessible. This is consistent with the observed solution properties of $(C_5Me_5)Ni(acac)$ and the postulate of an intramolecular, thermal, spin-equilibrium.

The plot of $1/\chi_M$ vs. T is linear for $(C_5Me_5)Co(acac)$ over the temperature range measured (5-300 K). This indictaes that either the HOMO-LUMO gap is small, so that relative population of the two levels does not change significantly with temperature, or the gap is still large but the orbital contribution to the moment of the two energy levels is very similar. The spectral evidence implies the former, since the level labeled b_2* has a' symmetry in the C_s point group (the true symmetry of the molecule). Orbitals with a' symmetry cannot yield an orbital contribution to the magnetic moment.[14] This means that the orbital contribution observed in both the solid-state magnetism and EPR spectrum for $(C_5Me_5)Co(acac)$ must be due to the electron partially residing in the b_2* orbital (which has a" symmetry in the C_s point group and can contribute to the magnetic moment). Since no curvature is observed in the variable temperature magnetic susceptibility plot, the relative population of the b_1* and b_2* orbitals does not

appear to change significantly with temperature, indicating that the energy gap between these two levels is small, certainly smaller than in $(C_5Me_5)Ni(acac)$.

If this theory is correct, the variable temperature ^1H NMR and magnetic susceptibility data of $(C_5Me_5)Ni(acac)$ should be modeled by using a simple Boltzmann distribution of electron spins. Kläui, *et al.* used the following formula to fit NMR data for spin equilibria in octahedral cobalt(III) complexes:[20]

$$\delta = \delta_{ls} + \frac{C}{T[1 + e^{(\Delta H^\circ - T\Delta S^\circ)/RT}]}$$

where δ is the observed chemical shift, δ_{ls} is the calculated shift for the diamagnetic species, ΔH° and ΔS° are the enthalpy and entropy, respectively, of the transition between low-spin and high-spin states, T is the absolute temperature, and C is a constant related to the molar susceptibility of the high-spin species. The results of the fitting for $(C_5Me_5)Ni(acac)$, where the equilibrium is between S=0 and S=1 states, are shown in Table 6. All of the thermodynamic values agree well with each other, and the extrapolated diamagnetic shifts are reasonably close to those found in $[(C_5Me_5)Ru(acac)]_2$[10] and $[(C_5Me_5)Rh(acac)](BF_4)_2$,[9] except for the C_5Me_5 signal. However, the error in the values for this signal are large, since the signal is several hundred hertz wide and shifts over nearly 90 ppm in the temperature range studied. The change in entropy is positive because there are more vibrational and rotational degrees of freedom in the high-spin state. The change in enthalpy is also positive because the metal radius is smaller for the low-spin state, so the bonds are shorter and presumably stronger in the low-spin state. These two contrary effects are in competition so that ΔH° favors the low-spin species at low temperatures, and the $T\Delta S^\circ$ term dominates at high temperatures, favoring the high-spin species. The values found yield a high spin-low spin equilibrium constant (K_{eq}) of 0.47 at 30 °C, where K_{eq} = [% high-spin] / [% low-spin].

Table 6. Fitted Parameters for $(C_5Me_5)Ni(acac)$ VT ^1H NMR Data.

	chemical shifts (ppm)			$\Delta H°(avg)^a$	$\Delta S°(avg)^a$	$\Delta G°^b$
Solvent	C_5Me_5	Me-acac	CH-acac	kcal/mol	cal/(mol·K)	kcal/mol
toluene-d_8	5.62	1.29	3.87	2.72	7.56	0.47
tetrahydrofuran-d_8	9.72	1.32	3.34	2.67	7.29	0.50
average	7.67	1.31	3.61	2.70	7.43	0.49
$[Cp^*Ru(acac)]_2$[10]	1.64	1.95	5.11	--	--	--
$[Cp^*Rh(acac)]_2(BF_4)_2$[9]	1.59	1.84	5.67	--	--	--

[a]Average of curve-fitting results for all three signals.
[b]Calculated for T = 298 K.

Crawford and Swanson describe the use of solution magnetic moment data to determine high spin-low spin equilibrium constants from known magnetic moments of the high-spin species by applying the following formula:[21]

$$K_{eq} = \frac{\mu^2_{obs}}{\mu^2_{para} - \mu^2_{obs}}$$

where K_{eq} is the high spin-low spin equilibrium constant, μ_{obs} is the moment observed in solution, and μ_{para} is the moment of the high-spin species. This equation yields a μ_{para} of 2.33 μ_B. Although this value is low (the spin-only moment is 2.83 μ_B), it is important to remember that the Evans' solution magnetic moment method assumes that the θ term of the Curie-Weiss expression is zero and this is a poor assumption in this case.

An important aspect of the spin equilibrium is the structural rearrangement involved in the change in spin state. Plausible mechanisms fall into two main categories, inter- and intramolecular. Equation 2 shows a simple example of a possible intermolecular exchange mechanism, where the acac ligand becomes monodentate and the vacated coordination site may be occupied by a solvent molecule. The intramolecular mechanism shown in equation 3 involves a more

subtle motion, where the acac ligand that is fixed in place by the "ene-allyl" distortion in the diamagnetic ground state rotates freely in the paramagnetic excited state. If the C_5Me_5 group is treated as a bidentate ligand coordinated through the C_b carbon atoms, then the intramolecular motion shown can be likened to the square planar-tetrahedral spin equilibria that have been observed in certain NiL_4 complexes.[22]

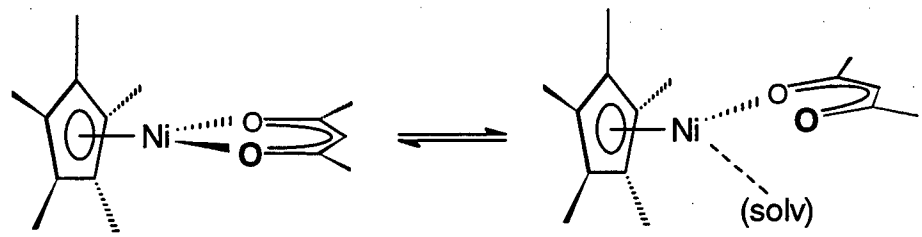

(2)

ground state excited state

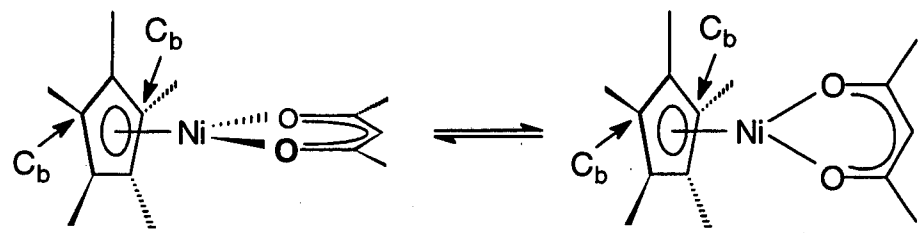

(3)

S = 0 ("Sq. Pl.") S = 1 ("Td")

Experimental evidence rules out solvent-assisted mechanisms, since identical behavior is seen in non-polar (toluene) and polar (tetrahydrofuran) solutions. The mechanism in equation 2 would be expected to show a pronounced solvent dependence of the averaged chemical shift since the equilibrium constant would be directly dependent on the identity of the coordinating solvent. In fact, any mechanism that involves a substantial change in the dipole moment of the nickel species is not consistent with the observed lack of dependence on the solvent

polarity. Furthermore, the solid-state magnetic data shows behavior consistent with a thermally accessible paramagnetic state. Since there is little freedom for conformational change in the solid state (low temperature X-ray crystallography studies show no fracturing of the crystals upon cooling to below -100 °C), this supports the argument that the geometrical differences between the two spin-states is likely to be minimal. The simplistic model shown in eq. 3 is only useful in that it is related to definitively assigned structural changes involved in other d^8 systems that exhibit spin equilibria. There is no evidence that favors one specific intramolecular exchange mechanism.

A final note about the distortion in the ground state as it relates to the fluxional behavior of $(C_5Me_5)Ni(acac)$ in solution. For the diamagnetic ground state with C_s symmetry, the C_5Me_5 signal should be split into 3 signals of relative intensity 2 : 2 : 1. Of course, with the equilibrium involving the high-spin state, the resonances are averaged and broadened. Even at the low end of the temperature range accessible in toluene solution, there is no sign of broadening or splitting of the C_5Me_5 signal. There are several mechanisms involving 1,2- or 1,3-shifts that will make the methyl groups of the ground state structure equivalent without accessing a paramagnetic excited state. Since the ^1H NMR lineshape conatins no information on the fluxional mechanism, nothing more can be said about the process occurring in solution to make the methyl groups equivalent.

An important point is that even though the "ene-allyl" distortion observed in $(C_5Me_5)Ni(acac)$ is comparable to that seen in $(C_5Me_5)Co(CO)_2$, the carbonyl complex is diamagnetic in solution at all accessible temperatures. An explanation for this disparity is shown in the frontier molecular orbital diagram in Figure 16, which was constructed by Klaui and Hofmann[23] to explain the spin-equilibrium observed for $(C_5H_5)Ni(S—S)$ (S—S = $[(C_5H_5)Ni(PMe_2S)_2]^-$). The

level labeled yz (b_2^* in Figure 11) is sensitive to π-interactions with the non-Cp ligands. The π-acceptor properties of CO stabilizes this level and increases the HOMO-LUMO gap, pairing the electrons and making $(C_5Me_5)Co(CO)_2$ diamagnetic. However, acac is not a π-acceptor and may have some π-donor capabilities, so the b_2^* level in $(C_5Me_5)Ni(acac)$ is destabilized relative to $(C_5Me_5)Co(CO)_2$, making the HOMO-LUMO gap smaller in $(C_5Me_5)Ni(acac)$. This smaller energy gap produces the spin-equilibrium behavior observed, indicated by the dashed electron shown in both the xz and yz levels in the rightmost section of Figure 16.

Figure 16. Destabilization of the HOMO in $CpML_2$ by π-donating L Groups.[23]

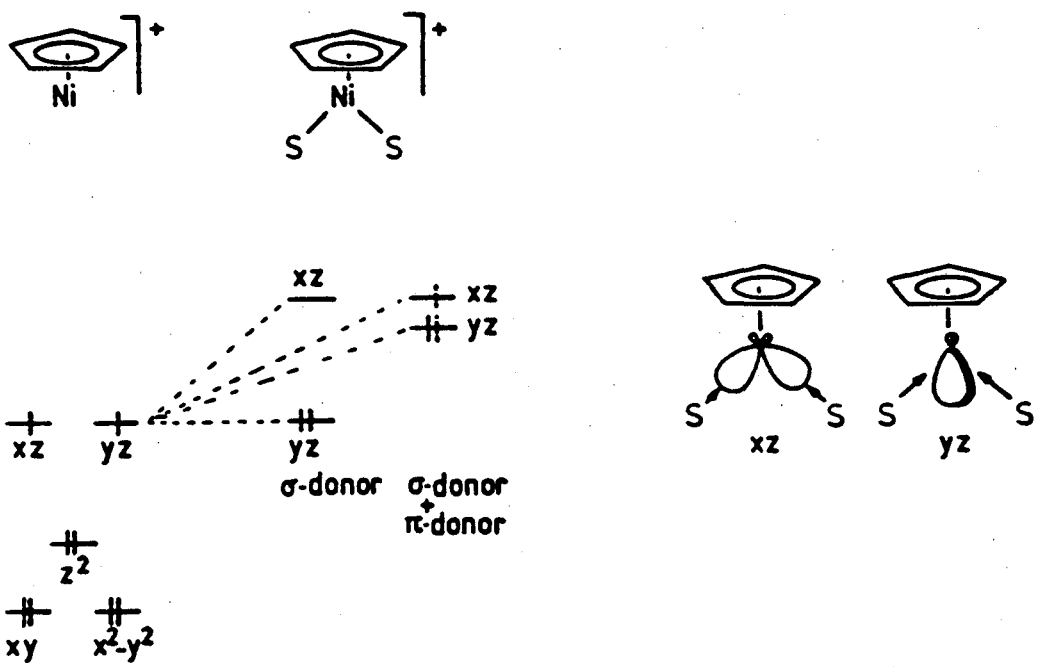

***xz*, *yz*, etc. stands for the $3d_{xz}$, $3d_{yz}$, etc. derived MO's.**

Reactions with Phosphines

Manriquez reported that reactions of the complexes, $(C_5Me_5)M(acac)$, with MeMgI under a CO atmosphere yielded the electronically saturated alkyl complexes (eq. 4). Also, reactions of $(C_5Me_5)M(acac)$ with NaCp produced the corresponding mixed ring metallocenes (eq. 5). However, no other reactions involving $(C_5Me_5)M(acac)$ were reported.[12]

$$(C_5Me_5)M(acac) + MeMgI \xrightarrow[THF]{CO,\ 1\ atm} [(C_5Me_5)M(CO)(Me)]_n + \text{"MgI(acac)"} \quad (4)$$

$M = Co, n = 2$

$M = Ni, n = 1$

$$(C_5Me_5)M(acac) + (C_5H_5)Na \xrightarrow{THF} (C_5Me_5)M(C_5H_5) + Na(acac) \quad (5)$$

$M = Co, Ni$

As mentioned in Chapter 1, the reaction of $(C_5Me_5)M(acac)$ with MeLi produces the trinuclear cluster $(C_5Me_5)_3M_3(\mu_3\text{-}CH)(\mu\text{-}H)$ for M = Co and Ni. The reaction was performed in the presence of a Lewis base (triethylphosphine) in an attempt to trap the proposed intermediate "$(C_5Me_5)M(CH_3)$". Indeed, $(C_5Me_5)M(CH_3)(PEt_3)$ is isolated, but the ^1H NMR spectrum indicates that the phosphine interacts with the starting material prior to addition of the alkylating agent (see Chapter 1). Complexes with the formula $(C_5Me_5)M(acac)(PR_3)$ with M = Co or Ni would be of interest to see if; phosphine exchange occurs in solution, the distortions in the C_5Me_5 ring are different than that seen for $(C_5Me_5)M(acac)$, and to determine if the acac ligand is mono- or bidentate. Bercaw, *et al.* have reported the synthesis of $(C_5Me_5)Fe(acac)(PMe_3)$ and its use as a starting material in a variety of reactions.[24] However, the only

characterization data presented for this compound is an elemental analysis and "a ^1H NMR spectrum indicative of a paramagnetic compound, i.e. with very broad peaks and chemical shifts that are very temperature dependent."[24] This is curious, since the isoelectronic $(C_5Me_5)Fe(acac)(CO)$ is diamagnetic[25] and paramagnetic, 18-electron compounds are unknown in permethylmetallocene chemistry.[26] Therefore, the 19-electron analogue, cobalt, and the 20-electron analogue, nickel, may yield some insight into the unexplained behavior of the iron compound and related complexes.

Crystallization of $(C_5Me_5)Ni(acac)$ from a pentane solution containing one equivalent of phosphine produces the base adduct in good yields (eq. 6).

$$(C_5Me_5)Ni(acac) + PR_3 \xrightarrow{\text{pentane}} (C_5Me_5)Ni(acac)(PR_3) \quad (6)$$

R = Me, 93% yield
R = Et, 80% yield

Infrared spectra for $(C_5Me_5)Ni(acac)(PMe_3)$ and $(C_5Me_5)Ni(acac)(PEt_3)$ are virtually identical except for the lower energy bands directly related to the phosphine groups. Both show the C-O/C-C combination band for the acac ligand at 1595 cm^{-1}. This is about 40 cm^{-1} higher than in $(C_5Me_5)Ni(acac)$, indicating that the acac has a weaker interaction with the nickel center in the phosphine complexes. Both complexes analyze as 1:1 adducts, so all evidence points towards $(C_5Me_5)Ni(acac)(PR_3)$ (R = Me, Et) being a stable complex in the solid state.

The cobalt analogs, if they exist, are much more fleeting. Addition of PEt_3 to a pentane solution of $(C_5Me_5)Co(acac)$ produces a mild color change towards a more orange shade of red, but crystallization only produces the starting material as judged by melting point, infrared, and elemental analysis data. The

use of ^1H NMR spectroscopy is not applicable since no resonances are observed for the cobalt complex under any conditions. Cobalt(II) is a labile metal center,[27] and addition of a Lewis base to $(C_5Me_5)Co(acac)$ would produce a 19-electron species. Both of these factors presumably disfavor the formation of a stable phosphine adduct.

Definitive proof for the existence of a discrete phosphine adduct of $(C_5Me_5)Ni(acac)$ lies in the X-ray crystal structure of the PMe_3 complex. Initial attempts were made to get X-ray quality crystals of the PEt_3 complex (for comparison purposes, since all other crystallographic studies of phosphine complexes presented herein utilize PEt_3), but the crystals inevitably shattered upon placement in the cold stream of the diffractometer. The PMe_3 adduct, $(C_5Me_5)Ni(acac)(PMe_3)$ produced thin prisms that were well-behaved, although they dissolved rapidly in the Paratone N oil releasing bubbles which presumably are PMe_3. A suitable crystal was isolated and refinement yielded the structure shown in Figure 17. The molecule has a crystallographically imposed mirror plane in the solid state, containing the nickel atom, the phosphorus atom, the γ-carbon atom (of the acac group), and one pair of ring and methyl carbons of the C_5Me_5 ligand (Figure 18). Bond distances and angles are listed in Tables 7 and 8, respectively.

Figure 17. ORTEP Diagram of $(C_5Me_5)Ni(acac)(PMe_3)$, Side View.

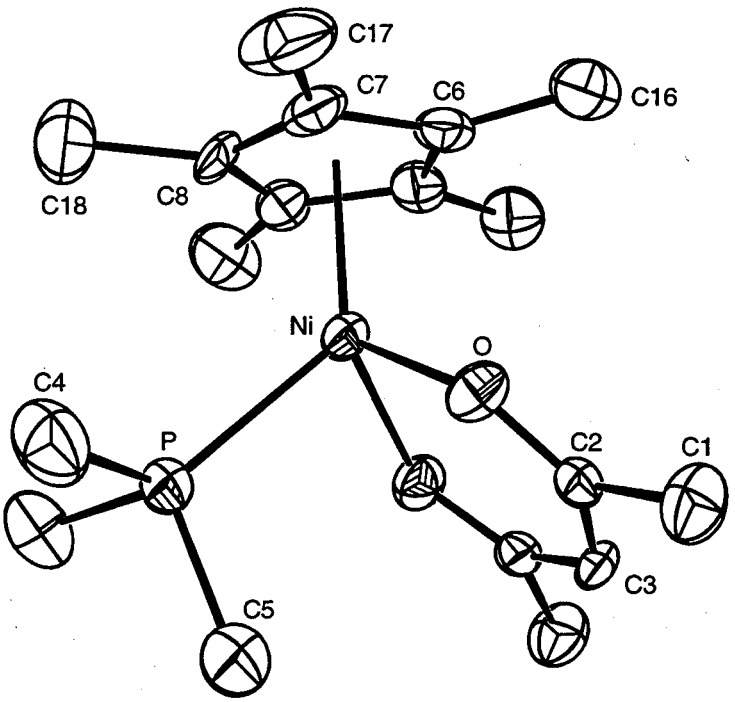

Figure 18. ORTEP Diagram of $(C_5Me_5)Ni(acac)(PMe_3)$, Overhead View.

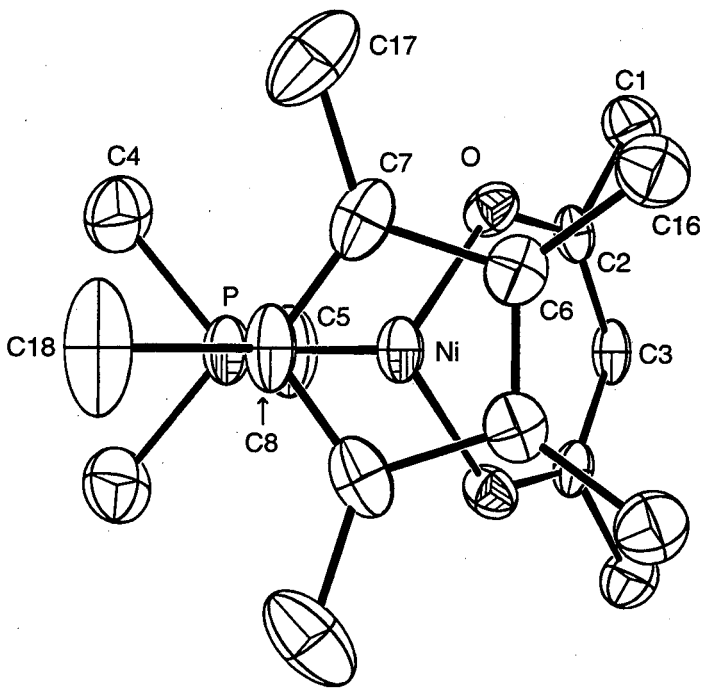

Table 7. Bond Distances for $(C_5Me_5)Ni(acac)(PMe_3)$ (Å).

Ni-O	2.035 (3)	O-C2	1.254 (6)
Ni-P	2.337 (2)	C1-C2	1.499 (7)
Ni-Cp	1.884	C2-C3	1.407 (6)
Ni-C6	2.249 (5)	C6-C6	1.395 (11)
Ni-C7	2.226 (5)	C6-C7	1.437 (7)
Ni-C8	2.231 (8)	C7-C8	1.404 (7)
		C6-C16	1.490 (8)
Ni-C (ave)	2.235 (4)	C7-C17	1.503 (9)
		C8-C18	1.510 (12)
P-C4	1.817 (7)		
P-C5	1.780 (10)		

Cp is the ring centroid of atoms C6-C8.

Table 8. Bond Angles for $(C_5Me_5)Ni(acac)(PMe_3)$ (°).

P-Ni-O	91.0(1)	Ni-P-C4	118.9(2)
O-Ni-O	91.0(2)	Ni-P-C5	110.6(3)
Cp-Ni-P	130.2	C4-P-C4	102.4(5)
Cp-Ni-O	121.6	C4-P-C5	101.7(3)
C6-C6-C7	108.1(3)	Ni-O-C2	125.0(3)
C6-C7-C8	107.2(5)		
C7-C8-C7	109.2(7)		

Variable-Temperature NMR Behavior

Both $(C_5Me_5)Ni(acac)(PMe_3)$ and $(C_5Me_5)Ni(acac)(PEt_3)$ exhibit shifted ^1H NMR signals that span a range of approximately 200 ppm at room temperature. The variable temperature ^1H NMR behavior of $(C_5Me_5)Ni(acac)(PEt_3)$ shows distinctly non-linear behavior with the C_5Me_5 and the acac methyl resonances broadening into the baseline upon cooling (Figures 19 and 20). This behavior indicates that some type of temperature dependent process is occurring in solution. Addition of excess PEt_3 (*ca.* 5 μL) to a sample of $(C_5Me_5)Ni(acac)(PEt_3)$ shifts all of the resonances and increases the relative intensities of the two signals in the diamagnetic region (at *ca.* δ 1.9 and 2.2), identifying them as the signals due to the methyl and methylene protons of the

PEt_3 group, respectively. No signals for uncoordinated PEt_3 were observed, so the coordinated phosphine must exchange with free phosphine rapidly relative to the NMR time scale. The variable temperature ^1H NMR spectrum of $(C_5Me_5)Ni(acac)(PEt_3)$ with added PEt_3 is also shown in Figures 19 and 20. The curves are superficially the same, but the C_5Me_5 and the acac methyl resonances broaden out at higher temperatures and the maxima in the acac γ-hydrogen curve shifts to a lower temperature.

Figure 19. δ vs. 1/T for $(C_5Me_5)Ni(acac)(PEt_3)$: $C_5\underline{Me}_5$ and $(\underline{Me}CO)_2CH$.

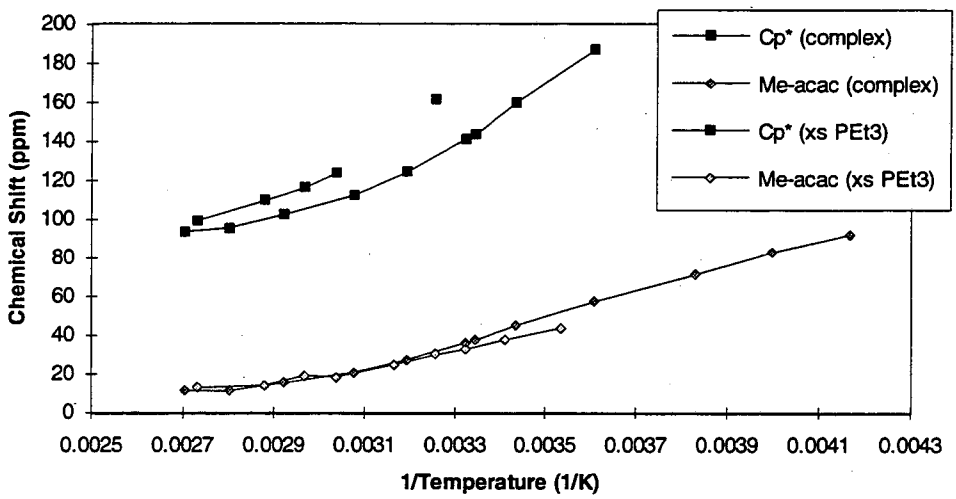

Figure 20. δ vs. 1/T for $(C_5Me_5)Ni(acac)(PEt_3)$: $(MeCO)_2C\underline{H}$ and PEt_3.

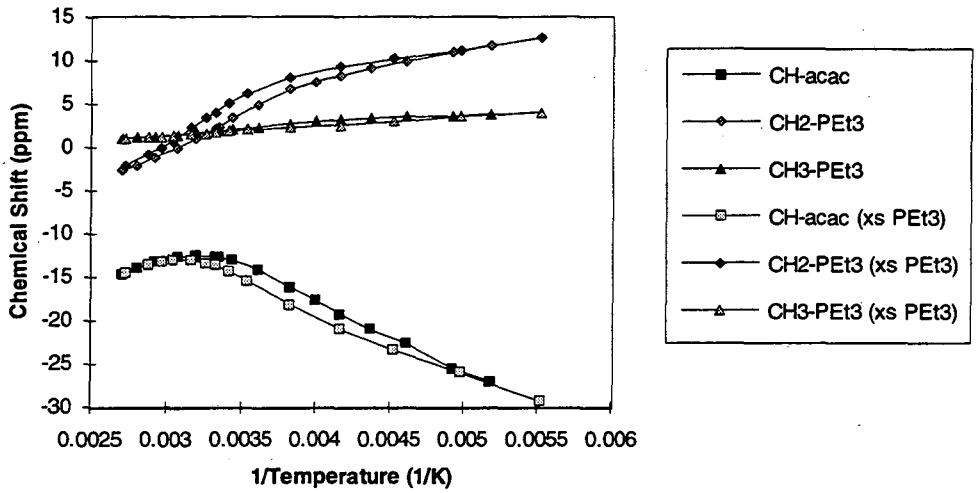

In contrast, the variable temperature ^1H NMR data for $(C_5Me_5)Ni(acac)(PMe_3)$ (Figure 21) exhibits essentially linear behavior, with the small deviations from linearity most likely due to a systematic error in temperature measurement. The C_5Me_5 resonance broadens into the baseline upon cooling, but at lower temperature (*ca.* -20 °C) than the corresponding resonance in $(C_5Me_5)Ni(acac)(PEt_3)$ (*ca.* 0 °C). Also, addition of excess PMe_3 does not shift the resonances, and a sharp singlet at 1.11 ppm, due to uncoordinated PMe_3, is observed in toluene-d_8 at all temperatures up to 106 °C. These results indicate that $(C_5Me_5)Ni(acac)(PMe_3)$ does not lose phosphine in solution.

Figure 21. δ vs. 1/T for $(C_5Me_5)Ni(acac)(PMe_3)$.

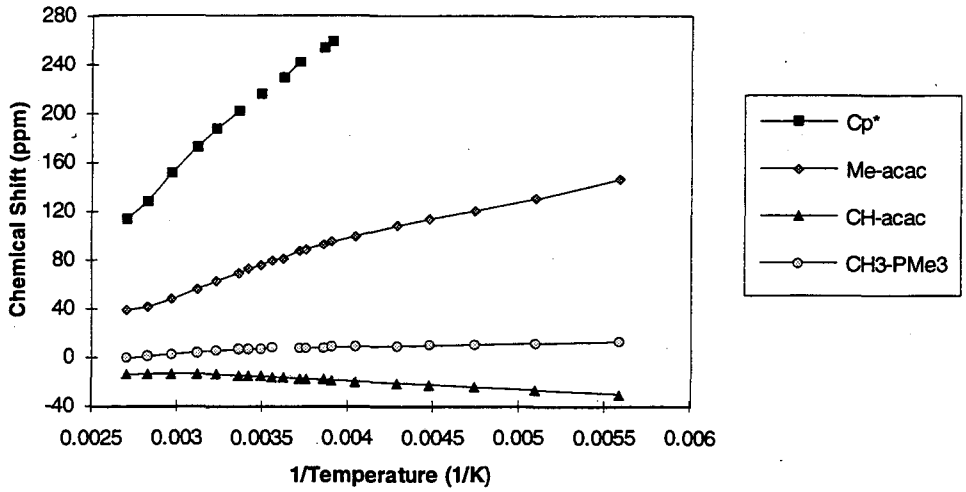

Interpretation of X-ray Crystallographic Data

The single crystal X-ray structure of $(C_5Me_5)Ni(acac)(PMe_3)$ shows some surprising results. In every case, the bond distances (Table 7) to nickel are longer than in the phosphine-free $(C_5Me_5)Ni(acac)$ (Table 3). The Ni-O and Ni-P distances are longer by 0.16 Å and 0.18 Å, respectively, than the corresponding distances in $(C_5Me_5)Ni(acac)$ and $(C_5Me_5)Ni(Br)(PEt_3)$ (Chapter 3, Table 5). The Ni-C distances are 0.04 Å longer than the longest Ni-C distance (Ni-C_c) in $(C_5Me_5)Ni(acac)$, and the Ni-centroid distance is 0.13 Å longer in the phosphine adduct. Also, the C-O distances of the acac ligand are slightly shorter (0.03 Å, qualitatively confirming the infrared data), but the magnitude of the difference is on the order of 3σ. Finally, and most importantly, all of the C-C distances in the C_5Me_5 ring are equivalent within the error of the measurements with $\Delta = 0.005$ Å (as defined for Table 5), indicating that an "ene-allyl" distortion is not detected.

Orbital Comparisons

Construction of a molecular orbital diagram for $(C_5Me_5)Ni(acac)(PMe_3)$ and subsequent comparison to the diagram for $(C_5Me_5)Ni(acac)$ (Figure 11) yields an explanation of the crystallographic results. Inspection of Table 8 shows that the ∠O-Ni-P and ∠O-Ni-O angles are identical. Thus, a reasonable first approximation for modeling $(C_5Me_5)Ni(acac)(PMe_3)$ is to treat the acac and PMe_3 ligands as three equivalent, unidentate ligands. The molecular orbital diagram for a pseudo-C_{3v} $CpML_3$ complex is shown in Figure 22.[28] Placement of 20 electrons in the C_{3v} model predicts a paramagnetic, S = 1 ground state for $(C_5Me_5)Ni(acac)(PMe_3)$. Reduction of the idealized symmetry from C_{3v} to C_s (the observed geometry of $(C_5Me_5)Ni(acac)(PMe_3)$) causes a splitting of the HOMO e* orbitals into two orbitals with a' and a" symmetry. This splitting will be smaller in magnitude than that in $(C_5Me_5)Ni(acac)$ because the two orbitals have a similar amount of overlap with the non-Cp ligands in the coordination sphere, unlike the b_1* and b_2* orbitals in $(C_5Me_5)Ni(acac)$. An "ene-allyl" distortion, like that seen for $(C_5Me_5)Ni(acac)$, would not be expected in the phosphine adduct, and the experimental evidence supports this conclusion. Furthermore, the lengthening of all of the bond distances to nickel, in excess of the amount expected by increasing the cooordination number by one, is explained, since the two additional electrons contributed by PMe_3 reside in strongly metal-ligand antibonding orbitals. In the solid state, $(C_5Me_5)Ni(acac)(PMe_3)$ should exhibit paramagnetic behavior at all but the lowest of temperatures. It should be noted that this model predicts that $(C_5Me_5)Fe(acac)(PMe_3)$ should be diamagnetic. Obviously, the properties of the iron analogue need to be investigated more completely.

Figure 22. Symmetry Orbital Diagram for C_{3v} $CpML_3$ (d^8 system).[28]

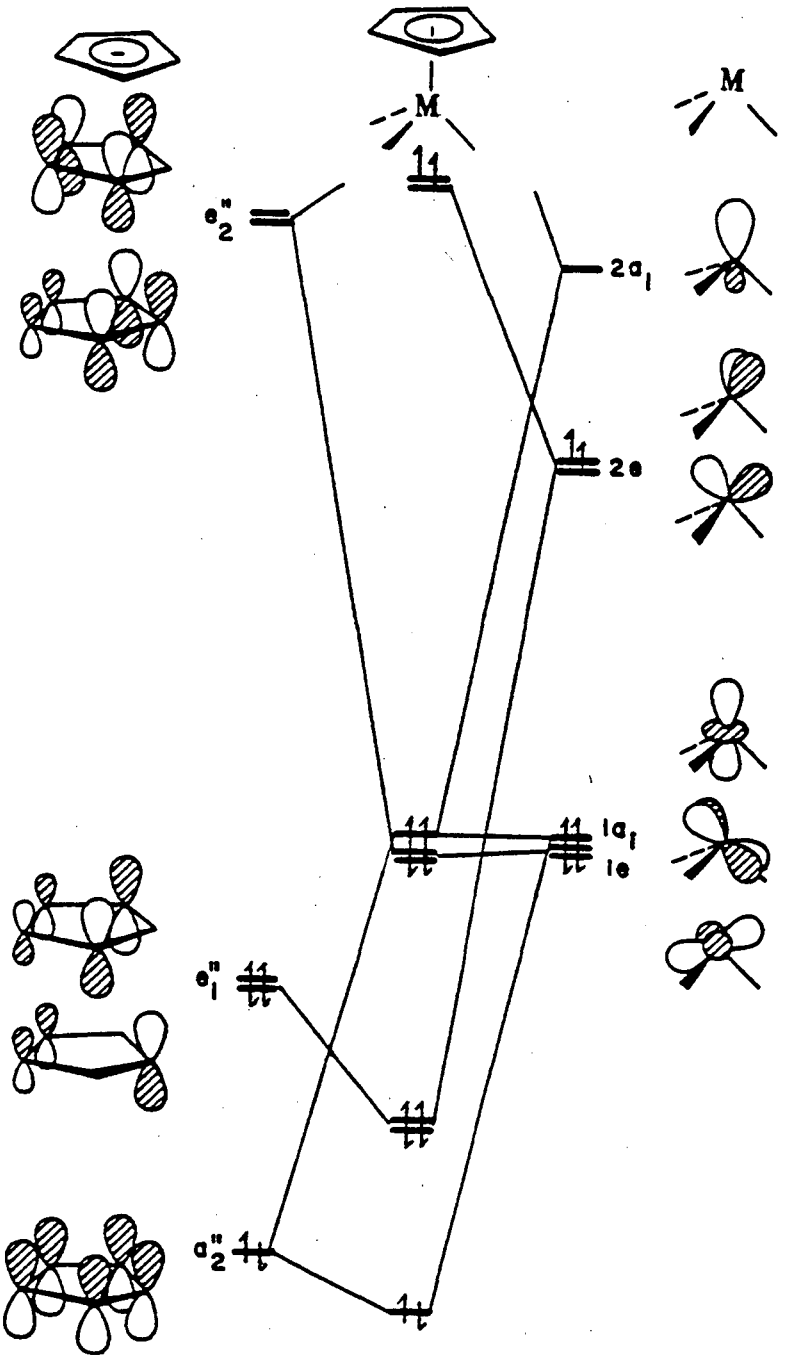

Solution Behavior

The prediction of a paramagnetic ground state for $(C_5Me_5)Ni(acac)(PMe_3)$ agrees well with the approximate Curie-Weiss behavior observed in the variable temperature ^1H NMR spectra. However, the differing solution behavior of $(C_5Me_5)Ni(acac)(PMe_3)$ and $(C_5Me_5)Ni(acac)(PEt_3)$ complicates the interpretation of the variable temperature data for $(C_5Me_5)Ni(acac)(PEt_3)$. $(C_5Me_5)Ni(acac)(PMe_3)$ shows no evidence of phosphine exchange in solution up to 106 °C. Since $(C_5Me_5)Ni(acac)(PEt_3)$ exchanges rapidly with free PEt_3 at all temperatures accessible in toluene solution, apparently PMe_3 binds more strongly to $(C_5Me_5)Ni(acac)$ than does PEt_3. This must be due to the larger steric bulk of PEt_3, since studies indicate that PEt_3 is a better base towards transition metals than PMe_3.[29] Any intramolecular processes that contribute to the non-linear behavior of the PEt_3 adduct's variable temperature NMR data are masked by both the phosphine exchange process and the presence of $(C_5Me_5)Ni(acac)$ in solution, since $(C_5Me_5)Ni(acac)$ itself displays non-linear behavior. Nothing further can be concluded from the variable temperature ^1H NMR results of $(C_5Me_5)Ni(acac)(PEt_3)$.

References

1. Cotton, F. A.; Wilkinson, G., "Advanced Inorganic Chemistry," 5th Ed., John Wiley and Sons: New York, **1988**.

2. Wilkinson, G.; Cotton, F. A., *Prog. Inorg. Chem.*, **1959**, *1*, 1; and references therein.

3. Shibata, S.; Onuma, S.; Iwase, A.; Inoue, H., *Inorg. Chim. Acta*, **1977**, *25*, 33.

4. (a) Shibata, S.; Onuma, S.; Inoue, H., *Inorg. Chem.*, **1985**, *24*, 1723.
   (b) Bullen, G. J.; Mason, R.; Pauling, P., *Inorg. Chem.*, **1965**, *4*, 456.
   (c) Bennett, M. J.; Cotton, F. A.; Eiss, R., *Acta Cryst.*, **1968**, *B24*, 904.

5. (a) Cotton, F. A.; Rice, G. W., *Nouv. J. Chim.*, **1977**, *1*, 301.
   (b) Cotton, F. A.; Elder, R. C., *Inorg. Chem.*, **1965**, *4*, 1145.

6. Ito, T.; Kiriyama, T.; Yamamoto, A., *Chem. Lett.*, **1976**, 835.

7. (a) Swallow, A. G.; Truter, M. R., *Proc. R. Soc. London*, **1962**, *A266*, 527.
   (b) Baba, S.; Ogura, T.; Kawaguchi, S., *Inorg. Nucl. Chem. Lett.*, **1971**, *7*, 1195; *Bull. Chem. Soc. Jpn.*, **1974**, *47*, 665.

8. Kawaguchi, S., *Coord. Chem. Rev.*, **1986**, *70*, 51; and references therein.

9. Rigby, N.; Lee, H-B.; Bailey, P. M.; McCleverty, J. A.; Maitlis, P. M., *J. Chem. Soc., Dalton Trans.*, **1979**, 387.

10. Kölle, U.; Kossakowski, J.; Raabe, G., *Angew. Chem., Int. Ed. Engl.*, **1990**, *29*, 773.

11. Smith, M. E.; Hollander, F. J.; Andersen, R. A., *Angew. Chem., Int. Ed. Engl.*, **1993**, *32*, 1294.

12. Bunel, E. E.; Valle, L.; Manriquez, J. M., *Organometallics*, **1985**, *4*, 1680.

13. Nakamoto, K.; McCarthy, P. J.; Martell, A. E., *J. Am. Chem. Soc.*, **1961**, *83*, 1272.

14. Jolly, W. H., "The Synthesis and Characterization of Inorganic Compounds," Prentice-Hall: Englewood Cliffs, NJ, **1970**.

15. Gerloch, M. R.; Mason, R., *J. Chem. Soc.*, **1965**, 296.

16. (a) Byers, L. R.; Dahl, L. F., *Inorg. Chem.*, **1980**, *19*, 277.
(b) Smith, A. E., *Inorg. Chem.*, **1972**, *11*, 165.

17. Hofmann, P., *Angew. Chem., Int. Ed. Engl.*, **1977**, *16*, 536.

18. Jesson, J. P., "NMR of Paramagnetic Molecules: Principles and Applications," LaMar, G. N.; Horrocks, W. DeW. Jr.; Holm, R. H., eds., Academic Press: New York, **1973**, Ch. 1.

19. Kläui, W.; Schmidt, K.; Bockmann, A.; Hofmann, P.; Schmidt, H.; Stauffert, P., *J. Organomet. Chem.*, **1985**, *286*, 407.

20. Kläui, W.; Eberspach, W.; Gütlich, P., *Inorg. Chem.*, **1987**, *26*, 3977.

21. Crawford, T. H.; Swanson, J., *J. Chem. Ed.*, **1971**, *48*, 382.

22. Holm, R. H.; Hawkins, C. J., "NMR of Paramagnetic Molecules: Principles and Applications," LaMar, G. N.; Horrocks, W. DeW. Jr.; Holm, R. H., eds., Academic Press: New York, **1973**, Ch. 7.

23. Kläui, W.; Schmidt, K.; Bockmann, A.; Brauer, D. J.; Wilke, J.; Lueken, H.; Elsenhans, U., *Inorg. Chem.*, **1986**, *25*, 4125.

24. Paciello, R. A.; Manriquez, J. M.; Bercaw, J. E., *Organometallics*, **1990**, *9*, 260.

25. Morrow, J.; Catheline, D.; Desbois, M.-H.; Manriquez, J. M.; Ruiz, J.; Astruc, D., *Organometallics*, **1987**, *6*, 2605.

26. Robbins, J. L., Ph.D. Thesis, University of California, Berkeley, **1981**.

27. Langford, C. H.; Gray, H. B., "Ligand Substitution Processes," W. A. Benjamin: London, **1966**.

28. Albright, T. A.; Burdett, J. K.; Whangbo, M. H., "Orbital Interactions in Chemistry," John Wiley and Sons: New York, **1985**.

29. Rahman, M.; Liu, H.-Y.; Eriks, K.; Prock, A.; Giering, W. P., *Organometallics*, **1989**, *8*, 1.

Chapter 3

Synthesis, Characterization and Reactivity of Pentamethylcyclopentadienyl Halide Complexes of Cobalt and Nickel

Initial investigations into the chemistry of coordinatively unsaturated metal alkyl complexes required starting materials of low coordination number with an easily metathesized leaving group. Complexes of the general formula $[(C_5Me_5)M(\mu\text{-}X)]_2$ with M = cobalt and nickel and X = halide fit these criteria. Although it was shown that these are not the ideal starting materials for making the desired complexes (as discussed in Chapter 1), study of the physical properties of these and related complexes would allow further insight into the nature of the bonding interactions in them. Several have been reported earlier,[1,2] but many details are either unreported or have yielded confusing results. In order to clarify these confusing reports an investigation of the solid-state and solution properties of the bridging halide complexes and the reaction products generated by oxidation or phosphine-induced cleavage was undertaken.

Literature Reports

Kölle initially reported the synthesis of the dimeric complexes $[(C_5Me_5)Co(\mu\text{-}X)]_2$[1a] (X = Cl, Br, I) from reaction of LiC_5Me_5 with the corresponding anhydrous cobalt(II) halide (eq. 1) at room temperature in tetrahydrofuran solution. His syntheses of the nickel analogues (X = Cl and Br) utilize the 1,2-dimethoxyethane (dme) adducts of the nickel(II) halides, since the anhydrous salts are insoluble in most solvents (eq. 2).[2]

$$2\,CoX_2 + 2\,LiC_5Me_5 \xrightarrow{THF} [(C_5Me_5)Co(\mu\text{-}X)]_2 + 2\,LiX \quad (1)$$
$$X = Cl, Br, I$$

$$2\,NiX_2(dme) + 2\,LiC_5Me_5 \xrightarrow[-10\,^\circ C]{THF} [(C_5Me_5)Ni(\mu\text{-}X)]_2 + 2\,LiX + 2\,dme \quad (2)$$
$$X = Cl, Br$$

The only characterizational data presented for the nickel complexes was a mass spectrum of $[(C_5Me_5)Ni(\mu\text{-}Br)]_2$.

Kölle reported that the solid-state magnetic susceptibility for $[(C_5Me_5)Co(\mu\text{-}Cl)]_2$ indicates that the unpaired spins, one for each cobalt center, are antiferromagnetically coupled with a coupling constant of 238 cm^{-1}.[1b] The molecular orbitals for a generic $L_nM\text{-}ML_n$ fragment of C_{nv} symmetry, as determined by Hoffmann and Pinhas,[3] indicate that the cobalt(II) halide bridged dimers should have a half-occupied HOMO with e_1^* symmetry. Reduction of the symmetry to C_s by puckering the planar unit splits this level into a_1^* and b_2^* symmetry orbitals, allowing pairing of the electrons. This explanation of the observed coupling is supported by inspection of the crystal structure of $(C_5Me_5)Co(\mu\text{-}NMe_2)(\mu\text{-}Cl)Co(C_5Me_5)$, which exhibits a significant puckering from the simple planar geometry expected for molecules of the type $[(C_5Me_5)Co(\mu\text{-}X)]_2$. Unfortunately, $[(C_5Me_5)Co(\mu\text{-}Cl)]_2$ yields crystals unsuitable for X-ray studies, and only preliminary data (of very poor quality) is available for $[(C_5Me_5)Co(\mu\text{-}Br)]_2$ (indicating a possibility of a puckered geometry).[1b]

The reported solution properties of the cobalt compounds are also somewhat unusual. Kölle reported that $[(C_5Me_5)Co(\mu\text{-}Cl)]_2$ exhibits a rhombic EPR signal centered at g = 2 that varies in intensity depending on the identity of the solvent used to make the sample glass.[1b] He noted distinct similarities to the

spectrum observed for $(C_5Me_5)Co(Cl)(pyridine)$, and interpreted the origin of the signal as being due to a solvated species, $(C_5Me_5)Co(Cl)(S)$, where S is the solvent used to prepare the sample. A disturbing feature of this scenario is that the same signal appears even in pentane and toluene solutions, which are poor Lewis bases. Finally, Kölle reports that $[(C_5Me_5)Co(\mu\text{-}Cl)]_2$ exhibits a ^1H NMR signal at *ca.* δ 40 ppm in toluene-d_8 and cyclohexane-d_{12} solutions. Kölle reports that these signals do not change position when the temperature is varied from 170 to 333 K, an unusual fact given the reported dependence of χ_M on temperature.[1b]

Detailed Investigations

The literature syntheses of $[(C_5Me_5)Co(\mu\text{-}Cl)]_2$ and $[(C_5Me_5)Co(\mu\text{-}Br)]_2$ were difficult to reproduce and gave yields of *ca.* 30%, far less than the reported 70-80%. Three modifications greatly improved the yields for the syntheses of the chloride and bromide dimers: a) larger quantities of solvent (typically 5 times the reported amount) were used to keep the starting materials in solution; b) use of the more soluble $(C_5Me_5)_2Mg$ instead of the lithium salt, again using starting materials that were soluble enough to keep the reaction homogenous; and c) performing the reaction at 0 °C (eq. 3). The cobalt complexes are not thermally sensitive in solution, so the need for doing the reaction at 0 °C is not obvious, though the yields increase.

$$2\ CoX_2 + Mg(C_5Me_5)_2 \xrightarrow[0\ °C]{THF} [(C_5Me_5)Co(\mu\text{-}X)]_2 + MgX_2 \quad (3)$$
$$X = Cl, Br$$

A cryptic reference in Kölle's synthesis says that "complete removal of the solvent [tetrahydrofuran] is not advisable since the product can be extracted only with difficulty from the completely dried reaction mixture."[1b] Indeed, concentration of the reaction mixture to an oil and subsequent extraction with, and crystallization from, pentane produces substantially higher yields than completely removing the volatile components from the reaction mixture (and subsequent workup) does. Kölle's EPR evidence that a solvated monomeric species, $(C_5Me_5)Co(X)(thf)$, is present in solution suggests that the presence of a solvated species may contribute to the difficulties in isolating the halide-bridged dimers in high yield. However, there is no simple explanation for the behavior observed during the synthesis of these complexes.

Unfortunately, these same modifications did not prove as successful with the nickel analogs, $[(C_5Me_5)Ni(\mu\text{-}X)]_2$. Although Kölle refers to the chloride analogue in the abstract and the initial reaction scheme of reference 2, no information (synthesis or characterization) is reported. Our repeated attempts to isolate $[(C_5Me_5)Ni(\mu\text{-}Cl)]_2$ resulted in failure, most likely due to the insolubility of $NiCl_2 \cdot dme$ in tetrahydrofuran at low temperatures. Since the bromide analog is unstable in solution above -10 °C, it is unlikely that $[(C_5Me_5)Ni(\mu\text{-}Cl)]_2$ will be successfully isolated using the route shown in eq. 2.

The bromide, $[(C_5Me_5)Ni(\mu\text{-}Br)]_2$ was isolated in reproducible yields of 15%, far lower than the 80% reported by Kölle.[2] Variation of the reaction temperature, solvent ratio, and pentamethylcyclopentadienyl transfer reagent had no significant effect on the yield of the product. The complex was isolated as dark red microcrystals by precipitation from pentane solution. The compound is much less volatile than the cobalt(II) analogues (which can be purified by sublimation at 120 °C at 10^{-4} torr), and attempts at sublimation resulted in decomposition. The low yields and thermal sensitivity of the complex rendered

crystallization difficult, so the material was used as obtained from the reaction mixture. Since pure material was not available, detailed investigation of the magnetic behavior and variable temperature ^1H NMR behavior of $[(C_5Me_5)Ni(\mu\text{-}Br)]_2$ was not pursued.

Magnetic Behavior

Both $[(C_5Me_5)Co(\mu\text{-}Cl)]_2$ and $[(C_5Me_5)Co(\mu\text{-}Br)]_2$ can be purified by sublimation (with only moderate loss of material due to decomposition) so that a study of the variable temperature solid state magnetism of the cobalt complexes can be made that are free of magnetic impurities, such as metal or metal halide impurities. The plots of (molar susceptibility)$^{-1}$ vs. temperature for the chloride and bromide complexes are shown in Figures 1 and 2, respectively.

Figure 1. Plot of $1/\chi_M$ vs. T for $[(C_5Me_5)Co(\mu\text{-}Cl)]_2$.

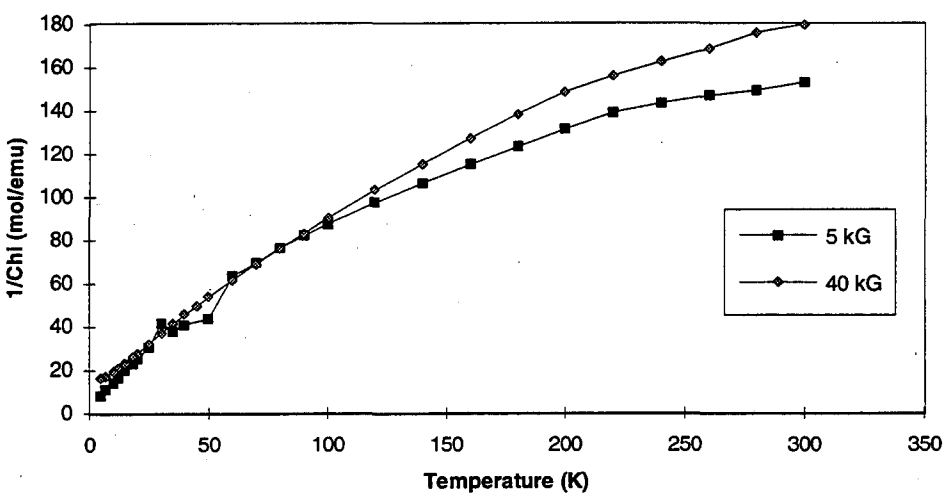

Figure 2. Plot of $1/\chi_M$ vs. T for $[(C_5Me_5)Co(\mu\text{-}Br)]_2$.

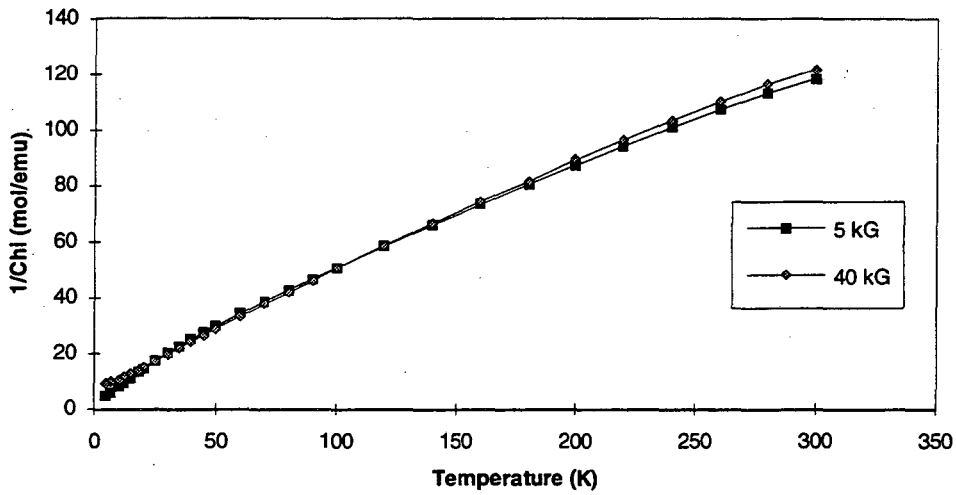

Both show Curie-Weiss behavior at low temperatures, with an increase in moment at higher temperatures. A summary of the resulting parameters of the linear least-squares fit for the two temperature regions is shown in Table 1. Both complexes exhibit moments indicative of 2 unpaired electrons at low temperature. The values obtained for the higher temperature region (> 160 K) are substantially larger. There is also a slight field dependence for both complexes, with the high field data (40 kG) yielding a larger low temperature moment but a smaller high temperature moment than the lower field data (5 kG) for both complexes. This might be due to a very small amount of magnetic impurities, which sublimation may not have completely removed.

Table 1. Magnetic Susceptibility Data for $[(C_5Me_5)Co(\mu\text{-}X)]_2$ (per dimer).

	5-50 K		160-300 K	
X	μ_{eff} (μ_B)	θ (K)	μ_{eff} (μ_B)	θ (K)
Cl	2.85	-7	5.09	-250
Br	3.98	-9	4.92	-67

Values are averaged results for 5 kG and 40 kG data.

Solution Studies

Measurement of the EPR spectra of sublimed samples of $[(C_5Me_5)Co(\mu\text{-}Cl)]_2$ and $[(C_5Me_5)Co(\mu\text{-}Br)]_2$ in methylcyclohexane glass at 2 K yielded no signal. Kölle sees a strong EPR signal at g = 2 in tetrahydrofuran solution, ascribed to $(C_5Me_5)Co(Cl)(thf)$.[1b] The significance of the discrepancies between our observations and Kölle's with respect to the paramagnetic species present in both solution and the solid-state will be discussed shortly.

The pentamethylcyclopentadienyl resonances in the ^1H NMR spectra of $[(C_5Me_5)Co(\mu\text{-}Cl)]_2$ and $[(C_5Me_5)Co(\mu\text{-}Br)]_2$ are quite broad ($\nu_{1/2}$ are *ca.* 500 Hz) and are shifted 30 to 40 ppm downfield from the expected position for this resonance in diamagnetic species. Once again, the results using sublimed material differs from those of Kölle's. The variable temperature behavior for these signals is shown in Figure 3. Both species exhibit distinctly non-linear behavior, which is most likely due to the occurrence of a temperature-dependent equilibrium in solution. The exact process occurring cannot be definitively determined, but a crossover experiment is informative.

Figure 3. Plot of δ vs. 1/T for $[(C_5Me_5)Co(\mu\text{-}X)]_2$ for X = Cl, Br.

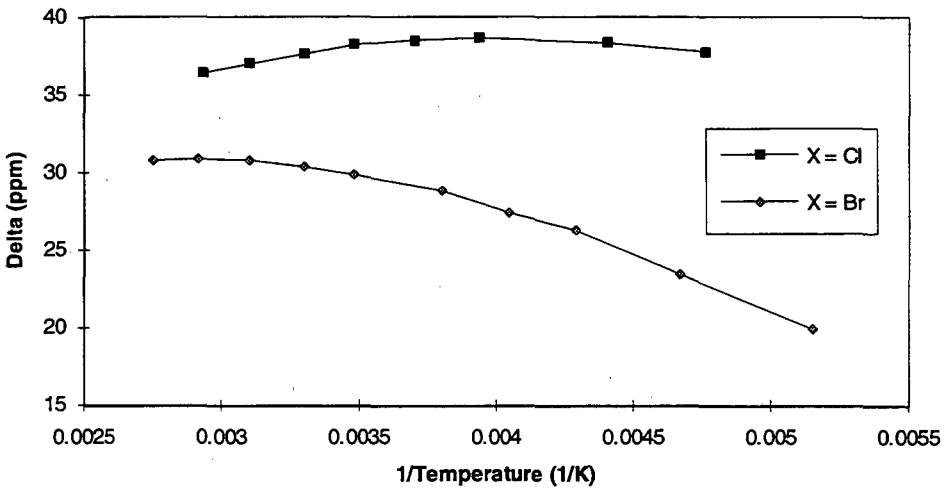

The variable temperature behavior for a 1:1 (molar) sample of $[(C_5Me_5)Co(\mu\text{-}Cl)]_2$:$[(C_5Me_5)Co(\mu\text{-}Br)]_2$ in toluene-d_8 is shown in Figure 4. Below 60 °C, the spectra show three signals in roughly a 1:2:1 intensity pattern. The lower intensity signals correspond to the chloride and bromide homo-dimers, compared to the measured spectra on the isolated complexes (Figure 3). The more intense signal occurs at the averaged chemical shift of the two symmetrical dimer species. At temperatures above 60 °C, the signals broaden into the baseline and coalesce into a single, extremely broad signal ($\nu_{1/2}$ > 1500 Hz).

Figure 4. Plot of δ vs. 1/T for $[(C_5Me_5)Co(\mu\text{-}Cl)]_2$:$[(C_5Me_5)Co(\mu\text{-}Br)]_2$ (1:1).

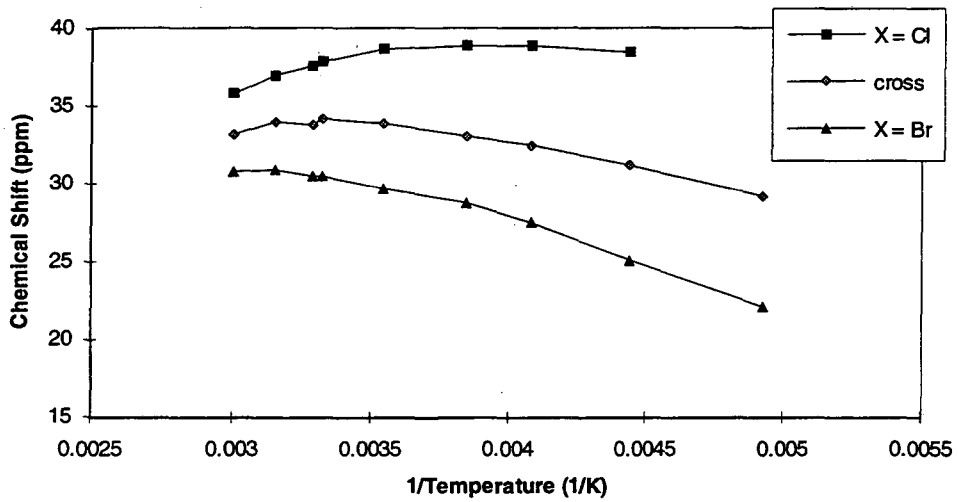

Discussion

Careful inspection of Kölle's results reveals some unusual behavior. The magnetic susceptibility data presented for $[(C_5Me_5)Co(\mu\text{-}Cl)]_2$ is very odd looking, with $1/\chi_M$ vs. T having a negative slope above 180 K. Also, there is still a residual magnetic moment at low temperature, which is attributed to "paramagnetic impurities [that are] always present in small proportions." The odd behavior at high temperature seems to indicate the presence of some

species of the formula $(C_5Me_5)Co(Cl)(L)$, since the curve approaches that reported for $(C_5Me_5)Co(Cl)$(pyridine) at higher temperatures.[1b] The presence of an EPR signal in hydrocarbon solvents that is attributed to a monomeric species solvated by the hydrocarbon is also suspicious.

The results obtained with sublimed samples of $[(C_5Me_5)Co(\mu\text{-}Cl)]_2$ and $[(C_5Me_5)Co(\mu\text{-}Br)]_2$ are much more consistent. The values summarized in Table 1 indicate the presence of two unpaired electrons per dimer at low temperature, with an increase in magnetic moment at higher temperatures. This could be due to thermal population of a high-spin state, as observed for monomeric $(C_5Me_5)Ni(acac)$ (Chapter 2). However, the results are also consistent with thermal population of a low-lying excited state that does not change the spin state, but significantly increases the spin-orbit coupling. In either case, the data is at odds with Kölle's results. Kölle's calculations were performed assuming θ = 0 K, which inspection of Table 1 shows to be an invalid assumption. Also, the moments were calculated per metal center, instead of for a dimeric molecular unit, which is not necessarily a valid treatment of the data.[4] Unfortunately, without definitive proof of the molecular geometry in the solid state, a microscopic (molecular) interpretation of the magnetic data is not possible.

The lack of an observable EPR signal in methylcyclohexane solution is consistent with an S = 1 ground state, as found by magnetic susceptibility. Zero-field splitting, which can be large for even-spin systems, could make the EPR spectrum unobservable.[5] Also, the lack of a signal in methylcyclohexane solution due to a "solvated" species is more reasonable than the results Kölle obtained in pentane and toluene solution.

Kölle's unusual EPR and magnetic data and the difficulties involved in the synthesis (related to the removal of tetrahydrofuran) all seem to indicate that $(C_5Me_5)Co(Cl)$(thf) is present in crystallized samples of $[(C_5Me_5)Co(\mu\text{-}Cl)]_2$.

Indeed, the crystals obtained from pentane solution for both halide dimers show evidence of solvent loss upon extended exposure to vacuum in order to remove traces of solvent. Since no EPR signal is observed in hydrocarbon solution with carefully sublimed material, a contamination of the dimer species with the thf adduct is the most reasonable explanation for the abnormalities noted in Kölle's results.

NMR Crossover Behavior

The variable temperature ^1H NMR behavior shown in Figure 3 indicates that a temperature-dependent equilibrium is present in solution for both $[(C_5Me_5)Co(\mu\text{-}Cl)]_2$ and $[(C_5Me_5)Co(\mu\text{-}Br)]_2$. The crossover experiment shown in Figure 4 exhibits a third resonance that occurs at the averaged position of the chloride and bromide homo-dimers, suggesting that it is due to the mixed bridge species shown in eq. 4. This behavior indicates that a monomer-dimer equilibrium, as originally proposed by Kölle, may be occurring in solution. The signals broaden and coalesce above 60 °C, apparently indicating that the exchange is too rapid above this temperature to observe signals due to the three discrete species. Unfortunately, the signals at all temperatures are extremely broad and defy line-shape analysis. There is no way to tell what process or processes are causing the exchange. Since EPR and other experiments indicate that tetrahydrofuran is not an "innocent" solvent for these systems, there is not much more that can be done with NMR to answer these questions.

$$[(C_5Me_5)Co(Cl)]_2 + [(C_5Me_5)Co(Br)]_2 \rightleftharpoons (C_5Me_5)Co\begin{matrix}\diagup Cl \diagdown \\ \diagdown Br \diagup\end{matrix}Co(C_5Me_5) \quad (4)$$

Oxidation Products

As discussed in Chapter 1, use of $[(C_5Me_5)Co(\mu\text{-}Cl)]_2$ as a starting material to make the cobalt cluster compounds was ultimately abandoned due to the presence of oxidation products. This led to the speculation that $[(C_5Me_5)CoCl(\mu\text{-}Cl)]_2$ (first reported by Kölle)[6] may be present in the starting material and that reaction of this cobalt(III) species with MeLi was producing the offending cobalt(III) cluster contaminating the product. Even though this did not prove true, a brief look into the properties of this cobalt(III) species was informative with regard to other reaction chemistry of the halide-bridged dimers.

Kölle's best synthetic route to $[(C_5Me_5)CoCl(\mu\text{-}Cl)]_2$ was discovered, presumably unintentionally, on his attempts to synthesize $(C_5Me_5)Co(Cl)(CO)$. The synthesis instead produced the valence disproportionation reaction products shown in eq. 5.[6]

$$2\,[(C_5Me_5)Co(Cl)]_2 + 4\,CO \xrightarrow{\text{pentane}} [(C_5Me_5)Co(Cl)_2]_2 + 2\,(C_5Me_5)Co(CO)_2 \quad (5)$$

Although the yields are quite good (> 80%), half of the cobalt ends up as an undesired carbonyl compound. Drawing on knowledge gained from studies of electron transfer reactions of Group 11 monohalides with low valent titanium and vanadium complexes,[7] reaction of $[(C_5Me_5)Co(\mu\text{-}Cl)]_2$ with anhydrous cuprous chloride in methylene chloride was found to produce the desired cobalt(III) species in virtually quantitative yield (eq. 6).

$$[(C_5Me_5)Co(\mu\text{-}Cl)]_2 + 2\,CuCl \xrightarrow{CH_2Cl_2} [(C_5Me_5)CoCl(\mu\text{-}Cl)]_2 + 2\,Cu^{\circ} \quad (6)$$

Kölle noticed that the spectral properties of $[(C_5Me_5)CoCl(\mu\text{-}Cl)]_2$ are dependent upon the polarity of the solvent used to make the physical measurements. The room temperature ^1H NMR signal for the C_5Me_5 ligand in benzene-d_6 appears at δ 0.75 ppm, but chemical shifts at δ 1.06 and 1.20 were found in CD_2Cl_2 and CD_3NO_2, respectively, by Kölle.[6] Also, solutions of $[(C_5Me_5)CoCl(\mu\text{-}Cl)]_2$ are green in non-polar solvents but aquamarine in polar solvents. This behavior is attributed to an equilibrium between a molecule with bridging and terminal chloride ligands (**A**) and a zwitterionic configuration with three bridging chlorides (**B**, eq. 7). Kölle contention is based upon the comparison with the properties of the complex $[(C_5Me_5)Co(\mu\text{-}Cl)_3Co(C_5Me_5)][PF_6]$, reported in the same article.

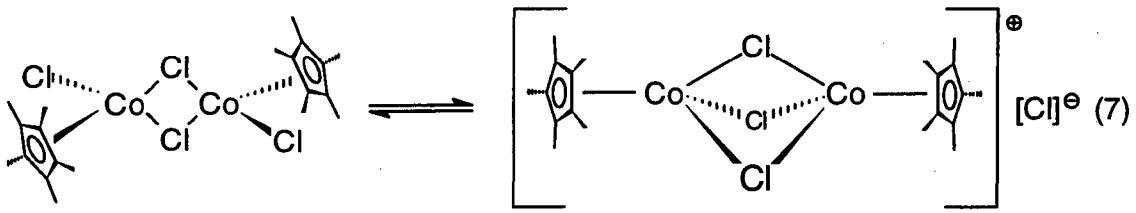

(7)

A **B**

Our mass spectroscopic data is not inconsistent with this explanation. Electron impact techniques on a solid sample yield a highest signal corresponding to loss of Cl_2, just as reported by Kölle.[6] However, use of fast-atom bombardment techniques on a sulfolane solution of the sample (which is aquamarine in color)[8] yields a heaviest ion corresponding to $(M - Cl)^+$, which is likely to be favored for isomer **B**. Though not definitive by itself, the mass spectroscopy of $[(C_5Me_5)CoCl(\mu\text{-}Cl)]_2$ supports the presence of the equilibrium in eq. 7.

Phosphine Adducts

Much of Kölle's reasoning about the halide-bridged dimers is based on comparisons with the properties of $(C_5Me_5)Co(Cl)(pyridine)$.[1b] This complex was synthesized by cleaving the chloride bridges in $[(C_5Me_5)Co(\mu\text{-}Cl)]_2$ with two equivalents of pyridine in pentane solution (eq. 8). Similar results were obtained using PMe_3 and PMe_2Ph with both the chloride and bromide dimers and with PPh_3 on the nickel bromide, $[(C_5Me_5)Ni(\mu\text{-}Br)]_2$.[2] However, in our hands performing the phosphine reactions with the cobalt(II) species in pentane produced a mixture of products, as judged by the isolation of two species, one red in color $[(C_5Me_5)Co(X)(PR_3)]$ and the other violet $[(C_5Me_5)Co(X)_2(PR_3)]$. Use of dichloromethane as a solvent was found to produce only the red species (the desired cobalt(II) complex). The synthesis of $(C_5Me_5)Co(Cl)_2(PEt_3)$ was accomplished using the same conditions with PEt_3 and $[(C_5Me_5)CoCl(\mu\text{-}Cl)]_2$ (eq. 9). Although only the PPh_3 adduct is reported by Kölle for the nickel systems,[2] Yamazaki and Mise have isolated this and related phosphine adducts *via* the routes shown in eqs. 10 and 11.[9]

$$[(C_5Me_5)M(\mu\text{-}X)]_2 + 2\,L \xrightarrow{\text{pentane or } CH_2Cl_2} 2\,(C_5Me_5)M(X)L \qquad (8)$$

$$M = Co,\ X = Cl, Br;\ M = Ni,\ X = Br$$
$$L = py,\ PR_3$$

$$[(C_5Me_5)CoCl(\mu\text{-}Cl)]_2 + 2\,PEt_3 \xrightarrow{CH_2Cl_2} 2\,(C_5Me_5)Co(Cl)_2PEt_3 \qquad (9)$$

$$[(C_5Me_5)Ni(CO)]_2 + I_2 \xrightarrow{Et_2O} 2\,(C_5Me_5)Ni(CO)I \quad (10a)$$

$$(C_5Me_5)Ni(CO)I + PR_3 \xrightarrow{Et_2O} (C_5Me_5)Ni(PR_3)I + CO \quad (10b)$$

$$(Ph_3P)_2NiX_2 + LiC_5Me_5 \xrightarrow{THF} (C_5Me_5)Ni(PPh_3)X + LiX + PPh_3 \quad (11)$$
$$X = Cl, Br$$

Both the cobalt and nickel phosphine adducts can be viewed as analogs of the $(C_5Me_5)M(acac)$ complexes since acac is a bidentate, three-electron ligand, and the combination of the halide and phosphine ligands is effectively the same. Structural and other characterizational data of the complexes $(C_5Me_5)M(X)(PR_3)$ (R = Me, Et; M = Co, X = Cl, Br; M = Ni, X = Br) were obtained for comparison to the acac complexes as well as to investigate the reaction chemistry of the bridging halide systems with Lewis bases. In addition, exploration of the utility of phosphine halides as synthons was needed.

General Properties

A summary of the properties of the phosphine complexes synthesized in this work is presented in Table 2. The detailed measurements presented later were performed on the PEt_3 complexes since they are more soluble than the PMe_3 complexes, allowing easier purification (all of the complexes decompose upon attempts at sublimation) and $(C_5Me_5)Co(Cl)(PMe_3)$ has been previously reported (values reported in Table 2 are for this work).[1b]

Table 2. Physical Properties of $(C_5Me_5)M(X)(PR_3)$ Complexes.

M	X	R	mp (°C)	color	EIMS
Co	Cl	Me	112 -115	dark red	M^+ observed
Co	Br	Me	121 -122	dark red	M^+ observed
Co	Cl	Et	160 -162	dark red	M^+ observed
Co	Br	Et	170 -171	dark red	M^+ observed
Co	Me	Et	94 - 95	dark red	M^+ observed
Ni	Br	Et	165 -167	clear red	M^+ observed
Ni	Me	Et	88 - 89	dark green	M^+ observed
Co	Cl_2	Et	140 -142	violet	as $[(C_5Me_5)Co(\mu\text{-}Cl)]_2$

The cobalt(II) halide species are all very similar. They crystallize as dark red plates from pentane solution, and yield weak molecular ions in the electron impact mass spectrum (a much stronger signal is observed for $(M - PR_3)^+$). The bromide species melt about 10 °C higher than their chloride analogues, and the PEt_3 complexes melt about 50 °C higher than their PMe_3 analogues. This is in contrast to the $(C_5Me_5)Ni(acac)(PR_3)$ species, where the PMe_3 and PEt_3 complexes melt at virtually the same temperature. $(C_5Me_5)Ni(Br)(PEt_3)$ crystallizes as air-stable, clear red plates from pentane solution. A strong molecular ion is observed in the EIMS (much more intense than for the cobalt(II) analog). This complex is diamagnetic ($\chi_M < 0$) in the solid state at all temperatures between 5 and 300 K. $(C_5Me_5)Co(Cl)_2(PEt_3)$ crystallizes as thin violet plates from diethyl ether and melts somewhat lower than its cobalt(II) analogue. The electron impact mass spectrum of $(C_5Me_5)Co(Cl)_2(PEt_3)$ shows the highest ion at 458, corresponding to $[(C_5Me_5)Co(\mu\text{-}Cl)]_2^+$. This is the same as the results observed for $[(C_5Me_5)CoCl(\mu\text{-}Cl)]_2$; apparently, the phosphine rapidly dissociates and the spectrum observed corresponds to that seen for the

cobalt(III) bridging chloride, with a highest mass peak due to $(M - Cl_2)^+$. The methyl complexes will be discussed later.

The solid-state magnetism of $(C_5Me_5)Co(Cl)(PEt_3)$ was measured to serve as a representative result for the whole class of cobalt(II) phosphine complexes. Magnetic susceptibility measurements (Fig. 5) exhibit Curie behavior, with a magnetic moment of 1.76 μ_B and θ = -1.5 K, indicating that these complexes have one unpaired electron that does not exhibit an orbital contribution to the magnetic moment.

Figure 5. Plot of $1/\chi_M$ vs. T for $(C_5Me_5)Co(Cl)(PEt_3)$.

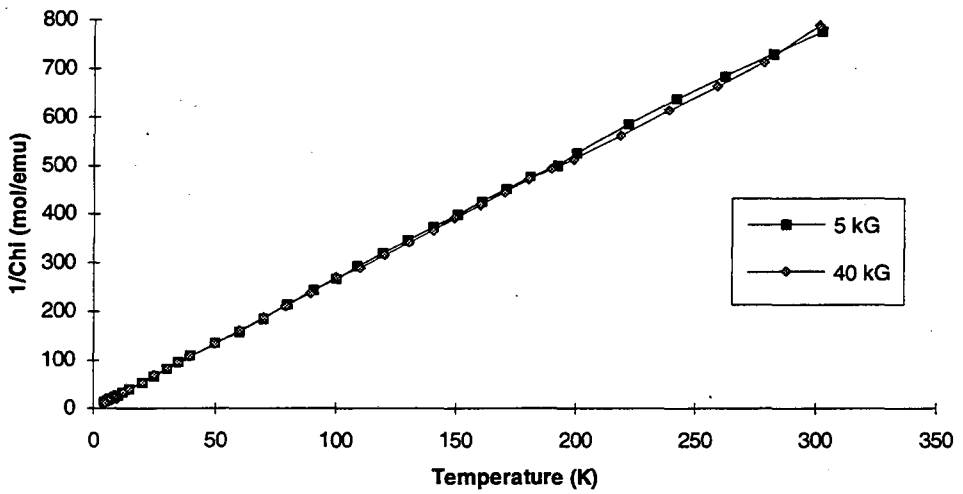

Crystallographic Studies

The X-ray crystal structures of $(C_5Me_5)Co(Cl)(PEt_3)$ and $(C_5Me_5)Ni(Br)(PEt_3)$ were measured to obtain comparisons between the phosphine halide complexes and the $(C_5Me_5)M(acac)$ complexes. The complexes are isomorphous, crystallizing in the space group $P\bar{4}$ (No. 81). Two views of each of the crystal structures of the phosphine halide complexes are shown in Figures 6 through 9, with the bond distances and angles listed in Tables 3 through 6. Important values for comparisons to the acac complexes are summarized in the discussion section.

Figure 6. ORTEP Diagram of $(C_5Me_5)Co(Cl)(PEt_3)$, Side View.

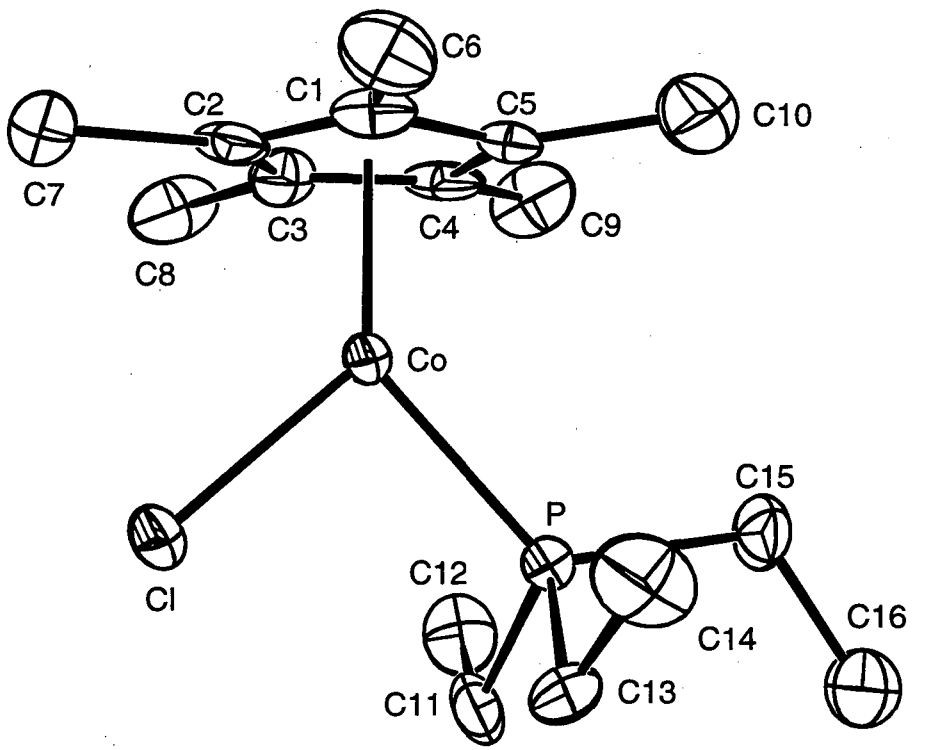

Figure 7. ORTEP Diagram of $(C_5Me_5)Co(Cl)(PEt_3)$, Edge View.

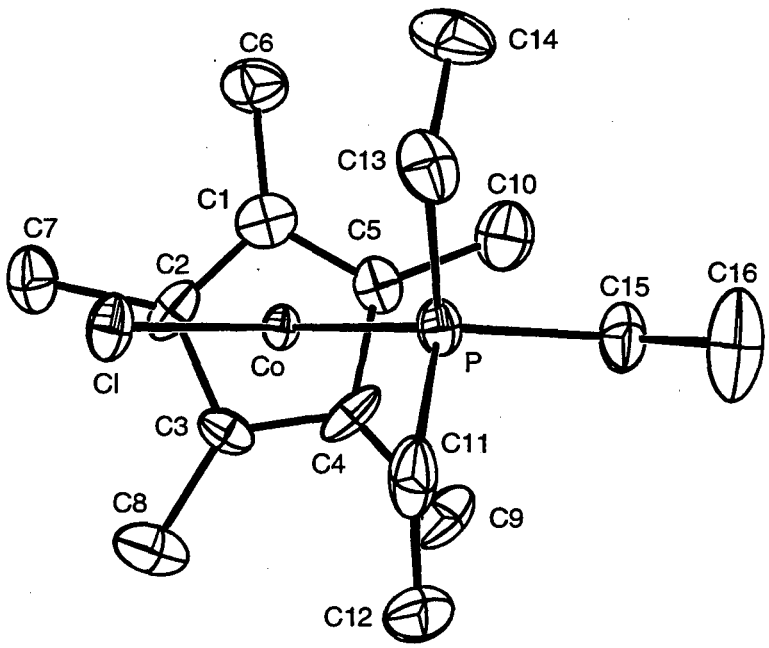

Table 3. Bond Distances for $(C_5Me_5)Co(Cl)(PEt_3)$ (Å).

Co-Cp	1.695	Co-P	2.207 (2)
		Co-Cl	2.214 (2)
Co-C1	2.119 (9)	C1-C2	1.404 (12)
Co-C2	2.040 (8)	C1-C5	1.415 (12)
Co-C3	2.092 (9)	C2-C3	1.437 (12)
Co-C4	2.057 (8)	C3-C4	1.369 (12)
Co-C5	2.076 (8)	C4-C5	1.429 (11)
Co-C_b (ave)	2.058 (6)	C_a-C_b (ave)	1.410 (9)
Co-C_c (ave)	2.075 (6)	C_b-C_c (ave)	1.433 (8)

Cp is the ring centroid of atoms C1-C5. C_a, C_b, and C_c refer to the labeling scheme in Figures 3 and 10 in Chapter 2.

Table 4. Bond Angles for $(C_5Me_5)Co(Cl)(PEt_3)$ (°).

P-Co-Cl	91.54 (8)	C2-C1-C5	105.4 (7)
Cp-Co-Cl	131.2	C1-C2-C3	110.5 (7)
Cp-Co-P	137.2	C2-C3-C4	105.9 (7)
		C3-C4-C5	109.6 (7)
C_a-C_b-C_c (ave)	109.5 (5)	C1-C5-C4	108.4 (7)
C_b-C_c-C_c (ave)	107.8 (5)		

Figure 8. ORTEP Diagram of $(C_5Me_5)Ni(Br)(PEt_3)$, Side View.

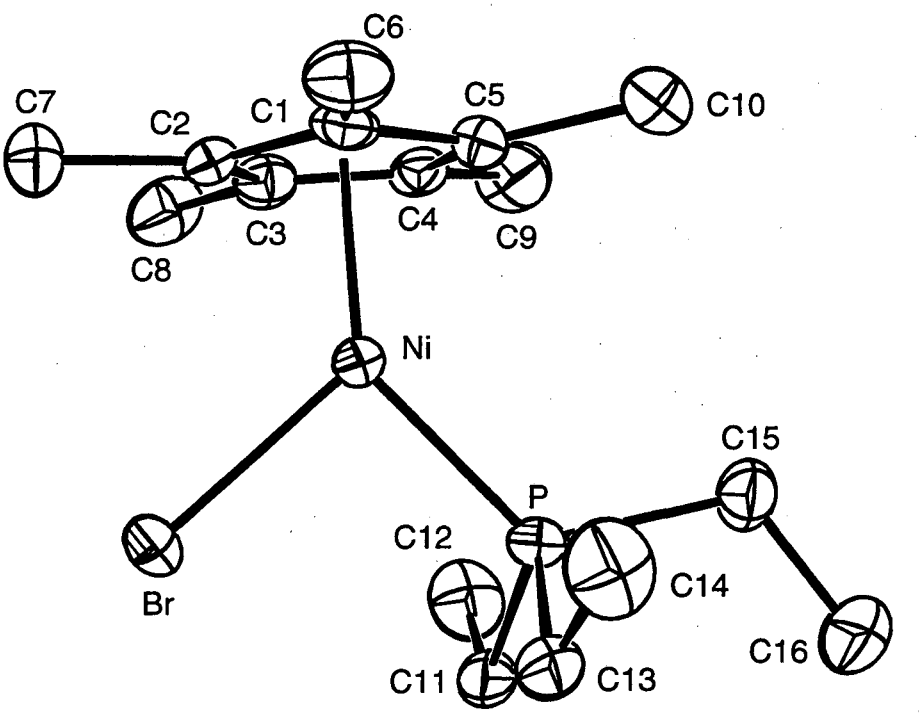

Figure 9. ORTEP Diagram of $(C_5Me_5)Ni(Br)(PEt_3)$, Edge View.

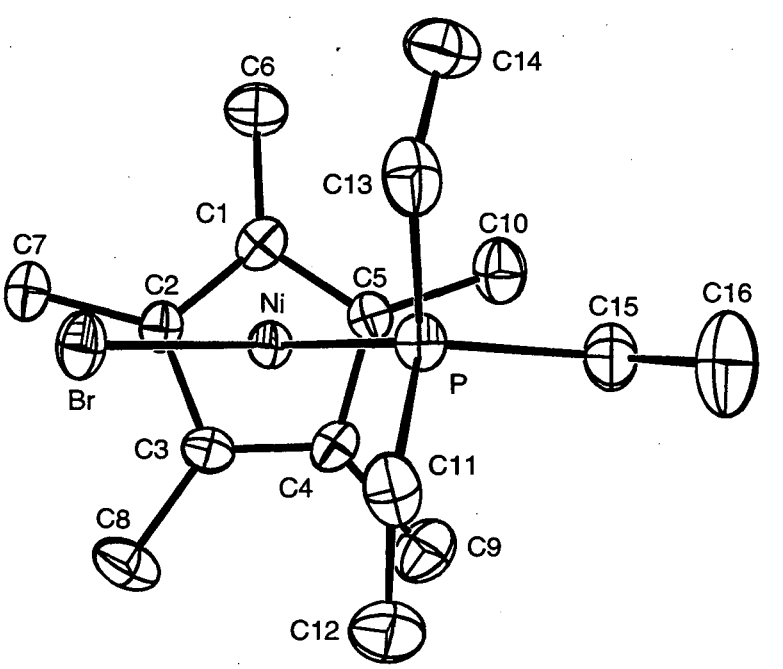

Table 5. Bond Distances for $(C_5Me_5)Ni(Br)(PEt_3)$ (Å).

Ni-Cp	1.755	Ni-P	2.160 (2)
		Ni-Br	2.335 (1)
Ni-C1	2.159 (7)	C1-C2	1.418 (9)
Ni-C2	2.112 (6)	C1-C5	1.428 (9)
Ni-C3	2.160 (7)	C2-C3	1.445 (9)
Ni-C4	2.148 (6)	C3-C4	1.368 (9)
Ni-C5	2.084 (6)	C4-C5	1.466 (9)
$Ni-C_b$ (ave)	2.098 (4)	C_a-C_b (ave)	1.423 (6)
$Ni-C_c$ (ave)	2.154 (5)	C_b-C_c (ave)	1.456 (6)

Cp is the ring centroid of atoms C1-C5. C_a, C_b, and C_c refer to the labeling scheme in Figures 3 and 10 in Chapter 2.

Table 6. Bond Angles for $(C_5Me_5)Ni(Br)(PEt_3)$ (°).

P-Ni-Br	92.46 (5)	C2-C1-C5	105.7 (6)
Cp-Ni-Br	127.7	C1-C2-C3	109.3 (6)
Cp-Ni-P	139.6	C2-C3-C4	108.6 (6)
		C3-C4-C5	107.4 (6)
$C_a-C_b-C_c$ (ave)	109.0 (4)	C1-C5-C4	108.7 (6)
$C_b-C_c-C_c$ (ave)	108.0 (4)		

Solution Properties

The EPR spectrum of $(C_5Me_5)Co(Cl)(PEt_3)$ is shown in Figure 10. The signal is rhombic at low temperatures and centered at g = 2, with each portion of the signal exhibiting hyperfine coupling with the ^{59}Co nucleus (I = 7/2). The high field term (g_3) also shows superhyperfine coupling to the ^{31}P nucleus. The EPR spectrum of $(C_5Me_5)Co(Br)(PEt_3)$, shown in Figure 11, is qualitatively the same as that of the chloride analog. However, the signal is broadened, most likely due to superhyperfine splitting by bromine (both ^{79}Br and ^{81}Br have I = 3/2).

Figure 10. EPR Spectrum of $(C_5Me_5)Co(Cl)(PEt_3)$ in C_7H_{14} Glass (77 K).

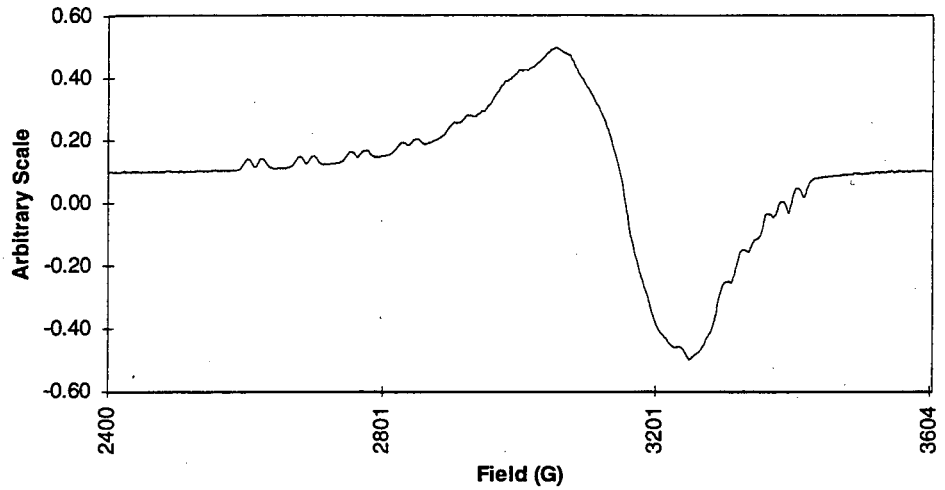

Figure 11. EPR Spectrum of $(C_5Me_5)Co(Br)(PEt_3)$ in C_7H_{14} Glass (81 K).

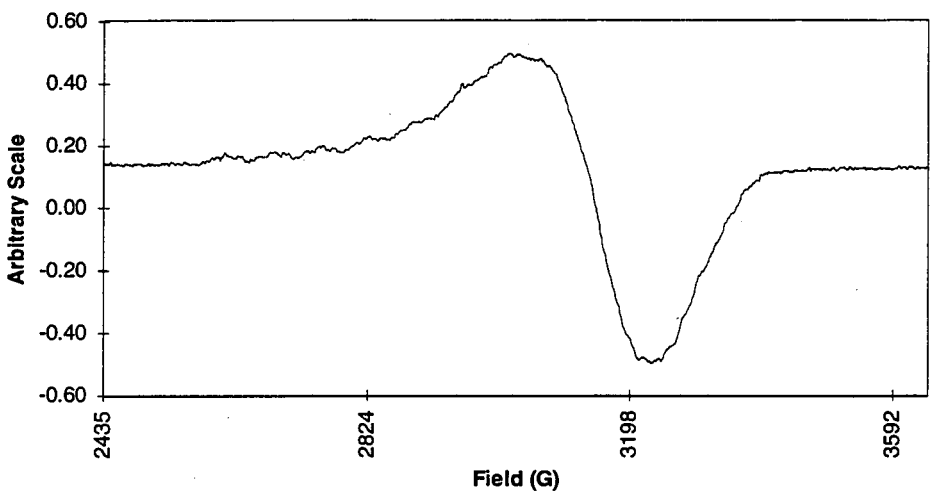

All of the cobalt(II) phosphine halide complexes exhibit a single, broad ($\nu_{1/2} \approx 150$ Hz) resonance in the ^1H NMR that is slightly upfield of 0 ppm, but do not have a $^{31}P\{^1H\}$ signal. When a small amount (*ca.* 5 μL) of the appropriate free phosphine was added to an NMR sample of $(C_5Me_5)Co(X)(PR_3)$, the single

observed signal shifted towards the diamagnetic region. No signal due to free phosphine was observed.

The ^1H NMR spectrum of $(C_5Me_5)Ni(Br)(PEt_3)$ shows narrow signals in the diamagnetic region that are invariant with temperature (coupling to ^{31}P is observed for all of the resonances). Also, a sharp singlet ($\nu_{1/2} \approx 5$ Hz) at δ 24.5 ppm is observed in the $^{31}P\{^1H\}$ NMR spectrum. When free PEt_3 was added to the nickel complex, the signals were unchanged and the spectrum exhibited signals attributable to uncoordinated PEt_3. The $^{31}P\{^1H\}$ spectra show this more clearly than the ^1H spectra because the signals do not overlap (uncoordinated PEt_3 has a ^{31}P chemical shift of δ -20 ppm) in the $^{31}P\{^1H\}$ spectra as they do in the ^1H spectra. This complex did not exhibit an EPR signal.

The solution behavior of $(C_5Me_5)Co(Cl)_2(PEt_3)$ is also unremarkable. The ^1H NMR has sharp signals, exhibiting ^{31}P coupling, just like that found in the nickel(II) complex. Its $^{31}P\{^1H\}$ signal is substantially broader ($\nu_{1/2} \approx 110$ Hz at δ 25.3 ppm) than that of the nickel(II) species, probably due to the large quadrupole moment of ^{59}Co. Addition of free PEt_3 does not perturb the signals due to the cobalt(III) complex, and signals due to uncoordinated PEt_3 are observed.

<u>$(C_5Me_5)M(Me)(PEt_3)$</u>

Curiously, the cobalt(II) phosphine adducts are unreactive towards methylating agents. Combining any of these complexes with MeLi, Me_2Mg, or Grignard reagents results in recovery of unreacted starting materials. Reaction with $AlMe_3$ in dichloromethane solution produces a color change, but attempts to isolate a discrete compound were unsuccessful. Yamazaki and Mise report that $(C_5Me_5)Ni(I)(PR_3)$ reacts with MeLi to produce $(C_5Me_5)Ni(Me)(PR_3)$ (R = Ph) and with LiC≡CPh to make $(C_5Me_5)Ni(C{\equiv}CPh)(PR_3)$ (R = Me).[9] However, both of

these reactions proceed in low yield (34 and 36%, respectively), and apparently the substitution reactions do not work for the chloride or bromide analogs.

Fortuitously, the desired complexes, $(C_5Me_5)M(Me)(PEt_3)$, were isolated from trapping experiments used to investigate the mechanism of formation of $(C_5Me_5)_3M_3(\mu_3\text{-}CH)(\mu\text{-}H)$ (as discussed in Chapter 1). Although it was later shown that PEt_3 coordinates to $(C_5Me_5)Ni(acac)$ (see Chapter 2), thus rendering the results useless from a mechanistic point of view, the reaction shown in eq. 12 is still an excellent route (and the only one) to $(C_5Me_5)M(Me)(PEt_3)$.

$$(C_5Me_5)M(acac) + PEt_3 + MeLi \xrightarrow[Et_2O]{} (C_5Me_5)M(Me)(PEt_3) + Li(acac) \quad (12)$$

yield: M = Ni, 81%
M = Co, 69%

Crystallographic Disorder of Methyl Complex

The X-ray crystal structure of $(C_5Me_5)Ni(Me)(PEt_3)$ was determined so that the "ene-allyl" distortion could be documented when the X-ligand is only a sigma donor. In addition, both $(C_5Me_5)M(Me)(PEt_3)$ complexes exhibit a small, sharp band around 2250 cm^{-1} in the infrared spectra. This is most likely an overtone combination of one or more of the strong bands due to PEt_3, but the band is only seen for the methyl complexes (none of the halide species have this band). The possibility that there is some unusual interaction of the methyl group with the metal centers provided added impetus for determination of the structure of $(C_5Me_5)Ni(Me)(PEt_3)$. The complex crystallizes in the same space group as the other two PEt_3 complexes ($P\bar{4}$), but suffers from disorder across a pseudo-mirror plane (Figure 12). Attempts to deconvolute the structure by treating it as a twinned crystal were unsuccessful. Instead, the pentamethylcyclopentadienyl ring had to be modeled by treating the methyl groups as two partial occupancy

carbons (relative populations of 2:1, with the lower occupancy sites denoted by an "a" in the label). The model of the disorder is shown in Figure 13, and bond distances and angles are in Tables 7 and 8, respectively. The pseudo-mirror plane contains the nickel atom, phosphorus atom, C2, C15, C16, and C17. The inaccuracy of the structure precludes any detailed discussion of the distortion in the C_5Me_5 ring.

Figure 12. ORTEP Diagram of $(C_5Me_5)Ni(Me)(PEt_3)$, Side View.

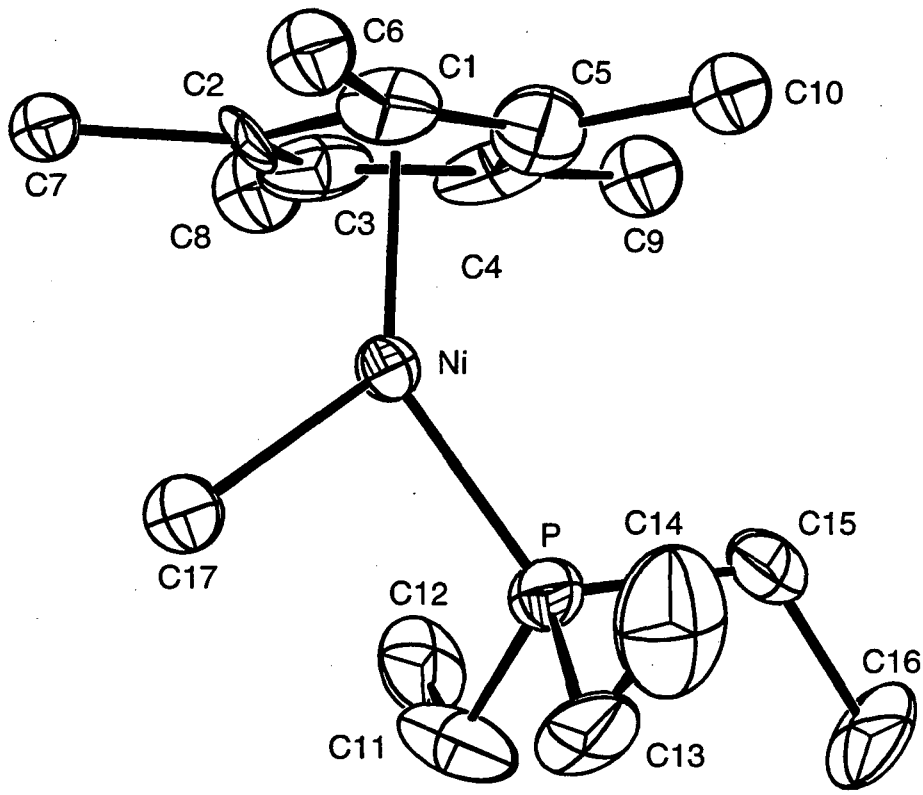

Figure 13. ORTEP Diagram of the Disorder Model of $(C_5Me_5)Ni(Me)(PEt_3)$.

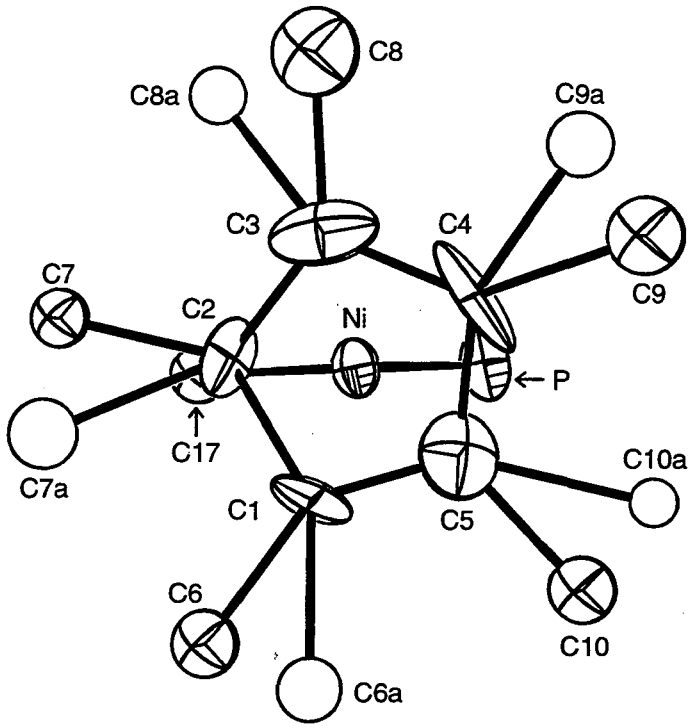

Table 7. Bond Distances for $(C_5Me_5)Ni(Me)(PEt_3)$ (Å).

Ni-Cp	1.76	Ni-P	2.109 (4)
		Ni-C17	1.96 (1)
Ni-C1	2.12 (2)	C1-C2	1.43 (2)
Ni-C2	2.05 (1)	C1-C5	1.33 (2)
Ni-C3	2.17 (2)	C2-C3	1.37 (2)
Ni-C4	2.14 (2)	C3-C4	1.42 (2)
Ni-C5	2.12 (2)	C4-C5	1.39 (2)

Cp is the ring centroid of atoms C1-C5.

Table 8. Bond Angles for $(C_5Me_5)Ni(Me)(PEt_3)$ (°).

P-Ni-C17	90.2 (4)	C2-C1-C5	105 (1)
Cp-Ni-C17	129	C1-C2-C3	112 (1)
Cp-Ni-P	141	C2-C3-C4	105 (1)
		C3-C4-C5	108 (1)
		C1-C5-C4	111 (2)

General and Solution Properties of Methyl Complexes

The alkyl, $(C_5Me_5)Co(Me)(PEt_3)$, crystallizes as dark red plates from pentane solution. The EPR spectrum is shown in Figure 14. The spectrum is of the same type as that observed for $(C_5Me_5)Co(Cl)(PEt_3)$, except that the lines are even sharper for the methyl complex, presumably due to the loss of electron-nuclear coupling with the chloride or bromide nuclear spins. The simulation of this spectrum (Figure 15) was used as a reference for beginning simulation of the chloride and bromide analogues, since the hyperfine coupling is better resolved for the methyl complex (the simulation program cannot model superhyperfine coupling - hence, the coupling to ^{31}P in g_3 is not present in the simulated spectrum).

As with the halide-phosphine complexes, $(C_5Me_5)Co(Me)(PEt_3)$ exhibits a single broad resonance in the ^1H NMR spectrum that is slightly upfield of 0 ppm. This signal shifts towards the diamagnetic region when excess PEt_3 is added to the sample. No signal due to free phosphine is observed under these conditions.

Figure 14. EPR Spectrum of $(C_5Me_5)Co(Me)(PEt_3)$ in C_7H_{14} Glass (84 K).

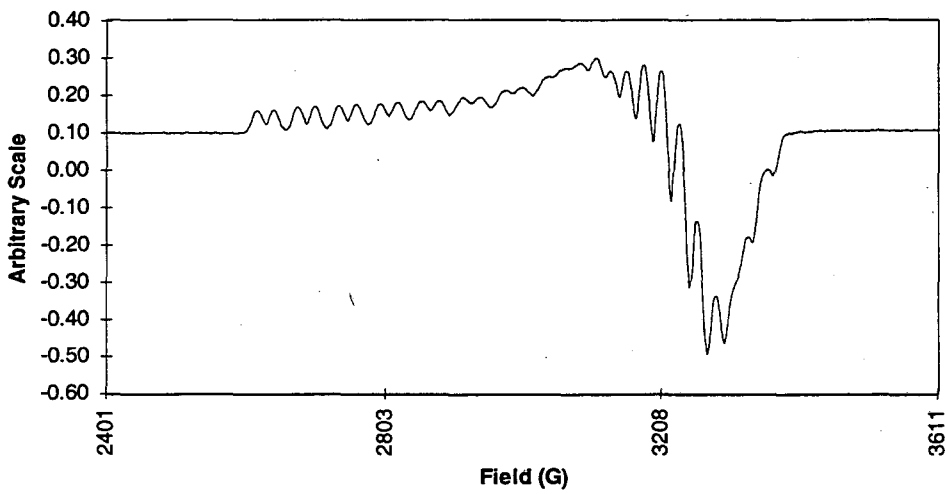

Figure 15. Simulated EPR Spectrum of $(C_5Me_5)Co(Me)(PEt_3)$.

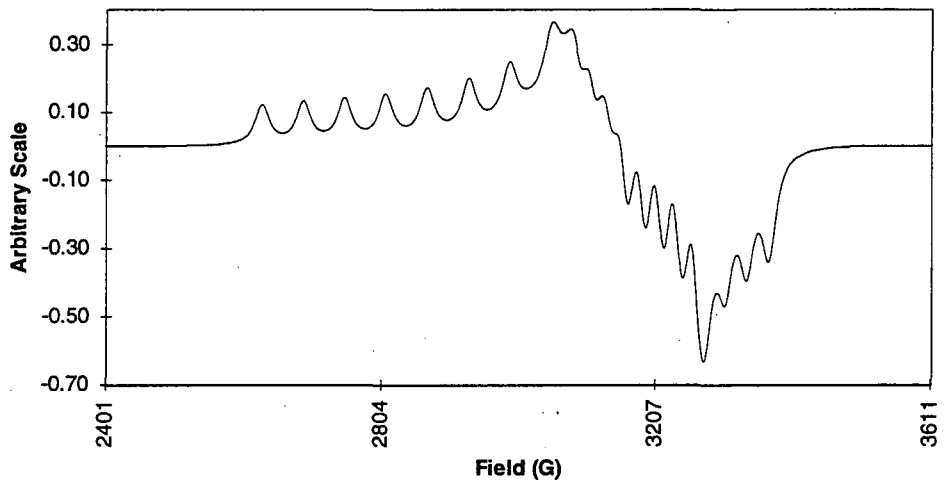

$(C_5Me_5)Ni(Me)(PEt_3)$ appears anomalous in that it crystallizes as dark green plates, instead of the ubiquitous red color found for all of the other divalent phosphine complexes. However, $(C_5Me_5)Ni(Me)(PPh_3)$ and $(C_5Me_5)Ni(C\equiv CPh)(PMe_3)$ are also reported as dark green solids,[9] and the ^1H NMR spectrum of $(C_5Me_5)Ni(Me)(PEt_3)$ is just as expected for a diamagnetic phosphine complex: sharp resonances, exhibiting coupling to the ^{31}P nucleus. The $^{31}P\{^1H\}$ NMR spectrum exhibits a single, sharp resonance ($\nu_{1/2} \approx 5$ Hz) at δ 34.9 ppm. Addition of free PEt_3 only produces a second set of signals attributable to uncoordinated PEt_3. No change in the signals due to $(C_5Me_5)Ni(Me)(PEt_3)$ is observed. No EPR signal was observed for $(C_5Me_5)Ni(Me)(PEt_3)$.

Comparison of Acac and Phosphine Complexes

The magnetic and EPR properties of the complexes $(C_5Me_5)Co(X)(PEt_3)$ and $(C_5Me_5)Ni(X)(PEt_3)$ differ markedly from that of the corresponding $(C_5Me_5)M(acac)$ complexes. The cobalt(II) phosphine complexes all exhibit EPR spectra with an average g value very close to 2, and the measured solid-state

magnetic moment of $(C_5Me_5)Co(Cl)(PEt_3)$ is 1.76 μ_B. This indicates that orbital angular momentum is quenched for the phosphine complexes, whereas this is not the case for $(C_5Me_5)Co(acac)$, which has μ_{eff} = 1.93 μ_B and an average g value of 2.099. Also, both $(C_5Me_5)Ni(Br)(PEt_3)$ and $(C_5Me_5)Ni(Me)(PEt_3)$ do not show any evidence of the spin-equilibrium observed for $(C_5Me_5)Ni(acac)$.

These differences can be explained by inspecting the molecular orbital diagrams used in Chapter 2 to explain these phenomena in $(C_5Me_5)M(acac)$ complexes (Figures 11 and 16 in that chapter). Even though the symmetry of the phosphine complexes is lower than that of the acac complexes, the general coordination geometry of a T-shaped $CpML_2$ molecule is maintained. Thus, the qualitative ordering of the molecular orbital levels in Figure 2-11 is unchanged. However, the acac ligand is capable of π-donation, producing a small HOMO-LUMO gap (as shown in Figure 2-16). For the phosphine complexes, only the halide ligands can act as π-donors, as the phosphine and methyl ligands are effectively only σ-donors. This has the effect of increasing the HOMO-LUMO gap relative to the acac complexes, and this increased gap produces the differences in the properties of the two classes of complexes. The incomplete quenching of the angular momentum of the unpaired electron in $(C_5Me_5)Co(acac)$ indicates that the unpaired electron must reside at times in both the HOMO and LUMO orbitals, since the HOMO has a' symmetry (which cannot have an orbital contribution to the moment)[10] in rigorous C_s symmetry (the labels b_1^* and b_2^* only denote the parentage of the hybrid orbitals based on the C_{2v} ML_2 fragment). Similarly, the spin-equilibrium observed for $(C_5Me_5)Ni(acac)$ is produced by thermal population of the LUMO. None of the phosphine complexes exhibit either of these phenomena, indicating that the HOMO-LUMO gap is indeed larger for these complexes.

This orbital model also explains the structural similarities of $(C_5Me_5)M(acac)$ and $(C_5Me_5)M(X)(PEt_3)$ seen in the X-ray crystallographic studies. Figure 16 shows the averaged carbon-carbon bond distances in the pentamethylcyclopentadienyl ring of the four related complexes. Both nickel complexes show a pronounced "ene-allyl" distortion, while the two cobalt complexes show a smaller variation in bond lengths, indicating that any distortion of this type in the cobalt complexes is on the order of the error of the experiment. However, $(C_5Me_5)Co(Cl)(PEt_3)$ shows a larger variation than does $(C_5Me_5)Co(acac)$, quite possibly due to the differing location of the unpaired electron in these complexes. As discussed in Chapter 2, the "ene-allyl" distortion is a direct result of the population of the b_2^* orbital, which has non-cylindrical π-electron density in the cyclopentadienyl ring orbitals. Since magnetic and EPR studies indicate that the electron is always in the b_2^* orbital for $(C_5Me_5)Co(Cl)(PEt_3)$, the "ene-allyl" distortion for this molecule would be expected to be larger than for $(C_5Me_5)Co(acac)$, whose unpaired electron partially occupies both b_1^* (which does not produce an "ene-allyl" distortion) and b_2^*. This corresponds exactly to the observed structural data for these two complexes. Table 9 summarizes the variations in the metal-ring carbon distances and the folding angle (ω) of these structures. The metal-ring carbon distances of the phosphine complexes are not as regular as those of the acac species, due to the asymmetric steric and electronic environment produced when the halide and phosphine ligands replace the two oxygens of the acac ligand. This asymmetry reduces the magnitude of the variation in the averaged metal-ring carbon distances, and reduces the significance of the value of ω. However, comparison of these distances and inspection of the edge views of the halide-phosphine structures (Figures 7 and 9) again shows that $(C_5Me_5)Ni(Br)(PEt_3)$ exhibits a large "ene-allyl" distortion while $(C_5Me_5)Co(Cl)(PEt_3)$ exhibits

variations that indicate that any distortion present is of a substantially smaller magnitude. Thus, the acac and halide-phosphine complexes exhibit similar solid-state distortions, even though they have different solution properties.

Figure 16. Averaged Bond Lengths (Å) of "Ene-allyl" Systems.

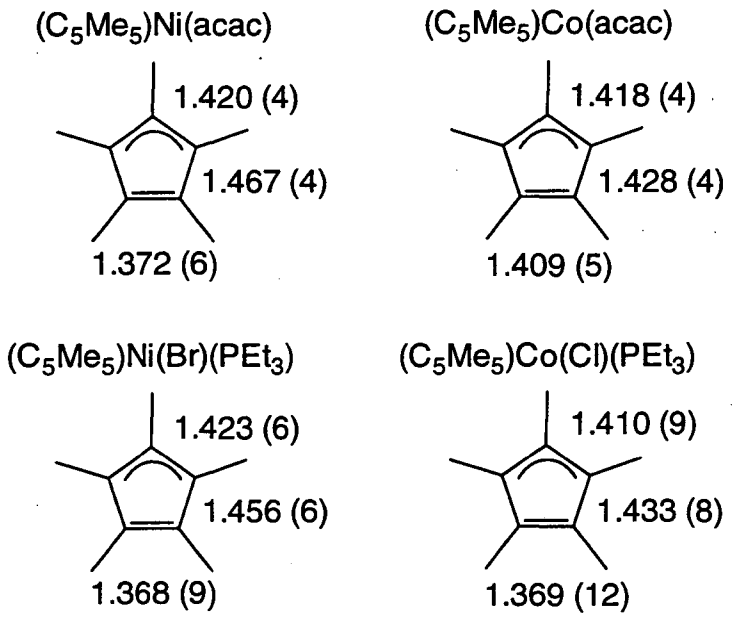

Table 9. Summary of Important Structural Parameters in "Ene-allyl" Systems

Compound	d(M-C_a)[a]	d(M-C_b)[a]	d(M-C_c)[a]	Δ	ω[b]
(C_5Me_5)Ni(acac)	2.133 (3)	2.068 (3)	2.192 (3)	0.124	9.3
(C_5Me_5)Co(acac)	2.105 (3)	2.056 (2)	2.089 (2)	0.033	4.2
(C_5Me_5)Ni(Br)(PEt_3)	2.159 (7)	2.098 (4)	2.154 (5)	0.056	5.2
(C_5Me_5)Co(Cl)(PEt_3)	2.119 (9)	2.058 (6)	2.075 (6)	0.017	3.2

[a]Averaged values in Å.

[b]Angle in degrees.

Unfortunately, extension of this analysis to the methyl-phosphine complexes was thwarted by the rotationally-disordered structure observed for $(C_5Me_5)Ni(Me)(PEt_3)$. Even though the complex crystallizes in the same space group as the halide-phosphine complexes ($P\bar{4}$), little useful information can be obtained from the structure. The disorder has the dual role of masking hydrogen atom positions on the methyl group (and thus any unusual interactions present) and rendering carbon-carbon and metal-ring carbon distances inaccurate enough to remove any evidence of an "ene-allyl" distortion (bond distances and angles in Tables 7 and 8, respectively). Thus, nothing more can be determined about the structural details of $(C_5Me_5)Ni(Me)(PEt_3)$.

Phosphine Exchange Studies

The isolation of a number of 17- and 18-electron phosphine complexes allows us to investigate the effects of electronic structure on ligand labilities. The standard experiment for determination of phosphine exchange in solution involves observing the NMR spectrum for the complex and then determining the changes in the spectrum upon addition of a small amount (3 to 5 μL) of free phosphine. These experiments were performed for all of the PEt_3 complexes presented in this work, and the results can be categorized by the metal centers studied, specifically Co(II), Ni(II), and Co(III).

As mentioned earlier, every cobalt(II) complex of the general formula $(C_5Me_5)Co(X)(PEt_3)$ showed evidence of rapid exchange between coordinated and free PEt_3 in solution. Also, the two nickel(II) species synthesized for this work, $(C_5Me_5)Ni(Br)(PEt_3)$ and $(C_5Me_5)Ni(Me)(PEt_3)$, exhibit no evidence of this exchange at room temperature. EPR data and X-ray structural analysis indicate that all of these complexes have virtually the same geometry, so the source of the differences in exchange rates must be electronic. Classical coordination

chemistry treats a cyclopentadienyl ligand as a tridentate ligand, since it takes up three of the six coordination sites in an octahedral coordination environment.[11] This makes the divalent phosphine complexes formally five-coordinate. In aqueous coordination chemistry, five-coordinate species can undergo ligand exchange by way of two general pathways: associative or dissociative. For associative processes, five-coordinate nickel(II) species react faster than the corresponding cobalt(II) species.[12] This is because association of a sixth ligand produces a transition state with electrons in strongly metal-ligand antibonding orbitals (in this case, the orbitals are of 2e parentage: see Figure 21 in Chapter 2 for the molecular orbital diagram of the $CpML_3$ transition state). Since the nickel(II) intermediate has one more electron in this antibonding level than the cobalt(II) intermediate, the exchange process is faster for nickel(II). The dissociative mechanism would involve loss of coordinated PEt_3, producing an intermediate of the general formula $(C_5Me_5)M(X)$ with 15 electrons for M = cobalt and 16 electrons for M = nickel. Although the geometry may be distorted, the intermediate can be considered pseudo-tetrahedral. In this case, cobalt(II) complexes are known to react faster than nickel(II) species,[12] since four-coordinate cobalt(II) low-spin complexes favor a tetrahedral geometry, whereas four-coordinate nickel(II) low-spin complexes favor a square-planar geometry. Hence, there is less reorganization energy needed for the cobalt(II) species to exchange ligands by a dissociative mechanism. Since phosphine exchange is rapid for $(C_5Me_5)Co(X)(PEt_3)$ at room temperature, yet is not observed for $(C_5Me_5)Ni(X)(PEt_3)$ at room temperature, it is most likely that the mechanism involved is of a dissociative nature. Of course, rigorous study of the phosphine exchange process by standard kinetic techniques is necessary to determine the mechanism that best models this process.

The lack of reactivity of $(C_5Me_5)Co(Cl)_2(PEt_3)$ with free PEt_3 is easier to explain. The compound is a pseudo-octahedral, low-spin cobalt(III) complex. Compounds of this type have been investigated extensively due to their conveniently slow ligand exchange rates.[12] These species have been found to undergo ligand exchange by way of mechanisms that are dissociative in nature.[12] Since $(C_5Me_5)Co(Cl)_2(PEt_3)$ does not show any evidence of phosphine exchange at room temperature, there probably isn't any significant amount of steric crowding around the cobalt(III) center, since steric crowding has been shown to greatly increase the rate of ligand exchange for dissociative systems.[12] As for the nickel(II) species, the fact that no exchange is observed at room temperature in the $^{31}P\{^1H\}$ NMR spectra merely indicates that any exchange occurring must be slow relative to the NMR timescale, which is not inconsistent with results seen with other cobalt(III) species. Further kinetic studies at higher temperatures are necessary to determine if exchange is occurring at all in the 18-electron systems.

References

1. (a) Kölle, U.; Khouzami, F.; Fuss, B., *Angew. Chem., Int. Ed. Engl.*, **1982**, *21*, 131.
(b) Kölle, U.; Fuss, B.; Belting, M.; Raabe, E., *Organometallics*, **1986**, *5*, 980.

2. Kölle, U.; Fuss, B.; Khouzami, F.; Gersdorf, J, *J. Organomet. Chem.*, **1985**, *290*, 77.

3. Pinhas, A. R.; Hoffmann, R., *Inorg. Chem.*, **1979**, *18*, 654.

4. Lukens, W. W., Jr., personal communication.

5. Drago, R. S., "Physical Methods in Chemistry," W. B. Saunders: Philadelphia, **1977**.

6. Kölle, U.; Fuss, B., *Chem. Ber.*, **1984**, *117*, 743.

7. Matsunaga, P. T., Ph.D. Thesis, University of California, Berkeley, **1991**.

8. Ogden, S., personal communication.

9. Mise, T.; Yamazaki, H., *J. Organomet. Chem.*, **1979**, *164*, 391.

10. Jolly, W. H., "The Synthesis and Characterization of Inorganic Compounds," Prentice-Hall: Englewood Cliffs, NJ, **1970**.

11. Albright, T. A.; Burdett, J. K.; Whangbo, M. H., "Orbital Interactions in Chemistry," John Wiley and Sons: New York, **1985**.

12. Langford, C. H.; Gray, H. B., "Ligand Substitution Processes," W. A. Benjamin: London, **1966**.

Chapter 4

Crystallographic Studies of Distortions in Metallocenes with C_5-symmetrical Cyclopentadienyl Rings

Since the discovery[1] and structural characterization[2,3] of ferrocene in the early 1950's, metallocenes have played a central role in studies involving physical properties and reactivity of organometallic complexes that are dependent on the electronic structure of the complexes. Over time, metallocenes have been synthesized using a wide variety of substituted cyclopentadienyl rings, and with the discovery of a convenient route to pentamethylcyclopentadiene,[4] the synthesis of decamethylmetallocenes for most of the first row transition metals has been achieved.[5] The bulk solution and solid-state properties of these complexes indicate that the permethylated species have the same electronic configurations as their unsubstituted analogues (with the exception of the manganocenes).[6,7] However, several of the X-ray crystal structures of the decamethylmetallocenes and their salts exhibit unusual distortions that have been attributed to static Jahn-Teller distortions.[8] Since these structures were performed at room temperature and D_5 symmetrical metallocenes have a history of producing problematic X-ray crystal structures (the confusion over the point symmetry of ferrocene in the solid state is one example),[9] low-temperature studies of the crystal structures of lower symmetry metallocenes are warranted. This work involves the systematic investigation of the X-ray crystallographic structures of pentamethylmetallocenes, $(C_5Me_5)M(C_5H_5)$, where M = Mn, Fe, Co, and Ni. Our hope is that the reduction in symmetry of the metallocenes to C_{5v} will improve the quality of the crystal structures by producing more well-ordered crystals than those seen for D_5-symmetrical metallocenes.

Previous Work

Table 1 shows a summary of unsubstituted and permethylated metallocenes for the metals discussed in this work, with their proposed electronic ground states, solution magnetic moments, and metal-centroid distances listed. The configurations are based on the standard molecular orbital diagram for D_{5d} metallocenes shown in Figure 1.[5a] The values show that for a given metal, the two metallocenes have the same electronic configuration, except for manganese, where the unsubstituted species is high spin and decamethylmanganocene is low spin. This is reflected in the metal-ring carbon distances for these complexes, where the carbons of the bulkier pentamethylcyclopentadienyl rings in $(C_5Me_5)_2Mn$ are *ca.* 0.25 Å closer to the manganese atom than the carbons in the unsubstituted cyclopentadienyl rings in $(C_5H_5)_2Mn$. For all of the low-spin complexes, the trend in bond lengths is directly related to the electronic structure, since population of the $2e_{1g}$ orbitals, which are metal-ligand antibonding orbitals, produces an increase in the metal-ring carbon distances, even though the ionic radii of the divalent metal ions decrease when moving from left to right across the periodic table.[10]

Table 1. Physical Properties of $(C_5R_5)_2M$.

	R = H[11]			R = Me[6,7,8]		
M	G.S.[a]	μ_{eff} (μ_B)	d(M-C)[b]	G.S.[a]	μ_{eff} (μ_B)	d(M-C)[b]
Mn	$^6A_{1g}$	5.9	2.38	$^2E_{2g}$	1.97	2.112 (3)
Fe	$^1A_{1g}$	0	2.06	$^1A_{1g}$	0	2.050 (2)
Co	$^2E_{1g}$	1.70	2.11	$^2E_{1g}$	1.56	2.105 (2)
Ni	$^3A_{2g}$	2.89	2.20	$^3A_{2g}$	2.89	2.170 (5)

[a]Electronic ground state term symbol.
[b]Averaged value in Ångstroms.

Figure 1. Symmetry Orbital Diagram for D_{5d} Metallocenes.[5a]

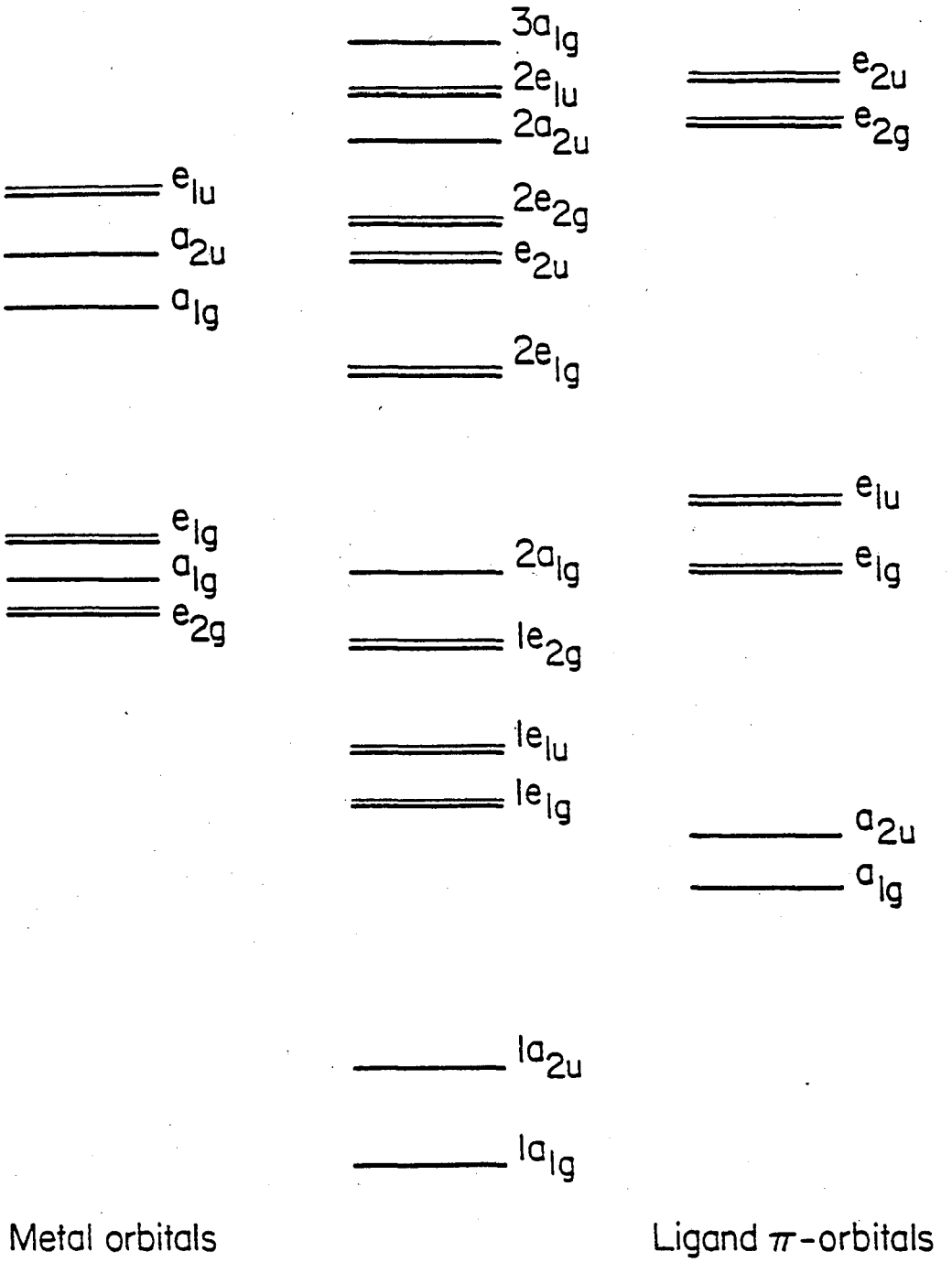

However, the unusual aspect of the structures of the permethylated complexes is the attribution of the ring distortions in the complexes with unsymmetrically populated e symmetry levels that is due to a static Jahn-Teller distortion. Inspection of Table 1 shows that $(C_5Me_5)_2Mn$ and $(C_5Me_5)_2Co$ both have ground states with E symmetry ($e_{2g}^3a_{1g}^2$ and $e_{2g}^4a_{1g}^2e_{1g}^1$, respectively), and these are Jahn-Teller active.[12] These two complexes are reported to have an unusually large variation in ring carbon-carbon bond lengths, which is attributed to a static Jahn-Teller distortion. However, unlike the "ene-allyl" distortions discussed earlier, there is no systematic pattern to the variations in the bond length that could be attributed to selective population of one of the two molecular orbitals that make up the unsymmetrically populated e_{1g} or e_{2g} levels. Also, extensive EPR studies by Ammeter indicate that the Jahn-Teller distortions present in D_5-symmetrical metallocenes with ^2E ground states are *dynamic*, in that they are only observable at extremely low temperatures (< 10 K) and are highly dependent upon the diamagnetic host used to measure the EPR spectra.[13] These distortions would not be expected to be observable at the relatively higher temperatures (≥ 140 K) that are accessible for X-ray crystallographic studies, except in the anisotropic thermal parameters of the carbon atoms.

Another distortion is observed in the hexafluorophosphate salts of the decamethylmetallocene cations, whose physical properties are shown in Table 2. All four cations have physical properties that indicate that they are isoelectronic with the related neutral decamethylmetallocenes.[6,7] However, in this case, the manganese and iron species exhibit a ring slippage, represented in Table 2 by the parameter Δ', which is the difference between the longest and shortest metal-carbon bond lengths in these structures.[8b] All of the molecules are isomorphous, crystallizing in the space group C2/m (No. 12, Z = 2), with the

decamethylmetallocene cations occupying a site with C_{2h} point symmetry (2/m). This means that the slippage of the two rings is symmetrical with respect to the inversion center that the metal atom occupies. However, no distortions within the rings themselves are observed (within the error of the experiments). Again, the variations in the bond lengths are attributed to a static Jahn-Teller distortion due to ^2E or ^3E electronic ground states. The nickel species also shows a substantial variation (0.23 Å), but the errors in this structure are substantially larger (2 to 3 times) than for the other three structures, so no definitive presence of this distortion was claimed for $[(C_5Me_5)_2Ni][PF_6]$, although it too has a ^2E electronic ground state.

Table 2. Physical Properties of $[(C_5R_5)_2M][PF_6]$.[6,7,8b]

M	G.S.[a]	μ_{eff} (μ_B)	d(M-C)[b]	Δ' (Å)[c]
Mn	$^3E_{2g}$	2.90	2.133 (8)	0.038
Fe	$^2E_{2g}$	2.40	2.097 (7)	0.031
Co	$^1A_{1g}$	0	2.050 (3)	0.014
Ni	$^2E_{1g}$	1.44	2.109 (5)	0.023

[a]Electronic ground state term symbol.
[b]Averaged value in Ångstroms.
[c]Δ' = d(M-C){longest} - d(M-C){shortest}

Pentamethylmetallocenes

The C_5-symmetrical pentamethylmetallocenes, $(C_5Me_5)M(C_5H_5)$, are known for the four metals discussed above (M = Mn, Fe, Co, Ni). $(C_5Me_5)Mn(C_5H_5)$ was synthesized by Matsunaga by the ring exchange reaction shown in eq. 1. This synthetic route takes advantage of the lability of the cyclopentadienyl rings in manganocene and decamethylytterbocene.[14] This route can also be used to synthesize pentamethylnickelocene.

$$(C_5Me_5)_2Yb + 2\,(C_5H_5)_2M \xrightarrow{\text{toluene}} 2\,(C_5Me_5)M(C_5H_5) + (C_5H_5)_2Yb \quad (1)$$
$$M = Mn, Ni$$

The mixed ring ferrocene, $(C_5Me_5)Fe(C_5H_5)$, was reported by Kölle and co-workers by treatment of "$(C_5Me_5)FeBr$", generated at low temperature, with C_5H_5Na (eq. 2).[15] However, this route produces a mixture of the desired mixed-ring ferrocene (48% yield) with the unsubstituted (36%) and permethylated ferrocenes (15%). The pain-staking separation of these species by fractional sublimation by Zanin and co-workers was necessary to isolate pure $(C_5Me_5)Fe(C_5H_5)$ for crystallographic analysis.[16]

$$FeBr_2(dme) + LiC_5Me_5 \xrightarrow[-80\ ^\circ C]{\text{THF}} "(C_5Me_5)FeBr" \quad (2a)$$

$$"(C_5Me_5)FeBr" + NaC_5H_5 \xrightarrow[-80\ ^\circ C]{\text{THF}} (C_5Me_5)Fe(C_5H_5) + (C_5R_5)_2Fe \quad (2b)$$
$$48\% \qquad R = H, 36\%$$
$$R = Me, 15\%$$

The cobaltocene, $(C_5Me_5)Co(C_5H_5)$, was synthesized by Manriquez and co-workers from $(C_5Me_5)Co(acac)$ and C_5H_5Li as mentioned in Chapter 2 (eq. 3).[17] Although Manriquez states that "spectroscopic and analytical data are in accord with literature values",[17] he does not report any of this data and the literature reference given only reports data for $(C_5Me_5)_2Co$.[18] The physical properties of $(C_5Me_5)Co(C_5H_5)$ were obtained as part of this work.

$$(C_5Me_5)M(acac) + NaC_5H_5 \xrightarrow{THF} (C_5Me_5)M(C_5H_5) + Na(acac) \quad (3)$$

$$M = Co, Ni$$

The nickel metallocene, $(C_5Me_5)Ni(C_5H_5)$, was first reported by Werner and Dernberger in 1980, who synthesized the complex from the reaction of $(C_5Me_5)Ni(Cl)(PPh_3)$ and C_5H_5Tl (eq. 4).[19] Manriquez synthesized the complex soon after, using the more convenient route in eq. 3.[17] Again, little characterizational data is presented in the literature, with Werner reporting only the elemental analysis and mass spectral data for $(C_5Me_5)Ni(C_5H_5)$,[19] so the physical properties of the nickel complex were also obtained for this study.

$$(C_5Me_5)Ni(Cl)(PPh_3) + TlC_5H_5 \xrightarrow[40\ °C]{THF} (C_5Me_5)Ni(C_5H_5) + TlCl + PPh_3 \quad (4)$$

Properties of Pentamethylcobaltocene and Pentamethylnickelocene

$(C_5Me_5)Co(C_5H_5)$ crystallizes as thin black plates from pentane solution. The material sublimes easily to produce large black polyhedra, thus insuring separation of the sample from metal and metal salt impurities. Figure 2 shows the variable temperature magnetic susceptibility data for $(C_5Me_5)Co(C_5H_5)$. The plot obeys the Curie-Weiss law, yielding a magnetic moment of 1.78 μ_B (θ = -7.5 K), which is slightly higher than the solution values obtained for the cobaltocene complexes listed in Tables 1. The complex does not exhibit a solution EPR, but does exhibit an extremely broad, axially distorted signal with g_{iso} = 1.861 in methylcyclohexane glass at very low temperatures (Figure 3). This is consistent with results found by Ammeter for $(C_5H_5)_2Co$[13] and Robbins, *et al.* for $(C_5Me_5)_2Co$,[6] and indicates that $(C_5Me_5)Co(C_5H_5)$ most likely has a $^2E_{1g}$ ground state, just like $(C_5H_5)_2Co$ and $(C_5Me_5)_2Co$.

Figure 2. Plot of $1/\chi_M$ vs. T for $(C_5Me_5)Co(C_5H_5)$.

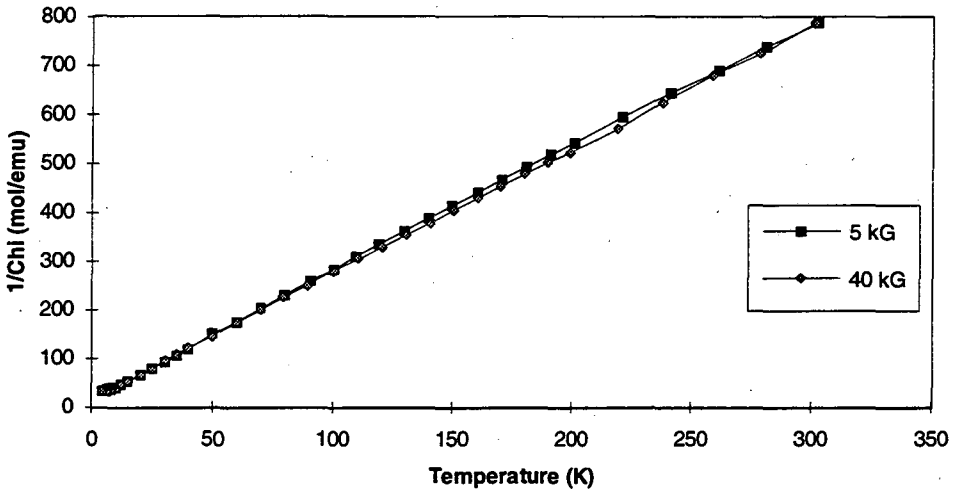

Figure 3. EPR Spectrum of $(C_5Me_5)Co(C_5H_5)$ in C_7H_{14} Glass (4.5 K).

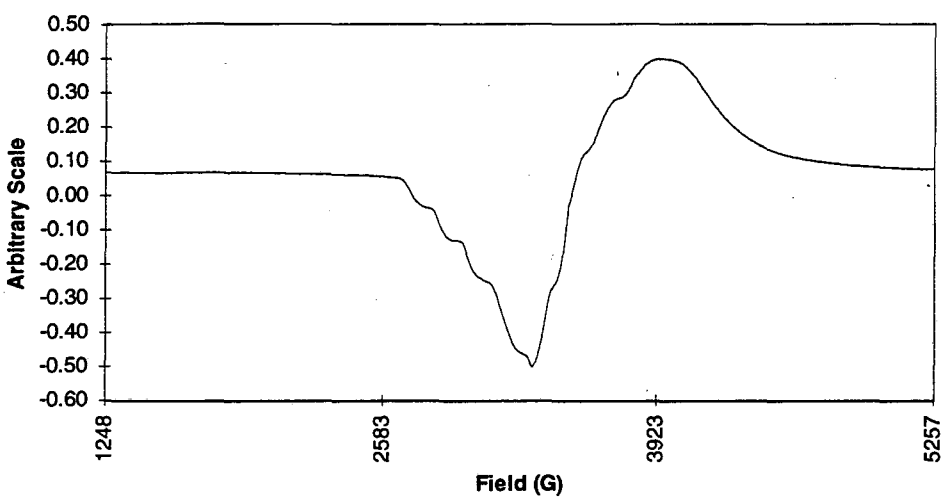

$(C_5Me_5)Ni(C_5H_5)$ forms bright green crystals, and is quite volatile, just like the cobalt analogue. The solid state magnetic susceptibility data for $(C_5Me_5)Ni(C_5H_5)$ is shown in Figure 4. Above 25 K, the plot obeys the Curie-Weiss law, yielding a μ_{eff} = 3.06 μ_B with θ = -49 K. Below this temperature, the species exhibits a temperature independent paramagnetism, indicative of a large

zero-field splitting (36.0 cm^{-1}).[20] $(C_5H_5)_2Ni$ (33.6 cm^{-1})[21] and $(C_5Me_5)_2Ni$ (30.5 cm^{-1})[5a] also exhibit large zero-field splitting values and similar temperature independent phenomena in their solid-state magnetic behavior. Consistent with this is the fact that no EPR signal is observed at any temperature for $(C_5Me_5)Ni(C_5H_5)$. In the ^1H NMR spectrum, $(C_5Me_5)Ni(C_5H_5)$ has two broad ($\nu_{1/2} \approx 400$ Hz), highly shifted resonances, one for each ring. The room temperature chemical shifts of these two resonances are similar to the room temperature values seen for $(C_5H_5)_2Ni$[22] and $(C_5Me_5)_2Ni$, as shown in Table 3. The variable temperture ^1H NMR behavior of $(C_5Me_5)Ni(C_5H_5)$, shown in Figure 5, also exhibits Curie-Weiss behavior. All of this is consistent with $(C_5Me_5)Ni(C_5H_5)$ having a $^3A_{2g}$ ground state, as do $(C_5H_5)_2Ni$ and $(C_5Me_5)_2Ni$.

Figure 4. Plot of $1/\chi_M$ vs. T for $(C_5Me_5)Ni(C_5H_5)$.

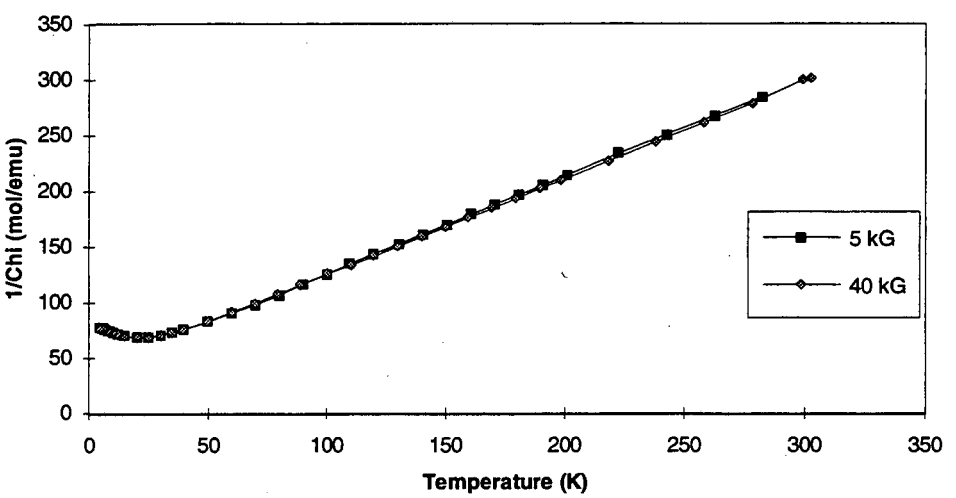

Table 3. ^1H NMR Chemical Shifts of C_5-symmetrical Nickelocenes.

Complex	δ (C_5H_5)	δ (C_5Me_5)	ref
$(C_5H_5)_2Ni$	-245	--	22
$(C_5Me_5)_2Ni$	--	235	this work
$(C_5Me_5)Ni(C_5H_5)$	-208	230	this work

Figure 5. δ vs. 1/T for $(C_5Me_5)Ni(C_5H_5)$.

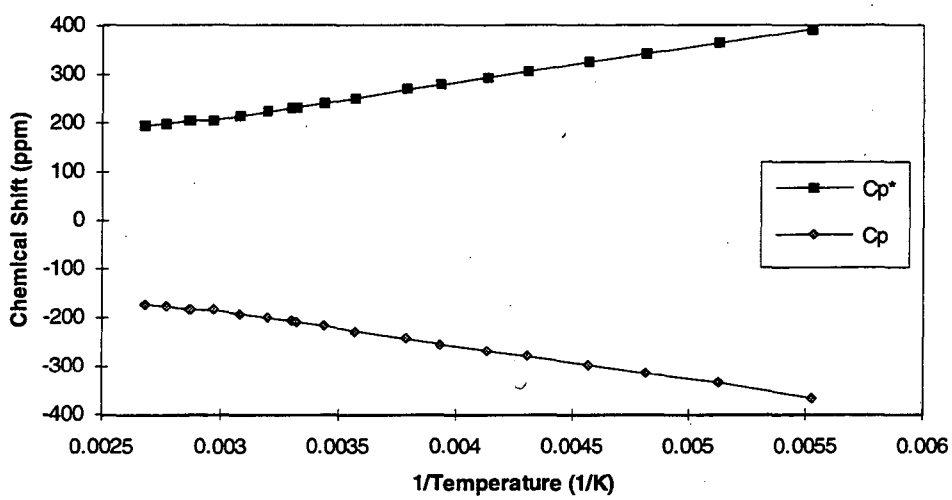

Crystallographic Studies

Since the pentamethylmetallocenes have been shown to have the same electronic ground states as the corresponding decamethylmetallocenes, a systematic crystallographic analysis of the mixed-ring complexes would be very useful in determining the significance of the distortions observed in some of the permethylated metallocene structures. The single crystal X-ray structures of $(C_5Me_5)Co(C_5H_5)$ and $(C_5Me_5)Ni(C_5H_5)$ are shown in Figures 6 and 7, respectively. The two complexes are isomorphous with the reported structures of $(C_5Me_5)Mn(C_5H_5)$[14] and $(C_5Me_5)Fe(C_5H_5)$,[16] with all four complexes crystallizing with an eclipsed geometry in $P\bar{1}$ (No. 2) with very similar cell

parameters (Table 4). The bond distances and angles for the cobalt and nickel structures are listed in Tables 5 through 8, and a summary of the most important values and the corresponding values for the manganese and iron structures are listed in Table 9.

Figure 6. ORTEP Diagram of $(C_5Me_5)Co(C_5H_5)$.

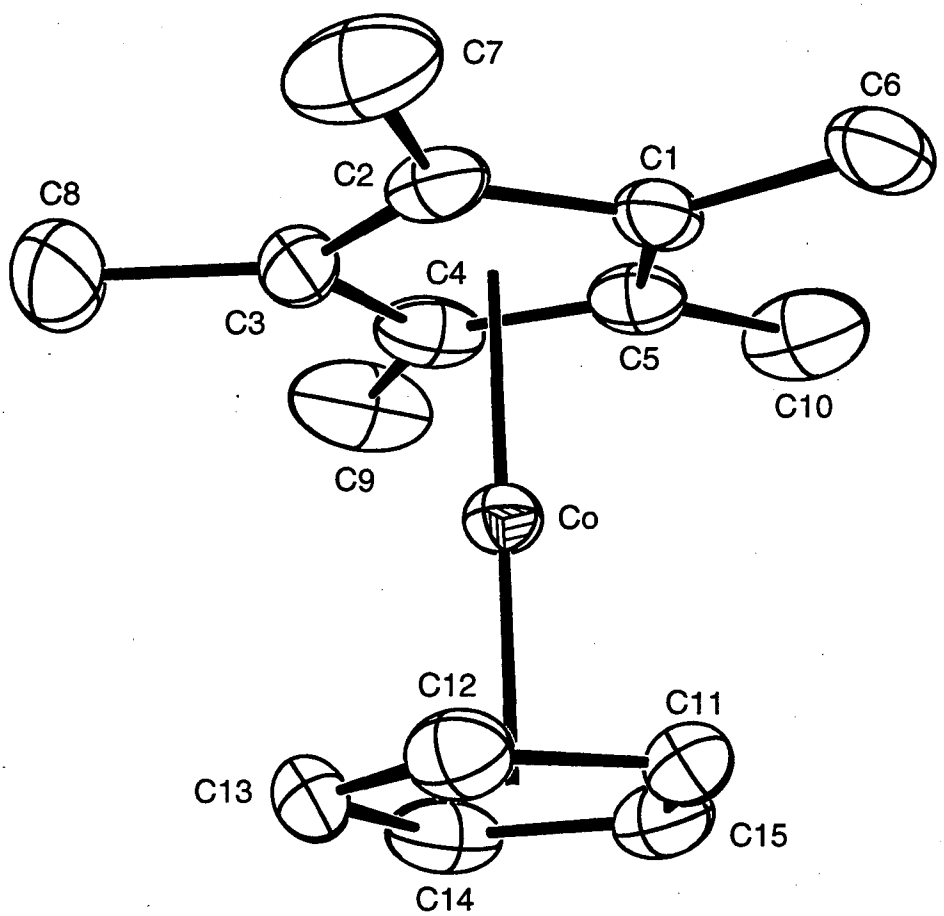

Figure 7. ORTEP Diagram of $(C_5Me_5)Ni(C_5H_5)$.

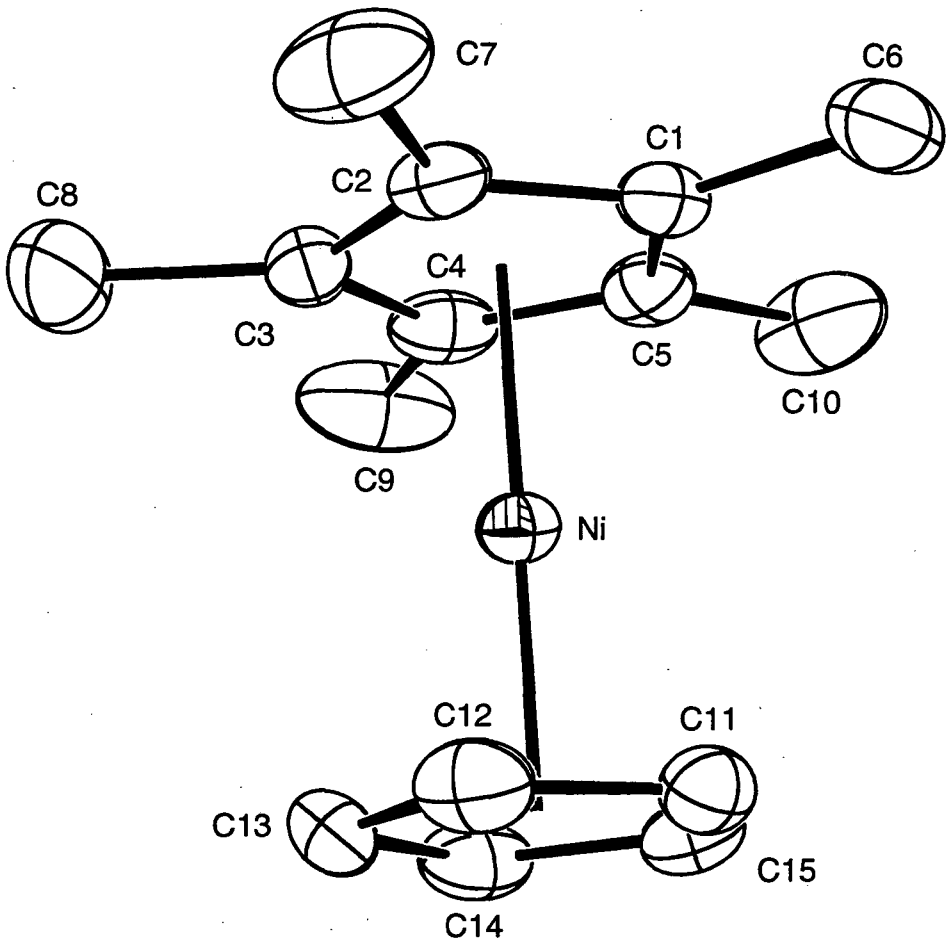

Table 4. Summary of Crystal Data for $(C_5Me_5)M(C_5H_5)$ (M = Mn, Fe, Co, Ni).

M	Mn	Fe*	Co	Ni
Formula	$C_{15}H_{20}Mn$	$C_{15}H_{20}Fe$	$C_{15}H_{20}Co$	$C_{15}H_{20}Ni$
FW (g/mol)	255.26	256.17	259.26	259.04
Space Group	$P\bar{1}$ (No. 2)	$P\bar{1}$ (No. 2)	$P\bar{1}$ (No. 2)	$P\bar{1}$ (No. 2)
a (Å)	7.865 (2)	7.720 (1)	7.713 (2)	7.860 (3)
b (Å)	8.204 (2)	8.178 (1)	8.197 (2)	8.204 (2)
c (Å)	12.163 (2)	12.143 (1)	12.210 (2)	12.285 (7)
α (°)	101.65 (2)	101.19 (1)	101.58 (2)	101.19 (2)
β (°)	96.99 (2)	95.33 (1)	96.94 (2)	97.79 (3)
γ (°)	118.49 (2)	118.21 (1)	118.18 (2)	118.57 (2)
V ($Å^3$)	653.5 (6)	639.0 (1)	645.4 (3)	658.1 (9)
Z	2	2	2	2
Temp (°C)	-90	-120	-114	-96

*The cell parameters of the reported structure of $(C_5Me_5)Fe(C_5H_5)$ were transformed to match the cell setting of the other three structures.[16]

Table 5. Bond Distances for $(C_5Me_5)Co(C_5H_5)$ (Å).

Co-C1	2.080 (2)	Co-C11	2.096 (2)
Co-C2	2.111 (2)	Co-C12	2.111 (2)
Co-C3	2.091 (2)	Co-C13	2.095 (3)
Co-C4	2.086 (2)	Co-C14	2.094 (3)
Co-C5	2.111 (2)	Co-C15	2.117 (2)
Co-Cp*	1.711	Co-Cp	1.730
C1-C2	1.423 (3)	C11-C12	1.402 (4)
C1-C5	1.424 (3)	C11-C15	1.407 (4)
C2-C3	1.419 (3)	C12-C13	1.397 (4)
C3-C4	1.434 (4)	C13-C14	1.416 (4)
C4-C5	1.411 (4)	C14-C15	1.402 (4)

Cp* and Cp are the ring centroids of atoms C1-C5 and C11-C15, respectively.

Table 6. Bond Angles for $(C_5Me_5)Co(C_5H_5)$ (°).

C2-C1-C5	108.4 (2)	C12-C11-C15	108.4 (2)
C1-C2-C3	107.8 (2)	C11-C12-C13	108.1 (2)
C2-C3-C4	107.7 (2)	C12-C13-C14	107.9 (2)
C3-C4-C5	108.3 (2)	C13-C14-C15	108.0 (3)
C1-C5-C4	107.7 (2)	C11-C15-C14	107.6 (2)

Table 7. Bond Distances for $(C_5Me_5)Ni(C_5H_5)$ (Å).

Ni-C1	2.161 (4)	Ni-C11	2.183 (4)
Ni-C2	2.159 (4)	Ni-C12	2.178 (4)
Ni-C3	2.164 (4)	Ni-C13	2.167 (4)
Ni-C4	2.160 (4)	Ni-C14	2.169 (4)
Ni-C5	2.164 (4)	Ni-C15	2.181 (4)
Ni-Cp*	1.795	Ni-Cp	1.821
C1-C2	1.417 (5)	C11-C12	1.392 (6)
C1-C5	1.420 (5)	C11-C15	1.397 (6)
C2-C3	1.415 (6)	C12-C13	1.398 (6)
C3-C4	1.413 (6)	C13-C14	1.402 (6)
C4-C5	1.419 (6)	C14-C15	1.404 (6)

Cp* and Cp are the ring centroids of atoms C1-C5 and C11-C15, respectively.

Table 8. Bond Angles for $(C_5Me_5)Ni(C_5H_5)$ (°).

C2-C1-C5	107.5 (3)	C12-C11-C15	108.7 (4)
C1-C2-C3	108.6 (3)	C11-C12-C13	107.6 (4)
C2-C3-C4	107.7 (3)	C12-C13-C14	108.4 (4)
C3-C4-C5	108.2 (3)	C13-C14-C15	107.6 (4)
C1-C5-C4	108.0 (3)	C11-C15-C14	107.7 (4)

Table 9. Summary of Important Bond Distances for $(C_5Me_5)M(C_5H_5)$.[16]

	d(M-C)[a]		Δ'(M-C)[b]		d(C-C)[a]		Δ'(C-C)[b]	
M	Cp	Cp*	Cp	Cp*	Cp	Cp*	Cp	Cp*
Mn	2.118	2.104	0.035	0.027	1.414	1.422	0.014	0.010
Fe	2.051	2.041	0.010	0.008	1.422	1.428	0.020	0.007
Co	2.103	2.096	0.023	0.031	1.405	1.422	0.019	0.023
Ni	2.176	2.162	0.016	0.005	1.399	1.417	0.012	0.007

[a]Averaged values in Ångstroms.

[b]Δ' = d(X-C){longest} - d(X-C){shortest}, for X indicated in the label.

Implications

The data in Table 9 for the pentamethylmetallocenes show a general trend of increasing metal-ring distances with increasing population of the e_1^* metal-ring antibonding orbitals (the mixed-ring metallocenes do not have inversion symmetry, so the *gerade/ungerade* labels do not apply), just as has been observed for the symmetrical metallocene systems. $(C_5Me_5)Mn(C_5H_5)$ and $(C_5Me_5)_2Mn$ have longer metal-ring distances than their iron analogues mainly because manganese(II) is slightly larger than iron(II) (r(Mn) = 0.81 Å, r(Fe) = 0.75 Å, for divalent ions with a coordination number of six).[10] Also, the low-spin manganocenes have one less electron in the e_2 level (compared to the ferrocenes), but this level is only very slightly metal-ring bonding in nature (formally, it would be considered a δ-bonding orbital).

However, the values summarized in Table 9 also show minimal structural distortions. The small variations in ring carbon-carbon distances (Δ'(C-C)) do not show any obvious dependence on the electronic ground states of the metallocenes. The argument made for a static Jahn-Teller distortion in $(C_5Me_5)_2Mn$ was based on room temperature measurements for this compound and $(C_5Me_5)_2Fe$.[8a] However, the two structures are in different space groups:

C2/c and Cmca for $(C_5Me_5)_2Mn$ and $(C_5Me_5)_2Fe$, respectively. The difference in site symmetry for the two molecules is that the ferrocene has an extra mirror plane that bisects the two C_5Me_5 rings. The carbon-carbon bond that would be bisected by this mirror plane in the manganese structure (if it were present) is the single, unusually long bond in the structure that is the evidence used to propose the presence of a static distortion. Considering the site disorder problem found in the room temperature structure of $(C_5H_5)_2Fe$ and the footnote in reference 8a that the low temperature structure of $(C_5Me_5)_2Mn$ is in the space group Cmca and exhibits a "somewhat altered distortion," it is not unreasonable to consider the possibility that a small amount of disorder across a pseudo-mirror plane may be responsible for the single long carbon-carbon bond length found in $(C_5Me_5)_2Mn$. Unfortunately, the data for the low temperature structure of $(C_5Me_5)_2Mn$ in Cmca was not available.

The ring slippage seen in the decamethylmetallocene cation structures is suspect, also. Although the variations in metal-carbon distances (Δ'(M-C) in Table 9) are larger for $(C_5Me_5)Mn(C_5H_5)$ and $(C_5Me_5)Co(C_5H_5)$ than they are for their iron and nickel analogues, the Δ' values alone do not guarantee the significance of any distortions present. The variations seen in $[(C_5Me_5)_2Mn][PF_6]$ and $[(C_5Me_5)_2Fe][PF_6]$ are geometrically the same, with the metal approaching one vertex of each C_5Me_5 ring, producing one short, two "normal," and two long metal-carbon bond distances. However, the variations in $(C_5Me_5)Mn(C_5H_5)$ (which is isoelectronic with $[(C_5Me_5)_2Fe][PF_6]$ and hence would be expected to show the same geometric distortions if the distortion is due to Jahn-Teller forces) are due to one long, two "normal," and two short bond distances, indicating that the slippage is towards an edge of the cyclopentadienyl rings, not a vertex. Also important is the unusual magnetic susceptibility behavior seen by Robbins, *et al.* for $[(C_5Me_5)_2Ni][PF_6]$.[6] The tetraflurorborate salt, $[(C_5Me_5)_2Ni][BF_4]$, exhibits

Curie-Weiss behavior, with a magnetic moment typical for 19-electron metallocenes (μ_{eff} = 1.62 μ_B). However, $[(C_5Me_5)_2Ni][PF_6]$, while exhibiting Curie-Weiss behavior at higher temperatures (μ_{eff} = 1.67 μ_B), shows a pronounced curvature in the plot of $1/\chi_M$ vs. T below 40 K; which is attributed by Robbins, *et al.* to intermolecular interactions between the ions, since $[(C_5Me_5)_2Ni][BF_4]$ shows no evidence of anything unusual. Therefore, even though the variations in metal-carbon bond distances in metallocenes with ^2E ground states are statistically significant, they do not specifically indicate the presence of a static Jahn-Teller distortion. It is more likely that they are due to packing forces of some kind, and that the increased magnitude of the variations observed for metallocenes with ^2E ground states may be related to the dynamic Jahn-Teller distortions of these complexes that have been exhaustively elucidated by Ammeter.[13] Indeed, Ammeter has shown that the nature of the host lattice plays a dramatic role in the EPR and magnetic properties of the dynamic Jahn-Teller systems.[13b]

The most important aspect of this study is that the variations in bond lengths observed for all of the metallocenes are quite small. The data summarized in Figure 16 and Table 9 in Chapter 3 show the variations in bond lengths observed in systems with "ene-allyl" distortions. For $(C_5Me_5)Ni(acac)$, which has one molecular orbital selectively populated that produces the "ene-allyl" distortion, the values corresponding to Δ'(M-C) and Δ'(C-C) in Table 9 are 0.124 Å and 0.095 Å, respectively. These variations are far larger than any variations seen in the metallocene systems. Of course, the Jahn-Teller distortions expected for the metallocenes would be smaller, but the low temperature X-ray studies of the pentamethylmetallocenes indicate that distortions of such small magnitude are most likely going to be obscured by the standard errors due to librational motion and packing effects, and that any

assignment of the variations observed to Jahn-Teller distortions should be made with reservation.

References

1. Kealy, T. J.; Pauson, P. L., *Nature (London)*, **1951**, *168*, 1039.

2. Wilkinson, G.; Rosenblum, M.; Whiting, M. C.; Woodward, R. B., *J. Am. Chem. Soc.*, **1952**, *74*, 2125.

3. Fischer, E. O.; Pfab, W., *Z. Naturforcsh.*, **1952**, *7b*, 377.

4. Threlkel, R. S.; Bercaw, J. E., *J. Organomet. Chem.*, **1977**, *136*, 1.

5. (a) Robbins, J. L., Ph.D. Thesis, University of California, Berkeley, **1981**.
   (b) Kölle, U.; Khouzami, F., *Chem. Ber.*, **1981**, *114*, 2929.

6. Robbins, J. L.; Edelstein, N. M.; Spencer, B.; Smart, J. C., *J. Am. Chem. Soc.*, **1982**, *104*, 1182.

7. (a) Smart, J. C.; Robbins, J. L., *J. Am. Chem. Soc.*, **1978**, *100*, 3936.
   (b) Robbins, J. L.; Edelstein, N. M.; Cooper, S. R.; Smart, J. C., *J. Am. Chem. Soc.*, **1979**, *101*, 3853.

8. (a) Freyberg, D. P.; Robbins, J. L.; Raymond, K. N.; Smart, J. C., *J. Am. Chem. Soc.*, **1979**, *101*, 892.
   (b) Raymond, K. N., unpublished results.

9. (a) Seiler, P.; Dunitz, J. D., *Acta Cryst.*, **1979**, *B35*, 1068 and 2020.
   (b) Takusagawa, F.; Koetzle, T. F., *Acta Cryst.*, **1979**, *B35*, 1074.

10. Douglas, B.; McDaniel, D. H.; Alexander, J. J., "Concepts and Models of Inorganic Chemistry," 2nd Ed., John Wiley and Sons: New York, **1983**.

11. Powell, P., "Principles of Organometallic Chemistry," 2nd Ed., Chapman and Hall: London, **1988**.

12. Douglas, B. E.; Hollingsworth, C. A., "Symmetry in Bonding and Spectra: An Introduction," Academic Press: Orlando, **1985**; and references therein.

13. (a) Ammeter, J. H.; Swalen, J. D., *J. Chem. Phys.*, **1972**, *57*, 678.
   (b) Bucher, R., Dissertation, Eidgenossischen Technische Hochschule, Zurich, **1977**.

14. Matsunaga, P. T.; Andersen, R. A., unpublished results.

15. Kölle, U.; Fuss, B.; Khouzami, F.; Gersdorf, J., *J. Organomet. Chem.*, **1985**, *290*, 77.

16. Zanin, I. E.; Antipin, M. Y.; Struchkov, Y. T.; Kudinov, A. R.; Ruebinskaya, M. I., *Metalloorganicheskaya Chimiya*, **1992**, *5*, 579.

17. Bunel, E. E.; Valle, L.; Manriquez, J. M., *Organometallics*, **1985**, *4*, 1680.

18. Kölle, U.; Khouzami, F.; Fuss, B., *Angew. Chem., Int. Ed. Engl.*, **1982**, *21*, 131.

19. Werner, H.; Dernberger, Th., *J. Organomet. Chem.*, **1980**, *198*, 97.

20. From: Prins, R.; Van Voorst, J. D. W.; Schinkel, C. J., *Chem. Phys. Lett.*, **1967**, *1*, 54. The high temperature (Curie-Weiss) magnetic susceptibility data was used to calculate $g_\perp$ from the following equation:

$$\chi_M = \frac{2N\mu_B^2}{9kT}(g_{\|}^2 + 2g_\perp^2)$$

where N is Avogadro's number, μB is the Bohr magneton, k is Boltzmann's constant, T is the temperature, and $g_{\|}$ is assumed to have the free electron value (2.0023). The low temperature (temperature independent) magnetic susceptibility data was then used to calculate the zero-field splitting (D, in cm^{-1}) from the following equation:

$$\chi_M = \frac{4N\mu_B^2}{3D}(g_\perp^2)$$

21. Baltzer, P.; Furrer, A.; Hulliger, J.; Stebler, A., *Inorg. Chem.*, **1988**, *27*, 1543.

22. Rettig, M. F., "NMR of Paramagnetic Molecules: Principles and Applications," LaMar, G. N.; Horrocks, W. DeW. Jr.; Holm, R. H., eds., Academic Press: New York, **1973**, Ch. 6.

Experimental Details

General

All reactions and product manipulations were carried out under an atmosphere of dry nitrogen using standard Schlenk and dry box techniques. Solvents and solutions were transferred between reaction vessels *via* stainless steel tubing. Filtrations were performed by attaching filters to one inch pieces of small-bore glass tubing secured to the ends of stainless steel tubing with epoxy. Pentane, hexane, toluene, diethyl ether, and tetrahydrofuran were distilled from sodium benzophenone ketyl under nitrogen immediately prior to use. Dichloromethane was distilled from calcium hydride under nitrogen immediately prior to use. All other chemicals were of reagent grade and purified according to standard procedures as necessary.[1] Deuterated solvents for NMR measurements were distilled from potassium under nitrogen and stored over sodium. $(Me_5C_5)_2Mg$[2] was prepared from pentamethylcyclopentadiene and bis(butyl)magnesium in heptane solution at reflux.

Infrared spectra were recorded on a Nicolet 5DX FTIR spectrometer as Nujol mulls between CsI or KBr plates. All ^1H, ^{13}C, and $^{31}P\{^1H\}$ nuclear magnetic resonance spectra were measured on a JEOL FX90Q FT NMR spectrometer operating at 89.6 (^1H) or 23.6 (^{13}C) MHz; or on one of several FT NMR spectrometers using Nicolet electronics assembled by Mr. R. Nunlist at the University of California, Berkeley Department of Chemistry NMR facility as noted. Chemical shifts for ^1H and $^{13}C\{^1H\}$ spectra were referenced to tetramethylsilane ($\delta = 0$) with positive values at higher frequency. Chemical shifts for $^{31}P\{^1H\}$ spectra were referenced to 85% H_3PO_4(aq.) ($\delta = 0$) with positive values at higher frequency. Electron paramagnetic resonance spectra were recorded on an IBM

ER-2090D-SRC spectrometer, and were measured in methylcyclohexane (solution or glass) unless otherwise noted. Simulation of the EPR spectra was accomplished by comparison of experimental spectra with calculated spectra obtained from a second-order calculation program written by Dr. E. Gamp and run on a SUN MP630 computer server. EPR spectra with rhombic symmetry have three g-tensors, g_1, g_2, g_3, and these labels were arbitrarily assigned so that $g_1 < g_2 < g_3$. Absolute assignment of the g-tensors is impossible since the relative orientation of the crystallographic and magnetic axes in the glass is not known. Melting points were measured on a Thomas-Hoover melting point apparatus in sealed capillaries and are uncorrected.

Solution magnetic moments were determined using the method described by Evans[3] using the aforementioned JEOL FX90Q FT NMR spectrometer or the UCB 300 MHz instrument. Specifically, the apparatus consists of a 2 mm tube placed concentrically within a 5 mm NMR tube and secured with epoxy. A known concentration solution of the compound in C_6D_6 was placed in the inner tube, which was capped with a septum, and neat C_6D_6 was placed in the outer chamber between the two tubes. The difference in chemical shift of the C_6D_5H signal for the solution (solute + C_6D_6) and the neat C_6D_6 ($\Delta\nu$, in Hz) was then measured and the following formula was used to calculate μ:[4]

$$\frac{\Delta\nu}{\nu_0} = (S_f \cdot m_0)\left[\chi_0 - \frac{1}{MW}\left(\chi_D + \frac{\mu^2}{8(T + \theta)}\right)\right]$$

where ν_0 is the spectrometer frequency in hertz, m_0 is the mass (in grams) of the compound dissolved in 1 mL of C_6D_6, χ_0 is the mass susceptibility of the solvent (-0.702×10^{-6} emu/g for benzene), χ_D is the molar magnetic susceptibility of the ligands (same as the diamagnetic correction used for solid-state magnetic susceptibility measurements), MW is the molecular weight of the compound, μ is the magnetic moment of the compound in μ_B, T is the absolute temperature in

Kelvin, θ is the Weiss constant for the compound from the Curie-Weiss equation (if known), and S_f is the shape factor, a correction term that is dependent on the type of magnet used in the experiment (it is $-2\pi/3$ for permanent magnets {JEOL} and $+4\pi/3$ for superconducting magnets {UCB 300}). Unless specifically mentioned, θ was ignored in the calculation either because it was unknown (not determinable from solid-state measurements) or it was small ($|\theta| < 10$ K) and not significant relative to the error of the experiment.

Solid-state magnetic susceptibility measurements (SQUID) were obtained from either a S.H.E. Corporation Model 905 or a Quantum Designs MPMS HP-150 superconducting magnetometer. Samples were prepared and handled according as previously described.[5] In all cases, the samples were purified by crystallization followed by sublimation, when possible. Susceptibility data were corrected for sample and container diamagnetism. Regions in the plot of $1/\chi_M$ vs. T that demonstrated Curie-Weiss behavior were fit to the Curie-Weiss law $1/\chi_M = (T - \theta) / C$, where θ is the Weiss constant and C is the Curie constant, using a linear-least squares program written by Dr. E. Gamp. Electron impact and fast-atom bombardment mass spectra were recorded by the mass spectrometry laboratory at the University of California, Berkeley. When molecular ions were observed, the isotopic cluster was reported as follows: ion amu (observed intensity, calculated intensity). Elemental analyses were performed by the analytical laboratories at the University of California, Berkeley.

Selected Starting Materials

$Co(acac)_2$

This complex was synthesized according to a published procedure.[6] To a solution of cobalt acetate tetrahydrate (54.3 g, 0.250 mol) in 250 mL of water was added 2,4-pentanedione (50.1 mL, 0.500 mol) in methanol (100 mL). The dark purple solution was heated to reflux for 15 minutes, then cooled slowly to room temperature. Crystallization of the solution at 0 °C yielded rose red crystals. Concentration of the mother liquor provided additional crops of crystals, which were combined and washed thoroughly with cold water, yielding $Co(acac)_2$ $2H_2O$ (49.8 g, 0.170 mol, 68.0% yield).

The water of hydration was removed *via* toluene azeotrope in three roughly equal portions. $Co(acac)_2 \cdot 2H_2O$ (18.0 g, 61.4 mmol) was slurried in toluene (*ca.* 150 mL) and the flask was equipped with a condensor with a Dean-Stark trap. Refluxing for 24 h produces a deep violet solution, which upon cooling to -80 °C yields $Co(acac)_2$ as a lavender purple solid. Additional crops of material were obtained by concentrating the mother liquor. The yield was quantitative except for manipulative losses. The IR spectrum was identical to that of the previously reported compound ($\nu_{CO/CC}$ 1590, 1516 cm^{-1} (Nujol); Lit. 1601, 1513 cm^{-1} (KBr)).[7,8]

$Ni(acac)_2$

This complex was synthesized according to a published procedure.[6] To a solution of nickel acetate tetrahydrate (54.2 g, 0.250 mol) in 250 mL of water was added 2,4-pentanedione (50.1 mL, 0.500 mol) in methanol (100 mL). The dark purple solution was heated to reflux for 15 minutes, then cooled slowly to room

temperature. Crystallization of the solution at 0 °C yielded aquamarine crystals. Concentration of the mother liquor provided additional crops of crystals, which were combined and washed thoroughly with cold water, yielding $Ni(acac)_2{\cdot}2H_2O$ (60.3 g, 0.206 mol, 82.3% yield).

The water of hydration was removed *via* toluene azeotrope in two roughly equal portions. $Ni(acac)_2{\cdot}2H_2O$ (31.0 g, 0.106 mol) was slurried in toluene (*ca.* 200 mL) and the flask was equipped with a condensor with a Dean-Stark trap. Refluxing for 24 h produces a forest green solution, which upon cooling to -80 °C yields $Ni(acac)_2$ as bright green microcrystals. Additional crops of crystals were obtained by concentrating the mother liquor. The yield was quantitative except for manipulative losses. The IR spectrum was identical to that of the previously reported compound ($\nu_{CO/CC}$ 1592, 1521 cm^{-1} (Nujol); Lit. 1598, 1514 cm^{-1} (KBr)).[7,8]

$[(C_5Me_5)Co(\mu\text{-}Cl)]_2$

This complex was synthesized using a modification of a published procedure.[9] A solution of bis(pentamethylcyclopentadienyl)magnesium (1.45 g, 4.92 mmol) in tetrahydrofuran (70 mL) was added to a slurry of $CoCl_2$ (1.24 g, 9.55 mmol) in tetrahydrofuran (50 mL) at 0 °C. Upon mixing, the solution immediately changed color from light blue to dark brown and a gray precipitate settled out. After stirring at 0 °C for 1 h, the solution was warmed to room temperature. The volatile materials were completely removed under reduced pressure and the residue was extracted with pentane (150 mL). The dark brown solution was filtered and the filtrate was concentrated to *ca.* 50 mL. Cooling to -80 °C afforded brown plates. Concentration of the mother liquor provided an additional crop of crystals for a total yield of 1.55 g (3.38 mmol, 70.8% yield). Mp 179-180 °C. IR: 2719 (m), 1508 (sh), 1351 (m), 1156 (m), 1070 (m), 1022 (s),

942 (m), 793 (m), 612 (w), 584 (m), 540 (w), 428 (s), 398 (m), 335 (m), 303 (w). ^{1}H NMR (C_7D_8, 303 K, 90 MHz): δ 37.6 ($\nu_{1/2}$ = 245 Hz). EIMS: 458 (100,100); 459 (20,22); 460 (66,67); 461 (13,15); 462 (12,12); 463 (2,2). Magnetic Susceptibility: 5kG (5-25 K), μ_{eff} = 2.67 μ_B, θ = -2.7 K; (160-300 K), μ_{eff} = 5.48 μ_B, θ = -287 K; 40kG (5-50 K), μ_{eff} = 3.03 μ_B, θ = -12 K; (160-300 K), μ_{eff} = 4.70 μ_B, θ = -207 K. No EPR signal was observed in methylcyclohexane glass (2 K).[9]

$[(C_5Me_5)Co(\mu\text{-}Br)]_2$

This complex was synthesized using a modification of a published procedure.[9] A solution of bis(pentamethylcyclopentadienyl)magnesium (1.25 g, 4.24 mmol) in tetrahydrofuran (75 mL) was added to a solution of $CoBr_2$ (1.94 g, 8.87 mmol) in tetrahydrofuran (60 mL) at 0 °C. Upon mixing, the solution immediately changed color from deep blue to deep brown and a gray precipitate settled out. After stirring at 0 °C for 1 h, the solution was warmed to room temperature. The volatile materials were completely removed under reduced pressure and the residue was extracted with pentane (250 mL). The dark brown solution was filtered and the filtrate was concentrated to *ca.* 100 mL. Cooling to -80 °C afforded brown plates. Concentration of the mother liquor provided an additional crop of crystals for a total yield of 1.96 g (3.58 mmol, 84.4% yield). Mp 203 °C (dec.). IR: 2719 (m), 1505 (m), 1352 (s), 1262 (w), 1159 (m), 1069 (m), 1023 (s), 941 (m), 791 (m), 612 (w), 584 (m), 543 (w), 427 (m), 393 (m), 353 (w). ^{1}H NMR (C_6D_6, 293 K, 90 MHz): δ 30.7 ($\nu_{1/2}$ = 225 Hz). EIMS: 546 (50,51); 547 (13,11); 548 (100,100); 549 (23,22); 550 (48,50); 551 (9,11). Magnetic Susceptibility: 5kG (5-50 K), μ_{eff} = 3.76 μ_B, θ = -4.4 K; (160-300 K), μ_{eff} = 4.96 μ_B, θ = -68.6 K; 40kG (5-50 K), μ_{eff} = 4.19 μ_B, θ =

-13.4 K; (180-300 K), μ_{eff} = 4.87 μ_B, θ = -64.8 K. No EPR signal was observed in methylcyclohexane glass (2 K).[9]

$[(C_5Me_5)Ni(\mu\text{-}Br)]_2$

This complex was synthesized using a modification of a published procedure.[10] A solution of bis(pentamethylcyclopentadienyl)magnesium (1.55 g, 5.26 mmol) in tetrahydrofuran (50 mL) was added to a slurry of $NiBr_2$(1,2-dimethoxyethane) (3.28 g, 10.6 mmol) in tetrahydrofuran (75 mL) at -10 °C. Upon mixing, the solution immediately changed color from tan to red-brown and a gray precipitate settled out. After stirring at -10 °C for 1 h, the volatile materials were completely removed under reduced pressure at -10 °C and the residue was extracted with cold pentane (-30 °C, 150 mL). The red-brown solution was filtered and the filtrate was concentrated to *ca.* 100 mL. Cooling to -80 °C afforded deep red microcrystals. Concentration of the mother liquor provided an additional crop of crystals for a total yield of 0.82 g (1.5 mmol, 14% yield). The compound did not melt to 330 °C. IR: 2724 (m), 1428 (m), 1262 (m), 1097 (m), 1067 (m), 1021 (s), 941 (w), 801 (s), 548 (w), 349 (s). ^{1}H NMR (C_6D_6, 293 K, 90 MHz): δ 258 ($\nu_{1/2}$ = 300 Hz). EIMS: 544 (67,36); 545 (36,8); 546 (100,99); 547 (47,24); 548 (81,100); 549 (34,25); 550 (41,49); 551 (16,13); 552 (11,15). The chlride analogue could not be prepared by a related reaction.

Chapter 1

$(C_5Me_5)_3Co_3(\mu_3\text{-}CH)(\mu\text{-}H)$

(a) From $(C_5Me_5)Co(acac)$

To a solution of sublimed $(C_5Me_5)Co(acac)$ (1.75 g, 5.97 mmol) in diethyl ether (120 mL) was added 7.7 mL of a 0.77M diethyl ether solution of methyllithium (5.9 mmol) at 0 °C. Upon mixing, the solution turned black and a flocculent precipitate formed after approximately 15 min. The reaction vessel was vented periodically to the nitrogen manifold to release pressure, presumably due to methane evolution. After stirring at 0 °C for 2 h, the volatile materials were removed under reduced pressure. The residue was extracted with pentane at room temperature (*ca.* 200 mL) and filtered. The filtrate was concentrated to *ca.* 120 mL and cooled to -30 °C, affording black prisms. Concentration of the mother liquor provided additional crops of crystals. Recrystallization of the combined crops of crystals from pentane yielded pure material (0.78 g, 1.3 mmol, 66% yield). The compound did not melt to 330 °C. IR: 2713 (m), 1409 (sh), 1371 (s), 1290 (w), 1158 (m), 1066 (m), 1024 (s), 976 (w), 946 (w), 900 (m), 856 (m), 834 (s), 609 (w), 539 (m), 487 (m), 409 (m), 371 (m). No resonances were observed in the ^1H NMR spectrum in C_6D_6 at room temperature. No distinct molecular ion was observed in the EIMS; instead a broad envelope approximately 20 amu wide, centered at 600 amu was observed. Magnetic Susceptibility (per cluster): 5kG (7-50 K), μ_{eff} = 2.41 μ_B, θ = -0.3 K; (160-300 K), μ_{eff} = 2.73 μ_B, θ = -40.7 K; 40kG (5-50 K), μ_{eff} = 2.42 μ_B, θ = -0.9 K; (160-300 K), μ_{eff} = 2.70 μ_B, θ = -35.9 K. Solution Magnetic Moment (303 K, C_6D_6, 300 MHz, θ = -38 K): 2.28 μ_B. EPR (powder, 2%, doped into

$(C_5Me_5)_3Co_3(\mu_3\text{-}CH)_2$): 1.7 K, g = 2.157 (broad), $g_{1/2}$ = 4.268. Anal. Calcd for $C_{31}H_{47}Co_3$: C, 62.4; H, 7.94. Found: C, 62.6; H, 7.94. If the $(C_5Me_5)Co(acac)$ was not purified by sublimation, then the overall yield is reduced and the isolated cluster is impure.

(b) From $[(C_5Me_5)Co(\mu\text{-}Cl)]_2$

To a solution of $[(C_5Me_5)CoCl]_2$ (0.50g, 1.1 mmol) in diethyl ether (70 mL) was added 3.4 mL of a 0.66M diethyl ether solution of MeLi (2.2 mmol) at 0 °C. Upon mixing, the solution slowly changed color from deep brown to black and a gray precipitate appeared. The reaction vessel was vented periodically to the nitrogen manifold to release pressure, presumably due to methane evolution. After stirring at 0 °C for 4 h, the solution was allowed to warm to room temperature and stirred for another 12 h. The volatile materials were completely removed under reduced pressure and the residue was extracted with pentane (70 mL). The black solution was filtered and the filtrate was concentrated to *ca.* 50 mL. Cooling to -30 °C afforded black prisms. Concentration of the mother liquor provided additional crops of crystals for a total yield of 0.26 g (0.44 mmol, 60% yield). This method is inferior because the isolated product has impurities that cannot be separated by fractional crystallization.

$(C_5Me_5)_3Ni_3(\mu_3\text{-}CH)(\mu\text{-}H)$

To a solution of sublimed $(C_5Me_5)Ni(acac)$ (0.92 g, 3.1 mmol) in diethyl ether (75 mL) was added 4.8 mL of a 0.77M diethyl ether solution of methyllithium (3.7 mmol) at 0 °C. Upon mixing, the solution turned a chocolate brown color and a flocculent precipitate formed after approximately 15 min. The reaction vessel was vented periodically to the nitrogen manifold to release pressure, presumably due to methane evolution. After stirring at 0 °C for 4 h, the

solution was allowed to warm to room temperature and stirred for another 12 h. The volatile materials were removed under reduced pressure. The residue was extracted with pentane (120 mL) and filtered. The filtrate was concentrated to *ca.* 70 mL and cooled to -30 °C, affording brown prisms. Concentration of the mother liquor provided additional crops of crystals. Recrystallization of the combined crops of crystals from pentane yielded pure material (0.38 g, 0.64 mmol, 61% yield). The compound did not melt to 330 °C. IR: 2715 (m), 1435 (sh), 1371 (s), 1261 (w), 1155 (m), 1065 (m), 1023 (s), 981 (m), 943 (w), 819 (s), 612 (w), 390 (m), 354 (s). No resonances were observed in the ^{1}H NMR in C_6D_6 at room temperature. EIMS, low res: 593 (83,86); 594 (29,40); 595 (100,100); 596 (38,41); 597 (56,54); 598 (21,21); 599 (22,21); 600 (8,8); 601 (7,6). EIMS, high res: Calcd: 593.1738 ($^{58}Ni_3$), 595.1693 ($^{58}Ni_2{}^{60}Ni$); Found: 593.1725, 595.1681. Magnetic Susceptibility (5-300 K) (per cluster): 5kG, μ_{eff} = 1.93 μ_B, θ = -8.23 K; 40kG, μ_{eff} = 1.86 μ_B, θ = -4.28 K. Solution Magnetic Moment (303 K, C_6D_6, 300 MHz): 1.77 μ_B. EPR: 298 K, g = 2.046; 88 K, $g_\perp$ = 2.114, $g_\parallel$ = 2.009. Anal. Calcd for $C_{31}H_{47}Ni_3$: C, 62.5; H, 7.95. Found: C, 62.9; H, 7.95.

$(C_5Me_5)_3Co_3(\mu_3\text{-}CH)_2$

(a) From carbon tetrachloride

To a solution of $(C_5Me_5)_3Co_3(\mu_3\text{-}CH)(\mu\text{-}H)$ (0.07 g, 0.1 mmol) in toluene (50 mL) was added 11.5 μL of CCl_4 (0.1 mmol). Upon mixing, the solution very gradually changed color from black to red-purple and a black precipitate settled out. After stirring at room temperature for 24 h, the volatile materials were completely removed under reduced pressure and the residue was extracted with pentane (65 mL). The red-purple solution was filtered and the filtrate was

concentrated to *ca.* 15 mL. Cooling to -80 °C afforded purple prisms for a total yield of 0.02 g (0.03 mmol, 27% yield). The compound did not melt to 330 °C. IR: 2714 (m), 1687 (s), 1484 (sh), 1406 (w), 1371 (s), 1160 (m), 1069 (m), 1024 (m), 989 (w), 945 (w), 906 (w), 856 (s), 836 (w), 611 (w), 570 (w), 538 (s), 450 (w), 409 (s). ^{1}H NMR (C_6D_6, 293 K, 90 MHz): δ 16.99 (s, 2H, μ^3-C<u>H</u>), 1.74 (s, 45H, C_5<u>Me$_5$</u>). EIMS: 608 (100,100); 609 (36,36); 610 (7,6). <u>Anal.</u> Calcd for $C_{32}H_{47}Co_3$: C, 63.2; H, 7.78. Found: C, 63.3; H, 8.02.

(b) From aqueous acid

To a solution of $(C_5Me_5)_3Co_3(\mu_3\text{-}CH)(\mu\text{-}H)$ (0.20 g, 0.33 mmol) in diethyl ether (70 mL) was added 0.15 mL of a 12M degassed aqueous solution of hydrochloric acid (1.8 mmol). Upon mixing, the solution slowly changed color from black to reddish-purple and a blue colored precipitate settled out ($CoCl_2$). After stirring at room temperature for 16 h, the volatile materials were completely removed under reduced pressure and the residue was extracted with pentane (70 mL). The red-purple solution was filtered and the filtrate was concentrated to *ca.* 30 mL. Cooling to -80 °C afforded purple prisms for a total yield of 0.03 g (0.05 mmol, 15% yield).

$(C_5Me_5)_3Co_3(\mu_3\text{-}CH)(\mu_2\text{-}H)_3$

A solution of $(C_5Me_5)_3Co_3(\mu_3\text{-}CH)(\mu\text{-}H)$ (0.22 g, 0.37 mmol) in hexane (150 mL) was placed in a Fischer-Porter high pressure reaction vessel. The atmosphere above the solution was flushed 3 times with hydrogen gas before a static pressure of hydrogen (11 atm) was applied to the system. Upon mixing, the solution very slowly changed color from dark brown to dark green. After stirring at room temperature for 9 days, the mixture was transferred to a Schlenk tube. The dark green solution was filtered and the filtrate was concentrated to

ca. 60 mL. Cooling to -30 °C afforded black plates. Concentration of the mother liquor provided an additional crop of crystals for a total yield of 0.19 g (0.32 mmol, 86% yield). Mp 297 °C. IR: 2713 (w), 1675 (m), 1407 (sh), 1357 (m), 1261 (m), 1186 (m), 1156 (w), 1098 (w), 1068 (w), 1022 (s), 942 (w), 854 (m), 832 (s), 804 (m), 732 (w), 611 (m), 557 (m), 541 (m), 413 (m), 401 (m). ^{1}H NMR (C_6D_6, 293 K, 400 MHz): δ 16.92 (s, 1 H, μ_3-C<u>H</u>), 1.77 (s, 45 H, C_5<u>Me</u>$_5$), -32.06 (s, 3 H, μ_2-<u>H</u>). EIMS $(M\text{-}H_2)^+$: 596 (100,100); 597 (34,34); 598 (7,6). FAB MS (M^+): 598 (100,100); 599 (34,34); 600 (8,6). <u>Anal.</u> Calcd for $C_{31}H_{47}Co_3$: C, 62.2; H, 8.25. Found: C, 62.2; H, 8.42.

Reaction of $(C_5Me_5)_3Ni_3(\mu_3\text{-}CH)(\mu\text{-}H)$ with CCl_4

To a solution of $(C_5Me_5)_3Ni_3(\mu_3\text{-}CH)(\mu\text{-}H)$ (0.16 g, 0.27 mmol) in toluene (65 mL) was added 28 μL of CCl_4 (0.29 mmol). Upon mixing, the solution gradually changed color from brown to very pale yellow and a tan precipitate formed. After stirring at room temperature for 12 h, the solution was filtered and the volatile materials were completely removed from the filtrate under reduced pressure. The resulting residue was extracted with pentane (40 mL). The clear solution was filtered and the filtrate was concentrated to *ca.* 10 mL. Cooling to -80 °C afforded white plates of (1-chloro)(1-chloromethyl)-3,4,5,6-tetramethylfulvene for a total yield of 0.04 g (0.18 mmol, 23% yield). Mp 103-105 °C. IR: 2854 (s), 1300 (w), 1260 (m), 1217 (m), 1099 (w), 1016 (w), 1002 (w), 962 (w), 904 (m), 827 (m), 755 (w), 742 (w), 683 (m), 600 (m), 578 (w), 528 (m). ^{1}H NMR (C_6D_6, 293 K, 400 MHz): δ 4.23 (s, 2 H, -C<u>H</u>$_2$Cl), 2.34 (s, 3 H), 2.17 (s, 3 H), 1.97 (s, 3 H), 1.76 (s, 3 H). ^{13}C NMR (C_6D_6, 293 K, 23.6 MHz): δ 135.1 (s), 134.7 (s), 134.3 (s), 133.6 (s), 133.2 (s), 132.9 (s), 42.4 (t, $^1J_{C\text{-}H}$ = 150 Hz), 18.0 (q, $^1J_{C\text{-}H}$ = 127 Hz), 16.9 (q, $^1J_{C\text{-}H}$ = 127 Hz), 16.8 (q, $^1J_{C\text{-}H}$ = 126 Hz), 15.8 (q, $^1J_{C\text{-}H}$ = 127 Hz). EIMS, low res: 216 (100,100); 217 (15,12); 218 (65,65);

219 (8,8); 220 (11,11). EIMS, high res: Calcd: 216.0472; Found: 216.0469. The initial tan precipitate was insoluble in all solvents and was identified by infrared spectroscopy as $NiCl_2$.

Reaction of $(C_5Me_5)_3Co_3(\mu_3\text{-}CH)(\mu\text{-}H)$ with CO

A solution of $(C_5Me_5)_3Co_3(\mu_3\text{-}CH)(\mu\text{-}H)$ (0.07 g, 0.1 mmol) in hexane (50 mL) was placed in a Fischer-Porter high pressure reaction vessel. The atmosphere above the solution was flushed 3 times with carbon monoxide before a static pressure of CO (3 atm) was applied to the system. Upon mixing, the solution gradually changed color from dark brown to red-brown. After stirring at room temperature for 4 days, the mixture was transferred to a Schlenk tube. The volatile materials were completely removed under reduced pressure and the residue was extracted with pentane (75 mL). The red-brown solution was filtered and the filtrate was concentrated to *ca.* 25 mL. Cooling to -80 °C afforded red-brown microcrystals. Concentration of the mother liquor provided an additional crop of crystals for a total yield of 0.04 g. Infrared analysis indicated the product was a mixture of $(C_5Me_5)Co(CO)_2$ (ν_{CO}: 2008, 1883 cm^{-1} (Nujol); Lit. 2011, 1949 cm^{-1} (methylcyclohexane))[11] and $(C_5Me_5)_3Co_3(\mu_3\text{-}CO)_2$ (ν_{CO}: 1678 cm^{-1} (Nujol); Lit. 1685 cm^{-1} (hexane)).[12]

Reaction of $(C_5Me_5)_3Co_3(\mu_3\text{-}CH)(\mu_2\text{-}H)_3$ with CO

A solution of $(C_5Me_5)_3Co_3(\mu_3\text{-}CH)(\mu_2\text{-}H)_3$ (0.03 g, 0.05 mmol) in hexane (40 mL) was placed in a Fischer-Porter high pressure reaction vessel. The atmosphere above the solution was flushed 3 times with carbon monoxide before a static pressure of CO (3 atm) was applied to the system. Upon mixing, the solution gradually changed color from dark brown to red-brown. After stirring at room temperature for 4 days, the mixture was transferred to a Schlenk tube.

The red-brown solution was filtered and the filtrate was concentrated to *ca.* 15 mL. Cooling to -80 °C afforded red-brown microcrystals for a total yield of 0.02 g. The IR spectrum was identical to that found in the reaction of $(C_5Me_5)_3Co_3(\mu_3\text{-}CH)(\mu\text{-}H)$ with CO.

Reaction of $(C_5Me_5)_3Ni_3(\mu_3\text{-}CH)(\mu\text{-}H)$ with CO

A solution of $(C_5Me_5)_3Ni_3(\mu_3\text{-}CH)(\mu\text{-}H)$ (0.05 g, 0.08 mmol) in hexane (35 mL) was placed in a Fischer-Porter high pressure reaction vessel. The atmosphere above the solution was flushed 3 times with carbon monoxide before a static pressure of CO (15 atm) was applied to the system. Upon mixing, the solution slowly changed color from brown to clear red. After stirring at room temperature for 14 h, the mixture was transferred to a Schlenk tube. The red solution was filtered and the filtrate was concentrated to approximately 15 mL. Cooling to -80 °C afforded red plates. Concentration of the mother liquor provided an additional crop of crystals for a total yield of 0.04 g (0.09 mmol, 72% yield). Characterizational data is consistent with the product being $[(C_5Me_5)NiCO]_2$ (Lit. ν_{CO}: 1857, 1815 cm^{-1} (cyclohexane)).[13] Mp 170-171 °C. IR: 3633 (m), 2735 (w), 2725 (w), 1859 (s), 1805 (vs), 1505 (m), 1355 (s), 1261 (m), 1151 (m), 1099 (w), 1067 (w), 1027 (s), 941 (m), 907 (w), 803 (m), 645 (vs), 611 (s), 587 (sh), 541 (m), 486 (s), 392 (sh), 374 (s). EIMS: 442 (100,100); 443 (25,25); 444 (78,80); 445 (23,22); 446 (30,28); 447 (9,8), 448 (8,8); 449 (2,2); 450 (2,2).

Chapter 2

$(C_5Me_5)Co(acac)$

A solution of bis(pentamethylcyclopentadienyl)magnesium (1.15 g, 3.90 mmol) in tetrahydrofuran (75 mL) was added to a slurry of bis(2,4-pentanedionato)cobalt(II) (2.01 g, 7.82 mmol) in tetrahydrofuran (50 mL). Upon mixing, the solution immediately changed color from pink to deep red. After stirring at room temperature for 1 h, the volatile materials were completely removed under reduced pressure and the residue was extracted with diethyl ether (125 mL). The deep red solution was filtered and the filtrate was concentrated to *ca.* 40 mL. Cooling to -80 °C afforded deep red plates. Concentration of the mother liquor provided an additional crop of crystals for a total yield of 1.86 g (6.34 mmol, 81.1% yield). Sublimation at 60 °C under dynamic vacuum (oil diffusion pump) is necessary to separate $(C_5Me_5)Co(acac)$ from a minor volatile impurity. Mp 112-113 °C. IR: 2743 (w), 2723 (w), 2457 (w), 1958 (w), 1530 (vs), 1383 (s), 1365 (s), 1281 (s), 1193 (m), 1161 (m), 1069 (m), 1025 (s), 935 (m), 798 (s), 780 (s), 686 (w), 660 (m), 634 (m), 626 (m), 590 (w), 470 (s), 420 (m), 398 (m), 352 (w). No resonances were observed in the ^1H NMR spectrum in C_6D_6 at room temperature. EIMS: 293 (100,100); 294 (17, 19); 295 (2,2). Magnetic Susceptibility (5-300K): 5kG, μ_{eff} = 1.94 μ_B, θ = -8.69 K; 40kG, μ_{eff} = 1.91 μ_B, θ = -6.53 K. Solution Magnetic Moment (303 K, C_6D_6, 90 MHz): 1.86 μ_B. EPR: 298 K, g = 2.099, A_0 = 45.17 G; 2 K, g_1 = 1.970, A_1 = 43.11 G, g_2 = 2.091, A_2 was not observed due to line width, g_3 = 2.241, A_3 = 105.47 G.

$(C_5Me_5)Ni(acac)$

A solution of bis(pentamethylcyclopentadienyl)magnesium (1.76 g, 5.97 mmol) in tetrahydrofuran (70 mL) was added to a solution of bis(2,4-pentanedionato)nickel(II) (3.01 g, 11.7 mmol) in tetrahydrofuran (70 mL). Upon mixing, the solution immediately changed color from bright green to deep red. After stirring at room temperature for 1 h, the volatile materials were completely removed under reduced pressure and the residue was extracted with diethyl ether (150 mL). The deep red solution was filtered and the filtrate was concentrated to *ca.* 60 mL. Cooling to -80 °C afforded deep red plates. Concentration of the mother liquor provided an additional crop of crystals for a total yield of 2.89 g (9.86 mmol, 84.3% yield). Mp 98-99 °C. IR: 2735 (w), 2721 (w), 2453 (w), 1956 (w), 1550 (vs), 1390 (vs), 1276 (s), 1262 (s), 1196 (m), 1154 (m), 1066 (w), 1022 (s), 933 (s), 791 (s), 775 (s), 687 (w), 659 (m), 627 (m), 619 (m), 587 (w), 575 (w), 549 (w), 464 (s), 420 (m), 386 (m), 356 (w). ^1H NMR (C_7D_8, 299 K, 90 MHz): δ 63.40 (15H, $C_5\underline{Me}_5$, $\upsilon_{1/2}$ = 30 Hz), -2.32 (6H, acac-$C\underline{H}_3$, $\upsilon_{1/2}$ = 3 Hz), -10.04 (1H, acac-C$\underline{H}$, $\upsilon_{1/2}$ = 5 Hz). EIMS: 292 (100,100); 293 (17,18); 294 (40,39); 295 (8,8); 296 (6,6). Solution Magnetic Moment (303 K, C_6D_6, 90 MHz): 1.32 μ_B. Magnetic susceptibility measurements (5-300K) have $\chi_M < 0$ below ~140 K, and $\chi_M > 0$ above this temperature.

$(C_5Me_5)Ni(acac)PMe_3$

To a solution of sublimed $(C_5Me_5)Ni(acac)$ (0.30 g, 1.0 mmol) in pentane (40 mL) was added 0.11 mL of trimethylphosphine (1.1 mmol). Upon mixing, the solution immediately changed color from red to red-orange. After stirring at room temperature for 15 min, the solution was concentrated to *ca.* 20 mL. Cooling to -80 °C afforded red-orange plates. Concentration of the mother liquor provided an additional crop of crystals for a total yield of 0.35 g (0.95 mmol, 93% yield).

Mp 75-77 °C. IR: 3078 (w), 2742 (w), 2718 (w), 1594 (vs), 1514 (s), 1400 (vs), 1320 (sh), 1304 (m), 1284 (m), 1254 (m), 1194 (m), 1014 (m), 949 (s), 919 (m), 839 (m), 797 (w), 791 (w), 755 (m), 733 (m), 671 (w), 651 (w), 629 (w), 619 (w), 557 (m), 465 (w), 409 (m). ^{1}H NMR (C_7D_8, 297 K, 90 MHz): δ 202 (15H, $C_5\underline{Me}_5$, $\upsilon_{1/2}$ = 300 Hz), 69.6 (6H, acac-C$\underline{H}_3$, $\upsilon_{1/2}$ = 145 Hz), 5.80 (9H, PC$\underline{H}_3$, $\upsilon_{1/2}$ = 20 Hz), -14.74 (1H, acac-C$\underline{H}$, $\upsilon_{1/2}$ = 35 Hz). Anal. Calcd for $C_{18}H_{31}NiO_2P$: C, 58.6; H, 8.46. Found: C, 58.3; H, 7.89.

$(C_5Me_5)Ni(acac)PEt_3$

To a solution of sublimed $(C_5Me_5)Ni(acac)$ (0.34 g, 1.2 mmol) in pentane (50 mL) was added 0.17 mL of triethylphosphine (1.2 mmol). Upon mixing, the solution immediately changed color from red to red-orange. After stirring at room temperature for 15 min, the solution was concentrated to *ca.* 25 mL. Cooling to -80 °C afforded very thin red-orange plates. Concentration of the mother liquor provided an additional crop of crystals for a total yield of 0.38 g (0.92 mmol, 80% yield). Mp 79-81 °C. IR: 3072 (m), 2741 (w), 2725 (w), 1595 (s), 1509 (s), 1402 (vs), 1380 (m), 1370 (m), 1331 (sh), 1254 (s), 1190 (m), 1039 (s), 1013 (m), 919 (m), 763 (s), 719 (m), 701 (w), 667 (w), 652 (w), 626 (w), 554 (m), 462 (w), 406 (m). ^{1}H NMR (C_7D_8, 301 K, 90 MHz): δ 141.3 (15H, $C_5\underline{Me}_5$, $\upsilon_{1/2}$ = 325 Hz), 36.1 (6H, acac-C$\underline{H}_3$, $\upsilon_{1/2}$ = 145 Hz), 2.22 (6H, PC$\underline{H}_2$CH$_3$, $\upsilon_{1/2}$ = 15 Hz), 1.92 (9H, PCH$_2$C$\underline{H}_3$, $\upsilon_{1/2}$ = 20 Hz), -12.6 (1H, acac-C$\underline{H}$, $\upsilon_{1/2}$ = 30 Hz). Anal. Calcd for $C_{21}H_{37}NiO_2P$: C, 61.3; H, 9.07. Found: C, 61.4; H, 9.31.

Chapter 3

$[(C_5Me_5)CoCl(\mu\text{-}Cl)]_2$

A solution of $[(C_5Me_5)CoCl]_2$ (0.29 g, 0.63 mmol) in dichloromethane (45 mL) was added to a slurry of CuCl (0.14 g, 1.4 mmol) in dichloromethane (25 mL). Upon mixing, the solution very gradually changed color from dark brown to deep green and finely divided copper metal settled out. After stirring at room temperature for 24 h, the deep green solution was filtered and the filtrate was concentrated to approximately 40 mL. The resulting solution was diluted with *ca.* 40 mL of pentane, and cooling this solution to -80 °C afforded deep green needles. Concentration of the mother liquor provided an additional crop of crystals for a total yield of 0.32 g (0.60 mmol, 96% yield). Mp 280 °C (dec.). IR: 2728 (w), 1486 (m), 1262 (s), 1164 (sh), 1097 (s), 1021 (s), 959 (w), 865 (m), 803 (s), 703 (w), 592 (w), 542 (w), 442 (m), 398 (m), 316 (w), 288 (m). ^{1}H NMR (C_6D_6, 293 K, 300 MHz): δ 0.75 ($\nu_{1/2}$ = 5 Hz) (Lit.[14] δ 1.06 (CD_2Cl_2), δ 1.20 (CD_3NO_2)). EIMS $(M\text{-}Cl_2)^+$: 458 (100,100); 459 (23,22); 460 (69,67); 461 (15,15); 462 (11,12); 463 (3,2). FAB MS (sulfolane; $(M\text{-}Cl)^+$): 493 (92,100); 494 (10,22); 495 (100,100); 496 (11,22); 497 (15,34).

$(C_5Me_5)Co(Cl)PMe_3$

To a solution of $[(C_5Me_5)CoCl]_2$ (0.20 g, 0.44 mmol) in dichloromethane (20 mL) was added 0.12 mL of trimethylphosphine (1.2 mmol). Upon mixing, the solution immediately changed color from deep brown to clear red. After stirring at room temperature for 1 h, the volatile materials were completely removed under reduced pressure and the residue was extracted with pentane (60 mL). The red solution was filtered and the filtrate was concentrated to *ca.* 30 mL.

Cooling to -30 °C afforded red plates. Concentration of the mother liquor provided an additional crop of crystals for a total yield of 0.24 g (0.78 mmol, 89% yield). Mp 112-115 °C. IR: 2728 (m), 1418 (m), 1355 (sh), 1299 (m), 1279 (s), 1274 (s), 1161 (m), 1130 (w), 1071 (m), 1024 (m), 956 (s), 850 (m), 794 (w), 735 (s), 673 (m), 586 (w), 518 (w), 414 (m), 374 (m), 334 (m), 292 (m). ^{1}H NMR (C_6D_6, 293 K, 90 MHz): δ -2.75 ($\nu_{1/2}$ = 190 Hz) (no other resonances were observed at this temperature). EIMS: 305 (100,100); 306 (15,15); 307 (34,33); 308 (5,5). Anal. Calcd for $C_{13}H_{24}CoClP$: C, 51.1; H, 7.91. Found: C, 50.6; H, 7.62.

$(C_5Me_5)Co(Br)PMe_3$

To a solution of $[(C_5Me_5)CoBr]_2$ (0.24 g, 0.44 mmol) in dichloromethane (40 mL) was added 0.10 mL of trimethylphosphine (0.97 mmol). Upon mixing, the solution immediately changed color from deep brown to clear red. After stirring at room temperature for 3 h, the volatile materials were completely removed by exposing the solid to dynamic vacuum overnight. The residue was extracted with a 3:1 hexane:dichloromethane mixture (40 mL). The red solution was filtered and the filtrate was concentrated to *ca.* 20 mL. Cooling to -30 °C afforded red plates for a total yield of 0.20 g (0.57 mmol, 65% yield). Mp 121-122°C. IR: 2728 (w), 1497 (sh), 1430 (sh), 1417(m), 1356 (w), 1298 (w), 1280 (s), 1274 (s), 1158 (m), 1071 (w), 1023 (m), 957 (s), 940 (sh), 850 (m), 794 (w), 732 (s), 728 (sh), 673 (s), 587 (w), 410 (m), 366 (m). ^{1}H NMR (C_6D_6, 293 K, 90 MHz): δ -1.89 ($\nu_{1/2}$ = 150 Hz) (no other resonances were observed at this temperature). EIMS: 349 (100,100); 350 (29,15); 351 (89,98), 352 (19,14). Anal. Calcd for $C_{13}H_{24}CoBrP$: C, 44.6; H, 6.91. Found: C, 44.5; H, 6.62.

$(C_5Me_5)Co(Cl)PEt_3$

To a solution of $[(C_5Me_5)CoCl]_2$ (0.22 g, 0.48 mmol) in dichloromethane (70 mL) was added 0.15 mL of triethylphosphine (1.0 mmol). Upon mixing, the solution immediately changed color from deep brown to clear red. After stirring at room temperature for 6 h, the volatile materials were completely removed under reduced pressure and the residue was extracted with pentane (90 mL). The red solution was filtered and the filtrate was concentrated to *ca.* 40 mL. Cooling to -30 °C afforded red blocks. Concentration of the mother liquor provided an additional crop of crystals for a total yield of 0.32 g (0.92 mmol, 96% yield). Mp 160-162 °C. IR: 2724 (w), 1421 (w), 1358 (w), 1250 (m), 1242 (m), 1157 (m), 1068 (w), 1034 (s), 984 (w), 970 (w), 944 (w), 770 (s), 718 (s), 675 (w), 633 (m), 586 (w), 541 (w), 433 (w), 404 (m), 346 (w), 328 (w), 291 (w). ^1H NMR (C_6D_6, 293 K, 90 MHz): δ -0.65 ($\nu_{1/2}$ = 160 Hz) (no other resonances were observed at this temperature). EIMS: 347 (100,100); 348 (19,18); 349 (33,34); 350 (7,6). Magnetic Susceptibility (5-300 K): 5kG, μ_{eff} = 1.75 μ_B, θ = -1.19 K; 40kG, μ_{eff} = 1.77 μ_B, θ = -1.82 K. EPR: 77 K, g_1 = 1.971, A_1 = 20.90 G, g_2 = 2.080, A_2 was not observed due to line width, g_3 = 2.279, A_3 = 77.89 G (^{31}P superhyperfine on g_3 (only) was 20.5 G). Anal. Calcd for $C_{16}H_{30}CoClP$: C, 55.3; H, 8.69. Found: C, 54.8; H, 9.10.

$(C_5Me_5)Co(Br)PEt_3$

To a solution of $[(C_5Me_5)CoBr]_2$ (0.34 g, 0.62 mmol) in dichloromethane (40 mL) was added 0.20 mL of triethylphosphine (1.4 mmol). Upon mixing, the solution immediately changed color from deep brown to clear red. After stirring at room temperature for 6 h, the volatile materials were completely removed under reduced pressure and the residue was extracted with pentane (100 mL). The red solution was filtered and the filtrate was concentrated to *ca.* 75 mL.

Cooling to -30 °C afforded red blocks. Concentration of the mother liquor provided additional crops of crystals for a total yield of 0.43 g (1.1 mmol, 88% yield). Mp 170-171 °C. IR: 2725 (w), 1497 (sh), 1420 (w), 1355 (w), 1250 (m), 1242 (m), 1158 (w), 1067 (w), 1035 (s), 984 (w), 972 (w), 941 (w), 769 (s), 718 (s), 673 (w), 635 (m), 432 (w), 401 (m), 328 (w). ^{1}H NMR (C_6D_6, 293 K, 90 MHz): δ -0.64 ($\nu_{1/2}$ = 100 Hz) (no other resonances were observed at this temperature). EIMS: 391 (100,100); 392 (18,18); 393 (96,99); 394 (16,18). EPR: 81 K, g_1 = 1.993, A_1 = 20.94 G, g_2 = 2.102, A_2 was not observed due to line width, g_3 = 2.302, A_3 = 70.04 G (^{31}P superhyperfine on g_3 was not resolvable due to splitting by $^{79/81}$Br). Anal. Calcd for $C_{16}H_{30}CoBrP$: C, 49.0; H, 7.71. Found: C, 48.7; H, 7.89.

$(C_5Me_5)Co(Me)PEt_3$

To a solution of $(C_5Me_5)Co(acac)$ (0.33 g, 1.1 mmol) and triethylphosphine (0.185 mL, 1.25 mmol) in diethyl ether (60 mL) was added 1.5 mL of a 0.77M diethyl ether solution of MeLi (1.2 mmol). Upon mixing, the solution remained red, and a gray precipitate formed. After stirring at room temperature for 20 h, the volatile materials were completely removed under reduced pressure and the residue was extracted with pentane (60 mL). The red solution was filtered and the filtrate was concentrated to *ca.* 20 mL. Cooling to -80 °C afforded red plates. A second recrystallization from pentane was necessary to remove a small amount of $(C_5Me_5)Co(acac)$, producing the phosphine complex in a yield of 0.24 g (0.73 mmol, 65% yield). Mp 94-95 °C. IR: 2715 (w), 2237 (w), 1433 (sh), 1400 (w), 1247 (m), 1161 (w), 1130 (m), 1106 (w), 1034 (s), 1021 (s), 999 (w), 985 (w), 965 (w), 765 (s), 713 (s), 667 (m), 628 (s), 586 (w), 505 (m), 433 (m). ^{1}H NMR (C_6D_6, 293 K, 90 MHz): δ -1.68 ($\nu_{1/2}$ = 100 Hz) (no other resonances were observed at this temperature). EIMS:

327 (100,100); 328 (24,19). EPR: 298 K, g = 2.138; 84 K, g_1 = 2.017, A_1 = 29.76 G, g_2 = 2.075, A_2 = 24.79 G, g_3 = 2.322, A_3 = 60.93 G (^{31}P superhyperfine on g_3 (only) was 25.6 G). Anal. Calcd for $C_{17}H_{33}CoP$: C, 62.4; H, 10.16. Found: C, 62.0; H, 10.41.

$(C_5Me_5)Ni(Br)PEt_3$

To a solution of $[(C_5Me_5)NiBr]_2$ (0.27 g, 0.49 mmol) in dichloromethane (60 mL) was added 0.15 mL of triethylphosphine (1.0 mmol) at -20 °C. Upon mixing, the solution immediately changed color from red-brown to clear red. After stirring at -20 °C for 3 h, the volatile materials were completely removed under reduced pressure and the residue was extracted with pentane (150 mL). The red solution was filtered and the filtrate was concentrated to *ca.* 60 mL. Cooling to -30 °C afforded red blocks. Concentration of the mother liquor provided an additional crop of crystals for a total yield of 0.26 g (0.66 mmol, 67% yield). Mp 165-167 °C (dec.). IR: 2726 (w), 1532 (w), 1420 (s), 1346 (s), 1250 (m), 1240 (m), 1156 (m), 1066 (w), 1034 (s), 1022 (sh), 982 (w), 972 (w), 942 (w), 768 (s), 720 (s), 678 (m), 636 (m), 618 (w), 570 (w), 540 (w), 439 (m), 377 (m), 329 (w). ^{1}H NMR (C_6D_6, 293 K, 300 MHz): δ 1.49 (d, 15 H, $C_5\underline{Me}_5$, $^4J_{P-H}$ = 1.5 Hz), 1.40 (d of q, 6 H, $C\underline{H}_2CH_3$, $^2J_{P-H}$ = 8.5 Hz, $^3J_{H-H}$ = 7.5 Hz), 0.93 (d of t, 9 H, $CH_2C\underline{H}_3$, $^3J_{P-H}$ = 16 Hz, $^3J_{H-H}$ = 7.5 Hz). ^{31}P{^{1}H} NMR (C_6D_6, 293 K, 121.5 MHz): δ 24.53. EIMS: 390 (72,73); 391 (14,13); 392 (100,100); 393 (20,19); 394 (33,33); 395 (7,7); 396 (5,5). Anal. Calcd for $C_{16}H_{30}NiBrP$: C, 49.0; H, 7.71. Found: C, 48.9 ; H, 7.80.

$(C_5Me_5)Ni(Me)PEt_3$

To a solution of $(C_5Me_5)Ni(acac)$ (0.83 g, 2.8 mmol) and triethylphosphine (0.41 mL, 2.8 mmol) in diethyl ether (60 mL) was added 3.7 mL of a 0.77M

diethyl ether solution of MeLi (2.8 mmol) at 0 °C. Upon mixing, the solution immediately changed color from red to brown and a gray precipitate formed. After stirring at 0 °C for 4 h, the volatile materials were completely removed under reduced pressure and the residue was extracted with pentane (75 mL). The brown solution was filtered and the filtrate was concentrated to *ca.* 30 mL. Cooling to -80 °C afforded deep green plates. Concentration of the mother liquor provided an additional crop of crystals for a total yield of 0.75 g (2.3 mmol, 81% yield). Mp 88-89 °C. IR: 2722 (w), 2268 (w), 1431 (sh), 1421 (sh), 1359 (m), 1249 (m), 1161 (w), 1143 (s), 1063 (w), 1035 (s), 1023 (s), 999 (sh), 985 (w), 965 (w), 945 (w), 767 (s), 715 (s), 669 (w), 631 (m), 587 (w), 545 (w), 515 (m), 445 (m), 405 (w), 363 (m), 332 (w), 303 (w). ^{1}H NMR (C_6D_6, 293 K, 300 MHz): δ 1.80 (d, 15 H, $C_5\underline{Me}_5$, $^4J_{P\text{-}H}$ = 0.8 Hz), δ 1.17 (d of q, 6 H, $C\underline{H}_2CH_3$, $^2J_{P\text{-}H}$ = 7.5 Hz, $^3J_{H\text{-}H}$ = 7.5 Hz), 0.84 (d of t, 9 H, $CH_2C\underline{H}_3$, $^3J_{P\text{-}H}$ = 15 Hz, $^3J_{H\text{-}H}$ = 7.5 Hz), -0.94 (3 H, Ni-$C\underline{H}_3$, $^3J_{P\text{-}H}$ = 6 Hz). $^{31}P\{^1H\}$ NMR (C_6D_6, 293 K, 121.5 MHz): δ 34.92. EIMS: 326 (100,100); 327 (19,19); 328 (40,40); 329 (9,9); 330 (6,6). Anal. Calcd for $C_{17}H_{33}NiP$: C, 62.4; H, 10.17. Found: C, 62.2; H, 10.74. The methyl complex did not react with either H_2 (18 atm) or ethylene (9 atm).

$(C_5Me_5)Co(Cl)_2PEt_3$

To a solution of $[(C_5Me_5)CoCl_2]_2$ (0.05 g, 0.09 mmol) in dichloromethane (40 mL) was added 28 μL of triethylphosphine (0.19 mmol). Upon mixing, the solution immediately changed color from deep green to violet. After stirring at room temperature for 10 min, the volatile materials were completely removed under reduced pressure and the residue was extracted with diethyl ether (60 mL). The violet solution was filtered and the filtrate was concentrated to *ca.* 25 mL. Cooling to -80 °C afforded violet prisms. Concentration of the mother liquor provided an additional crop of crystals for a total yield of 0.05 g (0.13 mmol, 69%

yield). Mp 140-142 °C. IR: 2734 (w), 1508 (w), 1424 (m), 1358 (sh), 1260 (m), 1161 (w), 1103 (w), 1071 (w), 1037 (s), 1023 (sh), 803 (w), 754 (s), 718 (s), 700 (sh), 684 (w), 660 (w), 624 (w), 610 (w), 540 (w), 446 (w), 405 (s), 329 (w), 291 (w). ^{1}H NMR (C_6D_6, 293 K, 300 MHz): δ 1.83 (d of q, 6 H, $C\underline{H}_2CH_3$, $^{2}J_{P-H}$ = 10 Hz, $^{3}J_{H-H}$ = 7.5 Hz), 1.00 (d, 15 H, $C_5\underline{Me}_5$, $^{4}J_{P-H}$ = 1.5 Hz), 0.97 (d of t, 9 H, $CH_2C\underline{H}_3$, $^{3}J_{P-H}$ = 14 Hz, $^{3}J_{H-H}$ = 7.5 Hz). $^{31}P\{^{1}H\}$ NMR (C_6D_6, 293 K, 162 MHz): δ 25.25 ($\nu_{1/2}$ = 110 Hz). FAB MS (sulfolane): 382 (100,100); 383 (68,17); 384 (78,61); 385 (41,11); 386 (14,10). Anal. Calcd for $C_{16}H_{30}CoCl_2P$: C, 50.2; H, 7.89. Found: C, 50.2; H, 8.11.

Chapter 4

$(C_5Me_5)Co(C_5H_5)$

This complex was synthesized according to a published procedure.[15] To a solution of $(C_5Me_5)Co(acac)$ (0.58 g, 2.0 mmol) in tetrahydrofuran (70 mL) was added 1.05 mL of a 1.88M tetrahydrofuran solution of cyclopentadienylsodium (1.97 mmol). Upon mixing, the solution immediately changed color from deep red to dark brown and a white precipitate formed. After stirring at room temperature for 4 h, the volatile materials were completely removed under reduced pressure and the residue was extracted with pentane (60 mL). The dark brown solution was filtered and the filtrate was concentrated to *ca.* 20 mL. Cooling to -80 °C afforded green-black plates. Concentration of the mother liquor provided an additional crop of crystals, which were combined and sublimed at 30 °C under dynamic vacuum (oil diffusion pump) for a total yield of 0.38 g (1.5 mmol, 74% yield). Mp 106-107 °C. IR: 3100 (m), 2721 (w), 1725 (m), 1639 (m), 1548 (m), 1465 (s), 1415 (m), 1355 (sh), 1260 (w), 1104 (m), 1068 (m), 1026 (s), 998 (s), 779 (vs), 725 (sh), 581 (m), 425 (m), 395 (w), 300 (m). No resonances were observed in the ^1H NMR spectrum in C_6D_6 at room temperature. EIMS: 259 (100,100); 260 (16,17). Magnetic Susceptibility (5-300 K): 5kG, μ_{eff} = 1.76 μ_B, θ = -7.78 K; 40kG, μ_{eff} = 1.77 μ_B, θ = -7.34 K. EPR: 4.5 K, $g_\perp$ = 1.946, $A_\perp$ = 163.47 G, $g_\parallel$ = 1.818, $A_\parallel$ was not observed due to line width. Anal. Calcd for $C_{15}H_{20}Co$: C, 69.5; H, 7.78. Found: C, 69.8; H, 8.22.

$(C_5Me_5)Ni(C_5H_5)$

This complex was synthesized according to a published procedure.[15] A solution of bis(cyclopentadienyl)magnesium (0.42 g, 2.6 mmol) in tetrahydrofuran

(70 mL) was added to a solution of $(C_5Me_5)Ni(acac)$ (1.50 g, 5.11 mmol) in tetrahydrofuran (100 mL) at 0 °C. Upon mixing, the solution immediately changed color from red to bright green and a white precipitate formed. After stirring at 0 °C for 4 h, the volatile materials were completely removed under reduced pressure and the residue was extracted with pentane (80 mL). The bright green solution was filtered and the filtrate was concentrated to *ca.* 50 mL. Cooling to -80 °C afforded bright green plates. Concentration of the mother liquor provided additional crops of crystals, which were combined and sublimed at 35 °C under dynamic vacuum (oil diffusion pump) for a total yield of 1.14 g (4.40 mmol, 86.1% yield). Mp 111-112 °C (Lit.[16] 116 °C). IR: 3101 (m), 2723 (w), 1734 (m), 1634 (m), 1539 (m), 1466 (m), 1423 (s), 1263 (w), 1067 (w), 1023 (s), 1003 (vs), 869 (w), 773 (vs), 731 (w), 587 (w), 398 (sh), 376 (s). ^1H NMR (C_6D_6, 293 K, 90 MHz): δ 230 (15 H, $C_5\underline{Me}_5$, $\nu_{1/2}$ = 350 Hz), -208 (5 H, $C_5\underline{H}_5$, $\nu_{1/2}$ = 430 Hz). EIMS: 258 (100,100); 259 (19,17), 260 (40,40); 261 (9,8); 262 (6,6). Magnetic Susceptibility (25-300 K): 5kG, μ_{eff} = 3.05 μ_B, θ = -48.3 K; 40kG, μ_{eff} = 3.07 μ_B, θ = -49.3 K. No EPR signal was observed in methylcyclohexane glass (4 K).

X-ray Crystallographic Studies

$(C_5Me_5)_3Co_3(\mu_3\text{-}CH)(\mu\text{-}H)$

Black hexagonal prisms of the complex were grown from a pentane solution at -30 °C. A crystal of approximate dimensions 0.42 mm × 0.30 mm × 0.26 mm was isolated and placed in Paratone N oil.[17] The crystal was mounted on the end of a cut quartz capillary tube and placed under a flow of cold nitrogen on an Enraf-Nonius CAD4 diffractometer.[18] The solidified oil held the crystal in place and protected it from the atmosphere. The temperature was stabilized at -98 °C with an automated flow apparatus.

After centering the crystal in the X-ray beam, a set of accurate cell dimensions and an orientation matrix were determined by a least-squares fit to the setting angles of the unresolved MoKα components of 24 symmetry related reflections. The dimensions and volume of the unit cell suggested trigonal symmetry with 2 molecules in the unit cell. Details of the unit cell, collection parameters, and structure refinement are listed in Table 1.

A set of three standard reflections (-6, 4, 1; 0, 7, -1; 2, -3, 6) was chosen to monitor intensity and crystal orientation. The intensity was checked after every hour of X-ray exposure time and showed no appreciable decay over the course of the data collection. The crystal orientation was checked after every 200 reflections and was reoriented if any of the standard reflections were offset from their predicted position by more than 0.1°. The crystal orientation matrix was reoriented one time during the data collection.

The 1960 raw data were converted to structure factor amplitudes and their esds by correction for scan speed, background, and Lorentz-polarization

effects.[19,20,21] An empirical absorption correction was applied to the data based on averaged azimuthal psi scans for three reflections with $\chi > 80°$.[22] Examination of the azimuthal scans showed a variation of $I_{min}/I_{max} = 0.75$ for the average relative intensity curve. Analysis of the data revealed no systematic absences, consistent with the space group $R\bar{3}$ (No. 148). Redundant data were averaged, with 83 reflections rejected as "bad" (difference between equivalent reflections > 5σ), yielding a final total of 1273 reflections.

The coordinates of the cobalt atoms were determined by direct methods (SHELXS).[23] The locations of all non-hydrogen atoms were determined through the use of standard Fourier techniques and refined by least-squares methods. All non-hydrogen atoms were refined anisotropically. The μ^3-methylidyne carbon was disordered on either side of the tricobalt triangular face, with an approximate occupancy ratio of 3:1. A difference Fourier map revealed the positions of the pentamethylcyclopentadienyl and methylidyne (major site only) hydrogen atoms. These atoms were placed in calculated positions and included in the structure factor calculations but not refined. All hydrogen atoms were given isotropic thermal parameters 1.3 times the B(iso) of the atom to which they were bonded. The position of the hydride hydrogen bound to the metal(s) was masked by the disorder of the capping carbyne fragment, and hence was not included in the structure solution.

Final refinement of the 105 variables using the 1041 data for which $F_o^2 > 3\sigma(F_o^2)$ gave residuals of R = 4.10 and $R_w = 5.40$. The R value based on all 1270 unique data was 5.19 and the goodness-of-fit parameter was 1.855. The least squares program minimized the expression, $\Sigma w(|F_o| - |F_c|)^2$, where w is the weight of a given observation. A value of 0.04 for the p-factor was used to reduce the weight of intense reflections in the refinements.[24] The analytical forms of the scattering factor tables for the neutral atoms[25] were used and all

non-hydrogen scattering factors were corrected for both real and imaginary components of anomalous dispersion.[26]

The data were evaluated through the residuals over ranges of $\sin\theta/\lambda$, $|F_o|$, parity, and individual indices. No unusual features or trends were observed. Prior to final refinement, 3 reflections were rejected as "bad" data due to their high values of $w \times \Delta^2$. The highest and lowest peaks in the final difference Fourier map had electron densities of 0.89 and -0.14 e/Å^3, respectively, and were associated with the methylidyne carbon atoms.

Table 1. Crystal Data for $(C_5Me_5)_3Co_3(\mu_3\text{-}CH)(\mu\text{-}H)$

Formula	$Co_3C_{31}H_{47}$
FW	596.51
Space Group	$R\bar{3}$ (No. 148)
a, Å	11.561 (2)
α, deg.	100.533 (19)
V, Å^3	1455.9 (14)
Z	22
F(000)	628
d_{calc}, g/cm^3	1.358
μ_{calc}, cm^{-1}	17.04
size, mm	0.42 × 0.30 × 0.26
temperature	-98 °C
diffractometer	Enraf-Nonius CAD4
radiation	MoKα (0.71073 Å)
monochromator	highly oriented graphite
scan range, type	$3.0° \leq 2\Theta \leq 45°$, Θ-2Θ
scan width, deg.	$\Delta\Theta = 0.90 + 0.35(\tan\Theta)$
octants collected	± h, + k, + l
reflections collected	1960
unique reflections	1270
reflections, $F_o^2 > 3\sigma(F_o^2)$	1041
variables	105
R	4.10
R_w	5.40
R_{all}	5.19
GOF	1.855
largest Δ/σ in final LS cycle	0.00

$(C_5Me_5)_3Ni_3(\mu_3\text{-}CH)(\mu\text{-}H)$

Brown hexagonal prisms of the complex were grown from a pentane solution at -30 °C. A crystal of approximate dimensions 0.34 mm × 0.42 mm × 0.51 mm was isolated and placed in Paratone N oil.[17] The crystal was mounted on the end of a cut quartz capillary tube and placed under a flow of cold nitrogen on an Enraf-Nonius CAD4 diffractometer.[18] The solidified oil held the crystal in place and protected it from the atmosphere. The temperature was stabilized at -92 °C with an automated flow apparatus.

After centering the crystal in the X-ray beam, a set of accurate cell dimensions and an orientation matrix were determined by a least-squares fit to the setting angles of the unresolved MoKα components of 24 symmetry related reflections. The dimensions and volume of the unit cell suggested trigonal symmetry with 2 molecules in the unit cell. Details of the unit cell, collection parameters, and structure refinement are listed in Table 2.

A set of three standard reflections (-2, -6, 2; -6, 0, -1; -1, 5, -5) was chosen to monitor intensity and crystal orientation. The intensity was checked after every hour of X-ray exposure time and showed no appreciable decay over the course of the data collection. The crystal orientation was checked after every 200 reflections and was reoriented if any of the standard reflections were offset from their predicted position by more than 0.1°. The crystal orientation matrix did not reorient during the data collection.

The 2536 raw data were converted to structure factor amplitudes and their esds by correction for scan speed, background, and Lorentz-polarization effects.[19,20,21] An empirical absorption correction was applied to the data based on averaged azimuthal psi scans for three reflections with $\chi > 80°$.[22] Examination of the azimuthal scans showed a variation of $I_{min}/I_{max} = 0.89$ for the

average relative intensity curve. Analysis of the data revealed no systematic absences, consistent with the space group $R\bar{3}$ (No. 148). Redundant data were averaged, with 3 reflections rejected as "bad" (difference between equivalent reflections > 5σ), yielding a final total of 1705 reflections.

The coordinates of the nickel atoms were determined by direct methods (SHELXS).[23] The locations of all non-hydrogen atoms were determined through the use of standard Fourier techniques and refined by least-squares methods. All non-hydrogen atoms were refined anisotropically, except for the μ^3-methylidyne carbon. The μ^3-methylidyne carbon was disordered on either side of the trinickel triangular face, with an approximate occupancy ratio of 3:2. A difference Fourier map revealed the positions of the pentamethylcyclopentadienyl hydrogen atoms. These atoms were placed in calculated positions and included in the structure factor calculations but not refined. All hydrogen atoms were given isotropic thermal parameters 1.3 times the B(iso) of the atom to which they were bonded. The positions of the methylidyne hydrogen and the hydride hydrogen bound to the metal(s) were masked by the disorder of the capping carbyne fragment, and hence were not included in the structure solution.

Final refinement of the 104 variables using the 1354 data for which $F_o^2 > 3\sigma(F_o^2)$ gave residuals of R = 3.69 and R_w = 5.24. The R value based on all 1705 unique data was 5.00 and the goodness-of-fit parameter was 2.162. The least squares program minimized the expression, $\Sigma w(|F_o| - |F_c|)^2$, where w is the weight of a given observation. A value of 0.03 for the p-factor was used to reduce the weight of intense reflections in the refinements.[24] The analytical forms of the scattering factor tables for the neutral atoms[25] were used and all non-hydrogen scattering factors were corrected for both real and imaginary components of anomalous dispersion.[26]

The data were evaluated through the residuals over ranges of $\sin\theta/\lambda$, $|F_o|$, parity, and individual indices. No unusual features or trends were observed. Prior to final refinement, 4 reflections were rejected as "bad" data due to their high values of $w \times \Delta^2$. The highest and lowest peaks in the final difference Fourier map had electron densities of 1.20 and -0.14 e/Å^3, respectively, and were associated with the methylidyne carbon atoms.

Table 2. Crystal Data for $(C_5Me_5)_3Ni_3(\mu_3\text{-}CH)(\mu\text{-}H)$

Formula	$Ni_3C_{31}H_{47}$
FW	595.85
Space Group	$R\bar{3}$ (No. 148)
a, Å	11.5557 (24)
α, deg.	100.399 (17)
V, Å^3	1456.1 (12)
Z	2
F(000)	634
d_{calc}, g/cm^3	1.359
μ_{calc}, cm^{-1}	19.47
size, mm	$0.34 \times 0.42 \times 0.51$
temperature	-92 °C
diffractometer	Enraf-Nonius CAD4
radiation	MoKα (0.71073 Å)
monochromator	highly oriented graphite
scan range, type	$3.0° \leq 2\Theta \leq 50°$, Θ-2Θ
scan width, deg.	$\Delta\Theta = 0.60 + 0.35(\tan\Theta)$
octants collected	± h, + k, + l
reflections collected	2536
unique reflections	1705
reflections, $F_o^2 > 3\sigma(F_o^2)$	1354
variables	104
R	3.69
R_w	5.24
R_{all}	5.00
GOF	2.162
largest Δ/σ in final LS cycle	0.00

$(C_5Me_5)_3Co_3(\mu_3\text{-}CH)_2$

Red-violet hexagonal prisms of the complex were grown from a pentane solution at -80 °C. A crystal of approximate dimensions 0.51 mm × 0.40 mm × 0.34 mm was isolated and placed in Paratone N oil.[17] The crystal was mounted on the end of a cut quartz capillary tube and placed under a flow of cold nitrogen on an Enraf-Nonius CAD4 diffractometer.[18] The solidified oil held the crystal in place and protected it from the atmosphere. The temperature was stabilized at -83 °C with an automated flow apparatus.

After centering the crystal in the X-ray beam, a set of accurate cell dimensions and an orientation matrix were determined by a least-squares fit to the setting angles of the unresolved MoKα components of 24 symmetry related reflections. The dimensions and volume of the unit cell suggested trigonal symmetry with 2 molecules in the unit cell. Details of the unit cell, collection parameters, and structure refinement are listed in Table 3.

A set of three standard reflections (8, -1, -3; 0, 3, 7; 1, -8, 3) was chosen to monitor intensity and crystal orientation. The intensity was checked after every hour of X-ray exposure time and showed the intensity "faded" briefly during the course of the data collection. The "fading" was adjusted for by removing 120 reflections, which were insignificant due to the collection of redundant data. The crystal orientation was checked after every 200 reflections and was reoriented if any of the standard reflections were offset from their predicted position by more than 0.1°. The crystal orientation matrix was reoriented one time during the data collection.

The 2521 raw data were converted to structure factor amplitudes and their esds by correction for scan speed, background, and Lorentz-polarization effects.[19,20,21] An empirical absorption correction based on averaged azimuthal

psi scans for three reflections with $\chi > 80°$[22] was attempted but found to be non-representative of the crystal. The initial refinements were performed on uncorrected data and an empirical absorption correction was applied to the resulting solution using a Fourier series determined by minimizing the sum of the squares of the residuals, using the correction program provided with the MoLEN structure analysis package (DIFABS).[20b] Maximum correction was 23%. Analysis of the data revealed no systematic absences, consistent with the space group $R\bar{3}$ (No. 148). Redundant data were averaged, with 97 reflections rejected as "bad" (difference between equivalent reflections > 5σ), yielding a final total of 1600 reflections.

The coordinates of the cobalt atoms were determined by direct methods (SHELXS).[23] The locations of all non-hydrogen atoms were determined through the use of standard Fourier techniques and refined by least-squares methods. All non-hydrogen atoms were refined anisotropically. A difference Fourier map revealed the positions of all hydrogen atoms. These atoms were included in the structure refinement.

Final refinement of the 169 variables using the 1409 data for which $F_o^2 > 3\sigma(F_o^2)$ gave residuals of R = 2.67 and R_w = 3.32. The R value based on all 1600 unique data was 3.17 and the goodness-of-fit parameter was 1.625. The least squares program minimized the expression, $\Sigma w(|F_o| - |F_c|)^2$, where w is the weight of a given observation. A value of 0.03 for the p-factor was used to reduce the weight of intense reflections in the refinements.[24] The analytical forms of the scattering factor tables for the neutral atoms[25] were used and all non-hydrogen scattering factors were corrected for both real and imaginary components of anomalous dispersion.[26]

The data were evaluated through the residuals over ranges of $\sin\theta/\lambda$, $|F_o|$, parity, and individual indices. No unusual features or trends were

observed. The highest and lowest peaks in the final difference Fourier map had electron densities of 0.29 and -0.12 e/Å^3, respectively, and were associated with the carbyne atoms.

Table 3. Crystal Data for $(C_5Me_5)_3Co_3(\mu_3\text{-}CH)_2$

Formula	$Co_3C_{32}H_{47}$
FW	608.53
Space Group	$R\bar{3}$ (No. 148)
a, Å	11.5003 (13)
α, deg.	100.132 (10)
V, Å^3	1439.9 (7)
Z	2
F(000)	640
d_{calc}, g/cm^3	1.403
μ_{calc}, cm^{-1}	17.24
size, mm	0.51 × 0.40 × 0.34
temperature	-83 °C
diffractometer	Enraf-Nonius CAD4
radiation	MoKα (0.71073 Å)
monochromator	highly oriented graphite
scan range, type	3.0° ≤ 2Θ ≤ 50°, Θ-2Θ
scan width, deg.	ΔΘ = 0.80 + 0.35(tan Θ)
octants collected	± h, + k, + l
reflections collected	2521
unique reflections	1600
reflections, $F_o^2 > 3\sigma(F_o^2)$	1409
variables	169
R	2.67
R_w	3.32
R_{all}	3.17
GOF	1.625
largest Δ/σ in final LS cycle	0.01

$(C_5Me_5)Co(acac)$

Clear red prisms of the complex were grown by sublimation at 60 °C at 10^{-4} torr. A crystal of approximate dimensions 0.50 mm × 0.39 mm × 0.20 mm was isolated and placed in Paratone N oil.[17] The crystal was mounted on the end of a cut quartz capillary tube and placed under a flow of cold nitrogen on an Enraf-Nonius CAD4 diffractometer.[18] The solidified oil held the crystal in place and protected it from the atmosphere. The temperature was stabilized at -110 ° C with an automated flow apparatus.

After centering the crystal in the X-ray beam, a set of accurate cell dimensions and an orientation matrix were determined by a least-squares fit to the setting angles of the unresolved MoKα components of 24 symmetry related reflections. The original cell found and used for data collection was a non-primitive doubled cell with C-centering. Upon transformation to a primitive cell, the dimensions and volume of the unit cell suggested triclinic symmetry with 4 molecules in the unit cell. Details of the unit cell, collection parameters, and structure refinement are listed in Table 4.

A set of three standard reflections (2, 5, -6; -6, -7, 8; 2, -1, -8) was chosen to monitor intensity and crystal orientation. The intensity was checked after every hour of X-ray exposure time and showed no appreciable decay over the course of the data collection. The crystal orientation was checked after every 200 reflections and was reoriented if any of the standard reflections were offset from their predicted position by more than 0.1°. The crystal orientation matrix did not reorient during the data collection.

The 7937 raw data were converted to structure factor amplitudes and their esds by correction for scan speed, background, and Lorentz-polarization effects.[19,20,21] An empirical absorption correction based on averaged azimuthal

psi scans for three reflections with $\chi > 80°$[22] was attempted but found to be non-representative of the crystal. The initial refinements were performed on uncorrected data and an empirical absorption correction was applied to the resulting solution using a Fourier series determined by minimizing the sum of the squares of the residuals, using the correction program provided with the MoLEN structure analysis package (DIFABS).[20b] Maximum correction was 17%. Analysis of the data revealed the following systematic absences: h k l, h + k odd, consistent with a C-centered cell. After the aforementioned cell transformation to the primitive cell was performed, the 3848 remaining reflections showed no systematic absences, consistent with the space group $P\bar{1}$ (No. 2).

The coordinates of the cobalt atoms were determined by Patterson methods. The locations of all non-hydrogen atoms were determined through the use of standard Fourier techniques and refined by least-squares methods. All non-hydrogen atoms were refined anisotropically. A difference Fourier map revealed the positions of the hydrogen atoms. These atoms were placed in calculated positions and included in the structure factor calculations but not refined. All hydrogen atoms were given isotropic thermal parameters 1.3 times the B(iso) of the atom to which they were bonded.

Final refinement of the 325 variables using the 2945 data for which $F_o^2 > 3\sigma(F_o^2)$ gave residuals of R = 4.22 and R_w = 5.40. The R value based on all 3848 unique data was 6.01 and the goodness-of-fit parameter was 1.694. The least squares program minimized the expression, $\Sigma w(|F_o| - |F_c|)^2$, where w is the weight of a given observation. A value of 0.05 for the p-factor was used to reduce the weight of intense reflections in the refinements.[24] The analytical forms of the scattering factor tables for the neutral atoms[25] were used and all non-hydrogen scattering factors were corrected for both real and imaginary components of anomalous dispersion.[26]

The data were evaluated through the residuals over ranges of $\sin\theta/\lambda$, $|F_o|$, parity, and individual indices. No unusual features or trends were observed. The highest and lowest peaks in the final difference Fourier map had electron densities of 0.53 and -0.12 e/Å^3, respectively, and were associated with the cobalt atoms.

Table 4. Crystal Data for $(C_5Me_5)Co(acac)$

Formula	$CoO_2C_{15}H_{22}$
FW	293.27
Space Group	$P\bar{1}$ (No. 2)
a, Å	8.539 (3)
b, Å	12.399 (4)
c, Å	15.505 (4)
α, deg.	70.39 (2)
β, deg.	81.04 (2)
γ, deg.	72.64 (2)
V, $Å^3$	1473.1 (6)
Z	4
F(000)	620
d_{calc}, g/cm^3	1.322
μ_{calc}, cm^{-1}	11.54
size, mm	$0.50 \times 0.39 \times 0.20$
temperature	-110 °C
diffractometer	Enraf-Nonius CAD4
radiation	MoKα (0.71073 Å)
monochromator	highly oriented graphite
scan range, type	$3.0° \leq 2\Theta \leq 45°$, Θ-2Θ
scan width, deg.	$\Delta\Theta = 1.00 + 0.35(\tan\Theta)$
octants collected	$+h, \pm k, \pm l$
reflections collected	7937
unique reflections	3848
reflections, $F_o^2 > 3\sigma(F_o^2)$	2945
variables	325
R	4.22
R_w	5.40
R_{all}	6.01
GOF	1.694
largest Δ/σ in final LS cycle	0.01

$(C_5Me_5)Ni(acac)$

Clear red plates of the complex were grown from a pentane solution at -80 °C. A crystal of approximate dimensions 0.50 mm × 0.42 mm × 0.25 mm was isolated and placed in Paratone N oil.[17] The crystal was mounted on the end of a cut quartz capillary tube and placed under a flow of cold nitrogen on an Enraf-Nonius CAD4 diffractometer.[18] The solidified oil held the crystal in place and protected it from the atmosphere. The temperature was stabilized at -103 °C with an automated flow apparatus.

After centering the crystal in the X-ray beam, a set of accurate cell dimensions and an orientation matrix were determined by a least-squares fit to the setting angles of the unresolved MoKα components of 24 symmetry related reflections. The dimensions and volume of the unit cell suggested triclinic symmetry with 4 molecules in the unit cell. Details of the unit cell, collection parameters, and structure refinement are listed in Table 5.

A set of three standard reflections (3, 5, 8; -4, -4, 2; 0, 3, -7) was chosen to monitor intensity and crystal orientation. The intensity was checked after every hour of X-ray exposure time and showed no appreciable decay over the course of the data collection. The crystal orientation was checked after every 200 reflections and was reoriented if any of the standard reflections were offset from their predicted position by more than 0.1°. The crystal orientation matrix was reoriented one time during the data collection.

The 3848 raw data were converted to structure factor amplitudes and their esds by correction for scan speed, background, and Lorentz-polarization effects.[19,20,21] An empirical absorption correction was applied to the data based on averaged azimuthal psi scans for three reflections with $\chi > 80°$.[22] Examination of the azimuthal scans showed a variation of $I_{min}/I_{max} = 0.84$ for the

average relative intensity curve. Analysis of the data revealed no systematic absences, consistent with the space group $P\bar{1}$ (No. 2).

The coordinates of the nickel atoms were determined by direct methods (SHELXS).[23] The locations of all non-hydrogen atoms were determined through the use of standard Fourier techniques and refined by least-squares methods. The data were evaluated through the residuals over ranges of $\sin\theta/\lambda$, $|F_o|$, parity, and individual indices. This revealed sections of poor data throughout the data set. A total of 114 data were rejected as "bad" before the structure refined properly. The problem resulted from a peculiarity in crystal mounting that caused misalignment of reflections with very high χ. All non-hydrogen atoms were refined anisotropically. A difference Fourier map revealed the positions of all of the hydrogen atoms. These atoms were placed in calculated positions and included in the structure factor calculations but not refined. All hydrogen atoms were given isotropic thermal parameters 1.3 times the B(iso) of the atom to which they were bonded.

Final refinement of the 325 variables using the 2964 data for which $F_o^2 > 3\sigma(F_o^2)$ gave residuals of $R = 4.81$ and $R_w = 6.26$. The R value based on all 3848 unique data was 6.17 and the goodness-of-fit parameter was 1.962. The least squares program minimized the expression, $\Sigma w(|F_o| - |F_c|)^2$, where w is the weight of a given observation. A value of 0.05 for the p-factor was used to reduce the weight of intense reflections in the refinements.[24] The analytical forms of the scattering factor tables for the neutral atoms[25] were used and all non-hydrogen scattering factors were corrected for both real and imaginary components of anomalous dispersion.[26]

The highest and lowest peaks in the final difference Fourier map had electron densities of 0.89 and -0.17 e/Å^3, respectively, and were associated with the nickel atoms.

Table 5. Crystal Data for $(C_5Me_5)Ni(acac)$

Formula	$NiO_2C_{15}H_{22}$
FW	293.05
Space Group	$P\bar{1}$ (No. 2)
a, Å	8.4857 (20)
b, Å	12.4969 (32)
c, Å	15.9013 (25)
α, deg.	68.608 (17)
β, deg.	77.179 (16)
γ, deg.	71.958 (21)
V, Å^3	1481.5 (6)
Z	4
F(000)	624
d_{calc}, g/cm^3	1.314
μ_{calc}, cm^{-1}	13.06
size, mm	$0.50 \times 0.42 \times 0.25$
temperature	-103 °C
diffractometer	Enraf-Nonius CAD4
radiation	MoKα (0.71073 Å)
monochromator	highly oriented graphite
scan range, type	$3.0° \leq 2\Theta \leq 45.0°$, Θ-2Θ
scan width, deg.	$\Delta\Theta = 0.80 + 0.35(\tan \Theta)$
octants collected	$+ h, \pm k, \pm l$
reflections collected	3848
unique reflections	3848
reflections, $F_o^2 > 3\sigma(F_o^2)$	2964
variables	325
R	4.81
R_w	6.26
R_{all}	6.17
GOF	1.962
largest Δ/σ in final LS cycle	0.01

$(C_5Me_5)Ni(acac)PMe_3$

Red-orange plates of the complex were grown from a pentane solution at -80 °C. A crystal of approximate dimensions 0.20 mm × 0.27 mm × 0.34 mm was isolated and placed in Paratone N oil.[17] The crystal was mounted on the end of a cut quartz capillary tube and placed under a flow of cold nitrogen on an Enraf-Nonius CAD4 diffractometer.[18] The solidified oil held the crystal in place and protected it from the atmosphere. The temperature was stabilized at -125 ° C with an automated flow apparatus.

After centering the crystal in the X-ray beam, a set of accurate cell dimensions and an orientation matrix were determined by a least-squares fit to the setting angles of the unresolved MoKα components of 24 symmetry related reflections. The dimensions and volume of the unit cell suggested orthorhombic symmetry with 4 molecules in the unit cell. Details of the unit cell, collection parameters, and structure refinement are listed in Table 6.

A set of three standard reflections (6, 2, -1; 1, 7, 4; 1, -1, 8) was chosen to monitor intensity and crystal orientation. The intensity was checked after every hour of X-ray exposure time and showed an abrupt fading near the middle of the data collection. The region from 4 0 0 to 6 6 2 was duplicated by recollection at the end of the data set. The crystal orientation was checked after every 200 reflections and was reoriented if any of the standard reflections were offset from their predicted position by more than 0.1°. The crystal orientation matrix was reoriented 2 times during the data collection.

The 1883 raw data were converted to structure factor amplitudes and their esds by correction for scan speed, background, and Lorentz-polarization effects.[19,20,21] An empirical absorption correction based on averaged azimuthal psi scans for four reflections with $\chi > 80°$[22] was attempted but found to be non-

representative of the crystal. The initial refinements were performed on uncorrected data and an empirical absorption correction was applied to the resulting solution using a Fourier series determined by minimizing the sum of the squares of the residuals, using the correction program provided with the MoLEN structure analysis package (DIFABS).[20b] Maximum correction was 15%. Analysis of the data revealed the following systematic absences: h k 0, h odd; 0 k l, k + l odd, consistent with the space group Pnma (No. 62). Redundant data were not averaged because comparison of the region from 4 0 0 to 6 6 2 showed that the fading during collection decreased the intensities of these reflections. Subsequently, the initial values of these reflections were discarded, yielding a final total of 1339 reflections.

The coordinates of the nickel and phosphorus atoms were determined by Patterson methods. The locations of all non-hydrogen atoms were determined through the use of standard Fourier techniques and refined by least-squares methods. All non-hydrogen atoms were refined anisotropically. A difference Fourier map revealed the positions of all hydrogen atoms not lying on the mirror plane. These atoms were placed in calculated positions and included in the structure factor calculations but not refined. All hydrogen atoms were given isotropic thermal parameters 1.3 times the B(iso) of the atom to which they were bonded.

Final refinement of the 109 variables using the 954 data for which $F_o^2 > 3\sigma(F_o^2)$ gave residuals of R = 4.36 and R_w = 5.80. The R value based on all 1339 unique data was 6.74 and the goodness-of-fit parameter was 2.096. The least squares program minimized the expression, $\Sigma w(|F_o| - |F_c|)^2$, where w is the weight of a given observation. A value of 0.04 for the p-factor was used to reduce the weight of intense reflections in the refinements.[24] The analytical forms of the scattering factor tables for the neutral atoms[25] were used and all

non-hydrogen scattering factors were corrected for both real and imaginary components of anomalous dispersion.[26]

The data were evaluated through the residuals over ranges of $\sin\theta/\lambda$, $|F_o|$, parity, and individual indices. No unusual features or trends were observed. The highest and lowest peaks in the final difference Fourier map had electron densities of 0.47 and -0.38 e/Å^3, respectively, and were associated with the nickel atom.

Table 6. Crystal Data for $(C_5Me_5)Ni(acac)PMe_3$

Formula	$NiPO_2C_{18}H_{31}$
FW	369.13
Space Group	Pnma (No. 62)
a, Å	13.3111 (30)
b, Å	13.8551 (17)
c, Å	10.6376 (34)
V, Å^3	1961.9 (8)
Z	4
F(000)	792
d_{calc}, g/cm^3	1.250
μ_{calc}, cm^{-1}	10.77
size, mm	$0.20 \times 0.27 \times 0.34$
temperature	-125 °C
diffractometer	Enraf-Nonius CAD4
radiation	MoKα (0.71073 Å)
monochromator	highly oriented graphite
scan range, type	$3.0° \leq 2\Theta \leq 45.0°$, Θ-2Θ
scan width, deg.	$\Delta\Theta = 0.80 + 0.35(\tan \Theta)$
octants collected	+ h, + k, + l
reflections collected	1883
unique reflections	1339
reflections, $F_o^2 > 3\sigma(F_o^2)$	954
variables	109
R	4.36
R_w	5.80
R_{all}	6.74
GOF	2.096
largest Δ/σ in final LS cycle	0.00

$(C_5Me_5)Co(Cl)PEt_3$

Dark red plates of the complex were grown from a pentane solution at -30 °C. A crystal of approximate dimensions 0.13 mm × 0.37 mm × 0.47 mm was isolated and placed in Paratone N oil.[17] The crystal was mounted on the end of a cut quartz capillary tube and placed under a flow of cold nitrogen on an Enraf-Nonius CAD4 diffractometer.[18] The solidified oil held the crystal in place and protected it from the atmosphere. The temperature was stabilized at -118 ° C with an automated flow apparatus.

After centering the crystal in the X-ray beam, a set of accurate cell dimensions and an orientation matrix were determined by a least-squares fit to the setting angles of the unresolved MoKα components of 24 symmetry related reflections. The dimensions and volume of the unit cell suggested tetragonal symmetry with 4 molecules in the unit cell. Details of the unit cell, collection parameters, and structure refinement are listed in Table 7.

A set of three standard reflections (7, -3, 2; -1, 8, 1; 2, -5, -4) was chosen to monitor intensity and crystal orientation. The intensity was checked after every hour of X-ray exposure time and showed no appreciable decay over the course of the data collection. The crystal orientation was checked after every 250 reflections and was reoriented if any of the standard reflections were offset from their predicted position by more than 0.1°. The crystal orientation matrix did not reorient during the data collection.

The 1807 raw data were converted to structure factor amplitudes and their esds by correction for scan speed, background, and Lorentz-polarization effects.[19,20,21] An empirical absorption correction was applied to the data based on averaged azimuthal psi scans for three reflections with $\chi > 80°$.[22] Examination of the azimuthal scans showed a variation of $I_{min}/I_{max} = 0.96$ for the

average relative intensity curve. Analysis of the data revealed no systematic absences, consistent with the space group $P\bar{4}$ (No. 81). Redundant data were averaged, with no reflections rejected as "bad" (difference between equivalent reflections > 5σ), yielding a final total of 1792 reflections.

The coordinates of the cobalt, chlorine and phosphorus atoms were determined by Patterson methods. The locations of all non-hydrogen atoms were determined through the use of standard Fourier techniques and refined by least-squares methods. All non-hydrogen atoms were refined anisotropically. A difference Fourier map revealed the positions of most of the hydrogen atoms. These atoms were placed in calculated positions and included in the structure factor calculations but not refined. All hydrogen atoms were given isotropic thermal parameters 1.3 times the B(iso) of the atom to which they were bonded.

Final refinement of the 172 variables using the 1614 data for which $F_o^2 > 3\sigma(F_o^2)$ gave residuals of R = 5.08 and R_w = 5.78. The R value based on all 1792 unique data was 5.68 and the goodness-of-fit parameter was 2.271. The least squares program minimized the expression, $\Sigma w(|F_o| - |F_c|)^2$, where w is the weight of a given observation. A value of 0.03 for the p-factor was used to reduce the weight of intense reflections in the refinements.[24] The analytical forms of the scattering factor tables for the neutral atoms[25] were used and all non-hydrogen scattering factors were corrected for both real and imaginary components of anomalous dispersion.[26]

The data were evaluated through the residuals over ranges of $\sin\theta/\lambda$, $|F_o|$, parity, and individual indices. Prior to final refinement, 31 reflections were rejected as "bad" data due to their high values of $w \times \Delta^2$. This was probably due to multiple diffraction, and reflections were rejected using an arbitrary cutoff of $\Delta / F_{obs} > 0.22$ for positive values of Δ. The highest and lowest peaks in the final

difference Fourier map had electron densities of 0.61 and -0.28 e/Å^3, respectively, and were associated with the cobalt atom.

Table 7. Crystal Data for $(C_5Me_5)Co(Cl)PEt_3$

Formula	$CoClPC_{16}H_{30}$
FW	347.78
Space Group	$P\bar{4}$ (No. 81)
a, Å	14.260 (3)
c, Å	8.725 (2)
V, Å^3	1774.2 (6)
Z	4
F(000)	740
d_{calc}, g/cm^3	1.302
μ_{calc}, cm^{-1}	11.93
size, mm	$0.13 \times 0.37 \times 0.47$
temperature	-118 °C
diffractometer	Enraf-Nonius CAD4
radiation	MoKα (0.71073 Å)
monochromator	highly oriented graphite
scan range, type	$3.0° \leq 2\Theta \leq 50.0°$, Θ-2Θ
scan width, deg.	$\Delta\Theta = 0.70 + 0.35(\tan\Theta)$
octants collected	+ h, + k, + l
reflections collected	1807
unique reflections	1792
reflections, $F_o^2 > 3\sigma(F_o^2)$	1614
variables	172
R	5.08
R_w	5.78
R_{all}	5.68
GOF	2.271
largest Δ/σ in final LS cycle	0.00

$(C_5Me_5)Ni(Br)PEt_3$

Red plates of the complex were grown from a pentane solution at -30 °C. A crystal of approximate dimensions 0.25 mm × 0.45 mm × 0.50 mm was isolated and placed in Paratone N oil.[17] The crystal was mounted on the end of a cut quartz capillary tube and placed under a flow of cold nitrogen on an Enraf-Nonius CAD4 diffractometer.[18] The solidified oil held the crystal in place and protected it from the atmosphere. The temperature was stabilized at -112 °C with an automated flow apparatus.

After centering the crystal in the X-ray beam, a set of accurate cell dimensions and an orientation matrix were determined by a least-squares fit to the setting angles of the unresolved MoKα components of 24 symmetry related reflections. The dimensions and volume of the unit cell suggested tetragonal symmetry with 4 molecules in the unit cell. Details of the unit cell, collection parameters, and structure refinement are listed in Table 8.

A set of three standard reflections (8, 1, 1; 6, -6, 1; 4, 6, -3) was chosen to monitor intensity and crystal orientation. The intensity was checked after every hour of X-ray exposure time and showed no appreciable decay over the course of the data collection. The crystal orientation was checked after every 200 reflections and was reoriented if any of the standard reflections were offset from their predicted position by more than 0.1°. The crystal orientation matrix did not reorient during the data collection.

The 1858 raw data were converted to structure factor amplitudes and their esds by correction for scan speed, background, and Lorentz-polarization effects.[19,20,21] An empirical absorption correction was applied to the data based on averaged azimuthal psi scans for three reflections with $\chi > 80°$.[22] Examination of the azimuthal scans showed a variation of $I_{min}/I_{max} = 0.75$ for the

average relative intensity curve. Analysis of the data revealed no systematic absences, consistent with the space group $P\bar{4}$ (No. 81). Redundant data were averaged, with 6 reflections rejected as "bad" (difference between equivalent reflections > 5σ), yielding a final total of 1842 reflections.

The coordinates of the nickel and bromine atoms were determined by Patterson methods. The locations of all non-hydrogen atoms were determined through the use of standard Fourier techniques and refined by least-squares methods. All non-hydrogen atoms were refined anisotropically. A difference Fourier map revealed the positions of most of the hydrogen atoms. These atoms were placed in calculated positions and included in the structure factor calculations but not refined. All hydrogen atoms were given isotropic thermal parameters 1.3 times the B(iso) of the atom to which they were bonded.

Final refinement of the 172 variables using the 1610 data for which $F_o^2 > 3\sigma(F_o^2)$ gave residuals of $R = 3.37$ and $R_w = 3.87$. The R value based on all 1842 unique data was 4.19 and the goodness-of-fit parameter was 1.355. The least squares program minimized the expression, $\Sigma w(|F_o| - |F_c|)^2$, where w is the weight of a given observation. A value of 0.04 for the p-factor was used to reduce the weight of intense reflections in the refinements.[24] The analytical forms of the scattering factor tables for the neutral atoms[25] were used and all non-hydrogen scattering factors were corrected for both real and imaginary components of anomalous dispersion.[26]

The data were evaluated through the residuals over ranges of $\sin\theta/\lambda$, $|F_o|$, parity, and individual indices. No unusual features or trends were observed. Prior to final refinement, 2 reflections were rejected as "bad" data due to their high values of $w \times \Delta^2$. The highest and lowest peaks in the final difference Fourier map had electron densities of 0.77 and -0.19 e/Å^3, respectively, and were associated with the nickel atom.

Table 8. Crystal Data for $(C_5Me_5)Ni(Br)PEt_3$

Formula	$NiBrPC_{16}H_{30}$
FW	1813.7
Space Group	$P\bar{4}$ (No. 81)
a, Å	14.416 (2)
c, Å	8.7271 (13)
V, Å^3	1813.7 (9)
Z	4
F(000)	840
d_{calc}, g/cm^3	1.458
μ_{calc}, cm^{-1}	33.33
size, mm	$0.25 \times 0.45 \times 0.50$
temperature	-112 °C
diffractometer	Enraf-Nonius CAD4
radiation	MoKα (0.71073 Å)
monochromator	highly oriented graphite
scan range, type	$3.0° \leq 2\Theta \leq 50.0°$, Θ-2Θ
scan width, deg.	$\Delta\Theta = 0.60 + 0.35(\tan\Theta)$
octants collected	+ h, + k, + l
reflections collected	1858
unique reflections	1842
reflections, $F_o^2 > 3\sigma(F_o^2)$	1610
variables	172
R	3.37
R_w	3.87
R_{all}	4.19
GOF	1.355
largest Δ/σ in final LS cycle	0.00

$(C_5Me_5)Ni(Me)PEt_3$

Dark green plates of the complex were grown from a pentane solution at -80 °C. A crystal of approximate dimensions 0.35 mm × 0.34 mm × 0.29 mm was isolated and placed in Paratone N oil.[17] The crystal was mounted on the end of a cut quartz capillary tube and placed under a flow of cold nitrogen on an Enraf-Nonius CAD4 diffractometer.[18] The solidified oil held the crystal in place and protected it from the atmosphere. The temperature was stabilized at -89 °C with an automated flow apparatus.

After centering the crystal in the X-ray beam, a set of accurate cell dimensions and an orientation matrix were determined by a least-squares fit to the setting angles of the unresolved MoKα components of 24 symmetry related reflections. The original cell found and used for data collection was a non-primitive doubled cell with C-centering. Upon transformation to a primitive cell, the dimensions and volume of the unit cell suggested tetragonal symmetry with 4 molecules in the unit cell. Details of the unit cell, collection parameters, and structure refinement are listed in Table 9.

A set of three standard reflections (-2, 4, 5; -7, -11, 2; 7, -11, -2) was chosen to monitor intensity and crystal orientation. The intensity was checked after every hour of X-ray exposure time and showed a slight linear intensity decay over the course of the data collection. The decay was expressed as a linear function and a correction was applied to the data, with a maximum correction of 1.8%. The crystal orientation was checked after every 200 reflections and was reoriented if any of the standard reflections were offset from their predicted position by more than 0.1°. The crystal orientation matrix did not reorient during the data collection.

The 3638 raw data were converted to structure factor amplitudes and their esds by correction for scan speed, background, and Lorentz-polarization effects.[19,20,21] An empirical absorption correction based on averaged azimuthal psi scans for three reflections with $\chi > 80°$[22] was attempted but found to be non-representative of the crystal. The initial refinements were performed on uncorrected data and an empirical absorption correction was applied to the resulting solution using a Fourier series determined by minimizing the sum of the squares of the residuals, using the correction program provided with the MoLEN structure analysis package (DIFABS).[20b] Maximum correction was 16%. Analysis of the data revealed the following systematic absences: h k l, h + k odd, consistent with a C-centered cell. After the aforementioned cell transformation to the primitive cell was performed, the 1814 remaining reflections showed no systematic absences, consistent with the space group $P\bar{4}$ (No. 81).

The coordinates of the nickel and phosphorus atoms were determined by Patterson methods. The locations of all non-hydrogen atoms were determined through the use of standard Fourier techniques and refined by least-squares methods. Only the following atoms were refined anisotropically: the nickel, the Cp* ring carbons, and all non-hydrogen atoms related to the PEt_3 ligand. The methyl carbon was refined isotropically. The structure revealed a disorder of the Cp* ligand across a pseudo-mirror plane containing the nickel and phosphorus atoms, the methyl carbon, and C2 of the Cp* ligand. The methyl carbons of the Cp* ligand were modeled using a 2:1 occupancy ratio of two sites displaced circumferentially by approximately 0.5 Å in either direction from the predicted location of the methyl carbon (based on an idealized geometry for the Cp* ligand). A difference Fourier map revealed the positions of the methyl and triethylphosphine hydrogen atoms. Only these atoms were placed in calculated positions. They were included in the structure factor calculations but not refined.

All hydrogen atoms were given isotropic thermal parameters 1.3 times the B(iso) of the atom to which they were bonded. The positions of the Cp* hydrogens were masked by the disorder, and hence were not included in the structure solution.

Final refinement of the 162 variables using the 1594 data for which $F_o^2 > 3\sigma(F_o^2)$ gave residuals of R = 8.51 and R_w = 10.65. The R value based on all 1814 unique data was 9.53 and the goodness-of-fit parameter was 3.245. The least squares program minimized the expression, $\Sigma w(|F_o| - |F_c|)^2$, where w is the weight of a given observation. A value of 0.04 for the p-factor was used to reduce the weight of intense reflections in the refinements.[24] The analytical forms of the scattering factor tables for the neutral atoms[25] were used and all non-hydrogen scattering factors were corrected for both real and imaginary components of anomalous dispersion.[26]

The data were evaluated through the residuals over ranges of $\sin\theta/\lambda$, $|F_o|$, parity, and individual indices. No unusual features or trends were observed. Prior to final refinement, 8 reflections were rejected as "bad" data due to their high values of $w \times \Delta^2$. The highest and lowest peaks in the final difference Fourier map had electron densities of 0.97 and -0.39 e/Å^3, respectively, and were associated with the C_5Me_5 ring carbon atoms.

Table 9. Crystal Data for $(C_5Me_5)Ni(Me)PEt_3$

Formula	$NiPC_{17}H_{33}$
FW	327.14
Space Group	$P\bar{4}$ (No. 81)
a, Å	14.455 (4)
c, Å	8.706 (2)
V, Å^3	1819.1 (6)
Z	4
F(000)	712
d_{calc}, g/cm^3	1.194
μ_{calc}, cm^{-1}	11.46
size, mm	$0.35 \times 0.34 \times 0.29$
temperature	-89 °C
diffractometer	Enraf-Nonius CAD4
radiation	MoKα (0.71073 Å)
monochromator	highly oriented graphite
scan range, type	$3.0° \leq 2\Theta \leq 50.0°$, Θ-2Θ
scan width, deg.	$\Delta\Theta = 1.00 + 0.35(\tan\Theta)$
octants collected	+ h, + k, + l
reflections collected	3638
unique reflections	1814
reflections, $F_o^2 > 3\sigma(F_o^2)$	1594
variables	162
R	8.51
R_w	10.65
R_{all}	9.53
GOF	3.245
largest Δ/σ in final LS cycle	0.01

$(C_5Me_5)Co(C_5H_5)$

Black polyhedra of the complex were grown by sublimation at 30 °C at 10^{-4} torr. A crystal of approximate dimensions 0.41 mm × 0.41 mm × 0.32 mm was isolated and placed in Paratone N oil.[17] The crystal was mounted on the end of a cut quartz capillary tube and placed under a flow of cold nitrogen on an Enraf-Nonius CAD4 diffractometer.[18] The solidified oil held the crystal in place and protected it from the atmosphere. The temperature was stabilized at -114 ° C with an automated flow apparatus.

After centering the crystal in the X-ray beam, a set of accurate cell dimensions and an orientation matrix were determined by a least-squares fit to the setting angles of the unresolved MoKα components of 24 symmetry related reflections. The dimensions and volume of the unit cell suggested triclinic symmetry with 2 molecules in the unit cell. Details of the unit cell, collection parameters, and structure refinement are listed in Table 10.

A set of three standard reflections (1, 1, -7; 3, -4, 4; -2, -3, 2) was chosen to monitor intensity and crystal orientation. The intensity was checked after every hour of X-ray exposure time and showed no appreciable decay over the course of the data collection. The crystal orientation was checked after every 200 reflections and was reoriented if any of the standard reflections were offset from their predicted position by more than 0.1°. The crystal orientation matrix was reoriented one time during the data collection.

The 3363 raw data were converted to structure factor amplitudes and their esds by correction for scan speed, background, and Lorentz-polarization effects.[19,20,21] An empirical absorption correction was applied to the data based on averaged azimuthal psi scans for three reflections with $\chi > 80°$.[22] Examination of the azimuthal scans showed a variation of $I_{min}/I_{max} = 0.87$ for the

average relative intensity curve. Analysis of the data revealed no systematic absences, consistent with the space group $P\bar{1}$ (No. 2). Redundant data were averaged, with 58 reflections rejected as "bad" (difference between equivalent reflections > 5σ), yielding a final total of 1682 reflections.

The coordinates of the cobalt atom was determined by Patterson methods. The locations of all non-hydrogen atoms were determined through the use of standard Fourier techniques and refined by least-squares methods. All non-hydrogen atoms were refined anisotropically. A difference Fourier map revealed the positions of all hydrogen atoms. These atoms were included in the structure refinement.

Final refinement of the 225 variables using the 1532 data for which $F_o^2 > 3\sigma(F_o^2)$ gave residuals of R = 2.09 and R_w = 2.83. The R value based on all 1682 unique data was 2.38 and the goodness-of-fit parameter was 1.560. The least squares program minimized the expression, $\Sigma w(|F_o| - |F_c|)^2$, where w is the weight of a given observation. A value of 0.02 for the p-factor was used to reduce the weight of intense reflections in the refinements.[24] The analytical forms of the scattering factor tables for the neutral atoms[25] were used and all non-hydrogen scattering factors were corrected for both real and imaginary components of anomalous dispersion.[26]

The data were evaluated through the residuals over ranges of $\sin\theta/\lambda$, $|F_o|$, parity, and individual indices. No unusual features or trends were observed. The highest and lowest peaks in the final difference Fourier map had electron densities of 0.21 and -0.30 e/Å^3, respectively, and were associated with the cobalt atom.

Table 10. Crystal Data for $(C_5Me_5)Co(C_5H_5)$

Formula	$CoC_{15}H_{20}$
FW	259.26
Space Group	$P\bar{1}$ (No. 2)
a, Å	7.7126 (16)
b, Å	8.1970 (17)
c, Å	12.2098 (24)
α, deg.	101.582 (17)
β, deg.	96.938 (16)
γ, deg.	118.182 (17)
V, $Å^3$	645.4 (3)
Z	2
F(000)	274
d_{calc}, g/cm^3	1.334
μ_{calc}, cm^{-1}	12.97
size, mm	$0.41 \times 0.41 \times 0.32$
temperature	-114 °C
diffractometer	Enraf-Nonius CAD4
radiation	MoKα (0.71073 Å)
monochromator	highly oriented graphite
scan range, type	$3.0° \leq 2\Theta \leq 45.0°$, Θ-2Θ
scan width, deg.	$\Delta\Theta = 0.60 + 0.35(\tan\Theta)$
octants collected	± h, ± k, ± l
reflections collected	3363
unique reflections	1682
reflections, $F_o^2 > 3\sigma(F_o^2)$	1532
variables	225
R	2.09
R_w	2.83
R_{all}	2.38
GOF	1.560
largest Δ/σ in final LS cycle	0.05

$(C_5Me_5)Ni(C_5H_5)$

Forest green plates of the complex were grown from a pentane solution at -80 °C. A crystal of approximate dimensions 0.20 mm × 0.47 mm × 0.50 mm was isolated and placed in Paratone N oil.[17] The crystal was mounted on the end of a cut quartz capillary tube and placed under a flow of cold nitrogen on an Enraf-Nonius CAD4 diffractometer.[18] The solidified oil held the crystal in place and protected it from the atmosphere. The temperature was stabilized at -96 °C with an automated flow apparatus.

After centering the crystal in the X-ray beam, a set of accurate cell dimensions and an orientation matrix were determined by a least-squares fit to the setting angles of the unresolved MoKα components of 24 symmetry related reflections. The original cell found and used for data collection was a doubled cell with pseudo-C-centering, caused by a near-perfect twinning of the crystal. The data was "untwinned" by the following procedure: First, the cell was transformed to match the unit cell of $(C_5Me_5)Co(C_5H_5)$ as closely as possible (all dimensions the same except for the c axis being doubled). Then, the reflections were sorted by their sin θ/λ values, producing pairs of reflections with identical values. These pairs were related by the twinning law: $h' = h$, $k' = -(h + k)$, $l' = h + 2k + l$. The intensities were then corrected using Dr. Fred Hollander's program UNTWIN by treating the data as coming from two crystals with relative sizes of 2:1. The data was deconvoluted using the equations:

$$I_t(n) = x \cdot I(n) + (1-x) \cdot I(n')$$
$$I_t(n') = x \cdot I(n') + (1-x) \cdot I(n)$$

where I_t is the intensity of the reflection in the twinned crystal, I is the intensity of the reflection if the crystal were single, x is the square of the percentage that the larger twin constitutes of the whole crystal (in this case, 0.8: $(2:1)^2 = 4:1$), and n

and n' represent the indices of the reflections due to the two fractions (h k l and h' k' l', respectively). After deconvolution, all of the reflections with n' indices had $F_o^2 < 3\sigma(F_o^2)$, yielding a non-primitive doubled cell with C-centering. Upon transformation to a primitive cell, the dimensions and volume of the unit cell suggested triclinic symmetry with 2 molecules in the unit cell. Details of the unit cell, collection parameters, and structure refinement are listed in Table 11.

A set of three standard reflections (2, 4, -4; 3, 3, 10; 3, 1, 10) was chosen to monitor intensity and crystal orientation. The intensity was checked after every hour of X-ray exposure time and showed no appreciable decay over the course of the data collection. The crystal orientation was checked after every 200 reflections and was reoriented if any of the standard reflections were offset from their predicted position by more than 0.1°. The crystal orientation matrix was reoriented 2 times during the data collection.

The 3441 raw data were converted to structure factor amplitudes and their esds by correction for scan speed, background, and Lorentz-polarization effects.[19,20,21] An empirical absorption correction was applied to the data based on averaged azimuthal psi scans for three reflections with $\chi > 80°$.[22] Examination of the azimuthal scans showed a variation of $I_{min}/I_{max} = 0.81$ for the average relative intensity curve. Analysis of the data revealed no systematic absences, consistent with the space group $P\bar{1}$ (No. 2).

The coordinates of the nickel atom was determined by Patterson methods. The locations of all non-hydrogen atoms were determined through the use of standard Fourier techniques and refined by least-squares methods. All non-hydrogen atoms were refined anisotropically. A difference Fourier map revealed the positions of most of the hydrogen atoms. These atoms were placed in calculated positions and included in the structure factor calculations but not

refined. All hydrogen atoms were given isotropic thermal parameters 1.3 times the B(iso) of the atom to which they were bonded.

Final refinement of the 145 variables using the 1580 data for which $F_o^2 > 3\sigma(F_o^2)$ gave residuals of R = 3.54 and R_w = 4.92. The R value based on all 1722 unique data was 4.06 and the goodness-of-fit parameter was 2.578. The least squares program minimized the expression, $\Sigma w(|F_o| - |F_c|)^2$, where w is the weight of a given observation. A value of 0.02 for the p-factor was used to reduce the weight of intense reflections in the refinements.[24] The analytical forms of the scattering factor tables for the neutral atoms[25] were used and all non-hydrogen scattering factors were corrected for both real and imaginary components of anomalous dispersion.[26]

The data were evaluated through the residuals over ranges of $\sin\theta/\lambda$, $|F_o|$, parity, and individual indices. No unusual features or trends were observed once the untwinning procedure was completed. The highest and lowest peaks in the final difference Fourier map had electron densities of 0.37 and -1.28 e/Å^3, respectively, and were associated with the nickel atom.

Table 11. Crystal Data for $(C_5Me_5)Ni(C_5H_5)$

Formula	$NiC_{15}H_{20}$
FW	259.04
Space Group	$P\bar{1}$ (No. 2)
a, Å	7.860 (3)
b, Å	8.204 (2)
c, Å	12.285 (7)
α, deg.	101.19 (2)
β, deg.	97.79 (3)
γ, deg.	118.57 (2)
V, Å^3	658.1 (9)
Z	2
F(000)	276
d_{calc}, g/cm^3	1.307
μ_{calc}, cm^{-1}	14.52
size, mm	0.20 × 0.47 × 0.50
temperature	-96 °C
diffractometer	Enraf-Nonius CAD4
radiation	MoKα (0.71073 Å)
monochromator	highly oriented graphite
scan range, type	$3.0° \leq 2\Theta \leq 45.0°$, Θ-2Θ
scan width, deg.	$\Delta\Theta = 0.65 + 0.35(\tan\Theta)$
octants collected	+ h, ± k, ± l
reflections collected	3441
unique reflections	1722
reflections, $F_o^2 > 3\sigma(F_o^2)$	1580
variables	145
R	3.54
R_w	4.92
R_{all}	4.06
GOF	2.578
largest Δ/σ in final LS cycle	0.00

References

1. (a) Perrin, D. D.; Armarego, W. L. F.; Perrin, D. R., "Purification of Laboratory Materials," Pergamon: Oxford, **1980**. (b) Gordon, A. J.; Ford, R. A., "The Chemist's Companion: A Handbook of Practical Data, Techniques, and References," Wiley-Interscience: New York, **1972**.

2. (a) Andersen, R. A.; Blom, R.; Boncella, J. M.; Burns, C. J.; Volden, H. V., *Acta Chem. Scand.*, **1987**, *A41*, 24. (b) Robbins, J. L.; Edelstein, N.; Spencer, B.; Smart, J. C., *J. Am. Chem. Soc.*, **1982**, *104*, 1882.

3. Evans, D. F., *J. Chem. Soc.*, **1959**, 2003.

4. Baker, M. V.; Field, L. D.; Hambley, T. W., *Inorg. Chem.*, **1988**, *27*, 2872.

5. Berg, D. J., Ph.D. Thesis, University of California, Berkeley, **1987**.

6. Charles, R. G.; Pawlikowski, M. A., *J. Phys. Chem.*, **1958**, *62*, 440.

7. Nakamoto, K.; McCarthy, P. J.; Martell, A. E., *J. Am. Chem. Soc.*, **1961**, *83*, 1272.

8. For assignment of infrared spectral bands of divalent metal acetylacetonates, see: Pinchas, S.; Silver, B. L.; Laulicht, I., *J. Chem. Phys.*, **1967**, *46*, 1506.

9. Kölle, U.; Fuss, B.; Belting, M.; Raabe, E., *Organometallics*, **1986**, *5*, 980.

10. Kölle, U.; Fuss, B.; Khouzami, F.; Gersdorf, J., *J. Organomet. Chem.*, **1985**, *290*, 77.

11. King, R. B.; Bisnette, M. B., *J. Organomet. Chem.*, **1967**, *8*, 287.

12. Olson, W. L.; Stacy, A. M.; Dahl, L. F., *J. Am. Chem. Soc.*, **1986**, 108, 7646.

13. Mise, T.; Yamazaki, H., *J. Organomet. Chem.*, **1979**, *164*, 391.

14. Kölle, U.; Fuss, B., *Chem. Ber.*, **1984**, *117*, 743.

15. Bunel, E. E.; Valle, L.; Manriquez, J. M., *Organometallics*, **1985**, *4*, 1680. Only an elemental analysis is reported for $(C_5Me_5)Co(C_5H_5)$.

16. Werner, H.; Dernberger, T., *J. Organomet. Chem.*, **1980**, *198*, 97.

17. Paratone N oil is a viscous commercial oil available from Exxon Chemical Company, Houston, TX. The oil was degassed prior to use.

18. Instrumentation at the University of California Chemistry Department X-ray Crystallographic Facility (CHEXRAY) consists of two Enraf-Nonius CAD-4 diffractometers controlled by a DEC Microvax II and equipped with departmentally constructed low temperature systems. Both use Enraf-Nonius software as described in the "CAD-4 Operations Manual, Version 5.0," Enraf-Nonius, Delft, The Netherlands, **1977**, updated **1989**.

19. All calculations were performed on a DEC Microvax II or a DEC Microvax 4000 using locally modified Nonius-SDP software operating under Micro-VMS operating system.

20. (a) Frenz, B. A., "Structure Determination Package Users Guide," Texas A & M University and Enraf-Nonius: College Station, TX and The Netherlands, **1985**. (b) Fair, C. K., "MoLEN Molecular Structure Solution Procedures," Enraf-Nonius, Delft Instruments, X-ray Diffraction B. V., The Netherlands, **1990**.

21. The data reduction formulae are:

$$F_o^2 = \frac{\omega}{L_p}(C - 2B) \qquad \sigma_o(F_o^2) = \frac{\omega}{L_p}(C + 4B)^{1/2}$$

$$F_o = (F_o^2)^{1/2} \qquad \sigma_o(F) = [F_o^2 + \sigma_o(F_o^2)]^{1/2} - F_o$$

where C is the total count in the scan, B is the sum of the two background counts, ω is the scan speed used in deg/min, and

$$\frac{1}{L_p} = \frac{\sin 2\Theta(1 + \cos^2 2\Theta_m)}{1 + \cos^2 2\Theta_m - \sin^2 2\Theta}$$

is the correction for Lorentz and polarization effects for a reflection with scattering angle 2Θ and radiation monochromatized with a 50% perfect single-crystal monochromator with scattering angle $2\Theta_m$.

22. Reflection used for azimuthal scans were located near $\chi = 90°$ and the intensities were measured at 10° increments of rotation of the crystal about the diffraction vector.

23. SHELXS-86 is a public domain direct methods solution algorithm written by G. M. Sheldrick; see "Crystallographic Computing 3," eds. Sheldrick, G. M.; Krüger, C.; Goddard, R., Oxford University Press: Oxford, **1985**, pp. 175-189.

24. $R = \frac{\Sigma \left| |F_o| - |F_c| \right|}{\Sigma |F_o|}$ $\qquad wR = \sqrt{\frac{\Sigma w(|F_o| - |F_c|)^2}{\Sigma w F_o^2}}$

$$GOF = \sqrt{\frac{\Sigma w(|F_o| - |F_c|)^2}{(n_o - n_v)}}$$

where n_o is the number of observations, n_v is the number of variable parameters, and the weights, w, were given by

$$w = \frac{1}{\sigma^2(F_o)} \qquad \sigma(F_o^2) = \sqrt{\sigma_o^2(F_o^2) + (pF^2)^2}$$

where $\sigma^2(F_o)$ was calculated as above from $\sigma(F_o^2)$ and where p is the factor used to lower the weight of intense reflections.

25. Cromer, D. T.; Waber, J. T., "International Tables for X-ray Crystallography," Vol. IV, The Kynoch Press: Birmingham, England, **1974**, Table 2.2B.

26. Cromer, D. T., *ibid.*, Table 2.3.1.

Appendix I. Tables of Positional and Thermal Parameters

$(C_5Me_5)_3Co_3(\mu_3\text{-}CH)(\mu\text{-}H)$

Table of Positional Parameters and Their Estimated Standard Deviations

Atom	x	y	z	B(A2)
Co	0.20850(1)	0.32733(1)	0.17723(1)	2.27(1)
C1	0.2423(4)	0.4190(4)	0.0405(4)	2.2(1)
C2	0.1173(4)	0.3667(4)	0.0181(4)	2.1(1)
C3	0.0713(4)	0.4159(4)	0.1166(4)	2.2(1)
C4	0.1700(4)	0.5006(4)	0.2024(4)	2.1(1)
C5	0.2751(4)	0.5029(4)	0.1552(4)	2.4(1)
C6	0.3206(5)	0.4037(5)	-0.0483(5)	3.3(1)
C7	0.0423(5)	0.2786(5)	-0.0953(5)	3.4(1)
C8	-0.0592(4)	0.3916(5)	0.1198(5)	3.0(1)
C9	0.1613(5)	0.5793(5)	0.3179(5)	3.4(1)
C10	0.3966(5)	0.5848(5)	0.2110(5)	3.9(1)
C11	0.3135(7)	0.314	0.314	2.31(6)
C11'	0.150(2)	0.15	0.15	1.9(6)*
H6A	0.31442(1)	0.46093(1)	-0.09732(1)	4.2*
H6B	0.40212(1)	0.41609(1)	-0.00625(1)	4.2*
H6C	0.29509(1)	0.32445(1)	-0.09786(1)	4.2*
H7A	0.01220(1)	0.32176(1)	-0.15213(1)	4.4*
H7B	0.09082(1)	0.22950(1)	-0.12876(1)	4.4*
H7C	-0.02342(1)	0.22900(1)	-0.07615(1)	4.4*
H8A	-0.09617(1)	0.44804(1)	0.08523(1)	3.9*
H8B	-0.09758(1)	0.31210(1)	0.07513(1)	3.9*
H8C	-0.06695(1)	0.39928(1)	0.20110(1)	3.9*
H9A	0.14283(1)	0.65254(1)	0.30237(1)	4.4*
H9B	0.09938(1)	0.53848(1)	0.34939(1)	4.4*
H9C	0.23612(1)	0.59658(1)	0.37482(1)	4.4*
H10A	0.40085(1)	0.65825(1)	0.18451(1)	5.1*
H10B	0.40849(1)	0.60124(1)	0.29639(1)	5.1*
H10C	0.45750(1)	0.54680(1)	0.18739(1)	5.1*
H11	0.37333(1)	0.37333(1)	0.37333(1)	4.0*

Starred atoms were included with isotropic thermal parameters. The thermal parameter given for anisotropically refined atoms is the isotropic equivalent thermal parameter defined as: $(4/3) \cdot [a^2 \cdot B(1,1) + b^2 \cdot B(2,2) + c^2 \cdot B(3,3) + ab(\cos\gamma) \cdot B(1,2) + ac(\cos\beta) \cdot B(1,3) + bc(\cos\alpha) \cdot B(2,3)]$ where a,b,c are real cell parameters, and B(i,j) are anisotropic betas.

$(C_5Me_5)_3Co_3(\mu_3\text{-}CH)(\mu\text{-}H)$

Table of Anisotropic Thermal Parameters - B's

Name	B(1,1)	B(2,2)	B(3,3)	B(1,2)	B(1,3)	B(2,3)	Beqv
Co	2.62(2)	2.43(2)	2.36(2)	1.15(2)	0.91(2)	1.06(2)	2.27(1)
C1	2.6(2)	1.9(2)	2.4(2)	0.5(1)	0.7(1)	0.9(1)	2.2(1)
C2	2.7(2)	1.8(2)	2.1(2)	0.5(1)	0.3(1)	0.9(1)	2.1(1)
C3	2.4(2)	1.9(2)	2.4(2)	0.6(1)	0.4(1)	0.8(1)	2.2(1)
C4	2.6(2)	1.9(2)	1.9(2)	0.7(1)	0.4(1)	0.6(1)	2.1(1)
C5	2.3(2)	2.1(2)	2.7(2)	0.3(2)	0.3(2)	0.8(1)	2.4(1)
C6	3.8(2)	3.2(2)	3.6(2)	1.1(2)	1.8(2)	1.6(2)	3.3(1)
C7	3.9(2)	3.0(2)	2.5(2)	-0.1(2)	0.2(2)	0.2(2)	3.4(1)
C8	2.5(2)	3.2(2)	3.4(2)	0.6(2)	0.6(2)	0.7(2)	3.0(1)
C9	4.0(2)	2.8(2)	2.7(2)	0.7(2)	0.4(2)	-0.1(2)	3.4(1)
C10	3.2(2)	3.5(2)	4.2(3)	-0.5(2)	0.4(2)	0.4(2)	3.9(1)
C11	2.5(2)	B(1,1)	B(1,1)	0.9(2)	B(1,2)	B(1,2)	2.31(6)

The form of the anisotropic temperature factor is: $\exp[-0.25\{h^2a^2 \cdot B(1,1) + k^2b^2 \cdot B(2,2) + l^2c^2 \cdot B(3,3) + 2hkab \cdot B(1,2) + 2hlac \cdot B(1,3) + 2klbc \cdot B(2,3)\}]$ where a,b, and c are reciprocal lattice constants.

$(C_5Me_5)_3Ni_3(\mu_3\text{-}CH)(\mu\text{-}H)$

Table of Positional Parameters and Their Estimated Standard Deviations

Atom	x	y	z	B(A2)
Ni	0.21025(1)	0.32721(1)	0.17798(1)	2.13(1)
C1	0.1692(4)	0.5021(3)	0.1994(4)	2.07(8)
C2	0.2748(4)	0.5042(4)	0.1534(4)	2.22(9)
C3	0.2448(4)	0.4204(3)	0.0393(4)	2.09(8)
C4	0.1194(4)	0.3653(3)	0.0175(3)	1.99(8)
C5	0.0722(4)	0.4159(3)	0.1142(4)	2.07(9)
C6	0.1602(4)	0.5829(4)	0.3136(4)	3.2(1)
C7	0.3953(4)	0.5882(4)	0.2100(5)	3.6(1)
C8	0.3242(4)	0.4051(4)	-0.0480(4)	3.1(1)
C9	0.0465(5)	0.2768(4)	-0.0952(4)	3.3(1)
C10	-0.0585(4)	0.3902(4)	0.1170(4)	2.9(1)
C11'	0.1566(7)	0.157	0.157	1.2(2)*
C11	0.329(1)	0.329	0.329	1.2(3)*
H6B	0.09899(1)	0.54285(1)	0.34655(1)	4.2*
H6C	0.23524(1)	0.60163(1)	0.37012(1)	4.2*
H6A	0.14069(1)	0.65525(1)	0.29616(1)	4.2*
H7B	0.40570(1)	0.60538(1)	0.29528(1)	4.6*
H7C	0.45759(1)	0.55106(1)	0.18825(1)	4.6*
H7A	0.39880(1)	0.66101(1)	0.18234(1)	4.6*
H8B	0.40533(1)	0.41791(1)	-0.00523(1)	4.0*
H8C	0.29956(1)	0.32578(1)	-0.09700(1)	4.0*
H8A	0.31821(1)	0.46201(1)	-0.09761(1)	4.0*
H9B	0.09623(1)	0.22844(1)	-0.12786(1)	4.2*
H9C	-0.01895(1)	0.22674(1)	-0.07637(1)	4.2*
H9A	0.01633(1)	0.31951(1)	-0.15270(1)	4.2*
H10B	-0.09561(1)	0.31041(1)	0.07298(1)	3.8*
H10C	-0.06677(1)	0.39815(1)	0.19818(1)	3.8*
H10A	-0.09629(1)	0.44580(1)	0.08152(1)	3.8*

Starred atoms were included with isotropic thermal parameters. The thermal parameter given for anisotropically refined atoms is the isotropic equivalent thermal parameter defined as: $(4/3) \cdot [a^2 \cdot B(1,1) + b^2 \cdot B(2,2) + c^2 \cdot B(3,3) + ab(\cos\gamma) \cdot B(1,2) + ac(\cos\beta) \cdot B(1,3) + bc(\cos\alpha) \cdot B(2,3)]$ where a,b,c are real cell parameters, and B(i,j) are anisotropic betas.

$(C_5Me_5)_3Ni_3(\mu_3\text{-}CH)(\mu\text{-}H)$

Table of Anisotropic Thermal Parameters - B's

Name	B(1,1)	B(2,2)	B(3,3)	B(1,2)	B(1,3)	B(2,3)	Beqv
Ni	2.50(2)	2.28(2)	2.48(2)	1.26(1)	1.24(2)	1.32(2)	2.13(1)
C1	2.5(2)	1.7(1)	2.1(2)	0.7(1)	0.4(1)	0.6(1)	2.07(8)
C2	2.4(2)	1.9(1)	2.3(2)	0.2(1)	0.4(1)	0.7(1)	2.22(9)
C3	2.6(2)	1.6(1)	2.5(2)	0.6(1)	0.8(1)	1.0(1)	2.09(8)
C4	2.6(2)	1.7(1)	1.8(1)	0.5(1)	0.4(1)	0.8(1)	1.99(8)
C5	2.3(2)	1.6(1)	2.4(2)	0.5(1)	0.3(1)	0.8(1)	2.07(9)
C6	3.7(2)	2.8(2)	2.9(2)	0.9(2)	0.6(2)	-0.1(2)	3.2(1)
C7	2.8(2)	3.0(2)	4.3(2)	-0.4(2)	0.5(2)	0.5(2)	3.6(1)
C8	3.6(2)	2.9(2)	3.4(2)	0.8(2)	1.6(1)	1.2(1)	3.1(1)
C9	3.8(2)	2.9(2)	2.6(2)	0.5(2)	0.0(2)	0.1(2)	3.3(1)
C10	2.4(2)	3.2(2)	3.1(2)	0.6(1)	0.4(1)	0.9(1)	2.9(1)

The form of the anisotropic temperature factor is: $\exp[-0.25\{h^2a^2 \cdot B(1,1) + k^2b^2 \cdot B(2,2) + l^2c^2 \cdot B(3,3) + 2hkab \cdot B(1,2) + 2hlac \cdot B(1,3) + 2klbc \cdot B(2,3)\}]$ where a,b, and c are reciprocal lattice constants.

$(C_5Me_5)_3Co_3(\mu_3\text{-}CH)_2$

Table of Positional Parameters and Their Estimated Standard Deviations

Atom	x	y	z	B(A2)
Co	0.28845(1)	0.32088(1)	0.17074(1)	1.307(5)
C1	0.3800(2)	0.4834(2)	0.1367(2)	1.74(4)
C2	0.2543(2)	0.4600(2)	0.0808(2)	1.87(4)
C3	0.2245(2)	0.3469(2)	-0.0036(2)	1.87(4)
C4	0.3310(2)	0.3005(2)	-0.0007(2)	1.81(4)
C5	0.4277(2)	0.3852(2)	0.0859(2)	1.81(4)
C6	0.4504(2)	0.5947(2)	0.2260(2)	2.77(5)
C7	0.1747(2)	0.5493(2)	0.0956(2)	2.76(5)
C8	0.1041(2)	0.2908(3)	-0.0859(2)	3.07(6)
C9	0.3401(2)	0.1860(2)	-0.0807(2)	2.79(5)
C10	0.5593(2)	0.3819(2)	0.1122(2)	2.50(5)
C11	0.3374(2)	0.337	0.337	1.35(2)
C12	0.1825(2)	0.183	0.183	1.33(2)
H6A	0.480(4)	0.655(4)	0.187(4)	8(1)*
H6B	0.387(3)	0.626(3)	0.268(3)	7(1)*
H6C	0.505(3)	0.577(3)	0.282(3)	6.0(8)*
H7A	0.177(2)	0.598(2)	0.034(2)	3.1(6)*
H7B	0.093(3)	0.512(3)	0.088(3)	5.3(8)*
H7C	0.204(3)	0.606(3)	0.175(3)	4.6(7)*
H8A	0.099(3)	0.316(3)	-0.156(3)	6.0(9)*
H8B	0.094(3)	0.213(3)	-0.100(3)	4.6(7)*
H8C	0.036(3)	0.313(3)	-0.044(3)	4.5(7)*
H9A	0.337(3)	0.198(3)	-0.155(3)	5.0(8)*
H9B	0.418(3)	0.172(3)	-0.063(3)	5.7(8)*
H9C	0.288(2)	0.123(2)	-0.071(2)	3.0(6)*
H10A	0.613(3)	0.457(3)	0.103(3)	4.8(7)*
H10B	0.583(2)	0.373(2)	0.189(2)	3.2(6)*
H10C	0.580(3)	0.318(3)	0.060(3)	5.0(8)*
H11	0.406(2)	0.406	0.406	0.2(4)*
H12	0.113(2)	0.113	0.113	0.2*

Starred atoms were included with isotropic thermal parameters. The thermal parameter given for anisotropically refined atoms is the isotropic equivalent thermal parameter defined as: $(4/3) \cdot [a^2 \cdot B(1,1) + b^2 \cdot B(2,2) + c^2 \cdot B(3,3) + ab(\cos\gamma) \cdot B(1,2) + ac(\cos\beta) \cdot B(1,3) + bc(\cos\alpha) \cdot B(2,3)]$ where a,b,c are real cell parameters, and B(i,j) are anisotropic betas.

$(C_5Me_5)_3Co_3(\mu_3\text{-}CH)_2$

Table of Anisotropic Thermal Parameters - B's

Name	B(1,1)	B(2,2)	B(3,3)	B(1,2)	B(1,3)	B(2,3)	Beqv
Co	1.393(9)	1.372(9)	1.173(9)	0.267(7)	0.279(7)	0.336(7)	1.307(5)
C1	2.13(8)	1.70(7)	1.40(7)	0.11(6)	0.35(6)	0.65(6)	1.74(4)
C2	2.59(8)	1.71(7)	1.58(7)	0.59(6)	0.56(6)	0.84(5)	1.87(4)
C3	2.23(8)	1.93(7)	1.31(7)	0.14(6)	0.15(6)	0.52(6)	1.87(4)
C4	2.29(8)	1.90(7)	1.28(7)	0.26(6)	0.55(6)	0.46(6)	1.81(4)
C5	2.01(7)	1.95(7)	1.61(7)	0.28(6)	0.61(6)	0.67(6)	1.81(4)
C6	3.4(1)	1.88(8)	2.50(9)	-0.19(8)	0.27(8)	0.36(7)	2.77(5)
C7	3.22(9)	2.84(8)	2.69(9)	1.49(7)	0.55(7)	1.04(7)	2.76(5)
C8	2.8(1)	3.7(1)	2.18(9)	0.37(8)	-0.46(8)	0.62(8)	3.07(6)
C9	3.9(1)	2.37(9)	2.05(8)	0.52(8)	1.01(7)	-0.06(7)	2.79(5)
C10	1.84(8)	3.08(9)	2.73(8)	0.33(7)	0.67(7)	1.03(7)	2.50(5)
C11	1.38(5)	B(1,1)	B(1,1)	0.37(6)	B(1,2)	B(1,2)	1.35(2)
C12	1.38(5)	B(1,1)	B(1,1)	0.42(6)	B(1,2)	B(1,2)	1.33(2)

The form of the anisotropic temperature factor is: $\exp[-0.25\{h^2a^2 \cdot B(1,1) + k^2b^2 \cdot B(2,2) + l^2c^2 \cdot B(3,3) + 2hkab \cdot B(1,2) + 2hlac \cdot B(1,3) + 2klbc \cdot B(2,3)\}]$ where a,b, and c are reciprocal lattice constants.

$(C_5Me_5)Co(acac)$

Table of Positional Parameters and Their Estimated Standard Deviations

Atom	x	y	z	B(A2)
Co1	0.24796(7)	0.11001(1)	0.76474(1)	2.02(1)
Co2	0.26345(7)	0.35832(1)	0.27482(1)	2.16(1)
O1	0.1224(3)	0.1221(2)	0.6706(2)	2.33(7)
O2	0.3804(4)	0.2065(3)	0.6879(2)	2.55(7)
O3	0.2201(4)	0.2102(3)	0.3026(2)	2.80(8)
O4	0.4736(4)	0.2971(3)	0.3198(2)	2.86(8)
C1	0.0253(6)	0.1798(4)	0.5241(3)	3.0(1)
C2	0.1409(5)	0.1808(4)	0.5862(3)	2.1(1)
C3	0.2566(5)	0.2459(4)	0.5501(3)	2.2(1)
C4	0.3681(5)	0.2559(4)	0.6012(3)	2.2(1)
C5	0.4850(6)	0.3314(4)	0.5550(3)	3.2(1)
C6	0.1603(6)	-0.0148(4)	0.8711(3)	2.7(1)
C7	0.3339(6)	-0.0442(4)	0.8753(3)	2.4(1)
C8	0.3705(5)	0.0563(4)	0.8822(3)	2.3(1)
C9	0.2183(5)	0.1440(4)	0.8904(3)	2.1(1)
C10	0.0905(5)	0.0995(4)	0.8826(3)	2.3(1)
C11	0.0642(7)	-0.0924(4)	0.8603(4)	4.4(1)
C12	0.4529(7)	-0.1609(5)	0.8765(4)	4.2(2)
C13	0.5376(6)	0.0732(5)	0.8831(3)	3.6(1)
C14	0.2040(7)	0.2601(4)	0.9030(3)	3.5(1)
C15	-0.0895(6)	0.1598(5)	0.8845(4)	3.7(1)
C21	0.2583(7)	0.0037(4)	0.3505(4)	4.5(2)
C22	0.3189(6)	0.1102(4)	0.3398(3)	2.8(1)
C23	0.4736(6)	0.0948(4)	0.3667(3)	3.2(1)
C24	0.5443(6)	0.1865(4)	0.3550(3)	2.9(1)
C25	0.7175(7)	0.1579(5)	0.3814(4)	4.6(1)
C26	0.0388(6)	0.4863(4)	0.2748(3)	2.7(1)
C27	0.1689(6)	0.5305(4)	0.2835(3)	2.6(1)
C28	0.2806(6)	0.5274(4)	0.2048(3)	2.8(1)
C29	0.2186(6)	0.4862(4)	0.1465(3)	2.8(1)
C30	0.0715(6)	0.4561(4)	0.1925(3)	2.5(1)
C31	-0.1123(6)	0.4786(5)	0.3385(4)	3.9(1)
C32	0.1829(7)	0.5755(4)	0.3589(4)	4.3(1)
C33	0.4389(6)	0.5631(5)	0.1872(4)	4.6(2)
C34	0.2925(7)	0.4751(5)	0.0547(4)	4.4(2)
C35	-0.0330(7)	0.4019(4)	0.1593(4)	4.2(1)
H1A	0.04885(1)	0.22559(1)	0.46320(1)	3.9*
H1B	0.03772(1)	0.10043(1)	0.52572(1)	3.9*
H1C	-0.08437(1)	0.21277(1)	0.54361(1)	3.9*
H5A	0.46772(1)	0.36438(1)	0.49134(1)	4.1*
H5B	0.46593(1)	0.39360(1)	0.58130(1)	4.1*
H5C	0.59495(1)	0.28385(1)	0.56338(1)	4.1*
H3	0.25928(1)	0.28619(1)	0.48604(1)	2.9*
H11A	0.03790(1)	-0.14235(1)	0.91901(1)	5.7*
H11B	-0.03430(1)	-0.04422(1)	0.83148(1)	5.7*
H11C	0.12812(1)	-0.13987(1)	0.82372(1)	5.7*

Table of Positional Parameters and Their Estimated Standard Deviations (cont.)

Atom	x	y	z	B(A2)
H12A	0.46423(1)	-0.21128(1)	0.93808(1)	5.4*
H12B	0.41328(1)	-0.19697(1)	0.84225(1)	5.4*
H12C	0.55667(1)	-0.14862(1)	0.85010(1)	5.4*
H13A	0.57158(1)	0.04220(1)	0.94415(1)	4.7*
H13B	0.61436(1)	0.03274(1)	0.84553(1)	4.7*
H13C	0.53225(1)	0.15550(1)	0.86024(1)	4.7*
H14A	0.19154(1)	0.25218(1)	0.96666(1)	4.6*
H14B	0.30044(1)	0.28526(1)	0.87703(1)	4.6*
H14C	0.11100(1)	0.31730(1)	0.87349(1)	4.6*
H15A	-0.13443(1)	0.14162(1)	0.94609(1)	4.8*
H15B	-0.10559(1)	0.24327(1)	0.85919(1)	4.8*
H15C	-0.14279(1)	0.13297(1)	0.84947(1)	4.8*
H21A	0.33861(1)	-0.06678(1)	0.37849(1)	5.8*
H21B	0.15869(1)	0.00761(1)	0.38783(1)	5.8*
H21C	0.23951(1)	0.00313(1)	0.29185(1)	5.8*
H25A	0.75865(1)	0.07440(1)	0.40665(1)	6.0*
H25B	0.78467(1)	0.18616(1)	0.32868(1)	6.0*
H25C	0.71862(1)	0.19515(1)	0.42575(1)	6.0*
H23	0.53546(1)	0.01611(1)	0.39521(1)	4.1*
H31A	-0.19463(1)	0.55162(1)	0.32073(1)	5.1*
H31B	-0.15222(1)	0.41625(1)	0.33539(1)	5.1*
H31C	-0.08566(1)	0.46303(1)	0.39948(1)	5.1*
H32A	0.12780(1)	0.65766(1)	0.34418(1)	5.6*
H32B	0.13418(1)	0.53327(1)	0.41431(1)	5.6*
H32C	0.29559(1)	0.56429(1)	0.36626(1)	5.6*
H33A	0.41880(1)	0.64516(1)	0.15376(1)	5.9*
H33B	0.48226(1)	0.54884(1)	0.24402(1)	5.9*
H33C	0.51564(1)	0.51796(1)	0.15269(1)	5.9*
H34A	0.24991(1)	0.54688(1)	0.00821(1)	5.7*
H34B	0.40857(1)	0.45979(1)	0.05338(1)	5.7*
H34C	0.26598(1)	0.41147(1)	0.04431(1)	5.7*
H35A	-0.11425(1)	0.46301(1)	0.12235(1)	5.4*
H35B	0.03403(1)	0.35353(1)	0.12410(1)	5.4*
H35C	-0.08507(1)	0.35467(1)	0.21043(1)	5.4*

Starred atoms were included with isotropic thermal parameters. The thermal parameter given for anisotropically refined atoms is the isotropic equivalent thermal parameter defined as: $(4/3) \cdot [a^2 \cdot B(1,1) + b^2 \cdot B(2,2) + c^2 \cdot B(3,3) + ab(\cos \gamma) \cdot B(1,2) + ac(\cos \beta) \cdot B(1,3) + bc(\cos \alpha) \cdot B(2,3)]$ where a,b,c are real cell parameters, and B(i,j) are anisotropic betas.

$(C_5Me_5)Co(acac)$

Table of Anisotropic Thermal Parameters - B's

Name	B(1,1)	B(2,2)	B(3,3)	B(1,2)	B(1,3)	B(2,3)	Beqv
Co1	2.03(2)	2.43(2)	1.71(2)	-0.95(2)	-0.10(2)	-0.48(2)	2.02(1)
Co2	2.21(2)	1.91(2)	2.28(2)	-0.31(2)	-0.15(2)	-0.74(2)	2.16(1)
O1	2.3(1)	2.7(1)	1.9(1)	-1.05(9)	-0.2(1)	-0.31(9)	2.33(7)
O2	2.5(1)	2.8(1)	2.4(1)	-1.08(9)	-0.2(1)	-0.42(9)	2.55(7)
O3	2.8(1)	2.2(1)	3.1(1)	-0.7(1)	0.1(1)	-0.5(1)	2.80(8)
O4	3.0(1)	2.7(1)	3.1(1)	-0.2(1)	-0.8(1)	-1.31(9)	2.86(8)
C1	3.1(2)	3.3(2)	2.5(2)	-1.2(1)	-0.3(2)	-0.6(1)	3.0(1)
C2	2.3(2)	2.2(1)	2.0(2)	-0.5(1)	-0.1(1)	-0.9(1)	2.1(1)
C3	2.7(2)	2.3(2)	1.6(2)	-0.8(1)	0.3(1)	-0.4(1)	2.2(1)
C4	2.1(2)	2.1(1)	2.5(2)	-0.7(1)	0.4(1)	-0.7(1)	2.2(1)
C5	2.9(2)	3.2(2)	3.4(2)	-1.5(1)	0.5(2)	-0.8(2)	3.2(1)
C6	3.6(2)	3.1(2)	1.7(2)	-1.9(1)	-0.1(2)	-0.4(1)	2.7(1)
C7	3.0(2)	2.3(2)	1.5(2)	-0.3(1)	-0.2(1)	-0.4(1)	2.4(1)
C8	2.0(2)	3.4(2)	1.6(2)	-1.0(1)	-0.4(1)	-0.5(1)	2.3(1)
C9	2.5(2)	2.5(2)	1.5(2)	-0.9(1)	-0.1(1)	-0.6(1)	2.1(1)
C10	2.3(2)	2.9(2)	1.8(2)	-1.0(1)	0.2(1)	-0.5(1)	2.3(1)
C11	6.5(2)	5.0(2)	3.0(2)	-4.0(2)	-0.3(2)	-1.0(2)	4.4(1)
C12	5.6(3)	3.0(2)	2.8(2)	0.0(2)	-0.2(2)	-0.5(2)	4.2(2)
C13	2.6(2)	5.4(2)	2.8(2)	-1.4(2)	-0.2(2)	-0.8(2)	3.6(1)
C14	4.7(2)	3.2(2)	3.0(2)	-1.5(2)	-0.7(2)	-1.0(1)	3.5(1)
C15	2.3(2)	5.1(2)	3.1(2)	-0.9(2)	-0.1(2)	-0.6(2)	3.7(1)
C21	4.7(3)	2.8(2)	5.5(3)	-1.4(2)	0.8(2)	-0.8(2)	4.5(2)
C22	3.1(2)	2.3(2)	2.7(2)	-0.7(1)	0.8(2)	-0.7(1)	2.8(1)
C23	3.9(2)	2.2(2)	2.5(2)	0.3(2)	-0.3(2)	-0.5(2)	3.2(1)
C24	3.7(2)	2.9(2)	2.1(2)	0.2(2)	-1.0(2)	-1.2(1)	2.9(1)
C25	4.3(2)	4.0(2)	5.3(2)	0.8(2)	-2.1(2)	-2.0(2)	4.6(1)
C26	2.9(2)	2.1(2)	2.9(2)	-0.4(1)	0.1(2)	-0.6(1)	2.7(1)
C27	3.1(2)	2.0(2)	2.8(2)	-0.1(1)	-0.4(2)	-1.3(1)	2.6(1)
C28	2.6(2)	1.5(2)	3.9(2)	-0.3(1)	-0.5(2)	-0.2(2)	2.8(1)
C29	2.9(2)	2.3(2)	2.6(2)	-0.3(2)	-0.4(2)	-0.2(1)	2.8(1)
C30	2.6(2)	2.1(2)	2.9(2)	-0.5(1)	-0.6(2)	-0.7(1)	2.5(1)
C31	3.2(2)	3.8(2)	4.1(2)	-0.5(2)	0.6(2)	-1.0(2)	3.9(1)
C32	5.5(3)	3.3(2)	4.8(2)	-0.6(2)	-1.2(2)	-2.2(2)	4.3(1)
C33	2.6(2)	3.4(2)	7.0(3)	-0.9(2)	-0.6(2)	-0.6(2)	4.6(2)
C34	4.5(3)	4.3(2)	2.8(2)	0.1(2)	0.5(2)	-0.6(2)	4.4(2)
C35	4.0(2)	3.8(2)	5.1(2)	-0.9(2)	-1.4(2)	-1.5(2)	4.2(1)

The form of the anisotropic temperature factor is: $\exp[-0.25\{h^2a^2 \cdot B(1,1) + k^2b^2 \cdot B(2,2) + l^2c^2 \cdot B(3,3) + 2hkab \cdot B(1,2) + 2hlac \cdot B(1,3) + 2klbc \cdot B(2,3)\}]$ where a,b, and c are reciprocal lattice constants.

$(C_5Me_5)Ni(acac)$

Table of Positional Parameters and Their Estimated Standard Deviations

Atom	x	y	z	B(A2)
Ni1	0.27915(8)	0.11027(1)	0.76275(1)	1.94(1)
Ni2	0.24010(8)	0.34860(1)	0.27000(1)	1.92(2)
O1	0.1523(4)	0.1295(3)	0.6721(2)	2.25(8)
O2	0.4241(4)	0.2053(3)	0.6891(2)	2.47(9)
O3	0.1810(4)	0.2058(3)	0.3002(2)	2.34(8)
O4	0.4458(4)	0.2881(3)	0.3167(2)	2.28(8)
C1	0.0652(7)	0.1995(5)	0.5269(3)	2.7(1)
C2	0.1814(6)	0.1926(4)	0.5892(3)	2.0(1)
C3	0.3043(6)	0.2538(4)	0.5541(3)	2.1(1)
C4	0.4175(6)	0.2579(4)	0.6036(3)	2.1(1)
C5	0.5407(7)	0.3316(5)	0.5570(4)	3.2(2)
C6	0.1725(7)	-0.0107(4)	0.8703(3)	2.3(1)
C7	0.3480(7)	-0.0452(4)	0.8766(3)	2.5(1)
C8	0.3878(6)	0.0544(4)	0.8812(3)	2.3(1)
C9	0.2310(6)	0.1433(4)	0.8937(3)	2.1(1)
C10	0.1014(6)	0.1035(4)	0.8863(3)	2.1(1)
C11	0.0707(8)	-0.0829(5)	0.8599(4)	3.5(1)
C12	0.4640(9)	-0.1638(5)	0.8790(4)	3.8(2)
C13	0.5548(7)	0.0683(5)	0.8817(4)	3.4(2)
C14	0.2196(8)	0.2585(5)	0.9070(4)	3.5(2)
C15	-0.0805(7)	0.1662(5)	0.8891(4)	3.1(1)
C21	0.2093(7)	-0.0001(5)	0.3564(4)	3.2(1)
C22	0.2766(7)	0.1043(4)	0.3393(3)	2.3(1)
C23	0.4293(7)	0.0881(4)	0.3655(3)	2.3(1)
C24	0.5088(7)	0.1756(4)	0.3528(3)	2.2(1)
C25	0.6770(8)	0.1433(5)	0.3821(4)	3.3(1)
C26	0.0067(7)	0.4839(4)	0.2774(3)	2.4(1)
C27	0.1312(6)	0.5262(4)	0.2845(3)	2.1(1)
C28	0.2575(6)	0.5214(4)	0.2054(4)	2.4(1)
C29	0.1955(7)	0.4876(4)	0.1452(3)	2.3(1)
C30	0.0487(7)	0.4535(4)	0.1931(3)	2.3(1)
C31	-0.1517(7)	0.4716(5)	0.3406(4)	3.4(2)
C32	0.1483(8)	0.5668(5)	0.3591(4)	3.7(2)
C33	0.4160(8)	0.5573(5)	0.1878(4)	3.7(2)
C34	0.2774(9)	0.4825(6)	0.0513(4)	4.0(2)
C35	-0.0578(7)	0.4024(5)	0.1618(4)	3.3(1)
H1C	-0.04645(1)	0.23318(1)	0.54790(1)	3.5*
H1A	0.09476(1)	0.24760(1)	0.46690(1)	3.5*
H1B	0.07432(1)	0.12189(1)	0.52656(1)	3.5*
H3	0.31227(1)	0.29666(1)	0.49089(1)	2.7*
H5A	0.52736(1)	0.36718(1)	0.49420(1)	4.2*
H5C	0.65086(1)	0.28247(1)	0.56347(1)	4.2*
H5B	0.52197(1)	0.39182(1)	0.58375(1)	4.2*
H11A	0.03509(1)	-0.13194(1)	0.91818(1)	4.6*
H11B	-0.02407(1)	-0.03140(1)	0.83079(1)	4.6*
H11C	0.13662(1)	-0.13125(1)	0.82402(1)	4.6*

Table of Positional Parameters and Their Estimated Standard Deviations (cont.)

Atom	x	y	z	B(A2)
H12A	0.46791(1)	-0.21419(1)	0.94031(1)	4.9*
H12B	0.42499(1)	-0.19823(1)	0.84587(1)	4.9*
H12C	0.57263(1)	-0.15421(1)	0.85226(1)	4.9*
H13A	0.58175(1)	0.03723(1)	0.94231(1)	4.4*
H13B	0.63593(1)	0.02643(1)	0.84533(1)	4.4*
H13C	0.55375(1)	0.15010(1)	0.85769(1)	4.4*
H14A	0.19785(1)	0.24938(1)	0.97019(1)	4.5*
H14B	0.32202(1)	0.28053(1)	0.88267(1)	4.5*
H14C	0.13155(1)	0.31859(1)	0.87670(1)	4.5*
H15A	-0.13107(1)	0.14951(1)	0.95047(1)	4.0*
H15B	-0.09285(1)	0.24933(1)	0.86206(1)	4.0*
H15C	-0.13288(1)	0.13935(1)	0.85634(1)	4.0*
H21C	0.19267(1)	-0.00288(1)	0.30015(1)	4.2*
H21A	0.28665(1)	-0.07100(1)	0.38517(1)	4.2*
H21B	0.10595(1)	0.00727(1)	0.39466(1)	4.2*
H23	0.48589(1)	0.00868(1)	0.39540(1)	3.0*
H25A	0.71329(1)	0.05947(1)	0.40762(1)	4.3*
H25C	0.67115(1)	0.17929(1)	0.42642(1)	4.3*
H25B	0.75393(1)	0.17057(1)	0.33102(1)	4.3*
H31A	-0.23225(1)	0.54595(1)	0.32772(1)	4.4*
H31B	-0.19362(1)	0.41433(1)	0.33236(1)	4.4*
H31C	-0.12948(1)	0.44666(1)	0.40179(1)	4.4*
H32A	0.08870(1)	0.64768(1)	0.34863(1)	4.9*
H32B	0.10413(1)	0.51962(1)	0.41594(1)	4.9*
H32C	0.26297(1)	0.55892(1)	0.36013(1)	4.9*
H33A	0.39653(1)	0.64044(1)	0.15749(1)	4.9*
H33B	0.45636(1)	0.53835(1)	0.24401(1)	4.9*
H33C	0.49644(1)	0.51617(1)	0.15081(1)	4.9*
H34A	0.23617(1)	0.55601(1)	0.00691(1)	5.2*
H34B	0.39490(1)	0.46784(1)	0.04831(1)	5.2*
H34C	0.25239(1)	0.42036(1)	0.03989(1)	5.2*
H35A	-0.13849(1)	0.46517(1)	0.12747(1)	4.2*
H35B	0.01062(1)	0.35621(1)	0.12498(1)	4.2*
H35C	-0.11301(1)	0.35367(1)	0.21325(1)	4.2*

Starred atoms were included with isotropic thermal parameters. The thermal parameter given for anisotropically refined atoms is the isotropic equivalent thermal parameter defined as: $(4/3) \cdot [a^2 \cdot B(1,1) + b^2 \cdot B(2,2) + c^2 \cdot B(3,3) + ab(\cos\gamma) \cdot B(1,2) + ac(\cos\beta) \cdot B(1,3) + bc(\cos\alpha) \cdot B(2,3)]$ where a,b,c are real cell parameters, and B(i,j) are anisotropic betas.

$(C_5Me_5)Ni(acac)$

Table of Anisotropic Thermal Parameters - B's

Name	B(1,1)	B(2,2)	B(3,3)	B(1,2)	B(1,3)	B(2,3)	Beqv
Ni1	1.99(2)	2.06(2)	1.42(2)	-0.75(2)	-0.35(2)	0.12(2)	1.94(1)
Ni2	2.02(3)	1.31(2)	2.00(2)	-0.17(2)	-0.50(2)	-0.11(2)	1.92(2)
O1	2.6(1)	2.5(1)	1.3(1)	-0.8(1)	-0.4(1)	0.0(1)	2.25(8)
O2	2.4(1)	2.2(1)	2.3(1)	-1.1(1)	-0.5(1)	0.3(1)	2.47(9)
O3	2.7(1)	1.6(1)	2.4(1)	-0.6(1)	-0.7(1)	0.1(1)	2.34(8)
O4	2.4(1)	1.9(1)	2.1(1)	-0.2(1)	-0.9(1)	0.0(1)	2.28(8)
C1	3.2(2)	2.4(2)	2.0(2)	-0.3(2)	-0.5(2)	-0.3(2)	2.7(1)
C2	2.2(2)	1.6(2)	1.9(2)	0.4(2)	-0.6(2)	-0.6(1)	2.0(1)
C3	2.5(2)	1.2(2)	1.6(2)	-0.3(2)	-0.1(2)	0.3(1)	2.1(1)
C4	1.9(2)	1.2(2)	2.3(2)	-0.1(1)	0.0(2)	-0.1(1)	2.1(1)
C5	3.0(2)	2.4(2)	3.4(2)	-0.9(2)	-0.2(2)	0.0(2)	3.2(2)
C6	3.0(2)	2.4(2)	1.3(2)	-1.3(1)	-0.1(2)	0.1(1)	2.3(1)
C7	3.4(2)	1.9(2)	1.1(2)	-0.2(2)	-0.4(2)	0.4(2)	2.5(1)
C8	2.6(2)	2.7(2)	1.4(2)	-0.8(2)	-0.7(1)	-0.0(1)	2.3(1)
C9	2.9(2)	1.9(2)	1.2(2)	-0.8(1)	-0.4(2)	-0.0(1)	2.1(1)
C10	2.0(2)	2.8(2)	1.2(2)	-0.6(2)	0.0(2)	-0.2(1)	2.1(1)
C11	4.6(3)	4.1(2)	2.2(2)	-2.5(2)	-0.2(2)	-0.5(2)	3.5(1)
C12	4.7(3)	2.6(2)	2.3(2)	0.6(2)	-0.7(2)	-0.0(2)	3.8(2)
C13	2.7(2)	4.6(3)	2.5(2)	-1.5(2)	-0.8(2)	0.1(2)	3.4(2)
C14	5.2(3)	2.5(2)	2.8(2)	-1.2(2)	-1.0(2)	-0.5(2)	3.5(2)
C15	2.5(2)	3.3(2)	2.5(2)	-0.4(2)	-0.4(2)	-0.0(2)	3.1(1)
C21	3.7(2)	2.3(2)	3.4(2)	-0.7(2)	-1.2(2)	-0.3(2)	3.2(1)
C22	3.2(2)	1.8(2)	1.8(2)	-0.8(2)	0.0(2)	-0.4(1)	2.3(1)
C23	2.7(2)	1.6(2)	2.3(2)	-0.4(2)	-0.5(2)	-0.2(1)	2.3(1)
C24	2.5(2)	2.2(2)	1.6(2)	-0.3(2)	-0.3(2)	-0.4(1)	2.2(1)
C25	3.6(3)	2.8(2)	3.1(2)	-0.4(2)	-0.9(2)	-0.6(2)	3.3(1)
C26	2.9(2)	1.4(2)	2.3(2)	-0.2(2)	-0.1(2)	-0.2(1)	2.4(1)
C27	2.0(2)	1.2(2)	2.8(2)	0.4(1)	-0.8(2)	-0.7(1)	2.1(1)
C28	2.1(2)	1.2(2)	3.1(2)	0.0(2)	-0.6(2)	0.2(2)	2.4(1)
C29	2.7(2)	1.4(2)	1.9(2)	0.2(2)	-0.5(2)	0.2(1)	2.3(1)
C30	2.8(2)	1.5(2)	2.1(2)	-0.4(2)	-0.7(2)	0.2(1)	2.3(1)
C31	2.5(2)	3.6(2)	3.2(2)	-0.3(2)	0.2(2)	-0.7(2)	3.4(2)
C32	4.9(3)	2.5(2)	3.8(2)	-0.4(2)	-1.1(2)	-1.1(2)	3.7(2)
C33	3.4(3)	2.4(2)	4.8(3)	-1.1(2)	-0.7(2)	-0.1(2)	3.7(2)
C34	4.7(3)	3.7(3)	2.1(2)	-0.2(2)	-0.1(2)	-0.2(2)	4.0(2)
C35	2.7(2)	2.9(2)	4.1(2)	0.1(2)	-1.5(2)	-1.0(2)	3.3(1)

The form of the anisotropic temperature factor is: $\exp[-0.25\{h^2a^2 \cdot B(1,1) + k^2b^2 \cdot B(2,2) + l^2c^2 \cdot B(3,3) + 2hkab \cdot B(1,2) + 2hlac \cdot B(1,3) + 2klbc \cdot B(2,3)\}]$ where a,b, and c are reciprocal lattice constants.

$(C_5Me_5)Ni(acac)PMe_3$

Table of Positional Parameters and Their Estimated Standard Deviations

Atom	x	y	z	B(A2)
Ni	0.08538(7)	0.25	-0.00197(9)	2.13(2)
P	-0.0887(2)	0.25	0.0260(2)	2.65(4)
O	0.0744(3)	0.1452(2)	-0.1353(3)	2.42(8)
C1	0.0792(5)	0.0715(4)	-0.3334(5)	3.3(1)
C2	0.0763(4)	0.1596(4)	-0.2517(5)	1.9(1)
C3	0.0741(6)	0.25	-0.3118(6)	2.2(2)
C4	-0.1473(5)	0.3522(5)	0.1040(7)	4.4(2)
C5	-0.1515(7)	0.25	-0.1218(9)	5.0(3)
C6	0.2404(4)	0.1997(4)	0.0504(5)	2.5(1)
C7	0.1696(4)	0.1674(4)	0.1433(5)	2.8(1)
C8	0.1291(6)	0.25	0.2005(7)	2.7(2)
C16	0.3030(5)	0.1356(5)	-0.0303(6)	3.3(1)
C17	0.1465(5)	0.0639(5)	0.1744(6)	4.8(2)
C18	0.0608(8)	0.25	0.3138(9)	6.3(3)
H1A	0.08053(1)	0.01539(1)	-0.28205(1)	4.3*
H1B	0.02128(1)	0.07010(1)	-0.38547(1)	4.3*
H1C	0.13778(1)	0.07311(1)	-0.38444(1)	4.3*
H3	0.07586(1)	0.25000(1)	-0.40097(1)	2.9*
H4A	-0.21779(1)	0.34217(1)	0.10863(1)	5.7*
H4B	-0.12073(1)	0.35849(1)	0.18650(1)	5.7*
H4C	-0.13397(1)	0.40941(1)	0.05768(1)	5.7*
H5A	-0.22205(1)	0.25000(1)	-0.10855(1)	6.5*
H5B	-0.13291(1)	0.30598(1)	-0.16779(1)	6.5*
H5B'	-0.13291(1)	0.19402(1)	-0.16779(1)	6.5*
H16B	0.26891(1)	0.07619(1)	-0.04342(1)	4.3*
H16C	0.31465(1)	0.16605(1)	-0.10895(1)	4.3*
H16A	0.36548(1)	0.12356(1)	0.01005(1)	4.3*
H17A	0.19070(1)	0.04217(1)	0.23848(1)	6.3*
H17B	0.07903(1)	0.05894(1)	0.20290(1)	6.3*
H17C	0.15503(1)	0.02527(1)	0.10140(1)	6.3*
H18A	0.10019(1)	0.25000(1)	0.38832(1)	8.1*
H18B	0.01961(1)	0.30598(1)	0.31227(1)	8.1*
H18B'	0.01960(1)	0.19402(1)	0.31226(1)	8.1*

Starred atoms were included with isotropic thermal parameters. The thermal parameter given for anisotropically refined atoms is the isotropic equivalent thermal parameter defined as: $(4/3) \cdot [a^2 \cdot B(1,1) + b^2 \cdot B(2,2) + c^2 \cdot B(3,3) + ab(\cos\gamma) \cdot B(1,2) + ac(\cos\beta) \cdot B(1,3) + bc(\cos\alpha) \cdot B(2,3)]$ where a,b,c are real cell parameters, and B(i,j) are anisotropic betas.

$(C_5Me_5)Ni(acac)PMe_3$

Table of Anisotropic Thermal Parameters - B's

Atom	B(1,1)	B(2,2)	B(3,3)	B(1,2)	B(1,3)	B(2,3)	Beqv
Ni	1.77(3)	3.25(4)	1.37(3)	0	-0.08(5)	0	2.13(2)
P	1.81(8)	4.1(1)	2.07(9)	0	0.05(8)	0	2.65(4)
O	2.9(2)	2.4(2)	1.9(1)	-0.3(2)	-0.0(2)	0.4(1)	2.42(8)
C1	4.0(3)	3.2(3)	2.6(2)	0.1(3)	0.3(3)	-0.7(2)	3.3(1)
C2	1.2(2)	2.9(2)	1.8(2)	0.1(2)	0.0(2)	-0.3(2)	1.9(1)
C3	1.8(3)	3.9(4)	0.9(3)	0	0.1(3)	0	2.2(2)
C4	2.9(3)	5.0(4)	5.3(3)	0.4(3)	0.6(3)	-0.2(3)	4.4(2)
C5	2.9(4)	8.5(7)	3.5(4)	0	0.1(4)	0	5.0(3)
C6	1.7(2)	3.2(2)	2.4(2)	0.2(2)	-0.5(2)	0.5(2)	2.5(1)
C7	2.5(3)	4.2(3)	1.8(2)	-0.5(2)	-0.6(2)	1.0(2)	2.8(1)
C8	2.5(4)	4.9(4)	0.7(3)	0	-0.2(3)	0	2.7(2)
C16	2.9(2)	3.5(3)	3.6(3)	0.5(2)	-0.2(2)	0.4(3)	3.3(1)
C17	4.1(3)	6.0(4)	4:3(3)	-1.2(3)	-1.2(3)	2.8(3)	4.8(2)
C18	3.6(5)	12.0(9)	3.2(4)	0	0.6(4)	0	6.3(3)

The form of the anisotropic temperature factor is: $\exp[-0.25\{h^2a^2 \cdot B(1,1) + k^2b^2 \cdot B(2,2) + l^2c^2 \cdot B(3,3) + 2hkab \cdot B(1,2) + 2hlac \cdot B(1,3) + 2klbc \cdot B(2,3)\}]$ where a,b, and c are reciprocal lattice constants.

$(C_5Me_5)Co(Cl)PEt_3$

Table of Positional Parameters and Their Estimated Standard Deviations

Atom	x	y	z	B(A2)
Co	0.23616(6)	0.26958(7)	0.1645(1)	1.35(1)
Cl	0.3386(1)	0.1629(1)	0.0874(2)	2.29(4)
P	0.2009(1)	0.3065(1)	-0.0743(2)	1.76(4)
C1	0.2674(6)	0.3549(6)	0.3567(9)	2.4(2)
C2	0.2640(5)	0.2590(6)	0.3932(8)	2.2(2)
C3	0.1718(6)	0.2220(5)	0.3655(9)	2.2(2)
C4	0.1214(5)	0.2939(6)	0.3019(9)	2.4(2)
C5	0.1781(6)	0.3764(5)	0.2953(8)	2.1(2)
C6	0.3464(6)	0.4233(6)	0.377(1)	3.3(2)
C7	0.3477(7)	0.2054(6)	0.463(1)	3.1(2)
C8	0.1439(7)	0.1212(6)	0.394(1)	3.6(2)
C9	0.0171(6)	0.2874(7)	0.263(1)	3.5(2)
C10	0.1402(7)	0.4715(7)	0.251(1)	3.6(2)
C11	0.1678(6)	0.2018(6)	-0.180(1)	3.0(2)
C12	0.0823(6)	0.1551(6)	-0.115(1)	3.3(2)
C13	0.3053(6)	0.3476(6)	-0.178(1)	2.6(2)
C14	0.3426(6)	0.4391(6)	-0.108(1)	3.6(2)
C15	0.1102(6)	0.3910(6)	-0.1259(9)	2.7(2)
C16	0.0939(7)	0.4020(8)	-0.297(1)	4.7(2)

$(C_5Me_5)Co(Cl)PEt_3$

Table of Positional Parameters and Their Estimated Standard Deviations (cont.)

Atom	x	y	z	B(A2)
H6A	0.34236(1)	0.45132(1)	0.47538(1)	4.3*
H6B	0.40457(1)	0.39135(1)	0.36734(1)	4.3*
H6C	0.34231(1)	0.47061(1)	0.30039(1)	4.3*
H7A	0.34583(1)	0.21048(1)	0.57141(1)	4.0*
H7B	0.34416(1)	0.14121(1)	0.43435(1)	4.0*
H7C	0.40464(1)	0.23148(1)	0.42582(1)	4.0*
H8A	0.11599(1)	0.11597(1)	0.49243(1)	4.6*
H8B	0.10023(1)	0.10192(1)	0.31801(1)	4.6*
H8C	0.19797(1)	0.08238(1)	0.38925(1)	4.6*
H9A	-0.01893(1)	0.30282(1)	0.35106(1)	4.5*
H9B	0.00287(1)	0.32995(1)	0.18261(1)	4.5*
H9C	0.00257(1)	0.22532(1)	0.23132(1)	4.5*
H10A	0.11860(1)	0.50327(1)	0.33957(1)	4.6*
H10B	0.18843(1)	0.50715(1)	0.20337(1)	4.6*
H10C	0.08962(1)	0.46377(1)	0.18081(1)	4.6*
H11A	0.21846(1)	0.15863(1)	-0.17765(1)	3.9*
H11B	0.15524(1)	0.21890(1)	-0.28366(1)	3.9*
H13A	0.28930(1)	0.35829(1)	-0.28231(1)	3.4*
H13B	0.35275(1)	0.30092(1)	-0.17247(1)	3.4*
H15A	0.12766(1)	0.45039(1)	-0.08569(1)	3.5*
H15B	0.05293(1)	0.37139(1)	-0.08029(1)	3.5*
H12A	0.06770(1)	0.10103(1)	-0.17410(1)	4.3*
H12B	0.09417(1)	0.13727(1)	-0.01213(1)	4.3*
H12C	0.03096(1)	0.19754(1)	-0.11814(1)	4.3*
H14A	0.39644(1)	0.45912(1)	-0.16308(1)	4.7*
H14B	0.29548(1)	0.48606(1)	-0.11360(1)	4.7*
H14C	0.35894(1)	0.42868(1)	-0.00376(1)	4.7*
H16A	0.04589(1)	0.44697(1)	-0.31435(1)	6.1*
H16B	0.15021(1)	0.42242(1)	-0.34496(1)	6.1*
H16C	0.07548(1)	0.34342(1)	-0.33956(1)	6.1*

Starred atoms were included with isotropic thermal parameters. The thermal parameter given for anisotropically refined atoms is the isotropic equivalent thermal parameter defined as: $(4/3) \cdot [a^2 \cdot B(1,1) + b^2 \cdot B(2,2) + c^2 \cdot B(3,3) + ab(\cos \gamma) \cdot B(1,2) + ac(\cos \beta) \cdot B(1,3) + bc(\cos \alpha) \cdot B(2,3)]$ where a,b,c are real cell parameters, and B(i,j) are anisotropic betas.

$(C_5Me_5)Co(Cl)PEt_3$

Table of Anisotropic Thermal Parameters - B's

Name	B(1,1)	B(2,2)	B(3,3)	B(1,2)	B(1,3)	B(2,3)	Beqv
Co	1.32(3)	1.38(3)	1.36(3)	0.28(3)	-0.05(4)	-0.04(3)	1.35(1)
Cl	2.14(7)	2.49(7)	2.25(7)	1.06(6)	-0.13(7)	-0.29(7)	2.29(4)
P	2.12(8)	1.67(7)	1.48(7)	0.47(6)	-0.04(7)	-0.05(7)	1.76(4)
C1	2.8(3)	3.1(3)	1.5(3)	-0.2(3)	0.5(3)	-0.7(3)	2.4(2)
C2	1.5(3)	3.6(4)	1.6(2)	0.7(3)	-0.0(3)	-1.4(3)	2.2(2)
C3	3.0(3)	1.7(3)	1.8(4)	-0.4(3)	0.3(3)	0.2(3)	2.2(2)
C4	1.1(3)	4.3(4)	1.6(3)	0.2(3)	-0.2(3)	-1.7(3)	2.4(2)
C5	3.1(3)	1.9(3)	1.2(3)	0.5(3)	0.1(3)	-0.6(3)	2.1(2)
C6	3.5(4)	2.7(3)	3.7(5)	-0.5(3)	0.1(4)	-0.9(3)	3.3(2)
C7	3.8(4)	2.9(4)	2.6(4)	0.9(3)	-0.6(3)	-0.0(3)	3.1(2)
C8	5.2(5)	3.0(4)	2.4(4)	-1.6(3)	-0.1(4)	0.1(3)	3.6(2)
C9	1.7(3)	5.7(5)	3.1(4)	-0.1(4)	0.1(3)	0.1(4)	3.5(2)
C10	3.5(4)	3.8(4)	3.4(4)	0.9(4)	0.0(4)	-0.3(4)	3.6(2)
C11	3.7(4)	2.3(3)	3.0(4)	1.7(3)	-1.3(4)	-0.9(3)	3.0(2)
C12	3.1(4)	2.8(4)	4.1(5)	-0.6(3)	-1.1(4)	-0.6(4)	3.3(2)
C13	3.4(4)	2.9(3)	1.5(3)	0.6(3)	0.9(3)	0.6(3)	2.6(2)
C14	3.7(4)	2.9(4)	4.2(5)	-0.9(3)	1.9(4)	0.1(4)	3.6(2)
C15	2.3(3)	2.9(3)	2.7(4)	1.0(3)	0.0(3)	0.7(3)	2.7(2)
C16	5.5(5)	5.6(5)	3.0(4)	3.3(4)	-0.7(4)	0.0(4)	4.7(2)

The form of the anisotropic temperature factor is: $\exp[-0.25\{h^2a^2 \cdot B(1,1) + k^2b^2 \cdot B(2,2) + l^2c^2 \cdot B(3,3) + 2hkab \cdot B(1,2) + 2hlac \cdot B(1,3) + 2klbc \cdot B(2,3)\}]$ where a,b, and c are reciprocal lattice constants.

$(C_5Me_5)Ni(Br)PEt_3$

Table of Positional Parameters and Their Estimated Standard Deviations

Atom	x	y	z	B(A2)
Br	0.33943(1)	0.15345(1)	0.08333(8)	2.50(1)
Ni	0.23716(1)	0.27060(1)	0.15803(9)	1.57(1)
P	0.2063(1)	0.3074(1)	0.9236(2)	1.88(3)
C1	0.2664(4)	0.3541(4)	0.3576(7)	2.0(1)
C2	0.2670(4)	0.2583(4)	0.3941(7)	1.8(1)
C3	0.1757(4)	0.2200(4)	0.3678(7)	2.0(1)
C4	0.1203(4)	0.2880(4)	0.3080(7)	1.9(1)
C5	0.1766(4)	0.3723(4)	0.2952(7)	1.8(1)
C6	0.3429(5)	0.4218(5)	0.3783(8)	2.9(1)
C7	0.3482(5)	0.2067(5)	0.4631(8)	2.6(1)
C8	0.1493(5)	0.1200(5)	0.3992(9)	3.2(2)
C9	0.0191(5)	0.2839(6)	0.2699(9)	3.3(2)
C10	0.1405(5)	0.4664(5)	0.2551(9)	3.0(1)
C11	0.1709(5)	0.2060(4)	0.8120(8)	2.6(1)
C12	0.0885(5)	0.1566(5)	0.884(1)	3.7(2)
C13	0.3087(5)	0.3494(5)	0.8245(9)	2.9(1)
C14	0.3474(5)	0.4384(5)	0.893(1)	3.7(2)
C15	0.1178(5)	0.3941(5)	0.8768(8)	2.7(1)
C16	0.0996(6)	0.4080(6)	0.7068(9)	4.5(2)

$(C_5Me_5)Ni(Br)PEt_3$

Table of Positional Parameters and Their Estimated Standard Deviations (cont.)

Atom	x	y	z	B(A2)
H6A	0.33901(1)	0.44855(1)	0.47758(1)	3.8*
H6B	0.40083(1)	0.39105(1)	0.36735(1)	3.8*
H6C	0.33797(1)	0.46927(1)	0.30315(1)	3.8*
H7A	0.34589(1)	0.21159(1)	0.57159(1)	3.4*
H7B	0.34514(1)	0.14316(1)	0.43440(1)	3.4*
H7C	0.40452(1)	0.23279(1)	0.42670(1)	3.4*
H8A	0.12361(1)	0.11516(1)	0.49909(1)	4.2*
H8B	0.10475(1)	0.10025(1)	0.32583(1)	4.2*
H8C	0.20289(1)	0.08191(1)	0.39217(1)	4.2*
H9A	-0.01629(1)	0.29425(1)	0.36017(1)	4.4*
H9B	0.00480(1)	0.33026(1)	0.19632(1)	4.4*
H9C	0.00455(1)	0.22451(1)	0.22923(1)	4.4*
H10A	0.11715(1)	0.49565(1)	0.34469(1)	3.8*
H10B	0.18929(1)	0.50280(1)	0.21331(1)	3.8*
H10C	0.09216(1)	0.46059(1)	0.18178(1)	3.8*
H11A	0.22153(1)	0.16402(1)	0.80616(1)	3.4*
H11B	0.15430(1)	0.22562(1)	0.71176(1)	3.4*
H12A	0.07204(1)	0.10449(1)	0.82335(1)	4.9*
H12B	0.10456(1)	0.13643(1)	0.98438(1)	4.9*
H12C	0.03733(1)	0.19803(1)	0.88998(1)	4.9*
H13A	0.29286(1)	0.36065(1)	0.72044(1)	3.7*
H13B	0.35527(1)	0.30294(1)	0.82944(1)	3.7*
H14A	0.40061(1)	0.45703(1)	0.83629(1)	4.8*
H14B	0.30163(1)	0.48574(1)	0.88745(1)	4.8*
H14C	0.36404(1)	0.42802(1)	0.99646(1)	4.8*
H15A	0.13698(1)	0.45184(1)	0.91855(1)	3.5*
H15B	0.06124(1)	0.37545(1)	0.92356(1)	3.5*
H16A	0.05298(1)	0.45392(1)	0.69354(1)	5.8*
H16B	0.15507(1)	0.42764(1)	0.65787(1)	5.8*
H16C	0.07933(1)	0.35125(1)	0.66287(1)	5.8*

Starred atoms were included with isotropic thermal parameters. The thermal parameter given for anisotropically refined atoms is the isotropic equivalent thermal parameter defined as: $(4/3) \cdot [a^2 \cdot B(1,1) + b^2 \cdot B(2,2) + c^2 \cdot B(3,3) + ab(\cos \gamma) \cdot B(1,2) + ac(\cos \beta) \cdot B(1,3) + bc(\cos \alpha) \cdot B(2,3)]$ where a,b,c are real cell parameters, and B(i,j) are anisotropic betas.

$(C_5Me_5)Ni(Br)PEt_3$

Table of Anisotropic Thermal Parameters - B's

Name	B(1,1)	B(2,2)	B(3,3)	B(1,2)	B(1,3)	B(2,3)	Beqv
Br	2.55(2)	2.51(2)	2.44(2)	0.96(2)	-0.06(3)	-0.36(3)	2.50(1)
Ni	1.66(3)	1.63(3)	1.42(2)	0.15(2)	-0.04(3)	-0.05(3)	1.57(1)
P	2.15(6)	1.98(6)	1.51(5)	0.32(5)	0.09(6)	-0.18(6)	1.88(3)
C1	2.0(2)	2.6(2)	1.6(3)	0.3(2)	0.1(2)	-0.8(2)	2.0(1)
C2	2.1(2)	2.0(2)	1.2(2)	0.3(2)	-0.2(2)	-0.2(2)	1.8(1)
C3	2.2(2)	2.1(2)	1.8(3)	-0.3(2)	0.3(2)	-0.0(2)	2.0(1)
C4	1.6(2)	2.8(3)	1.3(2)	0.2(2)	0.3(2)	-0.1(2)	1.9(1)
C5	2.1(2)	1.8(2)	1.6(2)	0.3(2)	0.1(2)	-0.1(2)	1.8(1)
C6	3.2(3)	2.8(3)	2.7(3)	-0.6(2)	-0.1(3)	-0.7(3)	2.9(1)
C7	2.5(3)	2.7(3)	2.6(3)	0.7(2)	-0.2(3)	0.3(3)	2.6(1)
C8	4.6(3)	2.5(3)	2.6(3)	-1.1(3)	-0.1(3)	0.3(3)	3.2(2)
C9	2.3(3)	4.5(3)	3.3(3)	0.3(3)	0.4(3)	0.0(3)	3.3(2)
C10	3.6(3)	2.6(3)	2.7(3)	0.8(3)	-0.2(3)	-0.5(3)	3.0(1)
C11	4.0(3)	2.1(2)	1.7(3)	0.6(2)	-0.8(3)	-0.5(2)	2.6(1)
C12	3.8(3)	2.8(3)	4.6(4)	-0.6(3)	-0.9(3)	-0.7(3)	3.7(2)
C13	3.2(3)	3.3(3)	2.1(3)	1.0(2)	0.7(3)	0.6(3)	2.9(1)
C14	3.2(3)	3.0(3)	4.8(4)	-0.6(3)	0.5(3)	0.6(3)	3.7(2)
C15	2.4(3)	3.0(3)	2.7(3)	0.6(2)	0.2(2)	0.7(3)	2.7(1)
C16	5.3(4)	5.4(4)	2.7(3)	2.2(3)	-0.4(3)	0.8(3)	4.5(2)

The form of the anisotropic temperature factor is: $\exp[-0.25\{h^2a^2 \cdot B(1,1) + k^2b^2 \cdot B(2,2) + l^2c^2 \cdot B(3,3) + 2hkab \cdot B(1,2) + 2hlac \cdot B(1,3) + 2klbc \cdot B(2,3)\}]$ where a,b, and c are reciprocal lattice constants.

$(C_5Me_5)Ni(Me)PEt_3$

Table of Positional Parameters and Their Estimated Standard Deviations

Atom	x	y	z	B(A2)
Ni	0.2304(1)	0.2669(1)	0.1564(2)	2.00(3)
P	0.2000(3)	0.2960(3)	-0.0756(4)	2.82(7)
C1	0.2744(8)	0.3353(9)	0.359(2)	2.9(3)
C2	0.2463(9)	0.2418(8)	0.386(1)	2.4(3)
C3	0.154(1)	0.230(1)	0.362(2)	4.0(3)
C4	0.1234(9)	0.317(1)	0.304(2)	4.3(4)
C5	0.198(1)	0.377(1)	0.307(2)	3.8(4)
C6	0.379(1)	0.352(1)	0.395(3)	2.7(4)*
C6A	0.353(3)	0.416(3)	0.378(5)	2.4(8)*
C7	0.293(1)	0.158(1)	0.452(2)	2.0(4)*
C7A	0.348(3)	0.201(3)	0.465(5)	2.9(8)*
C8A	0.137(2)	0.129(2)	0.395(4)	1.9(7)*
C8	0.077(2)	0.156(2)	0.383(3)	4.5(6)*
C9	0.029(2)	0.364(2)	0.264(3)	3.5(5)*
C9A	0.017(3)	0.296(3)	0.263(5)	2.6(8)*
C10A	0.141(2)	0.477(2)	0.256(4)	1.4(6)*
C10	0.207(1)	0.484(1)	0.273(2)	2.7(4)*
C11	0.159(1)	0.199(1)	-0.181(2)	5.1(4)
C12	0.072(1)	0.151(1)	-0.111(2)	5.2(4)
C13	0.299(1)	0.334(1)	-0.188(2)	5.2(4)
C14	0.348(1)	0.414(1)	-0.118(3)	5.8(5)
C15	0.118(1)	0.387(1)	-0.119(2)	4.3(4)
C16	0.098(1)	0.404(1)	-0.294(2)	6.4(4)
C17	0.3235(9)	0.1764(9)	0.092(2)	2.6(2)*

$(C_5Me_5)Ni(Me)PEt_3$

Table of Positional Parameters and Their Estimated Standard Deviations (cont.)

H11A	0.20682(1)	0.15407(1)	-0.18594(1)	6.6*
H11B	0.14356(1)	0.21868(1)	-0.28191(1)	6.6*
H13	0.27771(1)	0.35127(1)	-0.28757(1)	6.7*
H13B	0.34092(1)	0.28362(1)	-0.19744(1)	6.7*
H15A	0.14110(1)	0.44346(1)	-0.07706(1)	5.6*
H15B	0.06082(1)	0.37237(1)	-0.06985(1)	5.6*
H12A	0.05414(1)	0.10048(1)	-0.17335(1)	6.8*
H12B	0.08575(1)	0.13013(1)	-0.01032(1)	6.8*
H12C	0.02248(1)	0.19474(1)	-0.10629(1)	6.8*
H14A	0.39891(1)	0.43107(1)	-0.18062(1)	7.5*
H14B	0.30667(1)	0.46475(1)	-0.10873(1)	7.5*
H14C	0.36988(1)	0.39710(1)	-0.01860(1)	7.5*
H16A	0.05412(1)	0.45229(1)	-0.30517(1)	8.3*
H16B	0.15352(1)	0.41959(1)	-0.34477(1)	8.3*
H16C	0.07324(1)	0.34850(1)	-0.33757(1)	8.3*
H17A	0.35138(1)	0.14949(1)	0.18030(1)	3.3*
H17B	0.29481(1)	0.12935(1)	0.03261(1)	3.3*
H17C	0.36957(1)	0.20635(1)	0.03222(1)	3.3*

Starred atoms were included with isotropic thermal parameters. The thermal parameter given for anisotropically refined atoms is the isotropic equivalent thermal parameter defined as: $(4/3) \cdot [a^2 \cdot B(1,1) + b^2 \cdot B(2,2) + c^2 \cdot B(3,3) + ab(\cos \gamma) \cdot B(1,2) + ac(\cos \beta) \cdot B(1,3) + bc(\cos \alpha) \cdot B(2,3)]$ where a,b,c are real cell parameters, and B(i,j) are anisotropic betas.

$(C_5Me_5)Ni(Me)PEt_3$

Table of Anisotropic Thermal Parameters - B's

Name	B(1,1)	B(2,2)	B(3,3)	B(1,2)	B(1,3)	B(2,3)	Beqv
Ni	1.77(5)	2.19(5)	2.04(5)	0.54(5)	0.09(6)	-0.08(6)	2.00(3)
P	2.6(1)	3.6(2)	2.3(1)	1.1(1)	0.0(1)	0.2(1)	2.82(7)
C1	2.1(5)	3.7(6)	3.1(6)	-1.2(4)	-1.2(5)	-1.1(6)	2.9(3)
C2	3.2(6)	1.7(5)	2.4(5)	1.5(4)	1.1(5)	-0.4(5)	2.4(3)
C3	5.6(7)	4.3(6)	2.1(6)	-2.6(5)	0.7(6)	-0.3(6)	4.0(3)
C4	0.9(5)	10(1)	1.7(6)	2.1(6)	0.4(4)	-0.6(6)	4.3(4)
C5	3.4(6)	4.5(7)	3.4(7)	0.6(6)	1.2(6)	0.3(6)	3.8(4)
C11	3.7(7)	6.9(9)	4.6(8)	1.2(7)	-0.2(7)	-3.2(7)	5.1(4)
C12	6.8(9)	2.9(7)	6(1)	-0.2(6)	-2.5(8)	-1.5(7)	5.2(4)
C13	4.5(7)	8.3(9)	2.7(7)	3.9(6)	2.5(6)	1.9(7)	5.2(4)
C14	4.6(8)	4.6(8)	8(1)	-0.7(6)	1.3(9)	2.2(9)	5.8(5)
C15	6.6(9)	3.2(6)	3.1(7)	1.8(6)	-1.0(7)	-1.1(6)	4.3(4)
C16	7.5(9)	7.9(9)	3.8(8)	4.1(7)	-1.0(7)	2.5(7)	6.4(4)

The form of the anisotropic temperature factor is: $\exp[-0.25\{h^2a^2 \cdot B(1,1) + k^2b^2 \cdot B(2,2) + l^2c^2 \cdot B(3,3) + 2hkab \cdot B(1,2) + 2hlac \cdot B(1,3) + 2klbc \cdot B(2,3)\}]$ where a,b, and c are reciprocal lattice constants.

$(C_5Me_5)Co(C_5H_5)$

Table of Positional Parameters and Their Estimated Standard Deviations

Atom	x	y	z	B(A2)
Co	0.18720(1)	0.37020(1)	0.22678(1)	1.742(6)
C1	-0.0875(3)	0.3642(3)	0.1994(2)	2.10(5)
C2	0.0669(3)	0.5512(3)	0.2715(2)	2.36(5)
C3	0.1545(3)	0.5278(3)	0.3719(2)	2.70(6)
C4	0.0482(3)	0.3255(3)	0.3629(2)	2.71(5)
C5	-0.1035(3)	0.2258(3)	0.2580(2)	2.29(5)
C6	-0.2175(3)	0.3213(3)	0.0831(2)	3.25(6)
C7	0.1257(4)	0.7385(3)	0.2454(2)	4.15(7)
C8	0.3244(4)	0.6812(4)	0.4722(3)	5.24(8)
C9	0.0850(4)	0.2324(4)	0.4511(2)	5.06(7)
C10	-0.2570(4)	0.0130(3)	0.2139(2)	4.18(7)
C11	0.2576(3)	0.3062(3)	0.0691(2)	2.24(5)
C12	0.4136(3)	0.4906(3)	0.1380(2)	2.44(5)
C13	0.4962(3)	0.4708(3)	0.2393(2)	2.81(6)
C14	0.3930(3)	0.2716(3)	0.2321(2)	2.88(6)
C15	0.2476(3)	0.1699(3)	0.1260(2)	2.58(5)
H6A	-0.258(3)	0.193(3)	0.032(2)	4.7(6)*
H6B	-0.319(3)	0.334(3)	0.090(2)	4.8(6)*
H6C	-0.131(4)	0.426(3)	0.038(2)	6.9(8)*
H7A	0.028(3)	0.782(3)	0.262(2)	5.7(7)*
H7B	0.125(4)	0.730(3)	0.162(2)	6.1(7)*
H7C	0.243(4)	0.829(4)	0.291(3)	7.7(8)*
H8A	0.384(3)	0.786(3)	0.451(2)	3.3(5)*
H8B	0.279(3)	0.709(3)	0.537(2)	5.2(7)*
H8C	0.431(5)	0.654(4)	0.494(3)	9(1)*
H9A	0.032(4)	0.260(3)	0.518(2)	6.9(8)*
H9B	0.224(4)	0.315(3)	0.492(2)	7.8(9)*
H9C	0.042(6)	0.109(5)	0.420(3)	14(1)*
H10B	-0.201(4)	-0.059(3)	0.245(2)	6.3(7)*
H10C	-0.279(4)	-0.038(3)	0.125(2)	7.6(8)*
H10A	-0.367(3)	-0.013(3)	0.241(2)	5.2(7)*
H11	0.171(3)	0.276(2)	-0.005(2)	2.6(5)*
H12	0.450(3)	0.604(3)	0.119(2)	3.3(5)*
H13	0.604(3)	0.570(2)	0.298(2)	3.0(5)*
H14	0.418(3)	0.219(3)	0.287(2)	4.0(6)*
H15	0.142(3)	0.025(3)	0.096(2)	3.3(5)*

Starred atoms were included with isotropic thermal parameters. The thermal parameter given for anisotropically refined atoms is the isotropic equivalent thermal parameter defined as: $(4/3) \cdot [a^2 \cdot B(1,1) + b^2 \cdot B(2,2) + c^2 \cdot B(3,3) + ab(\cos\gamma) \cdot B(1,2) + ac(\cos\beta) \cdot B(1,3) + bc(\cos\alpha) \cdot B(2,3)]$ where a,b,c are real cell parameters, and B(i,j) are anisotropic betas.

$(C_5Me_5)Co(C_5H_5)$

Table of Anisotropic Thermal Parameters - B's

Name	B(1,1)	B(2,2)	B(3,3)	B(1,2)	B(1,3)	B(2,3)	Beqv
Co	1.685(8)	1.971(8)	1.73(1)	1.035(6)	0.570(7)	0.512(8)	1.742(6)
C1	1.93(6)	2.92(7)	1.99(8)	1.61(5)	0.70(6)	0.72(6)	2.10(5)
C2	2.49(7)	2.25(6)	2.90(9)	1.51(5)	1.30(6)	0.70(7)	2.36(5)
C3	2.17(7)	3.48(8)	2.02(9)	1.53(5)	0.39(6)	-0.20(7)	2.70(6)
C4	3.30(7)	4.47(7)	2.36(8)	2.91(5)	1.66(6)	1.97(6)	2.71(5)
C5	2.06(6)	2.44(7)	2.97(9)	1.29(5)	1.42(6)	1.16(7)	2.29(5)
C6	2.78(7)	5.44(9)	2.56(9)	2.89(5)	0.83(7)	1.05(8)	3.25(6)
C7	4.94(9)	2.98(7)	6.1(1)	2.60(6)	3.00(8)	2.01(8)	4.15(7)
C8	3.14(9)	6.5(1)	3.7(1)	2.06(8)	0.15(9)	-1.7(1)	5.24(8)
C9	6.16(9)	9.5(1)	3.7(1)	5.96(7)	2.84(8)	4.14(9)	5.06(7)
C10	3.44(9)	2.64(8)	6.5(1)	1.23(6)	2.83(8)	1.43(9)	4.18(7)
C11	2.19(7)	2.72(7)	1.83(8)	1.35(5)	0.65(6)	0.38(6)	2.24(5)
C12	2.33(7)	2.24(7)	3.00(9)	1.11(5)	1.31(6)	1.01(7)	2.44(5)
C13	1.60(7)	3.42(8)	2.35(9)	1.01(6)	0.14(6)	-0.35(8)	2.81(6)
C14	3.24(7)	4.46(7)	2.81(9)	2.93(5)	1.48(6)	1.88(7)	2.88(6)
C15	2.73(7)	2.32(7)	3.10(9)	1.53(5)	1.24(6)	0.65(7)	2.58(5)

The form of the anisotropic temperature factor is: $\exp[-0.25\{h^2a^2 \cdot B(1,1) + k^2b^2 \cdot B(2,2) + l^2c^2 \cdot B(3,3) + 2hkab \cdot B(1,2) + 2hlac \cdot B(1,3) + 2klbc \cdot B(2,3)\}]$ where a,b, and c are reciprocal lattice constants.

$(C_5Me_5)Ni(C_5H_5)$

Table of Positional Parameters and Their Estimated Standard Deviations

Atom	x	y	z	B(A2)
Ni1	0.18746(1)	0.36963(1)	0.22656(1)	1.81(1)
C1	-0.0926(5)	0.3647(5)	0.2012(3)	2.14(8)
C2	0.0646(5)	0.5512(4)	0.2721(3)	2.37(8)
C3	0.1505(5)	0.5309(5)	0.3737(3)	2.73(9)
C4	0.0463(5)	0.3314(5)	0.3662(3)	2.63(9)
C5	-0.1046(5)	0.2283(5)	0.2601(3)	2.37(9)
C6	-0.2221(5)	0.3207(6)	0.0853(4)	3.6(1)
C7	0.1243(6)	0.7384(6)	0.2443(4)	4.8(1)
C8	0.3212(6)	0.6895(7)	0.4725(4)	5.5(1)
C9	0.0836(6)	0.2406(6)	0.4549(4)	5.3(1)
C10	-0.2567(6)	0.0144(6)	0.2178(4)	4.2(1)
C11	0.2667(5)	0.3039(5)	0.0670(3)	2.33(9)
C12	0.4180(5)	0.4888(5)	0.1362(3)	2.55(9)
C13	0.5007(5)	0.4689(5)	0.2374(3)	2.9(1)
C14	0.3994(5)	0.2713(5)	0.2308(3)	2.96(9)
C15	0.2539(5)	0.1689(5)	0.1245(3)	2.71(9)
H6C	-0.26283(1)	0.19421(1)	0.03950(1)	4.7*
H6A	-0.33743(1)	0.32645(1)	0.09434(1)	4.7*
H6B	-0.14809(1)	0.41356(1)	0.04859(1)	4.7*
H7C	0.09779(1)	0.71443(1)	0.16319(1)	6.2*
H7A	0.04938(1)	0.79121(1)	0.27321(1)	6.2*
H7B	0.26365(1)	0.82801(1)	0.27877(1)	6.2*
H8C	0.40940(1)	0.79057(1)	0.44512(1)	7.2*
H8A	0.27028(1)	0.73970(1)	0.52701(1)	7.2*
H8B	0.39235(1)	0.63876(1)	0.50797(1)	7.2*
H9C	0.22192(1)	0.31408(1)	0.49523(1)	6.8*
H9A	0.00526(1)	0.23931(1)	0.50760(1)	6.8*
H9B	0.04704(1)	0.11120(1)	0.41786(1)	6.8*
H10C	-0.20051(1)	-0.05400(1)	0.24623(1)	5.5*
H10A	-0.37234(1)	-0.01055(1)	0.24432(1)	5.5*
H10B	-0.29355(1)	-0.02786(1)	0.13606(1)	5.5*
H11	0.18571(1)	0.27444(1)	-0.00711(1)	3.0*
H12	0.45780(1)	0.60715(1)	0.11801(1)	3.3*
H13	0.60739(1)	0.57180(1)	0.29990(1)	3.8*
H14	0.42465(1)	0.21665(1)	0.28792(1)	3.8*
H15	0.16296(1)	0.03229(1)	0.09659(1)	3.5*

Starred atoms were included with isotropic thermal parameters. The thermal parameter given for anisotropically refined atoms is the isotropic equivalent thermal parameter defined as: $(4/3) \cdot [a^2 \cdot B(1,1) + b^2 \cdot B(2,2) + c^2 \cdot B(3,3) + ab(\cos \gamma) \cdot B(1,2) + ac(\cos \beta) \cdot B(1,3) + bc(\cos \alpha) \cdot B(2,3)]$ where a,b,c are real cell parameters, and B(i,j) are anisotropic betas.

$(C_5Me_5)Ni(C_5H_5)$

Table of Anisotropic Thermal Parameters - B's

Name	B(1,1)	B(2,2)	B(3,3)	B(1,2)	B(1,3)	B(2,3)	Beqv
Ni1	1.54(1)	1.92(1)	1.89(2)	0.842(9)	0.52(1)	0.49(1)	1.81(1)
C1	1.7(1)	2.5(1)	2.2(1)	1.17(8)	0.6(1)	0.5(1)	2.14(8)
C2	2.6(1)	2.2(1)	3.1(1)	1.65(7)	1.5(1)	0.9(1)	2.37(8)
C3	2.0(1)	3.1(1)	2.3(1)	1.15(9)	0.6(1)	-0.3(1)	2.73(9)
C4	2.8(1)	3.8(1)	2.5(1)	2.30(8)	1.4(1)	1.5(1)	2.63(9)
C5	2.0(1)	2.2(1)	3.1(1)	1.04(8)	1.2(1)	0.9(1)	2.37(9)
C6	2.8(1)	5.7(2)	3.0(2)	2.6(1)	0.8(1)	1.1(1)	3.6(1)
C7	5.4(2)	3.3(1)	7.1(2)	2.6(1)	3.6(2)	2.3(2)	4.8(1)
C8	2.9(2)	6.5(2)	4.2(2)	1.8(1)	-0.3(2)	-2.1(2)	5.5(1)
C9	6.3(2)	9.5(2)	4.2(2)	6.0(1)	3.0(1)	4.2(1)	5.3(1)
C10	3.5(1)	2.6(1)	6.3(2)	1.1(1)	2.5(1)	1.2(2)	4.2(1)
C11	2.2(1)	2.8(1)	1.9(1)	1.33(8)	0.5(1)	0.5(1)	2.33(9)
C12	2.0(1)	2.4(1)	3.0(1)	0.87(9)	1.2(1)	0.8(1)	2.55(9)
C13	1.5(1)	3.6(1)	2.5(2)	0.97(9)	0.2(1)	-0.0(1)	2.9(1)
C14	3.2(1)	4.5(1)	3.0(1)	2.94(8)	1.3(1)	1.9(1)	2.96(9)
C15	2.6(1)	1.8(1)	3.8(2)	1.13(8)	1.3(1)	0.6(1)	2.71(9)

The form of the anisotropic temperature factor is: $\exp[-0.25\{h^2a^2 \cdot B(1,1) + k^2b^2 \cdot B(2,2) + l^2c^2 \cdot B(3,3) + 2hkab \cdot B(1,2) + 2hlac \cdot B(1,3) + 2klbc \cdot B(2,3)\}]$ where a,b, and c are reciprocal lattice constants.

LAWRENCE BERKELEY LABORATORY
UNIVERSITY OF CALIFORNIA
TECHNICAL INFORMATION DEPARTMENT
BERKELEY, CALIFORNIA 94720